**www.uhasselt.be**

Universiteit Hasselt | Campus Diepenbeek
Agoralaan | Gebouw D | BE-3590 Diepenbeek | België
Tel.: +32(0)11 26 81 11

Growth and characterization of phosphorus doped n-type CVD diamond films of various orientations and devices/applications based on these

Ileana Andrada LAZEA

# DOCTORAATSPROEFSCHRIFT

2009 | Faculteit Wetenschappen

## Growth and characterization of phosphorus doped n-type CVD diamond films of various orientations and devices/applications based on these

Proefschrift voorgelegd tot het behalen van de graad van
Doctor in de Wetenschappen, richting natuurkunde, te verdedigen door:

Ileana Andrada LAZEA

Promotor: prof. dr. Ken Haenen
Copromotor: prof. dr. Marc D'Olieslaeger

INSTITUUT VOOR
MATERIAALONDERZOEK

# DOCTORAATSPROEFSCHRIFT

2009 | Faculteit Wetenschappen

# Growth and characterization of phosphorus doped n-type CVD diamond films of various orientations and devices/applications based on these

Proefschrift voorgelegd tot het behalen van de graad van
Doctor in de Wetenschappen, richting natuurkunde, te verdedigen door:

Ileana Andrada LAZEA

Promotor: prof. dr. Ken Haenen
Copromotor: prof. dr. Marc D'Olieslaeger

universiteit hasselt
INSTITUUT VOOR
MATERIAALONDERZOEK

imec

D/2009/2451/30

Pentru cei mai minunaţi pãrinţi din lume:
Teodora şi Mircea LAZEA

# Jury

| | | |
|---|---|---|
| **chairman** | Prof. dr. Jean Manca | Dean Faculty of Sciences, UHasselt, Belgium |
| **promotor** | Prof. dr. Ken Haenen | UHasselt - IMEC vzw, IMO - IMOMEC, Belgium |
| **co-promotor** | Prof. dr. Marc D'Olieslaeger | UHasselt - IMEC vzw, IMO - IMOMEC, Belgium |
| **jury members** | Dr. Matthias Schreck | Universität Augsburg, Institut für Physik, Germany |
| | Dr. Julien Barjon | CNRS & Université de Versailles St-Quentin-en-Yvelines, Groupe d'Etude de la Matière Condensée (GEMaC), France |
| | Dr. Jo Verbeeck | Universiteit Antwerpen, EMAT, Belgium |
| | Prof. dr. Miloš Nesládek | UHasselt - IMEC vzw, IMO - IMOMEC, Belgium |
| | Dr. Jan D'Haen | UHasselt - IMEC vzw, IMO - IMOMEC, Belgium |
| | Dr. Vincent Mortet | UHasselt - IMEC vzw, IMO - IMOMEC, Belgium |

# Acknowledgments

Accepting a PhD subject resembles, in my opinion, playing the lottery. You never know if the goals of the thesis are realistic or not, but more importantly you never know what kind of people you will have around you. Luckily for me, I feel like I just won the jackpot, due to the lovely people around me who have helped me to reach this point.

I would like to start the list of thanks with Prof. dr. Ken Haenen, who is my supervisor. Thanks for choosing my CV from the bunch of applicants for this fellowship, even though I had a terrible picture on it. I fully appreciate the independence and autonomy he granted me, this has given me the opportunity to grow and develop myself. Also, big thanks for taking the time to listen to my problems and for the fruitful suggestions and comments he made on my work.

To Prof dr. Marc D'Olieslaeger, my co-promotor, I want to thank for supervising my work and for the opportunity to start my PhD under his initial supervising.

Thanks to Dr. Vincent Mortet who played a determining role in my research and provided me with his experience in material science, lithography processes and so on. I have enjoyed working in the lab with him and it was equally fun to have my desk facing his.

To the members of the jury, thanks for taking the time to come to Hasselt on May 15th. It must have been difficult to find a free day in your busy schedules. To Prof. dr Miloš Nesládek, who I appreciate for his knowledge in diamond growth in general and n-type doping in particular. Special thanks to dr. Jan D'Haen for providing me with the necessary surface and microstructural analyses presented in this thesis. My gratitude also for dr. Julien Barjon for the lovely CL analyses presented in this work.

My fellowship was done in the framework of European network DRIVE (MRTN-CT-2004-512224). I want to express my gratitude to all the senior researchers involved in this project, among who is the jury member Prof. dr. Matthias Schreck, for their kindness and support in solving the students problems. For all the "early stage researchers" and the "experienced researchers": Bianca, Hadwig, Rosaria, Zoya, Wenying, Alex, Fabio, Michelle, Ovidiu, Tanguy and Wojciech, I feel like we became friends and shared nice moments in conferences and network meetings. I must admit that the Hasselt Diamond Workshop 2009 - SBDD XIV was not the same without the DRIVER's.

I would not have managed to finish my PhD without the help of my IMO colleagues. Most of them already left our group, but some of them are still working here: Anna B., Andrey B., Olivier D, Wim D., Michael D., Oliver W and Johnny B. A big thank to Johnny for always being there to solve my lab-related problems. I particularly liked the joke with the gas flows at the end of my PhD. Also, the newcomers to our office: Stoffel J., Diden B., Paulius P. and Yaso B., thanks for making the office a funny and joyful place. Especially when

complaining about the noise level in the room. A special word also for colleagues from the other departments of IMO: Sylvia W., Koen V. and Jean-Christophe B.
For all the administrative work related to my PhD and the IMEC SAP account problems, I could always rely on the help of our institute secretaries Relinde H., Lea V. and Marina B and on the help of computer skillfully Erik T. Dank u well!
Thanks to Bart R., Christel W. and Hilde P. for supplement me with all the necessary analyses and requests I had in the lab on a daily basis.
I have to thank to my former supervisor Prof. dr. George Dinescu for keeping me in contact with the Romanian scientific community during my Belgian "refugee". Multumesc pentru usa mereu deshisa!
Also thanks to my friends, "old" and "new" ones, for their assistance and support: Angela B., Beatrice C., Codruţa A., Emilia I., Lenia G., Syrah M., Karin R. and Valentina D.
To my gentleman of significant importance Свилен С.: Много благодаря, мило мое.
Finally, thanks to my family. Pentru mama şi tata: Vã mulţumesc dragii mei pãrinţi pentru ceea ce sunt azi si pentru ceea ce voi fi începand de mâine. Pentru sora, fratele, cumnata si nepotu': vã mulţumesc şi vouã dragilor ca m-aţi sprijinit, de la distanţã, când am avut nevoie.

Ileana – Andrada LAZEA
May 2009

# Abstract

The fact that diamond is a fabulous material with special properties, which are explored in a wide range of applications, is already known by now. The aim of this thesis is to exploit the material's characteristics, namely the semiconducting property. The deposition and characterization of n-type Chemical Vapour Deposition (CVD) diamond thin films are presented in this study. The bottom-up approach used in this survey starts with chapter 1, in which an overview of the diamond structure and its growth history is given. The reasons behind choosing Microwave Plasma Enhanced Chemical Vapor Deposition (MW PE CVD) as the appropriated method for producing our layers are properly explained. Also, diamond doping and the selection of the dopants, used for either n or p-type doping, are discussed. Special attention is given to phosphorous as an element, since it's the only component which can trigger a substitutional doping process in diamond leading to useful n-type conduction. The chapter finishes with a section dedicated to applications and a correlation between diamonds properties and specific types of application is made. The simplest application, which makes use of the semiconducting properties of diamonds, is the "pn-junction", which is the main device addressed in my thesis.

The second chapter pursues an accurate description of all the experimental techniques used in this research for growth and characterization of P-doped diamond layers. As expected, the growth procedure employed in obtaining n-type diamond opens chapter 2. Experimental setups for discovery and identification of impurities in CVD diamond, such as photocurrent and Fourier-Transform Photocurrent Spectroscopy (FTPS), are described next. The techniques which can characterize the quality of the obtained layers (from surface topography and morphology up to its electrical properties) are also explained in this chapter. The description of the necessary procedure, used for fabrication of diamond-based pn-junctions, is closing this chapter.

With chapter 3 the experimental part of the thesis starts. This study segment is dedicated to the P incorporation into diamond thin films when {100} and {111}-oriented diamond substrates were used. The doping process on {111}-oriented samples obtained at IMO is discussed in the context of the existing literature and the results presented here show the progress made over the first year of my thesis. Motivated by the need to optimize the quality of the doping process, a specific $O_2/H_2$ pre-treatment plasma step was developed. This procedure allowed the reduction of crystallographic defects incorporated in the n-type films and originating from the substrate. This finding enabled a slight improvement in quality of our P-doped {111}-oriented diamond films.

The development of n-type doping on {100}-oriented diamonds is presented in the second half of chapter 3. For this purpose a new doping strategy, different from the current trend present in literature, was introduced. The main differences of our growth procedure were: the elevated substrate temperature and the increased methane concentration. After a careful inspection of the results it was concluded that the doping of P in our {100}-oriented samples failed when this set of plasma parameters was used.

The reproducible and efficient n-type P-doping of diamond was successfully achieved for {100} or {111}-oriented substrates in various groups located all around the world. In contrast, only a few attempts reported doping into {110}-oriented films and the plasma parameters employed there were similar as for {111}-oriented films. Chapter 4 is dedicated exclusively to the doping process into {110}-oriented diamond substrates, either in single crystalline or polycrystalline specimens. For polycrystalline substrates, the layers were first grown using the so-called {111}-oriented strategy. For comparative reasons, a second doping scheme was tried. This time the P incorporation was addressed by atypical plasma parameters, which were previously tested for doping of P in our {100}-oriented samples. For probing the resulting layers several investigations were carried out. This inquiry includes surface and microstructural analyses, defect spectroscopy and electrical measurements. The preliminary surface images showed the presence of microfacets at the diamond surface. Also cathodoluminescence data and Raman spectra are presented. Based on the aforementioned results the quality of the P-doped layers was established and a confirmation of P incorporation was done. The overall estimation of the polycrystalline n-type doping point out to a higher quality of our layers when compared with the films grown using the {111}-oriented strategy. Thus, a general conclusion for polycrystalline {110}-oriented diamond films can be drawn: the novel set of plasma conditions is suitable for P incorporation.

The successful results presented for P doping onto polycrystalline diamond specimens inspired the work towards doping of single crystalline {110}-oriented layers. After the growth of the CVD diamond layers, the presence of P-related features was firstly revealed from PC and FTPS investigations. The results were confirmed by cathodoluminescence spectra. Thus, the successful P incorporation into the single crystalline {110}-oriented diamond layers was achieved. This points to the general conclusion of the chapter: this particular set of plasma parameters is appropriate for P doping of {110}-oriented diamond layers, even though some questions regarding the influence of the microfacets upon the incorporation process are still to be addressed.

The last chapter of the thesis describes the necessary fabrication steps used in obtaining various applications based on the n-type diamond layers described in the previous chapters. Obtaining pn-junctions devices, based on single or polycrystalline diamond layers, is not an easy task and complicated techniques are requested, such as lithography. The development of such applications requires quality layers. The characterization of single crystalline diamond pn-junctions reveals a successful preparation process of diamond-based devices at IMO. Based on this training, polycrystalline pn-junctions were fabricated. Their characterization proves that the quality of our layers is high enough to obtain devices. Moreover, the procured devices can be compared with the results from literature and thus it was validated that the new set of plasma growth conditions are appropriate for applications. The chapter ends with extending the range of the diamond-based devices. From thermionic electron emission measurements of the polycrystalline P-doped films grown on metallic substrates it was established that this material may be suitable for thermionic electron emitters.

Finally, the conclusions of this work are presented in the chapter called “general conclusions and outlook” together with some perspectives on the research topic.

# Nederlandse samenvatting

Het feit dat diamant een fabelachtig materiaal met speciale eigenschappen is, dat voor een brede waaier van toepassingen wordt onderzocht, is onderhand gekend. Het doel van deze thesis is de eigenschappen van dit materiaal te exploiteren, met nadruk op de halfgeleidende eigenschappen. De depositie en de karakterisering van dunne n-type diamant films afgezet via chemische dampdepositie, ofwel “Chemical Vapour Deposition - CVD” voor het bekomen van n-type lagen, word voorgesteld in deze studie. De bottom-up benadering die in dit onderzoek wordt gebruikt begint met hoofdstuk 1, waarin een overzicht van de diamantstructuur en zijn de groeigeschiedenis wordt gegeven. De redenen achter het kiezen van de zogenaamde microgolg plasma versterkte chemische dampdepositie (MW PE CVD) als aangewezen methode om onze af te zetten, worden verklaard. Ook het doteren van diamant en de keuze van geschikte elementen voor n- of p-type dotering, worden besproeken. Speciale aandacht wordt besteed aan fosfor, aangezien dit het einge element is dat substitutioneel in het rooster kan geincorporeerd worden om tot een bruikbare n-type geleiding te komen. Het hoofdstuk eindingt met een sectie gewijd aan toepassingen waarbij de correlatie tussen de eigenschappen van diamant en de specifieke toepassing wordt gemaakt. De eenvoudigste toepassing, die gebruik maakt van de halfgeleidende eigenschappen van diamant, is de “pn-junctie”. Het is dan ook de belangrijkste toeassing die in mijn thesis wordt beljcht.

Het twede hoofdstuk streeft een nauwkeurige beschrijving van alle experimentele technieken na die in dit onderzoek voor de groei en karakterisering van P-gedoteerde diamantlagen worden gebruikt. Zoals verwacht, hoofstuk 2 gestart met de groieprocedure die wordt aangewend voor het verkrijgen van n-type diamant. Daarna worden de experimentele opstellingen voor detectie en identificatie van onzuiverheden in CVD diamant, zoals de fotostroom en Fourier-Transform fotostroomspectroscopie (FTPS). De technieken die de kwaliteit van de verkregen lagen, gaande van oppervlaktetopografie en morfologie tot de elektrische eigenschappen, kunnen kenmerken worden ook verklaard in dit hoofdstuk. De beschrijving van de noodzakelijke procedure voor de vervaardiging van diamant-gebaseerde pn-junctues, beindigt dit hoofdstuk.

Met hoofdstuk 3 begint het experimentele deel van de thesis. Dit studiesegment word gewijd aan de incorporatie van P in dunne diamantfilms wanneer {100}- en {111}-georiënteerde diamantsubstraten werden gebruikt. Het doterings-proces op {111}-georiënteerde monsters wordt besproken in de context van de bestaande literatuur en de hier voorgestelde resultaten tonen de vooruitgang die tijdens het eerste jaar van mijn thesis werd geboekt. Gemotiveerd door de behoefte om kwaliteit van het doterings-proces te optimaliseren, werd een specifieke $O_2/H_2$ plasmavoorbehandeling ontwikkeld. Deze procedure liet toe om kristallografische defecten die hun origine vinden in het substraat, in de n-type films te verminderen. Hierdoor was een lichte verbetering van de kwaliteit van onze P-gedoteerde {111}-georiënteerde diamantfilms mogelijk. De ontwikkeling van {100}-georiënteerde n-type diamntfilms wordt voorgesteld in de tweede helf van hoofdstuk 3. Met dit als doel, werd een nieuwe doterings-strategie geintroduceerd, gebaseerd op tendensen aanwezig in de literatuur. De belangrijkste verschillen van onze groeiprocedure waren: de hogere substraattemperatuur en de verhoogde methaanconcentratie. Na inspectie van resultaten werd besloten dat het doteren van P in {100}-georiënteerde monsters niet mogelijk was met de voorgestelde plasmaparameters.

Reproduceerbare en efficiënte n-tye P-dotering van diamant voor zowel {100}- als {111}-georiënteerde substraten werd reeds in diverse groepen van rondom de wereld met succes bereikt. In tegenstelling, er zijn slechts een paar gemelde pogingen voor het doteren van {110}-georiënteerde films, en de daar aangewende plasmaparameters zijn gelijkaardig aan die voor {111}-georiënteerde films. Hooftstuk 4 word uitsluitend gewijd aan het doteren van {110}-georiënteerde diamantfilms gebruik maken van mono- en polykristallijne specimens. Voor de polykristallijne substraten werd eerste gebruik gemaakt van de zogenaamde {111}-georiënteerde strategie. Om de resultaten te vergelijken werden ook andere doteringscondities gebruikt. Dit keer werd de incorporatie van P onderzocht gebruik maken van de atypische plasmaparameters, die eerder voor doteren van de {100}-georiënteerde lagen werden getest. Om de uiteindelijke films te bestuderen, werden verscheidene experimenten uitgevoerd. De studie omvat oppervlakte en microstructurele analyses, de fectspectroscopie en elektrische metingen. De beelden van het filmoppervlak toonden de aanwezigheid van microfacettens aan. Ook cathodoluminescentie en Raman spectra worden voorgesteld. Gebaseerd op de voornoemde resultaten werd de kwaliteit van de P-gedoteerde lagen duidelijk gemaakt en een succesvolle incorporatie van P werd bevestigd. Na een vergelijkind bleek dat kwaliteit van polykristallijne n-type lagen beter was dan films gegroei met de zogenaamde {111}-georiënteerde strategie. Aldus, een aalgemene conclusie voor polykristallijne {110}-georiënteerde diamantfilms kan worden getrokken: de nieuwe geintroduceerde plasmacondities zijn geschikt voor de incorporatie van P.

De succesvolle resultaten die behaald werden bij het P-doteren op basis van polykristallijne diamantspecimens, fungeerde als inspiratibron voor het doteren van monokristallijne {110}-georiënteerde lagen. Na de groei van de CVD diamantfilms, werd de incorporatie van P eerste aangetoond met PC en FTPS.

Daarna werden de resultaten bevestigd met behulp van cathodoluminescentie, waardoor we kunnen besluiten dat we met succes P hebben geincorporeerd. Dit leidt tot de algemene conclusie van dit hoofdstuk: de gebruikte depositieparameters zijn geschikt voor het doteren van {110}-georiënteerde diamantfilms, ondanks het feit dat sommige vragen betreffende de invloed van microfacetten op het incorporatieproces nog moeten worden onderzocht.

Het laatste hoofdstuk van de thesis beschrijft de noodzakelijke vervaardigingsstappen die nodig zijn het verkrijgen van diverse toepassingen gebaseerd op de n-type diamantlagen die in de vorige hoofdstukken werden beschreven. Het aabmaken van pn-juncties, ebaseerd op mono- of polykristalline films, is geen gemakkelijke taak en ingewikkelde tecjnieken, zoals lithografie, zijn vereist. De ontwikkeling van dergelijke toepassingen vereist kwalitatief lagen. De karakterisering van monokristalijne diamant pn-juncties, tonen aan dat een succesvol bereiding van pn-juncties binnen IMO mogelijk is. Gebaseerd hierop, werden polykrystalline pn-juncties vervaadigd. Hun karakterisering bewijst dat de kwaliteit van onze lagen genoeg hoog is om zulke devices te verkrijgen. Daarenboven zijn de behaalde resultaten vergelijkbaar met waarden uit literatuur en kan er besloten worden dat de nieuwe plasmaparameters geschikt zijn voor toepassingen. Het hoofdstuk eindigt met het uitbreiden van de op diamant-gebaseerde toepassingen. Thermionische elektronenemissie op basis van de polykristallijne P-gedoteerde films afgezet op metalen substraten, tonen aan dat dit materiaal geschikt is als themionische elektronenemitter.

Tot slot worden de conclusie van dit werk voorgesteld in het hoofdstuk ”Algemene conclusies en vooruitzichten” samen met sommige perspectieven op het onderzoekonderwerp.

# Table of Contents

# 1 Introduction: Diamond

The first chapter is dedicated to a general presentation of diamond, pointing out its specific properties, which makes it appropriate for microelectronic applications. After a quick overview of the classification of carbon based materials, diamond structure and crystallinity is discussed, followed by a short description of diamond types. The next section describes the main techniques involved in producing synthetic diamonds, focusing on where impurities and defects can be included in the lattice. The applications of diamond are listed in the last part of the chapter where diamond as a semiconducting material is explored, with emphasis on the doping process, which is the subject of this thesis.

Diamond is a very expensive material and the word itself is magical. It makes us dream about kings and queens, pirate's treasures, famous actors and people in love. But the story of diamond has become more complex since the discovery of its many applications in industry, thus the range of involved people includes nowadays discoverers, doctors or scientists.

The power of diamond was recognized long before our century, the Greeks and the Romans called the gem stone "adamante" (Greek) and "adamas" (Latin) which means **invincible**, due to its hardness. Indeed this fabulous material is the hardest mineral ever discovered and huge amounts of money are paid for it. And yet it is pure carbon....

## 1.1 Diamond as pure carbon

Natural diamonds are produced inside the earth, at about 200 km below the earth crust. Because of high temperature (above 1300°C), high pressure and the abundance of carbon-based compounds, the carbon will be arranged in a special way, forming a material with a regular lattice. This special structure makes diamond like no other material. The process is slow and could take around a thousand million years before diamonds are formed. Investigations of the radioactive isotopes indicate the age of diamond as being older than earth. There are still debates regarding interpretation of these data, but scientists agree that the containing material is dating at least from the earth's formation. Once diamonds are formed the volcanoes will bring them up to the surface. The first gem stones were discovered in India 2700 years ago and were used in commerce. Jewelleries made with diamonds are dated a couple of centuries later to their discovery, but their true beauty was fully exposed starting with the 14th and 15th century when faceting and polishing techniques were developed.

In order to understand diamond, from its growth process up to its applications, basic knowledge of its structure is necessary. Carbon is the element that forms diamonds lattice and is one of the most abundant in the universe by mass (it's on the 4th place for most widespread elements after hydrogen, helium and oxygen). Its presence includes everything that surrounds us: sun, stars, comets, atmospheres of planets and all living organisms (people, animals, plants). Discovered since prehistory and located in the 4th group in the periodic table, carbon is a non-metal element. One neutral atom is formed by an electronic shell with 6 electrons (in a $1s^22s^22p^2$ configuration (Pierson 1993)) and a nucleus (composed from 6 neutrons and 6 protons). It has four valence electrons and due to its ability to share them, to form chemical bonds, over ten million of carbon-based compounds are found, many of which are essential for life.

Carbon can exist in nature in numerous allotropic forms such as amorphous, graphite, diamond, fullerenes and many more. A new form was recently discovered, i.e. magnetic carbon nanofilm (Rode, Ellman et al. 2002), displaying interesting electronic properties. But in order to avoid any confusion in the tremendous number of carbon allotropes, specific classification criteria can be used. One way to classify is according to the type of chemical bonds, corresponding to the possible hybridization of carbon: sp, $sp^2$ and $sp^3$. Specific physical and chemical properties characterize every allotrope form, thus applications differ from amorphous carbon (soft material used in inks, paints or rubber fabrications) to diamond (hard and abrasive material used for instance in cutting or drilling procedures).

The name of the hybrid orbitals comes from the name of constituents atomic orbitals, therefore in $sp^3$ configuration (like the case of *diamond* (Pierson 1993)) it is amixed one s orbital with three p orbitals. It will generate four equivalent $sp^3$ hybrid orbitals due to the fact that four atomic orbital are mixed. For carbon, all of the four valence electrons are involved in $sp^3$ hybrid orbitals, arranged in a tetrahedral arrangement centred on the C atom (as schematically drawn in Table 1.1). The angle between them is 109.5° and these orbitals form strong σ bonds with four similar neighbouring atoms. The three dimensional structure of diamond makes diamond the strongest and hardest natural material ever discovered and details about this structure will be included in the next section.

In $sp^2$ configuration one s orbital will be mixed with two p orbitals, generating three equivalent $sp^2$ hybrid orbitals. Using its three valence electrons, carbon will form three σ covalent bonds with the neighbouring atoms. The fourth valence electron remains in a p orbital, which is perpendicular to the σ bond plane and it's involved in π bond. The three $sp^2$ hybrid orbitals form a triagonal planar arrangement with 120° between the orbitals. The structure is present in *graphite*.

*Table 1.1: Classification of the three possible hybridizations of the carbon atom.*

| **Type of atomic orbitals involved in hybridization** | **Hybrid orbitals generated** | **Number of hybrid orbitals formed** | **Spatial arrangement of the hybrid orbitals** |
|---|---|---|---|
| s, p | sp | 2 | Linear 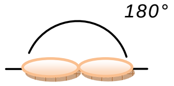 |
| s, p, p | $sp^2$ | 3 | Triagonal planar 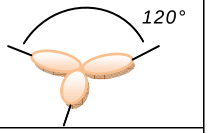 |
| s, p, p, p | $sp^3$ | 4 | Tetrahedral 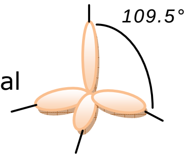 |

By mixing an s orbital with one p orbital two equivalent sp hybrid orbitals are generated. The carbon atom uses only two valence electrons for this configuration, the other two remain in the orthogonal p orbitals responsible for generation of π bonds. The set of sp orbitals has a linear arrangement, the angle between the orbitals being 180°. This hybridization is specific for *carbyne*.

In addition to the three distinct types, other forms exist and are called "transitional forms". These forms can be divided into two groups (Heimann, Evsyukov et al. 1997). The first one includes mixed short range-order carbon forms or less randomly arranged carbon atoms at different hybridization states: "amorphous" carbon, vitreous carbon, carbon black, soot, cokes, etc. Amorphous carbon is a disordered three-dimensional carbon allotrope in which both $sp^2$ and $sp^3$ hybridization are randomly found. It has no crystalline structure and depending on the amount of the "dominant" hybridization, included in the amorphous material, it exists in three forms (Kelires 1993). Evaporated amorphous carbon (a-C) is the form in which $sp^2$ local bonding dominates. When the percentage of the $sp^3$ sites increased, and all $sp^3$ carbon atoms are bonded to one or two hydrogen atoms, then we can speak about hydrogenated amorphous carbon films (a-C:H). Diamond like carbon (DLC) is an amorphous network solid, containing significant fraction of carbon $sp^3$ sites, but also $sp^2$ sites and hydrogen (Robertson 2008). These variations in composition between diamond-like and graphite-like crystallites play a determinant role in using of the material in "soft" or "hard" applications.

As part of the second group we have carbon forms with intermediate degree of hybridization written as $sp^n$, with "n" a fractional number. This group can be further divided in: a) when 1<n<2 such as cyclo[N]carbons, and b) when 2<n<3 such as fullerenes, carbon onions, nanotubes, etc. Differences between materials which are part of the same category are observed. For instance, fullerenes are simple clusters, consisting of minimum 20 carbon atoms ($C_{60}$), while nanotubes may be composed from one or multiple graphene sheets. For this reason carbon nanotubes will be preferred for applications as carbon-carbon composites, as catalysts or as materials with special electronic properties (Scharff 1998).

Size, dimensionality and shape play important roles in magnetic and optical properties of materials. The size matters when it becomes comparable to the length of a certain physical phenomenon that is concerned (Wu, Yang et al. 2004). Therefore, carbonic materials can be classified by a second criterion: spatial dimensionality of the structures. According to the aforementioned criterion, we have the following classes: three-dimensional (3D), two-dimensional (2D), one-dimensional (1D) and zero-dimensional (0D) carbonic compounds, as it is perfectly illustrated in Figure 1.1.

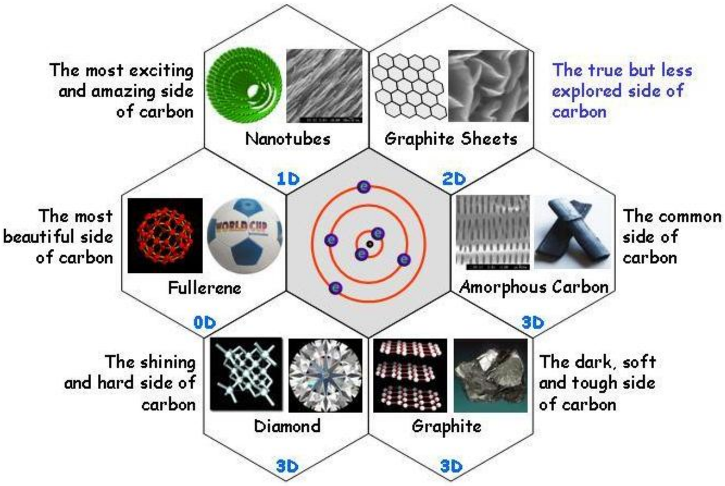

*Figure 1.1: Classification of carbon allotropes by dimensionality (Wu 2008).*

The range of 0D carbon allotropes is represented by cubes/spheres, like fullerenes and diamond clusters. 1D is defined by wires/tubes/rods and is observed in nanotubes. The definition of 2D refers to the simple shapes as sheets, seen in graphite and graphene. The 3D structures are more complex materials and include amorphous carbon, graphite and diamond.

### *1.1.1 Material crystallographic structure and properties*

Cubic diamond (or simply diamond), graphite and lonsdaleite (or hexagonal diamond) are the three possible crystallographic structures; their different crystal structures are presented in Figure 1.2 a). These structures can be visualised as stacking of puckered planes, ABCABC or ABAB, formed by six-member saturated carbon rings.

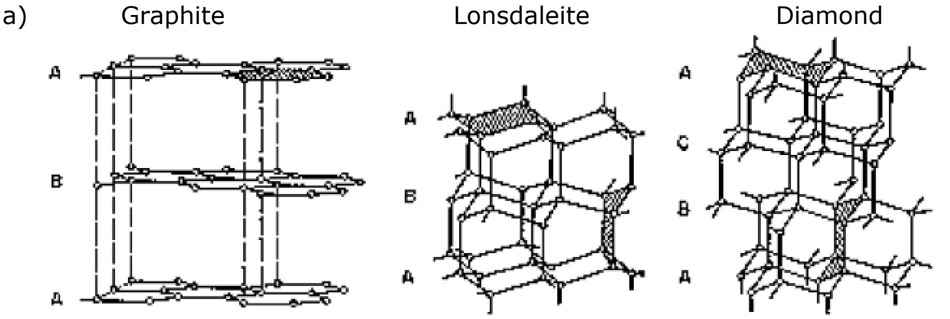

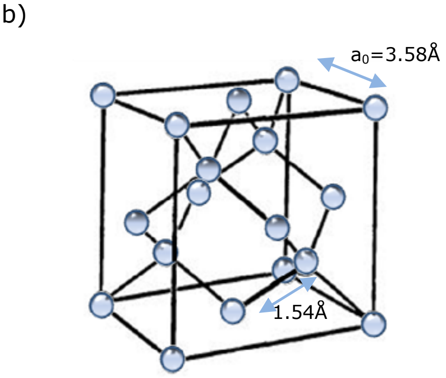

*Figure 1.2: a) Schematic diagrams of the three possible crystalline structures of carbon: graphite, hexagonal lonsdaleite and cubic diamond (Liu and Dandy 1995);*
*b) Diamond crystallographic structure.*

In graphite the structure is represented by flat sheets of carbon atoms strongly connected to their neighbouring atoms, but only weakly connected to other sheets. The polymorph of diamond, lonsdaleite, can adopt a (2H) hexagonal structure, but is rarely found in nature (Frondel and Marvin 1967).

In pure cubic diamond carbon atoms are bound together by single σ bonds (0.154nm) oriented along [111] directions (Blank 2003). The $sp^3$ hybridization and specific tetrahedron arrangement of this crystal were already explained in the previous section. The diamond structure is a face-centered cubic (fcc) Bravais lattice (Figure 1.2 b)). The unit cell is composed of two interpenetrating single fcc lattices which are shifted with respect to each other along the cube diagonal by a quarter of its length. This is similar to a primitive basis containing two atoms at (0,0,0) and (¼,¼,¼) associated with each lattice point. The edge of the conventional cubic cell is the lattice constant and has a length of $a_0$ = 0.357nm (3.57Å) at room temperature (Blank 2003). Its crystal structure is responsible for the fundamental properties of diamond, properties which will be discussed at the end of this section.

Natural diamond occurs in several crystal shapes (or habits), starting from simple shapes, as it is the case for the {100} cube (Strong 1989), the {110} dodecahedron and the {111} octahedron, and including other more complicated shapes. In order to understand the appearances of these crystal forms it is necessary to define the simplest crystallographic planes (100, 110 and 111) found in a cubic crystal.

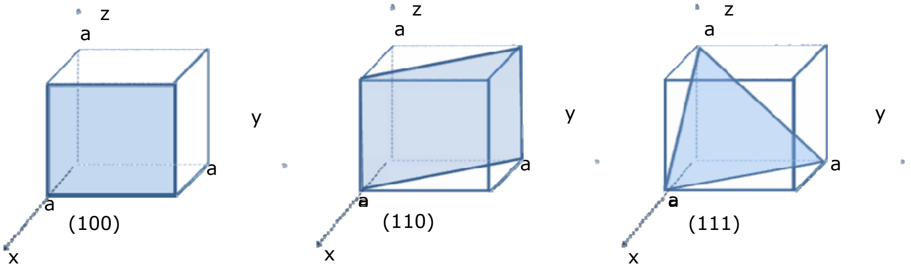

*Figure 1.3: Schematic illustrations of the three main crystallographic planes in diamond: (100), (110) and (111).*

A simple method to define the lattice planes and lattice directions in a crystal is to use Miller indices (hkl)(Sze 1981). By using these indices, the orientation of a surface or a crystal plane may be considered as how the plane (or any parallel plane with it) intersects the main crystallographic axes of the solid. A set of rules was established in order to determine these indices and they are calculated by the intercepts of the plane with three basis axes in terms of the lattice constant. Then the reciprocals of these numbers are considered and by reducing them to the smallest three integers the values of Miller indices are found. These values are enclosed in parenthesis (hkl), but when the plane intercepts the x axis on the negative side of the origin then (ħkl) is used. {hkl} is the notation used for planes of equivalent symmetry, [hkl] stands for the directions of a crystal, while <hkl> represents a full set of equivalent directions.

Figure 1.3 indicates the principal planes for a cubic crystal system.

The result of the diamond special kind of packaging is a tight covalent crystal and is the reason for diamond's *hardness*. Using the so called Mohs hardness scale (scratching test), natural diamond gets 10/10 and is considered the hardest terrestrial material. Although, recently new discovered materials, such as ultra hard fullerite (3D $C_{60}$) (Blank, Buga et al. 1998) and beta carbon nitride ($\beta$-$C_3N_4$) (Badzian 2001), can threaten diamond's leader position.

Due to the small size of the C atoms (Pierson 1993) the C-C bonds are considered to be short. The large overlap of the orbitals of the C atoms involved in a C-C bond causes a large energy separation between the occupied bonding orbitals and the unoccupied antibonding orbitals. This determines a very large forbidden energy gap between the valence and conduction band states in the electronic structure of diamond. As a result, diamond is a *wide bandgap material*, if not an insulator, with a minimal indirect band gap of 5.47eV at 300K (Sze 1981).

The highest *thermal conductivity* at room-temperature of any conventional solid is also explained because of the specific rigid covalent bonds present in diamond's structure. Due to these bonds, the transfer of the atomic vibrations through the crystal is efficient. Natural diamond has a thermal conductivity five times higher compared with metallic copper.

Diamond is *chemically inert* and *highly tolerant to irradiation*, properties dictated also by its crystal structure.

Another fundamental property is *optical transparency*. It is well know by now that due to its indirect band gap of 5.47eV, defect-free diamond absorbs electromagnetic radiation with a wavelength of ~227nm or lower. UV light or photons with higher energies will create electron-hole pairs. The process can be accompanied by near-ultraviolet light emitting, during the radiative recombination of an electron drop from conduction band minimum into a hole at the top of the valence band. The indirect bandgap presence in diamond and the phonons involvement makes the process inefficient. Therefore, diamond is transparent over a range from the near-ultraviolet, through the visible, to the far-infrared, and even at wavelengths beyond ~100 μm.

The following table summarizes mechanical, thermal, optical and electronic properties of diamond, many of which explain the material's great potential for applications.

*Table 1.3: Table with mechanical, thermal, optical and electronic properties of diamond. (Pierson 1993; Blank 2003; Schreck 2008; Teraji 2008)*

| **Property** | **Value** |
|---|---|
| Crystalline structure | Cubic (diamond) |
| Atom | C |
| Carbon atomic radii | 0.077nm |
| Atomic weight of carbon | 12.0107(8) u<br>1.9944 (1) x $10^{26}$kg |
| Lattice constant (300K) | 0.356nm |
| Bond length (300K) | 0.154nm |
| Bond angle (the tethraedal angle) | 109.4° |
| Density (300K) | 3515.25kg $m^{-3}$ |
| Packing density (fraction) | 0.34 |
| Atomic concentration (300K) | 1.763 x $10^{23}$$cm^{-3}$ |
| Hardness (Mhor scale) | 10 |
| Knoop hardness | 100GPa |
| Young's modulus | 1050GPa |
| Linear expansion coefficient (300K) | 1.05 x $10^{-6}$ $K^{-1}$ |
| Melting point | 3773K (4027°C) |
| Thermal conductivity | |
| at 300K | 2190W $m^{-1}$ $K^{-1}$ |
| at 500K | 1120W $m^{-1}$ $K^{-1}$ |
| at 600K | 960W $m^{-1}$ $K^{-1}$ |
| Debye temperature | 2067°C |
| Raman frequency (first order) | ~ 1132$cm^{-1}$ |
| Refractive index | |
| at 546.1 nm | 2.424 |
| at 589 nm | 2.419 |
| at 591 nm | 2.41 |
| visible light range | ~ 2.40-2.46 |
| Indirect bandgap | |
| at 300K | 5.47eV |
| at 500K | 5.42eV |
| at 600K | 5.38eV |
| Carrier mobility | |
| at 300K | |
| Electron (Hall) | 660$cm^{2}$ $V^{-1}$ $s^{-1}$ |

| | |
|---|---|
| Electron (TOF) | 4500cm$^2$ V$^{-1}$ s$^{-1}$ |
| Hole (Hall) | 1650cm$^2$ V$^{-1}$ s$^{-1}$ |
| Hole (TOF) | 3800cm$^2$ V$^{-1}$ s$^{-1}$ |
| at 500K | |
| Electron (Hall) | 270cm$^2$ V$^{-1}$ s$^{-1}$ |
| Hole (Hall) | 500cm$^2$ V$^{-1}$ s$^{-1}$ |
| at 600K | |
| Electron (Hall) | 130cm$^2$ V$^{-1}$ s$^{-1}$ |
| Hole (Hall) | 250cm$^2$ V$^{-1}$ s$^{-1}$ |
| Dielectric constant (300K) | 5.7 |
| Activation energy (300K) | |
| n-type (P) | ~570meV |
| p-type (B) | ~360meV |

### *1.1.2 Classification of diamond*

Two diamonds are never the same in terms of composition and properties, therefore it is possible to use different schemes of classifications. For instance, one standard rule to compare diamond gemstones is the 4C's rule, which is a concept from the jewellery sector that refers to the following words: Carat, Colour, Clarity and Cut.

However, synthetic and natural diamonds are classified in a unique way, based on the nature and amount of impurities contained within the structure and consists of two main types. The classification is done according to the optical absorption of nitrogen, boron and hydrogen-related defects and paramagnetic absorption of single substitutional nitrogen.

Nitrogen is the most detectable impurity and its presence is indicated by optical absorption in 98% in all natural diamonds (Pierson 1993). This foreign element can form optically active defects in many ways: single isolated atoms, multi-atoms complexes and complexes of atoms with other elements or with the lattice.

Another element which is frequently observed is boron. Its presence makes the identification of different classes of diamond possible. An explicit description of the type I and II diamonds was done in 2001 (Zaitsev 2001) and figure 1.4 is a schematic representation of this complex classification.

'**Type I**' diamonds have significant nitrogen impurities and further sub classification according to the aggregation of the nitrogen atoms in the lattice is possible. The '**Type II**' has low or undetectable nitrogen amounts and here the presence of boron distinguishes between the IIa and IIb sub categories.

Further details of type I and II are listed below.

**Type I:**

**Type Ia** – are the most common crystals in nature and have a nitrogen concentration up to 0.3% (3000ppm). The impurity is present in aggregates of substitutional atoms, in nonparamagnetic form. It is further divided in:

- **Type IaA** - the majority of nitrogen is present in the form of A aggregates (a nearest-neighbour substitutional pair), up to 500ppm.
- **Type IaB** - the B aggregates are specific for this category (four substitutional atoms surround a vacancy) and such diamonds are rare in nature.
- **Type IaB'** – comprises diamonds with B′-defects (platelets) as well as nitrogen organized as $N_3$ centre (three substitutional nitrogen that surround a vacancy). In this category is also included: type IaB′ regular, type IaB′ irregular and type IaB without B′.

**Type Ib** – are rare in nature (<0.1%) and nitrogen exists as isolated substitutional impurities with concentrations up to 500ppm. The strong yellow coloration is due to the increased light absorption towards the blue end of the spectrum. The category includes most high pressure high temperature synthetic diamond, but only 1 in 1000 natural diamonds fit in this category.

**Type Ic** – represents diamonds containing high concentrations of dislocations.

**Type II:**

**Type IIa** – comprises diamonds which do not present optical absorption due to the presence of boron and hydrogen impurities in the lattice and the content of nitrogen is less the $10^{18}$ $cm^{-3}$. This type of material is the most optically transparent and is usually colourless.

**Type IIb** – shows boron-related optical absorption, the material exhibiting significant p-type semiconductivity. Due to this factor the absorption of light happens toward the red end of the visible part of the spectrum, generating a slight blue colour of the diamond.

**Type IIc** – is represented by diamonds with dominating hydrogen defects.

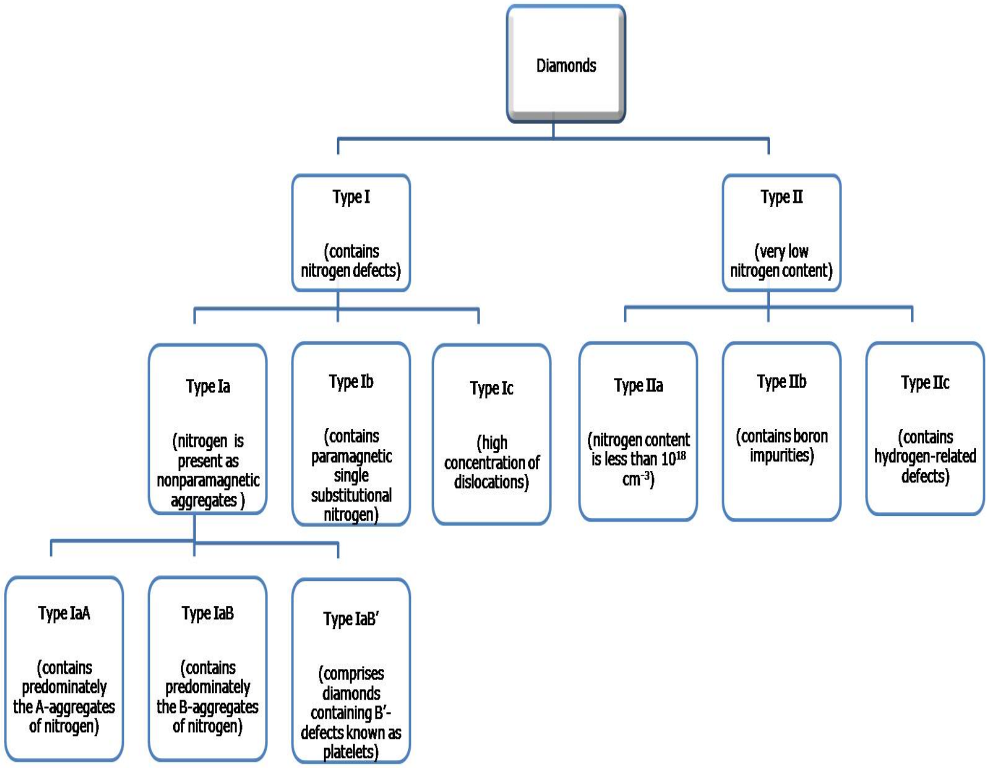

*Figure 1.4: Classification scheme of diamonds: type I – nitrogen is the dominant impurity and type II – nitrogen concentration is below* $10^{17}$ *cm*$^{-3}$.

### 1.1.3 Synthesis of artificial diamond

Diamonds are naturally produced at high pressure and temperature in volcanic shafts. The physical, chemical and many other properties of the resulted material are generally appreciated to be suitable for applications. However, gemstones are scarce and expensive and these were the reasons motivating the research in synthesis of artificial diamond.

In terms of modern diamond terminology, nowadays we can discuss about four distinct categories of materials:

- Natural diamond – being the only source of natural gemstones and a leader regarding acquisition prices;
- High-pressure high-temperature (HPHT) synthetic diamond – mimics diamond formation conditions relevant in earth (Siebert, Guyot et al. 2005) and are preferred for industry, in wear and abrasive applications;
- CVD diamond – it has potential for industrial applications and the process of obtaining it will be explained below;
- Diamond-like carbon (DLC) – is produced by physical vapour deposition and is a mixture of $sp^3$ bonded and $sp^2$ bonded carbon (see explanations regarding carbon allotropes presented earlier), it is preferred in optical applications.

Generally speaking synthetic diamond can be produced by two main techniques: HPHT and CVD. The main focus of this thesis is represented by CVD diamond, but details about HPHT synthetic diamond are also presented. Therefore the next paragraphs of this section will deal separately with the two processes and their detailed description and background.

#### 1.1.3.1 High Pressure High Temperature synthesis (HPHT)

Historical review of the important events that lead to the current development of high-pressure synthetic diamond are listed below (table 1.3.). As can be observed from the list a first success in HPHT diamond precipitation was achieved in 1955, but the process was continuously improved during the years and thus gem-quality diamonds of 3 carats (0.6 grams) are nowadays commercially available.

*Table 1.4: Historical development of HPHT diamond (Pierson 1993; Gemesis 1996).*

| | |
|---|---|
| 1814 | Carbon nature of diamond demonstrated by Davy |
| 1880 | Sealed-tube experiments of Harvey |
| 1894 | Carbon-arc experiments of Moissant |
| 1920 | Unsuccessful synthesis attempts by Parson |
| 1943 | Inconclusive synthesis experiments of Gunther |

| | |
|---|---|
| 1955 | First successful solvent-catalyst synthesis by General Electric, AESA, Sweden and in the Soviet Union |
| 1957 | Commercial production of grit by General Electric |
| 1965 | Successful shock-wave experiments by Dupont |
| 1983 | Production of a six-carat stone by De Beers |
| 1990 | Commercial production of 1.4 carat stones by Sumitomo |
| 2000's | Production of gem-quality (fancy yellow Ib) "cultured" diamonds, up to 3 carats nowadays, by Gemesis |

The high pressure, high temperature process is indicated in the phase diagram of carbon (as region A). As observed from figure 1.5., representing a complete pressure-temperature phase diagram, graphite is the stable form at 1 atm and room temperature, while diamond is formed by crystallization if a certain temperature occurs and high pressures are encountered. In HPHT synthesis the formation of diamond is possible by heating the carbon-based material at extreme pressures, between 5 and 10 GPa, and 1800-2300K. Also the presence of an ambient catalyst-solvent fluid metal layer is necessary to obtain diamond (Bundy, Bassett et al. 1996).

The transformation of diamond to graphite is also possible. Low pressure and the presence of the same metals (nickel, iron, cobalt, chromium, platinum, and palladium (Strong 1989)) is required, but this process is mostly of academic interest.

The addition of a catalyst to the process increases the growth speed to obtain diamond (several hours compared with millions of years needed for natural diamonds), although the efficiency of the conversion process can be affected by nitrogen and hydrogen-related impurities (Liang, Jia et al. 2005). Most of the crystals obtained by this technique are classified as Ib (see sub-section 1.1.2.). The presence of additional catalytic elements causes the incorporation of metallic inclusions in the crystals and thus limits the range of HPHT synthetic diamond applications to industrial methodologies that include cutting, drilling, grinding and milling.

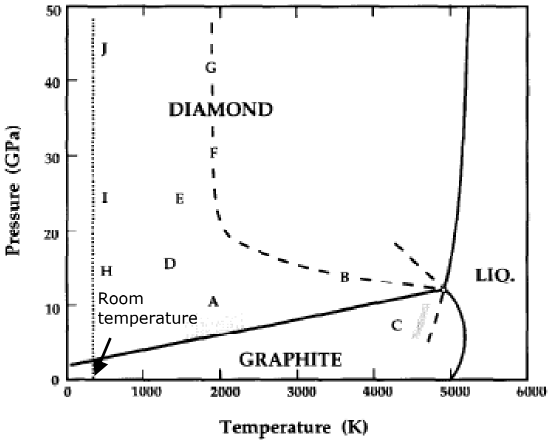

*Figure 1.5: Pressure-temperature (P/T) phase diagram illustrated by Bundy et al. in 1996, where A corresponds to commercial synthesis of diamond from graphite by using catalysts, B marks the P/T threshold of very fast (less then 1ms) solid-solid transformation of graphite to diamond, C: P/T threshold of very fast transformation of diamond to graphite, D: single crystal hexagonal graphite transforms to retrievable hexagonal-type diamond, E: are the regions where hexagonal-type diamond, F: upper ends of shock compression/quench cycles that convert hex-type graphite to cubic-type diamond. The B,G,F line represents the threshold of fast P/T cycles, however generated, that convert either type of graphite or hexagonal diamond into cubic-type diamond, H,I,J: path along which a single crystal hex-type graphite compressed in the c-direction at room temperature loses some graphite characteristics and acquires properties consistent with diamond-like polytype (Bundy, Bassett et al. 1996).*

#### *1.1.3.2 Chemical Vapour Deposition (CVD)*

The terms "vapour-phase diamond", "coating diamond" or "CVD diamond" refer to the material obtained by a low pressure vapour-phase process. Diamond grown in CVD conditions can be formed at near-atmospheric pressures and temperatures ranges from 100 (Tsugawa, Isihara et al. 2007) up to 1000°C, conditions where graphite is more stable thermodynamically (Bundy, Hall et al. 1955). A gas containing carbon (usually $CH_4$), diluted with hydrogen, is necessary for the process. Heating the substrate surface, destined to grow diamond on, to a certain temperature will lead to a decomposition of the methane gas and will create highly reactive carbon-containing radical species such as methyl ($CH_3$) and other growth species (Evans and Angus 1996). Most of the diamond-depositions methods require plasma and a list of techniques that can induce the requested decomposition step includes hot filament or oxy-acetylene torch methods (activation is induced by thermal means), or using microwave, DC or RF electrical discharges (radicals are produced by plasma activation).

Atomic hydrogen is also produced by activation of the gas mixture and has a key function in the prevention of the graphitization at sample surfaces, by terminating the dangling carbon bonds and the formation of 3D $sp^3$ bonds. Graphite and diamond are both deposited during the CVD growth and the selective etching of the planar graphitic layers is done by O or H atoms or OH radicals (when $O_2$ is present), while diamond is comparatively inert. The "preferential" etching role of hydrogen is well known by now (Angus, Will et al. 1968), but its presence might affect the film morphology and quality (Tang, Neves et al. 2005). Oxygen is an alternative solution to hydrogen (Sauer 1999), having the advantage of a higher etching rate, but it doesn't promote the $sp^3$ bonding (Evans and Angus 1996).

By low-pressure technique it is possible to grow diamond over a range of gas compositions, the carbon concentration in the gas phase being the main responsible factor for graphite deposition (Bachmann, Hagemann et al. 1995). Other plasma parameters, such as substrate temperature and pressure, can also be modified if one wants to induce lattice changes. The incorporation of defects and impurities is strongly correlated with these parameters, and more details about the doping process of diamond will follow in the next section.

Hot filament (HF) and microwave (MW) CVD are the two most common techniques used in CVD diamond generation (Werner and Locher 1998), each of them having advantages and disadvantages.

The HF CVD method makes use of metallic filaments (tungsten, tantalum or rhenium) to thermally activate the molecules of the gas mixtures and is widely used based on its simplicity. Moreover, it is suitable for 3D coatings which make this technique especially spread in tool applications or protective coatings. Recently it was possible to grow diamonds at relatively low substrate temperatures which could be a step forward in depositing diamond on temperature sensitive materials (Piazza, Gonzalez et al. 2006). The major drawbacks are the unwanted contamination of the diamond thin film with metal impurities, which is caused by the filament deterioration, and the impossibility to use oxygen or halogens due to the fact that these gases will destroy even more aggressively the filament.

The microwave plasma enhanced (MWPE) CVD process makes use of electron collisions to heat up and activate the gas mixtures. The use of liquid precursors is also possible. Due to the well controlled shape of the plasma ball this process is cleaner compared with HF, generating an outstanding quality for the materials prepared this way. Another advantage is the possibility to use oxygen and

halogens in the gas mixture, but one of its few weaknesses refers to the role of chamber geometry in defining the plasma shape and location.
An historical perspective of the major CVD developments was presented by H. Pierson in 1993 (Table 1.4.) and since then the continuous efforts in improving the processes lead to synthesis of high quality diamonds at a relatively high grow rate (Apollo Diamond 2008) .

*Table 1.5: Chronology of major developments in CVD diamonds (Pierson 1993; Apollo Diamond 2008; Schreck 2008).*

| | |
|---|---|
| 1950's | Early work on low-pressure synthesis mostly at Union Carbide, Case Western University and in the Soviet Union |
| 1956 | Development of low pressure synthesis by Derjaguin and others in the Soviet Union |
| 1974 | NIRIM and other Japanese laboratories develop high grow rate by CVD process. Development of NIRIM-type reactor by Matsumoto S., Sato Y., Kamo M. et al. |
| 1985 | Consortium formed at Pennsylvania State University to promote diamond research in the U.S. |
| 1988 | Development of diamond tweeter diaphragm by Sumimoto Electric |
| 1989 | Development of diamond-coated boring and drilling tools by Mitsubishi Metals |
| 1992 | Commercial production of free-standing shapes up to 1mm thick by Norton, General Electric and others. |
| Since 1990 | Growth of CVD diamond with high grow rate and ultrahigh mobilities. Developement of n-type and superconducting synthetic diamond |
| 2007 | Commercialization of cultured diamonds by Apollo Diamond, which are generally undistinguishable from mined diamonds with conventional gemmological tools |

### 1.1.4 Impurities and defects

As it was pointed out in section 1.1.2., diamond is almost never free of defects and/or impurities. Those lattice imperfections will affect diamond's physical properties and even small amounts of foreign elements included in the diamond's rigid structure can cause drastic changes, as it is the case for nitrogen for example.

Regarding the dimensionality of the defects, CVD diamond films can present the following types (Liu and Dandy 1995):

1. Point lattice defects such as vacancies, interstitials and substitutional defects;
2. Line lattice defects: dislocations;
3. Planar lattice defects: microtwins, stacking faults and grain boundaries;
4. Volume lattice defects: voids and inclusions (as is the case for graphite inclusions).

These defects are detrimental to electronic, optical, thermal and mechanical properties of diamond thin films, however the effect can also be neutral or beneficial. In some cases when a certain impurity is introduced in its lattice the so-called "doping" process takes place.

The impurities can be categorized in: lattice impurities, which consist of foreign elements incorporated in the lattice, the atom replacing a carbon atom; with donors or acceptors inclusions which are considered the second type and they refer to separate particles that are not part of the lattice, usually represented by silicates, aluminium, magnesium or calcium (Pierson 1993).

In general impurities can also alter a multitude of diamond's properties, such as: electrical properties (the doping process will be explained later on in this chapter), optical properties (change in diamond's colour, as observed in figure 1.6.), and mechanical properties (strength) or lattice parameter (stress engineering). The three dominant impurities present in the current CVD diamonds are nitrogen, boron and hydrogen.

*Figure 1.6: The difference in colour caused by impurities in the diamond lattice: image of nitrogen containing HPHT diamond crystals (left) and a picture of natural boron-doped diamond, the famous Hope diamond (right) (Schreck 2008).*

Hydrogen is easily incorporated as interstitials in the bulk diamond due to its small atom size, smaller than carbon. Also, hydrogen is a necessary ingredient of the CVD growth and is highly reactive. Nitrogen and boron are also easily incorporated, as substitutional defects, since their atoms are similar in size to carbon: the radius of nitrogen is 0.075nm that of boron is 0.082nm, while 0.077nm is the radius of carbon. The nitrogen source is present in commercial available bottles of hydrogen and also any leakage in the deposition system. It has five valence electrons, being a donor impurity in diamond, while boron with a valence of three is an electron acceptor. The *deep* donor status of nitrogen is dictated by its high activation energy 1.7eV (Walker 1979), which is 31% of the host material's bandgap. The boron acceptor is considered shallow using the same consideration: its activation energy is only 0.37eV (Collins and Lightowlers 1968).

The presence of other impurities in the diamond lattice was reported and Li and Na where estimated from theoretical calculations to be interstitial donors, while P will be a substitutional donor (Sauer 1999). As the focus of this thesis is on the later element, the state of the art in phosphorous doping will be detailed in the following section.

## 1.2 Diamond as a semiconductor: state of the art of doping

This study was aimed to point out the excellent semiconductor properties of diamond and its great potential as a semiconductor material. As it was previously explained, diamond is an indirect bandgap semiconductor and moreover the width of its bandgap is among the highest from the semiconductors.

By heating a semiconductor, the probability of an electron transfer from the valence band into the conduction band due to the thermal excitation will increase, and exceeding a critical temperature the material will no longer function as a semiconductor. Diamond has the highest upper limit for semiconductor materials, which is 500°C, compared with 150°C for silicon and 250°C for GaAs (Pierson 1993).

Diamond can be changed from an intrinsic to an extrinsic semiconductor at room temperature by introducing different impurities in its lattice, even though the extremely compact diamond lattice can't allow substitutional doping for many elements, still some dopant species like B, N, Si, P, Ni and S are possible to be taking up (Koizumi, Nebel et al. 2008). The intake of impurities is done either while growing by CVD or HPHT, either by ion implantation or diffusion.

The following sections refer to the process of doping and emphasis on the CVD growth of p or n-type semiconducting diamond will be presented.

### 1.2.1 p-Type doping

p-Type semiconducting diamond is obtained when acceptor impurities are introduced in the diamond lattice and thus discrete acceptor energy levels are formed above the valence band. Up till now, boron is the only dopant element that can cause p-type conductance. Natural diamonds type IIb are p-type semiconducting diamonds due to the presence of boron discovered inside their crystal structure (Chrenko 1973). Initially the role of the acceptor was attributed to aluminium, but detailed studies reveal the nature of the acceptor as being substitutional boron (Collins and Lightowlers 1968; Chrenko 1973). In the previous page it was established the reason behind considering boron a shallow acceptor, but even with such a low activation energy ($E_a$=0.368eV) (Collins and Williams 1971), the necessary energy is still too large compared with $k_BT$ at room temperature (≈25meV). Consequently, thermal excitation of holes in the valence band is hindered, and only 4-5% activation of the acceptor levels (even at 500K) is possible in the low doping regime. This explains why high concentrations of boron atoms, as high as $10^{19}$-$10^{20}$, are necessary for practical sheet conduction.

A first trial to obtain synthetic boron doped CVD diamonds was achieved in 1986 and a couple of years later the activation energy was reported to be close to the value for natural IIb diamonds (Fujimori, Nakahata et al. 1990). The necessary atom concentrations are possible by introducing high purity diborane ($B_2H_6$) or trimethylboron ($B(CH_3)_3$) to the source gas during the plasma growth process. Almost at the same time with the successful incorporation of B in diamond by the CVD method, p-type doping was also achieved by HPHT technique, using ion implantation and annealing techniques (Braunstein and Kalish 1983). At the moment homoepitaxial growth by CVD can yield mobilities as high as the best natural diamonds, thus values beyond 1500cm$^2$/Vs at 290K can be regularly obtained using this doping technique (Yamanaka, Watanabe et al. 1998; Teraji, Arima et al. 2004). Starting with 2004 the superconducting properties of super heavily B-doped synthetic diamond layers were explored (Bustarret, Kacmarcik et al. 2004; Ekimov, Sidorov et al. 2004). B-NCD stands for boron-doped nanocrystalline films and the conduction mechanism of those layers is believed to be of a semiconducting type, but metallic conduction can be obtained when B-acceptor concentrations reaches 2x10$^{21}$cm$^{-3}$ (Koizumi, Nebel et al. 2008).

Numerous studies presented details about B incorporation in the diamond films depending on the substrate type (mono or polycrystalline (Gheeraert, Deneuville et al. 1999)), the gas concentrations or the changes induced by substrate temperature variations (Nebel and Ristein 2004; Koizumi, Nebel et al. 2008) but their content is not discussed here.

### 1.2.2 n-Type doping

Contrary to p-type diamond, n-type is not found in nature and therefore must be synthetically produced, by both HPHT and CVD methods. By introducing an atom which creates a donor level into the diamond bandgap an n-type semiconducting diamond is obtained. Due to the diamond rigid structure and small size of the carbon atom, it is hard to find elements suitable for n-type doping. Mainly phosphorous is used as an impurity for the doping process, but nitrogen and sulphur were considered alternative donors.

#### Nitrogen doping

Nitrogen is one of the three most common impurities in diamond and its atomic radius permits the incorporation in the diamond lattice. However, due to the displacement of N atoms from the tetrahedral position in the lattice a deep donor state at 1.7 eV below the conduction band minimum is formed (Koizumi 2003). This energy, attributed to the substitutional nitrogen atoms, is too high to create active n-type conductivity at room temperature.

The recent progress in N doping of synthetic diamond layers showed that the addition of small quantities of nitrogen into the gas-phase mixtures will induce minor variations in morphology and crystal quality of the processed sample, while drastic influences were observed for higher concentrations (Locher, Wild et al. 1994; Bohr, Haubner et al. 1996; Tallaire, Achard et al. 2005; Tallaire, Collins et al. 2006; Achard, Silva et al. 2007). The quality of the crystals was close to that of HPHT type Ib diamonds. Also $N_2$ addition during the growth will increase the CVD growth rate, recently super high growth rates of 100μm$h^{-1}$ were reported, and tends to form (100) facets (Koizumi, Nebel et al. 2008).

The addition of N in ultrananocrystalline diamond (UNCD) growth leads to an n-type conductivity material (Williams, Curat et al. 2004). Here the N doesn’t act as a donor but the rather high incorporation of it creates a transport path related to a highly conductive subsystem of π-states located in the grain boundaries (William, Nesladek et al. 2008). Thus, reasonable conductivity at room temperature was calculated and metallic conductivity is attributed to the nitrogenated UNCD films (Mares, Hubik et al. 2006).

From theoretical calculations it was suggested that besides N, Li, Na and P impurities can be shallow donors (Kajihara, Antonelli et al. 1991). Li and Na can be located at interstitial sites acting thus as interstitial donors with donor states at 0.1 eV and 0.3 eV respectively, below the bottom of the conduction band. For substitutional P a donor level of 0.2 eV was approximated. In order to find suitable dopants one must consider its energy level but also its solubility and due to the calculated low values of their solubitilies in the diamond lattice, the process of effectively doping these impurities will be ion implantation. Li n-type doping by ion implantation was unsuccessful due to the fact that lithium becomes inactive after the long annealing procedure needed to remove the implanted induced defects, a process explained by possible trapping of diffused Li at implantation-induced lattice defects sites (Vavilov 1978). In 1993 it was found that Li and Na implantation could show conductivities due to the impurity incorporation in the lattice, but different conduction mechanisms were present (Prawer, Uzan-Saguy et al. 1993).

**Phosphorous doping**

Phosphorous is the only impurity, up to now, that can form a "shallow" n-type dopant in diamond and CVD is the main method used to achieve this type of conductivity, despite the multitude of experimental researches before 1996 (Koizumi 2003). It was demonstrated in 1997 by Koizumi et al. that P can be in-situ doped using phosphine ($PH_3$) as a dopant source during the CVD diamond growth (Koizumi, Kamo et al. 1997). The substrates used were {111}-oriented Ib synthetic diamonds and the temperature during the growth was around 950°C. The measured donor ionization energy was 0.6eV (Koizumi, Teraji et al. 2000) and a mobility maximum of $240cm^2V^{-1}s^{-1}$ at room temperature was obtained. The value of activation energy was continuously revised by different techniques such as photocurrent spectroscopy (Haenen, Meykens et al. 1999; Haenen, Meykens et al. 1999_a; Nesladek, Meykens et al. 1999_a; Haenen, Meykens et al. 2000_a) or Fourier Transform Infrared Spectroscopy (FTIR) (Gheeraert, Kozumi et al. 1999; Gheeraert, Koizumi et al. 2000; Gheeraert, Koizumi et al. 2000_a; Gheeraert, Casanova et al. 2001) and values between 0.5 and 0.6eV were found. Nowadays, Hall mobilities of $660cm^2 V^{-1}s^{-1}$ at room temperature can be reached and the reproducibility of the samples is not an issue anymore (Koizumi, Suzuki et al. 2008). Koizumi et al. reported the realization of a successful pn-junction used for formation of an ultraviolet (UV) light emitting diode (Koizumi, Watanabe et al. 2001).

An alternative for n-type doping was tried by deuteration of boron-doped diamond, which points out the formation of shallow donors and boron-multideuterium complexes such as (B, $D_2$) (Teukam, Chevallier et al. 2003). A more recent paper indicated that after the deuteration process the electron concentration, at room temperature, is higher in the deuterated boron-doped samples compared with the P-doped samples grown using tertiarybutylphosphine (TBP) as a doping source (Pinault, Barjon et al. 2007). A major drawback of this process is that at high temperatures the deuterated samples are going back to their p-type conductivity due to the dissociation of deuterium-related donors (Teukam, Chevallier et al. 2003). According to Pinault et al., these two different dopants are complementary dopants depending on the temperature range the samples are measured.

Contrary to B-doping, which is easily incorporated in {100}-oriented diamonds, the P-doping on {100} orientated substrates was unsuccessful for some years and a first positive result came in 2005 (Kato, Yamasaki et al. 2005). Based on this breakthrough, it was possible to fabricate pn and pin-junctions with good diode characteristics on {100}-oriented substrates (Makino, Kato et al. 2005; Makino, Tokuda et al. 2006). Nowadays, due to the progress in this direction made by Kato et al. it is possible to obtain Hall mobilities as high as 780cm$^2$/Vs (Kato, Tokuda et al. 2008) and almost similar phosphorous concentrations with to the ones obtained from {111} P-doped diamonds (Kato, Makino et al. 2007).

Another restriction, which can create a bottleneck in the development of diamond electronic devices over larger areas, was the preparation of polycrystalline doped diamonds. Again, B-doped CVD diamond films were easier to achieve compared to P-doped films. The n-type polycrystalline films were reported in 2003 (Nesladek, Haenen et al. 2003) and from Hall measurements a mobility of 12 cm$^2$V-$^1$s$^{-1}$ was found (Nesladek 2005). The same paper presents the characterization of the first polycrystalline diamond pn-junction.

At the end of this review on n-type diamond doping it is worth wile mentioning that sulphur was considered to be a successful n-type dopant and in 1999 the incorporation of sulphur was studied either by CVD or by ion implantation (Hasegawa, Takeuchi et al. 1999; Sakaguchi, Gamo et al. 1999). In the aforementioned studies a shallower donor level, when compared with P, was found, but the conductivity was attributed to the boron impurities present in the diamond layer rather than the active sulphur donors (Kalish, Reznik et al. 2000). This result made sulphur doping unattractive and contributed to the concentration of efforts towards research in P doping. Therefore this thesis will focus on this subject and separate chapters will deal with P incorporation in single and polycrystalline diamonds.

### *1.2.3 Applications of diamond*

For natural and HPHT synthetic diamonds grinding, grooving, cutting, sharpening, etching and polishing are the main industrial applications. Other applications in optics, thermal management (heat sinks) or even in surgery (surgical knifes or scalpels) are also possible. Although these applications have a large market, they are limited because of the size and high cost of the used crystals (Pierson 1993). Therefore CVD diamond offers a broader range of sizes, costs and other advantages such as exploitation of its intrinsic properties, which will make this type of diamonds more popular for applications. These advantages recommend it for areas like semiconductors, lasers, optics, opto-electronics, sensors and many more. Table 1.5 makes an overview of the actual applications of CVD diamond as seen by Liu et al. (Liu and Dandy 1995). Since then the presented list was continuously upgraded with sophisticated new examples of applications such as biosensors from diamond, diamonds as particle detectors, diamond-based acoustics devices and so on (Koizumi, Nebel et al. 2008).

*Table 1.6: Applications of CVD diamond (Liu and Dandy 1995) .*

| **Application area** | **Application examples** | **Physical properties of diamond utilized in the application** |
|---|---|---|
| Grinding/cutting tools | Inserts<br>Twist drills<br>Whetstones<br>Industrial knives<br>Circuit-board drills<br>Oil drilling tools<br>Slitter blades<br>Surgical scalpels<br>Saws | Great hardness<br>Great wear resistance<br>High strength and rigidity<br>Good lubricating properties<br>General chemical inertness |
| Wear parts | Bearings<br>Jet-nozzle coatings<br>Slurry valves<br>Extrusion dies<br>Abrasive pump seals<br>Computer disk coatings<br>Engine parts<br>Mechanical implants<br>Ball bearings<br>Drawing dies<br>Textile machinery | Great hardness<br>Great wear resistance<br>High strength and rigidity<br>Good lubricating properties<br>General chemical inertness |
| Acoustical coatings | Speaker diaphragms | High sound propagation speed<br>High stiffness<br>Low weight |
| Diffusion/corrosion protection | Crucibles<br>Ion barriers (sodium)<br>Fibre coatings<br>Reaction vessels | General chemical inertness<br>High strength and rigidity<br>Good temperature resistance |
| Optical coatings | Laser protection | Transparency from UV through visible into IR |

| | | |
|---|---|---|
| | Fibre optics | |
| | X-ray windows | Good radiation resistance |
| | Anti reflection | |
| | UV to IR windows | |
| Photonic devices | Radiation detectors | Large bandgap |
| | Switches | |
| Thermal management | Heat-sink diodes | High thermal conductivity |
| | Heat-sink PC boards | High electrical resistivity |
| | Thermal printers | |
| | Target heat-sinks | |
| Semiconductor devices | High-power transistors | High dielectric strength |
| | High-power microwave | High thermal conductivity |
| | Photovoltaic elements | Good temperature resistance |
| | Resistors | Good radiation resistance |
| | Capacitors | High power capacity |
| | Field-effect transistors | Good high-frequency performance |
| | UV sensors | Low saturation resistance |
| | Integrated circuits | |

As it is listed in the above table, diamond properties are the cause for making it a material with a great potential in semiconductor devices industry. Its applications operate in conditions in which traditional semiconductor materials, such as silicon, will fail. The most basic semiconductor device is the *pn-junction*. The realisation of such a structure requires the fabrication of n and p type semiconducting material by doping diamond with donor or acceptor impurities. The process of obtaining p-type diamond is easier, since it occurs naturally in diamond and is classified as type IIb.

The difficulty of obtaining a shallow donor was presented in the previous section and the only dopant is phosphorous. The progress made in this direction was recognized when an ultraviolet-light-emitting pn junction was fabricated from B-doped p-type and P-doped n-type diamond layers (Koizumi, Watanabe et al. 2001), paving the way for other P-doped devices with improved UV detection (Suzuki, Yoshida et al. 2004; Tajani, Tavares et al. 2004; Makino, Kato et al. 2005; Nesladek 2005; Tavares, Tajani et al. 2005; Makino, Tokuda et al. 2006). The diamond p-i-n diode has also shown good responsivity to deep UV (VUV) light detection with complete solar-blind characteristics (BenMoussa, Schuhle et al. 2004). The diamond VUV photodetectors with high sensitivity were chosen to be launched onboard satellite PROBA-2 (PRoject for ON-Board Autonomy) for solar UV radiation analysis (BenMoussa, Schuhle et al. 2006; BenMoussa, Soltani et al. 2008). This later application clearly shows the case where cost is secondary to performance.

## 1.3 Aims of this investigation

Since the success in exploiting diamond as a semiconductor material researchers all over the world have tried to work on some problems regarding its electronic properties (lack of shallow donors) and the practical production of bipolar diamond devices. The study presented here is also concentrated in this direction and there are three principal aims of this project:

- Continuing the investigations of defects by growing CVD diamond and introducing P in the crystal lattice, using single or polycrystalline diamond substrates of various orientations;
- The progress in n-type doping is discussed and the fabrication process and characterisation of pn-junctions is presented in detail, mainly when polycrystalline layers are used;
- Investigations of n-type diamond layers grown on non-diamond substrates are shown at the end of the study.

## 1.4 References

Achard, J., F. Silva, et al. (2007). "Coupled effect of nitrogen addition and surface temperature on the morphology and the kinetics of thick CVD diamond single crystals." Diamond and Related Materials **16**(4-7): 685-689.

Angus, J. C., H. A. Will, et al. (1968). "Growth of Diamond Seed Crystals by Vapor Deposition." Journal of Applied Physics **39**(6): 2915-2922.

Apollo Diamond. (2008). "Apollo Diamond home page." from http://www.apollodiamond.com/.

Bachmann, P. K., H. J. Hagemann, et al. (1995). "Thermal-Properties of C/H-Grown, C/H/O-Grown, C/H/N-Grown and C/H/X-Grown Polycrystalline Cvd Diamond." Diamond and Related Materials **4**(5-6): 820-826.

Badzian, A. (2001). "Diamond challenged by hard materials: a reflection on developments in the last decades." Materials Chemistry and Physics **72**(2): 110-113.

BenMoussa, A., U. Schuhle, et al. (2004). "PIN diamond detector development for LYRA, the solar VUV radiometer on board PROBA II." Physica Status Solidi a-Applied Research **201**(11): 2536-2541.

BenMoussa, A., U. Schuhle, et al. (2006). "Radiometric characteristics of new diamond PIN photodiodes." Measurement Science & Technology **17**(4): 913-917.

BenMoussa, A., A. Soltani, et al. (2008). "New developments on diamond photodetector for VUV solar observations." Semiconductor Science and Technology **23**(3): 1-7.

Blank, E. (2003). Structural imperfections in CVD diamond films. Thin film diamond I. C. Nebel and J. Ristein, Elsevier, ISBN 0-12-752185-2. **76**.

Blank, V. D., S. G. Buga, et al. (1998). "Structures and physical properties of superhard and ultrahard 3D polymerized fullerites created from solid C-60 by high pressure high temperature treatment." Carbon **36**(5-6): 665-670.

Bohr, S., R. Haubner, et al. (1996). "Influence of nitrogen additions on hot-filament chemical vapor deposition of diamond." Applied Physics Letters **68**(8): 1075-1077.

Braunstein, G. and R. Kalish (1983). "Effective P-Type Doping of Diamond by Boron Ion-Implantation." Journal of Applied Physics **54**(4): 2106-2108.

Bundy, F. P., W. A. Bassett, et al. (1996). "The pressure-temperature phase and transformation diagram for carbon; Updated through 1994." Carbon **34**(2): 141-153.

Bundy, F. P., H. T. Hall, et al. (1955). "Man-Made Diamonds." Nature **176**(4471): 51-55.

Bustarret, E., J. Kacmarcik, et al. (2004). "Dependence of the superconducting transition temperature on the doping level in single-crystalline diamond films." Physical Review Letters **93**(23): 237005_1-237005_4.

Chrenko, R. M. (1973). "Boron, Dominant Acceptor in Semiconducting Diamond." Physical Review B **7**(10): 4560-4567.

Collins, A. T. and E. C. Lightowlers (1968). "Photothermal ionization and photon-induced tunneling in the acceptor photoconductivity spectrum of semiconducting diamond." Physical Review **171**(3): 843.

Collins, A. T. and A. W. Williams (1971). "Nature of Acceptor Centre in Semiconducting Diamond." Journal of Physics Part C Solid State Physics **4**(13): 1789-1800.

Ekimov, E. A., V. A. Sidorov, et al. (2004). "Superconductivity in diamond." Nature **428**(6982): 542-545.

Evans, E. A. and J. C. Angus (1996). "Microbalance studies of diamond nucleation and growth rates." Diamond and Related Materials **5**(3-5): 200-205.

Frondel, C. and U. B. Marvin (1967). "Lonsdaleite a Hexagonal Polymorph of Diamond." Nature **214**(5088): 587-589.

Fujimori, N., H. Nakahata, et al. (1990). "Properties of Boron-Doped Epitaxial Diamond Films." Japanese Journal of Applied Physics Part 1-Regular Papers Short Notes & Review Papers **29**(5): 824-827.

Gemesis. (1996). "Gemesis home page." from http://www.gemesis.com/index.cfm.

Gheeraert, E., N. Casanova, et al. (2001). "Low temperature excitation spectrum of phosphorus in diamond." Diamond and Related Materials **10**(3-7): 444-448.

Gheeraert, E., A. Deneuville, et al. (1999). "Influence of diborane on the growth rate and phase stability of diamond films." Carbon **37**(1): 107-111.

Gheeraert, E., S. Koizumi, et al. (2000_a). "Electronic transitions of electrons bound to phosphorus donors in diamond." Solid State Communications **113**(10): 577-580.

Gheeraert, E., S. Koizumi, et al. (2000). "Electronic states of phosphorus in diamond." Diamond and Related Materials **9**(3-6): 948-951.

Gheeraert, E., S. Kozumi, et al. (1999). "Electronic states of boron and phosphorus in diamond." Physica Status Solidi a-Applied Research **174**(1): 39-51.

Haenen, K., K. Meykens, et al. (1999). "Low temperature photoconductivity detection of phosphorus in diamond." Physica Status Solidi a-Applied Research **174**(1): 53-58.

Haenen, K., K. Meykens, et al. (2000_a). "Temperature dependent spectroscopic study of the electronic structure of phosphorus in n-type CVD diamond films." Diamond and Related Materials **9**(3-6): 952-955.

Haenen, K., K. Meykens, et al. (1999_a). "Study of the electronic structure of the phosphorus level in n-type CVD diamond." Physica Status Solidi a-Applied Research **174**(1): R1-R2.

Hasegawa, M., D. Takeuchi, et al. (1999). "n-type control by sulfur ion implantation in homoepitaxial diamond films grown by chemical vapor deposition." Japanese Journal of Applied Physics Part 2-Letters **38**(12B): L1519-L1522.

Heimann, R. B., S. E. Evsyukov, et al. (1997). "Carbon allotropes: a sugested classification scheme based on valence orbital hybridization." Carbon Letters to the Editor **35**(10-11): 1654-1658.

Kajihara, S. A., A. Antonelli, et al. (1991). "Nitrogen and Potential Normal-Type Dopants in Diamond." Physical Review Letters **66**(15): 2010-2013.

Kalish, R., A. Reznik, et al. (2000). "Is sulfur a donor in diamond?" Applied Physics Letters **76**(6): 757-759.

Kato, H., T. Makino, et al. (2007). "N-type diamond growth by phosphorus doping on (001)-oriented surface." Journal of Physics D-Applied Physics **40**(20): 6189-6200.

Kato, H., N. Tokuda, et al. (2008). Electrical activity of doped phosphorus atom in (001) n-type diamond Hasselt Diamond Workshop 2008 - SBDD XIII, Hasselt, Belgium.

Kato, H., S. Yamasaki, et al. (2005). "n-type doping of (001)-oriented single-crystalline diamond by phosphorus." Applied Physics Letters **86**(22): 222111_1-222111_3.

Kelires, P. C. (1993). "Structural-Properties and Energetics of Amorphous Forms of Carbon." Physical Review B **47**(4): 1829-1839.

Koizumi, S. (2003). n-Type diamond growth. Thin-film diamond. C. Nebel and J. Ristein, Elsevier, ISBN 0-12-752185-2. **76**.

Koizumi, S., M. Kamo, et al. (1997). "Growth and characterization of phosphorous doped {111} homoepitaxial diamond thin films." Applied Physics Letters **71**(8): 1065-1067.

Koizumi, S., C. Nebel, et al. (2008). Physics and applications of CVD diamond, Wiley-VCH, ISBN 978-3-527-40801-6, Edited by S. Koizumi, C. Nebel and M. Nesladek.

Koizumi, S., M. Suzuki, et al. (2008). n-Type doping of diamond. Physics and applications of CVD diamond. S. Koizumi, C. Nebel and M. Nesladek, Wiley-VCH Verlag GmbH & Co. KGaA, ISBN 978-3-527-40801-6.

Koizumi, S., T. Teraji, et al. (2000). "Phosphorus-doped chemical vapor deposition of diamond." Diamond and Related Materials **9**(3-6): 935-940.

Koizumi, S., K. Watanabe, et al. (2001). "Ultraviolet emission from a diamond pn junction." Science **292**(5523): 1899-1901.

Liang, Z. Z., X. Jia, et al. (2005). "The influences of N and H on diamond synthesized with Ni-Mn-Co catalyst by HPHT." Diamond and Related Materials **14**(2): 243-247.

Liu, H. and D. S. Dandy (1995). Diamond chemical vapour deposition - Nucleation and early growth stages, Noyes Publications, ISBN 0-8155-1380-1.

Locher, R., C. Wild, et al. (1994). "Nitrogen Stabilized (100) Texture in Chemical-Vapor-Deposited Diamond Films." Applied Physics Letters **65**(1): 34-36.

Makino, T., H. Kato, et al. (2005). "Strong excitonic emission from (001)-oriented diamond P-N junction." Japanese Journal of Applied Physics Part 2-Letters & Express Letters **44**(37-41): L1190-L1192.

Makino, T., N. Tokuda, et al. (2006). "High-efficiency excitonic emission with deep-ultraviolet light from (001)-oriented diamond p-i-n junction." Japanese Journal of Applied Physics Part 2-Letters & Express Letters **45**(37-41): L1042-L1044.

Mares, J. J., P. Hubik, et al. (2006). "Weak localization in ultrananocrystalline diamond." Applied Physics Letters **88**(9): 092107_1-092107_3.

Nebel, C. E. and J. Ristein (2004). Thin-film diamond II, Elsevier, ISBN 0-12-752186-0, Edited by C. Nebel and J. Ristein.

Nesladek, M. (2005). "Conventional n-type doping in diamond: state of the art and recent progress." Semiconductor Science and Technology **20**(2): R19-R27.

Nesladek, M., K. Haenen, et al. (2003). "N-type P-doped polycrystalline diamond." Physica Status Solidi a-Applied Research **199**(1): 77-81.

Nesladek, M., K. Meykens, et al. (1999_a). "Low-temperature spectroscopic study of n-type diamond." Physical Review B **59**(23): 14852-14855.

Piazza, F., J. A. Gonzalez, et al. (2006). "Diamond film synthesis at low temperature." Diamond and Related Materials **15**(1): 109-116.

Pierson, H. O. (1993). Handbook of Carbon, Graphite, Diamond and Fullerenes - Properties, Processing and applications. New Jersey, USA.

Pinault, M. A., J. Barjon, et al. (2007). "The n-type doping of diamond: Present status and pending questions." Physica B-Condensed Matter **401**: 51-56.

Prawer, S., C. Uzan-Saguy, et al. (1993). "Can n-type doping of diamond be achieved by Li or Na ion-implantation." Applied Physics Letters **63**(18): 2502-2504.

Robertson, J. (2008). "Comparison of diamond-like carbon to diamond for applications." Physica Status Solidi a-Applications and Materials Science **205**(9): 2233-2244.

Rode, A. V., R. G. Ellman, et al. (2002). "Electronic and magnetic properties of carbon nanofoam produced by high-repetition-rate laser ablation." Applied Surface Science **197-198**: 644-649.

Sakaguchi, I., M. N. Gamo, et al. (1999). "Sulfur: A donor dopant for n-type diamond semiconductors." Physical Review B **60**(4): R2139-R2141.

Sauer, R. (1999). "Synthetic diamond - Basic research and applications." Crystal Research and Technology **34**(2): 227-241.

Scharff, P. (1998). "New carbon materials for research and technology." Carbon **36**(5-6): 481-486.

Schreck, M. (2008). Diamond growth - Tutorial. Diamond 2008, Sitges, Spain.

Siebert, J., F. Guyot, et al. (2005). "Diamond formation in metal-carbonate interactions." Earth and Planetary Science Letters **229**(3-4): 205-216.

Strong, H. M. (1989). "Early Diamond Making at General-Electric." American Journal of Physics **57**(9): 794-802.

Suzuki, M., H. Yoshida, et al. (2004). "Electrical characterization of phosphorus-doped n-type homoepitaxial diamond layers by Schottky barrier diodes." Applied Physics Letters **84**(13): 2349-2351.

Sze, S. M. (1981). Physics of semiconductor devices, J. Wiley & sons INC, ISBN 0-471-09837-x.

Tajani, A., C. Tavares, et al. (2004). "Homoepitaxial {111}-oriented diamond pn junctions grown on B-doped Ib synthetic diamond." Physica Status Solidi a-Applied Research **201**(11): 2462-2466.

Tallaire, A., J. Achard, et al. (2005). "Homoepitaxial deposition of high-quality thick diamond films: effect of growth parameters." Diamond and Related Materials **14**(3-7): 249-254.

Tallaire, A., A. T. Collins, et al. (2006). "Characterisation of high-quality thick single-crystal diamond grown by CVD with a low nitrogen addition." Diamond and Related Materials **15**(10): 1700-1707.

Tang, C. J., A. J. Neves, et al. (2005). "Characterization of chemical vapour deposited diamond films: correlation between hydrogen incorporation and film morphology and quality." Journal of Physics-Condensed Matter **17**(10): 1687-1695.

Tavares, C., A. Tajani, et al. (2005). "{111}-oriented diamond films and p/n junctions grown on B-doped type Ib substrates." Diamond and Related Materials **14**(3-7): 522-525.

Teraji, T. (2008). Chemical vapour deposition of homoepitaxial diamond films. Physics and applications of CVD diamond. S. Koizumi, C. Nebel and M. Nesladek, Wiley-VCH Verlag GmbH & Co. KGaA, ISBN 978-3-527-40801-6.

Teraji, T., K. Arima, et al. (2004). "High-quality boron-doped homoepitaxial diamond grown by high-power microwave-plasma chemical-vapor deposition." Journal of Applied Physics **96**(10): 5906-5908.

Teukam, Z., J. Chevallier, et al. (2003). "Shallow donors with high n-type electrical conductivity in homoepitaxial deuterated boron-doped diamond layers." Nature Materials **2**(7): 482-486.

Tsugawa, K., M. Isihara, et al. (2007). "Large-area and low-temperature nanodiamond coating by microwave plasma chemical vapor deposition." New Diamond and Frontier Carbon Technology **16**(6): 337-346.

Vavilov, V. S. (1978). "Ion-Implantation into Diamond." Radiation Effects and Defects in Solids **37**(3-4): 229-236.

Walker, J. (1979). "Optical-Absorption and Luminescence in Diamond." Reports on Progress in Physics **42**(10): 1605-1659.

Werner, M. and R. Locher (1998). "Growth and applications of undoped and doped diamond films." Reports on Progress in Physics **61**: 1665-1710.

William, O. A., M. Nesladek, et al. (2008). Growth and properties of nanocrystalline diamond films. Physics and applications of CVD diamond. S. Koizumi, C. Nebel and M. Nesladek, Wiley-VCH Verlag GmbH &Co. KGaA, ISBN 978-3-527-40801-6.

Williams, O. A., S. Curat, et al. (2004). "n-type conductivity in ultrananocrystalline diamond films (vol 85, pg 1680, 2004)." Applied Physics Letters **85**(21): 5106-5106.

Wu, Y. (2008). "Spintronics and Nanowalls." from http://www.ece.nus.edu.sg/stfpage/elewuyh/wuyihong.htm.

Wu, Y., B. Yang, et al. (2004). "Carbon nanowalls and related materials." Journal of Materials Chemistry **14**: 469-477.

Yamanaka, S., H. Watanabe, et al. (1998). "High-quality B-doped homoepitaxial diamond films using trimethylboron." Japanese Journal of Applied Physics Part 2-Letters **37**(10A): L1129-L1131.

Zaitsev, A. M. (2001). Optical Properties of Diamond, Springer, ISBN 3-540-41448-7, Edited by A. M. Zaitsev.

# 2 Experimental techniques

Chapter 2 presents the experimental techniques employed in the growth and characterization of P-doped diamond layers. The growth procedure used to realise the n-type diamond thin films, microwave plasma enhanced chemical vapour deposition (MW PE CVD), is described in the first part of the chapter. Section 2 describes the photocurrent theory behind the main defect spectroscopic techniques: photocurrent method (PC) and Fourier-Transform Photocurrent Spectroscopy (FTPS) followed by a presentation of their experimental set-ups. In the following sections techniques which can characterize the quality of the n-type layers (from surface topography and morphology up to the electrical properties) are presented. Last part of this chapter is reserved for the necessary procedures involved in fabrication of diamond-based devices, with emphasis on the fabrication procedure for pn-junctions.

## 2.1 Growth of n-type diamond films

### *2.1.1 Microwave plasma enhanced CVD method*

As it was explained in sub-section 1.1.3.2, the MW PE CVD is one of the most frequently used methods for thin film diamond growth and the most extensively studied.

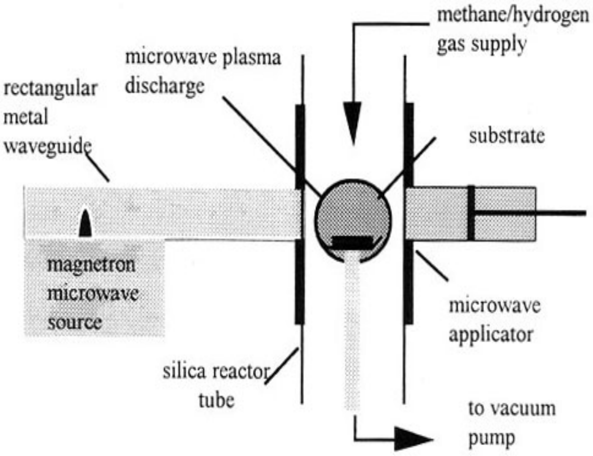

*Figure 2.1: Schematic diagram of a NIRIM-type reactor.*

These attributes are explained by the stability and reproducibility of this kind of plasma, the high efficiency, large surface depositions and by the high quality of the material obtained by this procedure. There exist a multitude of MW CVD reactor types and the choice for using one type or the other depends on the resulted attributes of the diamond film. It should be noted that in some reactors the substrate temperature, which is one of the key parameters in diamond growth, cannot be controlled independently from other parameters, while in others the substrates must have a certain size for a uniform growth.

In commonly used systems, as presented in figure 2.1, carbon-containing gases (such as methane) typically diluted in hydrogen are introduced in the discharge chamber and the chamber is permanently connected to a vacuum pump. The first microwave CVD reactor was using a quartz tube, which is pumped down to 10-100torr, and it was designed at NIRIM (Kobashi 2005) receiving its name after the place where it was invented (NIRIM-type reactor). The microwave source is coupled to the discharge chamber where gases are mixed and an electrical discharge in the gas mixture can be sustained by means of microwave radiation at a frequency of 2.45GHz (NIRIM-type reactor, ASTeX systems of 1.5kW or 5kW, SAIREM reactor of 1.2kW or AIXTRON reactor of 6kW) or 915MHz (ASTeX-type reactor of 100kW, WAVEMAT reactor of 30kW or AIXTRON system of 60kW) (Liu and Dandy 1995; Kobashi 2005).

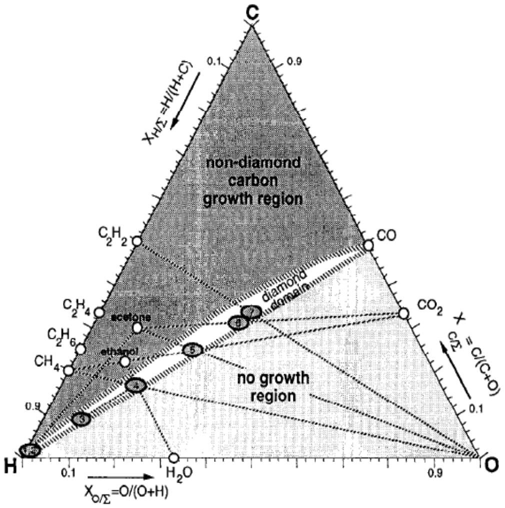

*Figure 2.2: C/H/O diagram of CVD diamond by Bachmann et al. (Bachmann, Hagemann et al. 1995).*

The gas mixture and hydrogen molecules are dissociated within the discharge and various types of reactive radicals, atoms, ions and electrons are formed. These species continue their journey towards the final target: the substrate surface. The sample placed in the middle of the discharge chamber, is in contact or immersed in the plasma, and its high temperature facilitates the chemical reactions necessary for formation of diamond. It is suggested that a variety of carbon species from $C_2$ up to $C_2H_2$ play a role in the growth process, but it is generally stated that diamond growth is possible due to methyl radicals addition and the presence of atomic hydrogen (May, Ashfold et al. 2007). The importance of other species for the process was studied by Bachmann et al. (Bachmann, Hagemann et al. 1995) and it was found that, independent of the deposition system or gas mixture, the diamond growth regime is constricted to a specific region, near the H-CO tie-line, close to the centre of the C/H/O diagram. The aforementioned region is presented in figure 2.2.

### *2.1.2 ASTeX-type reactor*

An advantage of the NIRIM-type reactor is the low cost of exchanging the quartz tube, in case of contaminations, leaks, etc. Nevertheless, disadvantages like incorporation of unwanted impurities (Si or O) in the diamond layers or low attainable base pressure make its spread restricted. An alternative is the use of steel chamber-type reactors. The specific design of the reactor enables the presence of a plasma ball just above the substrate surface, restricting the incorporation of unwanted impurities in the CVD diamond.

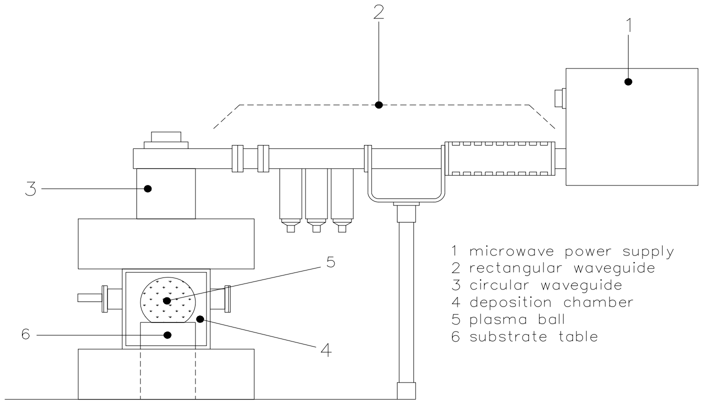

*Figure 2.3: Schematic illustration of the ASTeX-type reactor used for this thesis (Haenen 2002).*

Also, by additionally heating or cooling the substrate stage the effect of plasma heating is minimized, thus almost independent control of plasma and substrate parameters are possible. The base pressure can reach values up to $10^{-7}$torr by using turbo and rotary pumps, suppressing the residual gas phase impurities. One of the few disadvantages of this kind of reactor is that the replacement of the steel growth chamber is expensive.

The working principle of this system is a bit different from the NIRIM-type reactor and a schematic drawing of an ASTeX-type reactor used for the growth of P-doped CVD diamonds employed in this thesis is presented in figure 2.3. This design uses rectangular (2) and cylindrical (3) waveguides for the propagation of the microwaves (generated by a microwave generator – 1). The role of the three-rod tuner present on the trajectory of waveguide 2 is to regulate the impedance so that the reflected microwaves are suppressed. The generation of the plasma ball (5) occurs in the region where the local electric field is the highest, into the cylindrical deposition chamber (4) that is. The movable substrate stage (6) allows further tuning of the microwave circuit and thus the cavity geometry is adjusted.

The microwave output of the ASTeX PDS 17 reactor at IMO is in the range of 500 and 5000W. This deposition system is only used for n-type doping, but similar systems are available at IMO for growth of p-doped diamond films. A picture of the apparatus is showed in figure 2.4 (left). Also the plasma ball during the growth process of an n-type diamond is illustrated here (figure 2.4 (right)).

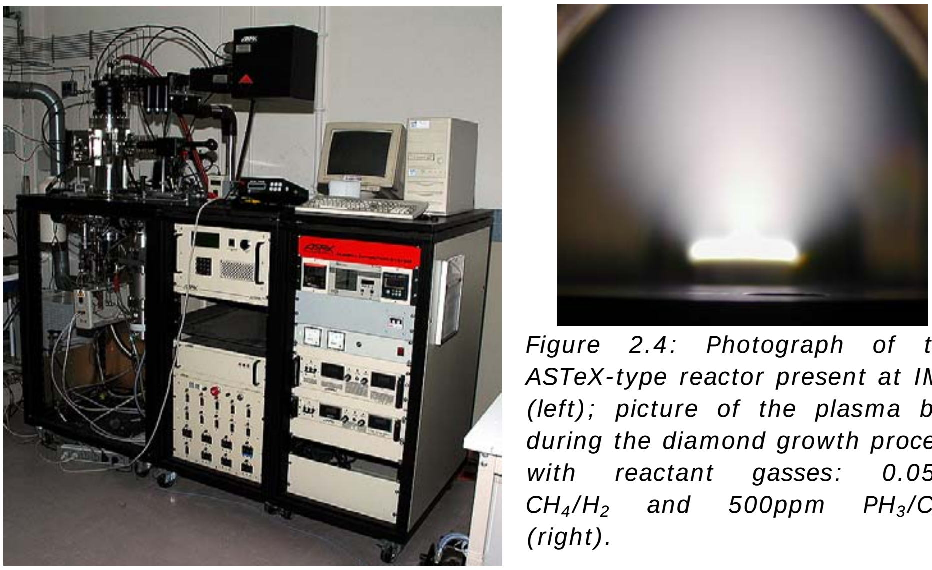

*Figure 2.4: Photograph of the ASTeX-type reactor present at IMO (left); picture of the plasma ball during the diamond growth process with reactant gasses: 0.05% $CH_4/H_2$ and 500ppm $PH_3/CH_4$ (right).*

A typical gas mixture is formed from a carbon gas source (methane is used for the growth of the diamond samples presented in this study), molecular hydrogen ($H_2$) and a P gas source (phosphine was used for this thesis). All the gases have a high purity (~99.9999%) and the plasma ball has a white-purple coloration as presented in the figure above. The concentration of the gases in the mixture is controlled by mass flow controllers and typically concentrations between 0.05 and 1% of $CH_4$ in $H_2$ were used, while the $PH_3$ flow was concentrated in the range of ppm compared with $CH_4$ (50 up to 10000). During the synthesis, gas is evacuated from the deposition chamber by a process pump and pressures up to 180 torr can sustain the plasma. Substrate orientation and type plays a major role in choosing the appropriate process parameters for n-type doping and detailed experimental conditions will be presented in chapters 3 and 4.

The ASTeX PDS 17 system is equipped with substrate cooling, allowing working with high power plasmas at the same time keeping the temperature in the range between 600 and 1200°C, typically the range necessary for diamond growth. Specific for P incorporation, temperatures around 900°C. The used substrate temperature is monitored, during the growth process, by means of an optical pyrometer (Pyrometer Instrument CO., INC Northvale, NJ, USA).

As shown in figure 2.4 (right side), the plasma ball forms just above the substrate when the aforementioned conditions are used and molybdenum substrate holders place the diamond substrates inside the growth chamber at a precise position. The design of the substrate holder is very important and a specific substrate holder was fabricated at IMO, its effect being translated into the possibility to reduce the MW power to sustain the plasma at certain gas pressures and to generate at the same time a plasma of small diameter just in the region of the concentrated electric field lines (Bogdan 2007).

## 2.2 Defect spectroscopy techniques

The discovery and identification of impurities or imperfections in CVD diamond is studied by specific techniques and this section describes the characterization techniques used to analyze defects. Sensitive methods of measuring the optical absorption of thin diamond films are important to clarify the quality of the investigated material. Such defect spectroscopy techniques allow the characterization of defect levels in the forbidden diamond gap and the associated electronic fine structure of the defect can be obtained.

### *2.2.1 Photocurrent measurements (PC)*

In order to determine the electronically-active defects and dopants in diamond photocurrent-based techniques are chosen due to their high sensitivity (ppb range) and universality. Opto-electronic details of the defect levels present in the forbidden band gap will be observed only when measurable charge carriers are produced. In this way defect-rich surfaces are ignored and features that are normally hidden, when normal absorption experiments are performed, will become visible. These advantages recommend photocurrent techniques as ideal tools for bulk analyses and are attractive to detect and classify the defects or to study their electronic structure. A short overview of the photocurrent theory used throughout this thesis will be given and, at the end of this section, the experimental set-up is presented in detail.

#### *2.2.1.1 Quasi-steady-state photocurrent phenomena*

The basic concepts in photoconductivity are described by the following terms: optical absorption by which free carriers are created, electrical transport by which free carriers contribute to the electrical conductivity of the material, and the capture of free carriers leading either to recombination or trapping (Bube 1992).

Optical absorption of light is described through the absorption coefficient $\alpha$. If the reflection or interference effects are neglected, the intensity of transmitted light I can be approximated by Beer's law:

$$I=I_0\exp(-\alpha d) \tag{2.1}$$

where $I_0$ is the incident light on a material of thickness d with an absorption constant $\alpha$.

The absorption of light by a material determines the raising of electrons to higher energy levels. The intrinsic optical absorption process corresponds to the raising of an electron from the valence band to the conduction band. These processes, also called interband transitions, are determined only by photons with at least the energy equal to the band gap value. The probability of such transitions to occur is very high since there are plenty of electrons in the valence band and many unoccupied states in the conduction band. Most of the absorption is limited near the surface.

Extrinsic optical absorption corresponds to the raising of an electron from the valence band to an imperfection or from an impurity level to the conduction band. These transitions are produced by photons with sub band gap energy and involve localized states inside the forbidden band. These localized states, formed by lattice imperfections, impurities and dopants, influence the electronic properties of the photoconductors and their investigation is one of the goals of the present study.

A basic type of photocurrent measurement is the quasi-steady-state photocurrent technique. This method measures the photoexcited current in function of the energy of the photons of the incident light. Due to the periodic illumination the term "quasi"-steady-state is used to describe the state of the investigated material and the present section describes the theory behind this method.

The total number of photoexcitated carriers, in the steady state, is given by:

$$N_{ph} = F\tau \qquad (2.2)$$

where F is the total generation rate of free electrons (per second) and τ is the lifetime of a free electron (Rose 1963).

The photocurrent is derived from the previous equation by dividing by the transit time and will be:

$$I = N_{ph}e/T_r = eF\tau/T_r \qquad (2.3)$$

where e is electron charge and $T_r$ is the transit time of a free electron from one electrode to the other. In the simplest case, neglecting the interference of light as is the case in a thin sample, the equation will become:

$$I \approx eN(1-R)[1-\exp(-\alpha d)]\eta\mu\tau F \qquad (2.4)$$

where N is the number of incident photons, $N(1-R)[1-\exp(-\alpha d)]$ is the number of absorbed photons in the sample, η is the quantum efficiency for generation of free electrons, μ is the free electron mobility, τ is their life time, and F is the applied electric field. A similar expression stands for holes.

The parameters μ and τ are characteristic parameters for the investigated material and their modification is derived from the particular set of defect states present in the forbidden zone of photoconductors (Rose 1963).

A free electron can be captured by defect levels and, depending on the position in the forbidden gap, traps or recombination centres are defined. The traps are states close to the conduction or valence band and are in "thermal contact" with the band. It means that a free electron captured into an unoccupied trap will be thermally reexcited into the conduction band (Rose 1963), participating again to the transport process. When capture of an electron happens at a recombination center (deeper states) it will be eliminated from the transport process.

In steady-state, e.g. with an external excitation (illumination in our case), the photoconductor is not in a thermal equilibrium state and we may use the Fermi distribution to describe the electron and hole densities in the bands, using the quasi-Fermi levels (Boer 1990). The quasi-Fermi level for electrons $E_{fn}$ is defined according to the definition:

$$n = N_C \exp(|E_{fn}-E_C|/kT) \qquad (2.5)$$

where $E_{fn}$-$E_C$ is the energetic distance between the conduction band and steady-state Fermi levels, k is the constant of Boltzman, T is the absolute temperature, $N_C$ describes the density of states at the bottom of conduction, and n is the density of electrons in the conduction band. For holes a similar expression is found.

#### 2.2.1.2 PhotoThermal Ionisation Spectroscopy (PTIS)

Photothermal conductivity is a very sensitive technique and the photothermal response of donors or acceptors is a result of a two-step process. First, the electrons (or holes) are excited from their ground state to a higher bound state by irradiation with light. Then, a subsequent excitation to the free conduction (or valence band) occurs by interaction with thermal phonons (Jongbloets 1979).
The line intensity I, which is proportional to the average number of ionizations, is defined for both donors and acceptors by:

$$I = A[1+(1/gg')\exp(\Delta E/kT)]^{-1} \qquad (2.6)$$

here, ΔE is the energy difference between the intermediate level and the band edge, g is the degeneracy of the excited level and g' is the degeneracy of the band. The factor A is proportional to the concentration of the impurity and the optical transition probability for the considered spectral line and to the concentration of the impurity.
The PTIS experimental set-up is similar to the PC-measurement which will be described in the following section and all the PTIS data are included when PC spectra are recorded.

#### 2.2.1.3 Experimental set-up

The present subsection describes the experimental set-up used for the classical photocurrent technique. In figure 2.5 a photograph and a schematic representation of the experimental configuration based on detecting a steady photocurrent are shown.
The light, from a xenon or a halogen lamp source, is modulated by a mechanical chopper prior to passing through a monochromator. The illumination of the sample with modulated monochromatic light of varying wavelengths will generate photocurrent. The signal will be amplified by a lock-in amplifier and thus detection of low photocurrent values is permitted. The spectral dependency of the light beam intensity is monitored by splitting the beam by a spectrally independent beamsplitter ($CaF_2$ beamsplitter in our case). A part of the beam is monitored by a pyrodetector, while the other part is focused on the sample.

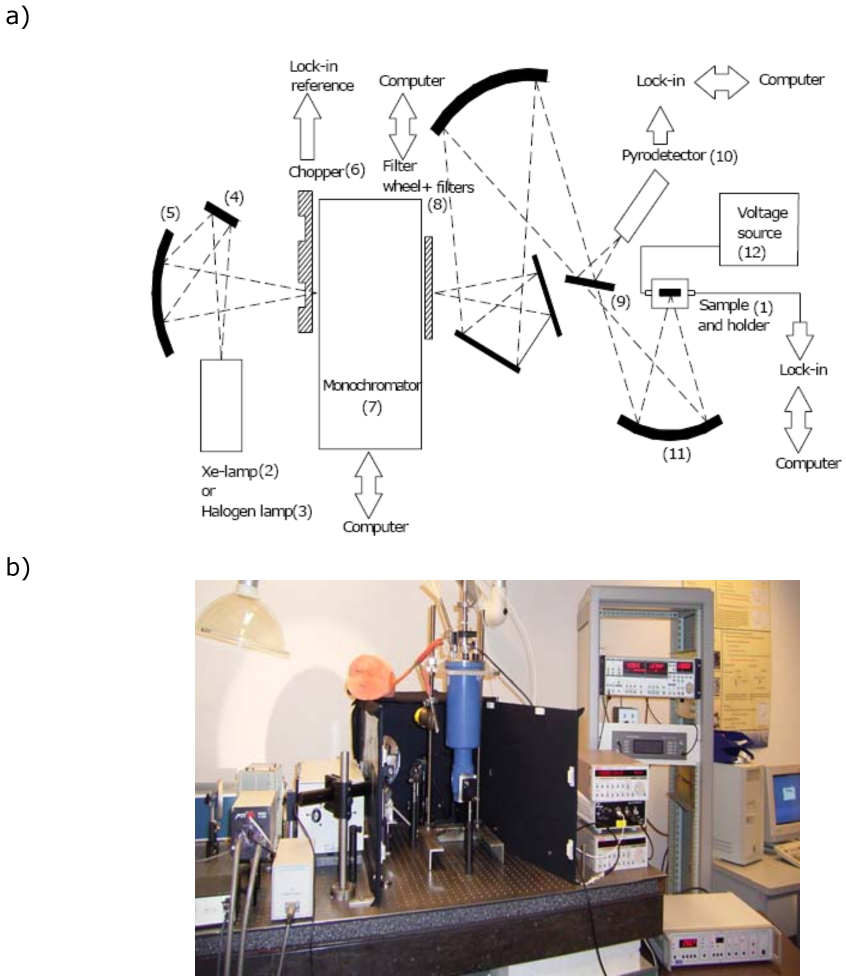

*Figure 2.5: a) Schematic representation of the PC set-up, b) Photograph of the photocurrent configuration at IMO.*

For all the spectra presented in this thesis the sample was placed inside an Oxford Instruments Optistat$^{DN}$ equipped with sapphire windows enabling photocurrent signals to be measured in a wide range of temperatures (from 77K up to room temperature). The necessary metal contacts used for signal capture are made out of aluminium (figure 2.6) and are connected to a Keithley 487

Voltage Source. All the PC experiments are automated and computer controlled, by means of a LabVIEW program.

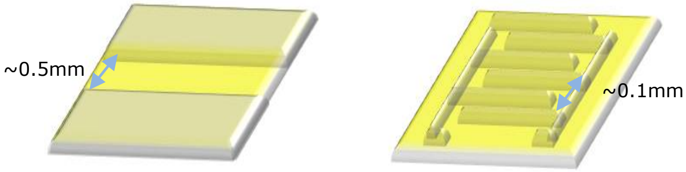

*Figure 2.6: Schematic representation of the two metallic contacts types used for PC measurements: (left) coplanar contacts - will cover the entire surface of the sample except for a portion in the centre of the specimen, (right) interdigital contacts - are situated in the centre of the sample with smaller space between them.*

### 2.2.2 Fourier-Transform Photocurrent Spectroscopy (FTPS)

This technique is based on Fourier-transform which is known for its high sensitivity in the IR spectral region. A traditional Fourier Transform InfraRed (FTIR) apparatus is used to measure the photocurrent signal. It is also a non-destructive method, as the PC techniques presented in section 2.2.1, but this method presents the following advantages when compared to the standard PC techniques: short acquisition time, high resolution and good signal to noise ratio obtained due to the high light throughput.

Using the FTPS method one can make qualitative investigations (investigate the electronic structure of the impurities) and/or make a quantitative analysis of the defects and dopants present in the investigated material. In 1997 (Tomm, Jaeger et al. 1997) the use of Fourier transform spectroscopy for measuring photocurrent in a higher energy range (near-IR and visible) was reported for the first time, and it is generally referred to as FTPC. A few years later, Vanecek et al. used Fourier-Transform Photocurrent Spectroscopy (FTPS) to develop a quantitative interpretation of the results (Vanecek and Poruba 2002). Nowadays, this method is commonly used in investigation of various materials. For this particular study it was used for analysing wide-band gap photosensitive materials, such as CVD doped diamonds, revealing thus interesting data about the defects and dopants in the material.

#### 2.2.2.1 The infrared spectrometer

Wavelenghts in the range between 750 nm and 1 mm, corresponding to photon energies of about 1.2 meV and 1.7 eV, represent the infrared (IR) region of the electromagnetic spectrum. Irradiation of materials with such energies may lead to absorption phenomena and, depending on the photon energy, different types of vibrational modes typically for covalently bonded solids may occur. The IR absorption process is a material-dependent process and for monoatomic solids, such as diamond, the technique is very sensitive to the presence of defects or impurities in the lattice.

One of the most used apparatuses for IR absorption analyses is the FTIR spectrometer. Fourier-transform spectroscopy is based on the possibility to calculate (evaluate) the spectrum by means of a two-beam interferometer and Fourier transformation.

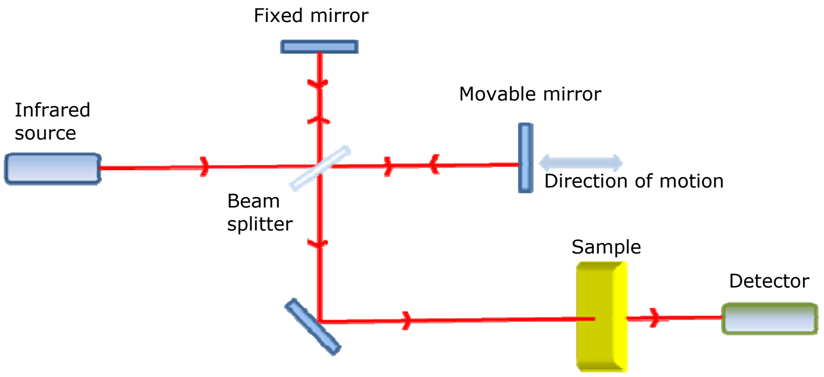

*Figure 2.7: Schematic view of Michelson interferometer.*

FTIR is a system using transmittance/reflectance of light and a Michelson interferometer is a key element for this. Its schematic drawing is presented in figure 2.7. The output beam from an infrared source is directed towards a beam splitter (a "half" silvered mirror). This optic element divides the incident light into two halfs: one is reflected toward the fixed mirror while the other 50% of the radiation is transmitted toward the movable mirrors. The mirrors are mutually perpendicular plane mirrors ("fully silvered"). The IR radiation from these mirrors is reflected to the beam splitter where they interfere, creating an output beam. Here, half of the total is transmitted back to the source and is discarded, while the other half is reflected to a new path toward the sample. Due to the interference, the intensity of the output beam depends on the optical path difference (retardation) between the two mirrors. The spectrum is calculated from the interferogram (interference effects measured as a function of the optical path difference between the fixed and movable mirrors of the Michelson interferometer) by computing its cosine Fourier transform.

#### 2.2.2.2 Experimental set-up

The first FTPS experiments ever realized on CVD diamonds were done for a continuous scan of the moving mirror using dc amplification systems (Kravets, Ogorodniks et al. 2002). For experiments presented in this thesis a Nicolet 8700 Fourier-transform infrared spectrometer was used, with an external light beam output and an external detector option. The contacts used for these investigations have the same specifications as in the case of standard photocurrent measurements presented earlier (coplanar or interdigital geometry electrodes). Diamond samples were placed as external detectors and their signal was normalized to the baseline FTIR signal. Measurements were done in a wide range of temperatures, but most of the times 77K is preferred. The samples were placed inside an Oxford Instruments Optistat$^{DN}$ equipped with sapphire windows. A pyroelectric detector was used as a reference detector and the signal from the sample is normalized by the signal of this spectrally independent detector. The rest of the electronic circuit used for acquisition of the spectra is similar as described in the literature (Vanecek, Kravets et al. 2003; Kravets, Vanecek et al. 2004).

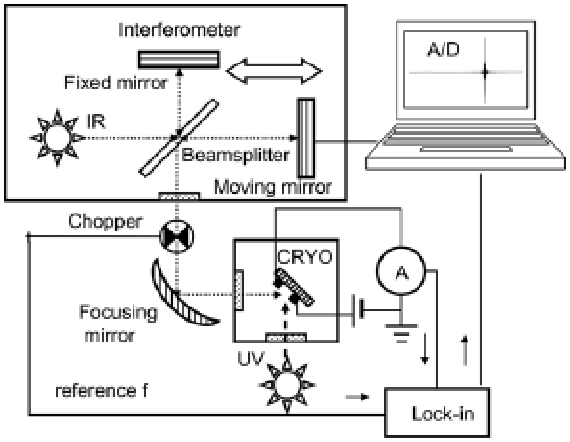

*Figure 2.8: Sketch of an experimental set-up for AMFTPS: the interferometer with IR source, beam splitter, fixed and moving mirrors, chopper, sample and cryostat, stable voltage source, current preamplifier (A), lock-in amplifier and A/D convertor. The computer records the AC photocurrent amplitude as a function of the moving retardation.*

Recently, highly sensitive IR photocurrent spectroscopy called AMFTPS was developed, using the FTIR setup for step-scan amplitude modulation (AM) experiments (Remes, Nesladek et al. 2007). In this case the IR light is modulated periodically by mechanical chopping and an experimental set-up is shown in figure 2.8.

The signal from the sample is first fed externally to a lock-in amplifier referenced to the same modulation frequency. The analog output from the lock-in amplifier is connected to the external analog input of the FTIR apparatus. Prior the interferogram scan, the lock-in output is off-set to zero. The maximized in phase signal is then digitized, recorded as an interferogram and Fourier transformed to obtain the photocurrent spectrum. The amplitude modulation allows the AC frequency to be tuned in a relatively wide range of frequencies, between 10 and $10^4$Hz. This contrast with continuous scan, which is restricted to lower ranges of frequencies (Remes, Nesladek et al. 2007). AMFTPS completely removes the frequency response normalization of the spectra and allows measuring practically all diamond samples even at very low (fA) photocurrent levels of the total IR photocurrent.

## 2.3 Microscopic surface imaging techniques

The diamond growth mechanism when the CVD process is used implies absorption of hydrocarbon species, abstraction of hydrogen atoms in order to create new growth sites and, when doping is wanted, introducing a specific impurity in the diamond lattice. All the mentioned procedures are complicated and obtaining a defect-free diamond surface is difficult due to the fact that during the growth process the properties of diamond (i.e. mechanical properties or lattice parameter) are altered. The evaluation of the CVD diamond thin film morphology used for this thesis is done by standard techniques for surface analysis: Optical Microscope (OM), Scanning Electron Microscopy (SEM) and Atomic Force Microscopy (AFM). Details of the structure of the diamond surface can be studied by Differential Interference Contrast Microscopey (DICM) and SEM, while AFM is optimal for investigations of defects on the atomic to the micron level.

### 2.3.1 Optical Microscopy: Differential Interference Contrast Microscopy (DICM)

Optical microscopy is a simple, non-destructive and powerful technique used to gather information about surface morphology of materials. A comparison of the images obtained before and after the growth of a CVD layer can be useful for the film growth history. In this thesis special attention was directed towards specific defects observed at the diamond surface due to the incorporation of the impurities.

DIC (differential interference contrast) investigations can be done either in transmitted or reflected light, depending if the information we want to gather refers to the structure or to the material surface. DICM, with reflected light, is a sophisticated and highly efficient technique and allows the identification of small differences in height (such as macro steps, round hillocks or etch pits on the diamond surface in the plane of focus), while SEM is most suited for 3D features (shape of crystallites in the layer). DIC is also known as Nomarski Interference Contrast (NIC). For this thesis the reflection DICM was used for surface investigations and therefore the focus of this sub-section is the working principle of this technique (figure 2.9).

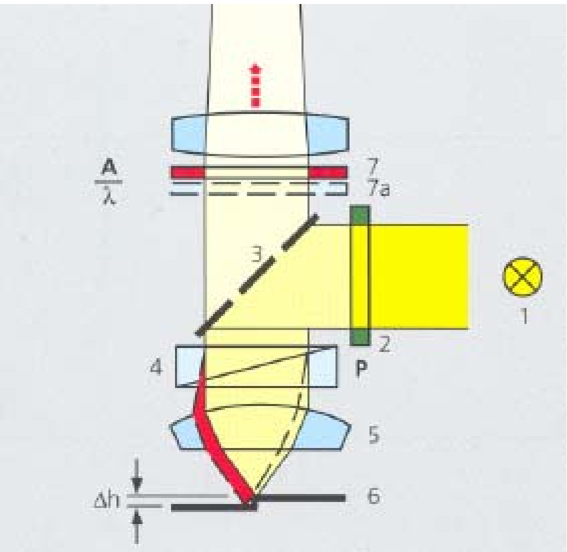

*Figure 2.9: Schematic view of a DICM apparatus (using reflected light): 1-light source, 2-polarizer, 3-mirror with oval holes, 4-birefringent prism, 5-objective, 6-sample, 7-analyzer, 7a-lambda plate (used to convert contrast into colours).*

DICM in reflected light is a method that allows visualisation of minute elevation differences in surfaces. A birefringent prism (4) is used, which splits the polarized light beam into two partial beams on its way to the sample (6). These partial beams hit the sample with lateral displacement from each other. If the surface is completely flat nothing will happen. However, if there is a small step between the two partial beams, one of the two beams must travel a path difference which is 2Δh longer and is assigned this path difference. Once the partial beams have returned, via the DIC prism (4) and the analyzer (7), they can interfere with each other in the intermediate image. The path difference assigned on the surface then changes into grey values which can be seen by the eye: steps become visible as a relief. As an auxiliary object, the plate (7a) changes grey values into colours again (Axiovert). At IMO, the microscope used for investigating the sample surfaces is an Axiovert 40 MAT microscope equipped with DIC as well as polarization or darkfield contrasting methods.

### 2.3.2 Scanning Electron Microscopy (SEM)

Scanning electron microscopes are scientific instruments used to image sample surfaces on a very fine scale by scanning it with an energetic electron beam. The SEMs are versatile apparatuses and can yield information regarding topography, external morphology (texture), chemical composition or crystallographic structure, and orientation of the materials making up the sample. In this sub-section the working principle of the SEM used for imaging surfaces and the Electron BackScatter Diffraction (EBSD) method, used for crystallographic structure and orientation investigations, are presented in detail.

#### 2.3.2.1 Surface imaging

Basically, in an SEM, a small sized beam of electrons (in the range of 10nm) scans the sample surface, while the electron-sample interactions are analysed by several detectors, revealing information about the sample topography, morphology, etc. The electrons are generated by a tungsten filament or a field emission gun. Once generated, the electrons are focused onto the sample by a set of electromagnetic lenses and accelerated to an energy which is in the range of 1-30keV. Their penetration depth is dependent on the energy of the impinging electrons. The information depth is in the order of several microns for diamond when 20kV beams are used.

SEMs are routinely used to generate low to high-resolution images and magnifications ranging between 30 and 1 milion times. This instrument is widely used to precisely image features less than 10nm in size.

Electron-sample interactions are quite diverse (see figure 2.10) and a multitude of signals are emitted. This can be explained by the fact that in a sample the primary electrons experience elastic as well as inelastic scattering processes. The kinetic energy of the primary electron will be mostly transferred into heat, whereas a part of the energy can leave the sample as X-rays, CL, light, secondary electrons (SE) and backscattered electrons (BSE).

The images used in this thesis are both SE and BSE, and therefore both of them will be briefly explained. The SE have an energy loss less than 50eV and they result from inelastic scattering of the electron beam with valence electron of the target atoms. They are generated from different regions underneath the sample surface, but only those electrons very close to the surface (in the range of nm) can actually leave the sample and give a topographical contrast. SE images are mostly used to reveal the surface morphology of the specimen and SE image contrast is usually generated by differences in SE emission efficiency with topography.

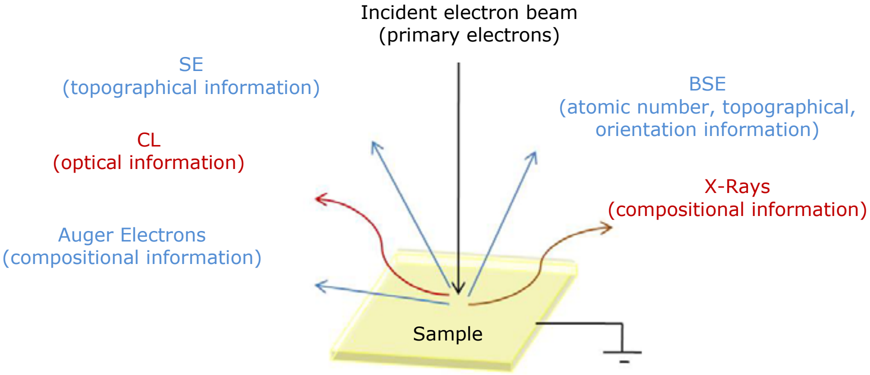

*Figure 2.10: Electron – sample interactions and different emitted signals in a scanning electron microscope.*

BSE are the result of an elastic scattering process, a primary electron interacts with the nuclei of the target atoms and the elastically scattered electrons might proceed in a different direction compared with the primary electrons. However, their energies remain the same (in the order of several keV). The deviation of the beam electrons from their original direction of travel will lead to a "diffusion" process of the electrons through the analyzed material. The backscatter electron yield is a function of the elemental atomic number of the scattering atom (Z-contrast), while the angular distribution of the backscatter electrons is a function of the angle between the impinging electron beam and the surface.

If the tilt of the angle between the impinging electron beam and the specimen surface normal is increased, the interaction volume becomes smaller. Due to this particularity, the backscattered electrons also have a strong dependence on the surface topography.

As diffraction depends on the crystallography of the sample, the analysis of BSE can yield a crystallographic contrast. Orientation contrast (OC) or channelling contrast defines the contrast which is due to a different crystallographic orientation. The wavelength of the impinging electrons and the angle of incidence play an important role in formations of the OC images. This is due to the fact that those factors determine the extent to which electrons can penetrate into (or exit) a material. Their contribution to the formation of OC images is shown in figure 2.11. The images represent the same region of a polished diamond sample, with different accelerating voltages or specimen tilt conditions. Because the sample is a diamond specimen, the Z contrast is not present. Also, due to the fact that the sample surface was polished, the influence of topography on the image is excluded. Thus, the only information observed in the figures refers to the orientation contrast.

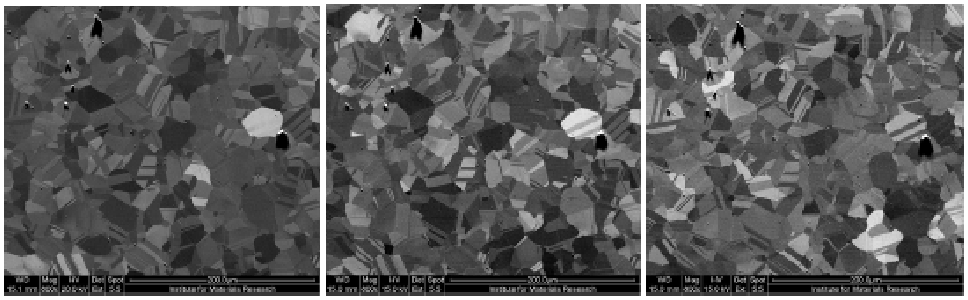

a) *20kV, 70°* b) *15kV, 70°* c) *15kV, 68°*

*Figure 2.11: Comparison between three OC images of a certain region on a diamond sample, taken with different accelerating voltages and specimen tilt angles (Vanstreels 2007).*

From the aforementioned results we can conclude that the images show that the intensity of the forward BSE changes with both the accelerating voltage and tilt angle, pointing out that the obtained OC is non-quantitative, as the intensity of the forward BSE can not be related to the orientation (Vanstreels 2007).
A SEM type Quanta 200-FEG manufactured by FEI is available at IMO and this apparatus was used for acquiring surface or crystallographic information of the samples presented in this thesis. When the investigated samples are conductive a detectable signal by the SEM detectors is generated. For most instruments vacuum is a must, thus samples likely to outgas at high vacuum conditions are unsuitable for SEM investigations. However, "low vacuum" or "environmental" SEM exists nowadays. When insulating samples are used, an electrically conductive coating must be applied (commonly carbon, gold or some other metal or alloy), unless low vacuum mode is used. The samples investigated in this thesis (semiconducting diamond samples with diameters less than ~3mm) fulfil all the aforementioned conditions necessary for SEM investigations.

#### *2.3.2.2 Electron BackScatter Diffraction (EBSD)*

Electron BackScatter Diffraction is a microstructural-crystallographic technique which allows crystallographic information to be obtained from a sample when investigating it in a scanning electron microscope (SEM). From the crystallographic data of the analyzed materials the texture or preferred orientation of any crystalline or polycrystalline sample can be obtained. EBSD is widely used to index and identify the crystal systems and for crystal orientation mapping, defect studies, phase identification, grain boundary or morphology studies. Until the invention of the SEM in the ‘60s, these types of analysis were carried out by transmission electron microscopy (TEM) or by X-ray diffraction (XRD) (Randle 1992). However due to the rather tedious and difficult sample preparation (for TEM) or the limited lateral resolution (the case for XRD) EBSD is preferred nowadays.

The working principle of the technique is the following: accelerated electrons of the primary electron beam (from a SEM apparatus) touch the sample surface and the interaction mainly behaves like a point source that scatters electrons incoherently (with little loss of energy but loss of phase coherence) in all directions. Electrons can be diffracted by atomic layers in crystalline materials and these diffracted electrons are detected when they impinge on a phosphorous screen and generate visible lines (Prior, Boyle et al. 1999). Those lines are called Kikuchi bands or electron backscatter patterns (EBSP’s). Such patterns are effectively projections of the geometry of the lattice planes in the crystal giving direct information about crystalline structure and crystallographic orientation of the grain from which they originate.

The sample is placed within a SEM apparatus such that a small angle, typically 20°, is made between the incident electron beam and the specimen surface, as presented in figure 2.12. The detector is a camera equipped with a phosphorous screen and is mounted as close as possible to the sample. The pattern of Kikuchi lines on the phosphorous screen is electronically digitized and processed to recognize the individual Kikuchi lines. These data are then used to identify the phase, to index the pattern and to determine the orientation of the crystal from which the pattern was generated.

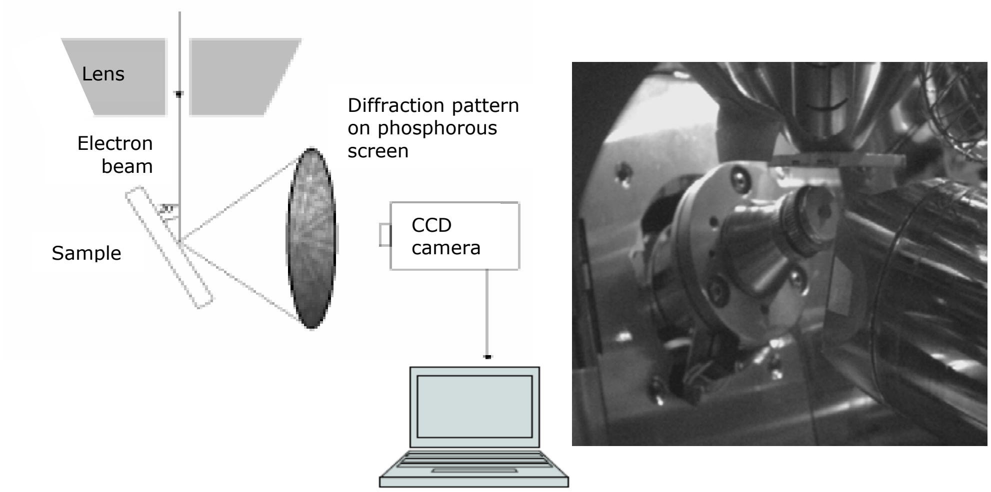

*Figure 2.12: (left) Schematic view of an EBSD apparatus and (right) the sample-detector configuration of the SEM system type Quanta 200-FEG present at IMO. The apparatus is equipped with an EBSD system from HKL Technology and a Nordlys II camera.*

Modern EBSD systems can determine the orientation of individual measurement points with an accuracy better than 1° (Demirel, El-Dasher et al. 2000). The graphical representation of the EBSD results, called mapping, is a very useful and intuitive method and depending on the specific orientation of each data point, a colour scheme can be attributed, thus interpretation of the obtained results becomes easier. A typical example is shown in figure 2.13, where figure 2.13a presents the orientation map for a polycrystalline diamond sample, with colours corresponding to the crystallographic orientation of each point as defined by the unit triangle colouring scheme (see figure 2.13b).

The representation of textures by their proximity to one or more ideal orientation is possible. This method allows to identify and describe the textures shown by the samples by their representation of proximity to one or more perfect orientations (commonly {100}, {111} and {110} planes are used for FCC materials like diamond). These representations are called pole figures. A pole figure is the intersection point of the surface normal of a certain lattice plane with a reference sphere. The stereographic projection of all the poles on the upper sphere for a given family of planes onto the equatorial plane yields the corresponding pole figure. An inverse pole figure is a representation which describes the material textures (i.e. rotational symmetry with only one preferred axis).

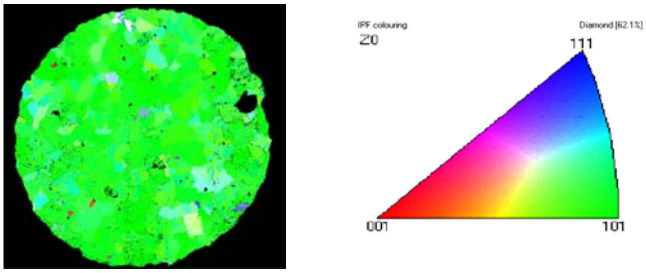

a) b)

*Figure 2.13: Top view EBSD mapping of a polycrystalline diamond sample: a) Inverse pole figure mapping, showing the crystallographic orientation with respect to the film normal direction (Z-direction) and b) unit triangle colouring scheme.*

EBSDs systems are the fastest and most reliable method to acquire data for crystalline structure and orientation in a solid crystalline phase, with a rather high lateral resolution. Most systems include sophisticated software to generate and modify graphical displays of the results. A larger area can be examined with EBSD (when compared with TEM) (Randle 1992) and the spatial resolution of this method is a function of step size, material, accelerating voltage, etc. For our measurements typically areas of 800x800μm$^2$ are scanned, with a step size of 1μm. One of the few drawbacks is that EBSP's are generated in the very shallow depths within the sample (10-50nm), thus being a surface sensitive technique and not giving volume information.

### 2.3.3 Scanning Probe Microscopy

In the most general sense, scanning probe microscopes reveal information about the surface properties of materials by scanning or "rastering" the surface with a small probe. Information about the interaction of the probe with the surface is transmitted, via an Electronic Interface Unit (EIU), to a computer where an image of the surface is generated. The first instrument of this type, the scanning tunneling microscope or STM, was invented in the early 1980's. In the STM, a sharp metal tip is brought to within a few angstroms of a conducting or semiconducting surface. If a voltage is applied to the sample, a current which varies exponentially with distance, flows between the tip and surface. This is called the tunnelling current. The surface topography is revealed by scanning the tip over the surface in parallel lines while keeping the current constant. The STM is most commonly used on conducting surfaces.

#### 2.3.3.1 Atomic Force Microscopy (AFM)

The Atomic Force Microscope (AFM) is one type of this new family of instruments called "scanning probe microscopes" and is a method of measuring surface topography on a scale from angstroms to 100 microns. The AFM was developed a few years after the STM. Unlike the STM, the surface studied by the AFM does not need to be conductive. The surface is scanned by a probe or a tip with radius of 20nm, which may touch the surface or be a few angstroms away. The contact between the probe and sample is used to generate an image of the surface topography. The probe can vibrate at its resonant frequency (wavemode) to make intermittent contact with the sample. This method has the advantage that lateral forces are almost totally eliminated. The forces generated in an AFM are several orders of magnitude lower than in an earlier type of surface profiler called a "profilometer", although much of the patent history in the field dates back to profilometers. The contact force between tip and surface is much smaller in an AFM, in the nanonewton range compared to tens of micronewtons for the profilometer. The net result is that whereas "profilometry" often damages the surface because of the large forces and contact surface area, AFM reveals the surface topography with much higher spatial resolution and at the same time leaves the surface undamaged.

An AFM apparatus is made up of the following components: a small tip or probe attached to a scanner supported by a stage, an electronic interface unit (EIU) and a computer (see figure 2.14). As the probe is "scanned" over the surface, the EIU maintains a condition of constant force between surface and probe by adjusting the height (z dimension) of the probe support. The movement of the tip over the surface is controlled by a piezoelectric ceramic, which can move in the x, y and z directions in response to applied voltages. Movement of the piezo in the x and y directions scan the sample. A feedback circuit controls voltage applied to the z piezo so that the bending of the probe cantilever is held constant as the tip is scanned across the surface.

In the AFM, the tip is attached to a spring in the form of a cantilever. As the tip moves over the surface, the cantilever bends back and forth in the z direction. A laser beam is directed onto the cantilever and as the cantilever bends, the movement of the reflected beam is detected by a photo diode. A feedback circuit integrates this signal and applies a feedback voltage to the z piezo to exactly balance the cantilever bending, since the probe force is proportional to the cantilever bending. The image of the surface is built up as a series of scan lines, each displaced in the y direction from the previous one.

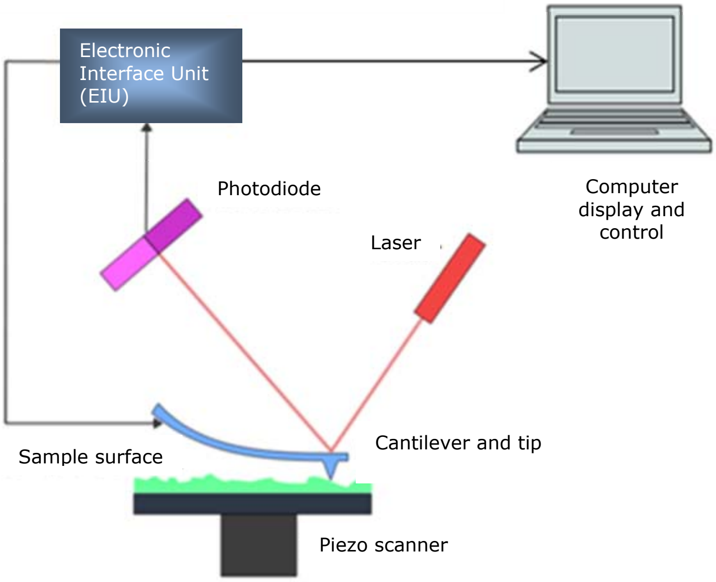

*Figure 2.14: Schematic diagram of an AFM apparatus.*

Many AFM modes have been developed for special purposes while the technique is becoming more mature. Most of the times three different operation modes are used: contact mode, non-contact mode and tapping mode. In contact mode the tip scans the sample in close contact and the force on the tip is repulsive. A new era in imaging was opened when a system operating in non-contact mode was developed, used in situations when tip contact might alter the sample in subtle ways. In this case the attractive forces (Van der Waals) acting between the tip and the sample surface are detected and topographic images are constructed by scanning the tip above the surface (50 – 150Å above the surface). Tapping mode is a key operating mode that solves the problems encountered when contact or non-contact modes are used. Problems such as damaging the surface, trapping the probes in the fluid layer at the sample surface or other problems associated with friction, adhesion or electrostatic forces can be avoided. This potent technique allows high resolution topographic imaging of sample surfaces by alternately placing the tip in contact with the surface to provide high resolution and then lifting the tip off the surface to avoid dragging the tip across the surface. During scanning, the vertically oscillating tip alternatively touching the surface and lifting off, generally at a frequency of 50,000 to 500,000 cycles per second, is observed. As the oscillating begins to intermittently contact the surface, the cantilever oscillation is necessarily reduced due to energy loss caused by the tip contacting the surface. The reduction in oscillation is used to identify and measure surface features.

A Veeco multimode AFM with NanoScope IIIa controller electronics and equipped with scanning probes made out of $n^+$-silicon material (resonance frequency between 204-497kHz) was used to perform tapping mode investigations of the n-type diamonds presented in this thesis.

## 2.4 Defect observation and characterization techniques

Secondary ion mass spectrometry (SIMS) and cathodoluminescence (CL) spectroscopy are two different techniques that can be combined to quantify the amount of impurities in diamond and their working principle is the purpose of this section.

### *2.4.1 Cathodoluminescence (CL)*

When an electron and a hole are excited to a higher energy state there are three fundamental processes by which the energy can be given up when the carriers returns to its thermal equilibrium state. The excess of energy can be given up by: emitting photons (is a radiative recombination phenomenon and describes the luminescence process), emitting phonons either simultaneously or sequentially (this is a non-radiative process) or raising free carriers (electrons or holes) to higher energy states in their bands (another non-radiative process called Auger recombination) (Bube 1992). This section is presenting the cathodoluminescence technique, which is part of the luminescence processes. This category of methods refers to any process in which energy is emitted from a material at a different wavelength from that at which it is absorbed. Depending on the way the charge carriers are excited, the following luminescence techniques exists:

- Photoluminescence (optical excitation)
- Cathodoluminescence (electron-beam excitation)
- Electroluminescence (excitation by carrier injection)
- α, β, γ or X-rays techniques (excitation by high energy nuclear radiation).

The mechanisms leading to the emission of light in a semiconductor are similar for different forms of excitation energy as soon the excitation is higher than the bandgap energy. The technique known as photoluminescence (PL) is the most commonly used spectroscopic method of excitation and by means of optical excitation (absorption of photons) electron-hole pairs are produced. Another radiatively recombination technique is cathodoluminescence (CL), in which irradiation of the sample with electron beams can create electron-hole pairs.

The luminescence from a light-emitting diode is an example of electroluminescence (EL) in which electrons and holes are electrically injected. Luminescence spectroscopies are sensitive tools for dopant quantification in semiconductors and the main luminescence technique used in this thesis is CL.

#### 2.4.1.1 Theory – CL in diamond

As it is presented in figure 2.10, interaction of an electron beam with a semiconductor leads to a variety of processes and electronic excitations that produce useful signals for material characterization. Backscattered electrons, secondary electrons, X-rays and photons emitted in the ultraviolet, visible and infrared spectral ranges are a few examples of signals. Cathodoluminescence is the emission of light as the result of electron bombardment of a specimen and due to the interactions of electrons with the material a large number of electron-hole pairs are generated. The subsequent recombination of electrons and holes produces luminescence. The working principle of CL is schematically represented in figure 2.15.

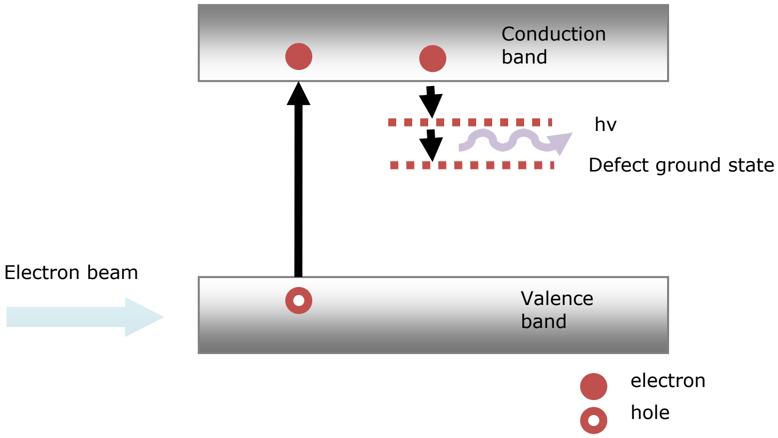

*Figure 2.15: Schematic working principle of a CL phenomenon. The generation of electron-hole pairs due to the incoming electron beam and the recombination process at defect centres with luminescence generation.*

CL is a non-contact and non-destructive method with high spatial resolution used for microcharacterization of semiconductors and shallow impurity studies. The electron beam is typically produced in a SEM apparatus and attachment of cathodoluminescence microscopy can be found for electron microscopes.

Another advantage of CL is the ability to obtain detailed depth-resolved information by varying the electron-beam energy. However, as a low energy electron beam (tens of kV) deposits its energy in a thin surface layer of a few µm, CL originates from the top layers of specimen's surface.

Generally, CL emission spectra can be divided in: *intrinsic*, fundamental or band-edge emission and *extrinsic*, activated or characteristic CL. The intrinsic spectrum is due to the recombination of electrons and holes across the fundamental energy gap, so it is an "intrinsic" property of the host lattice. This edge emission band (arising from conduction-band to valence-band transitions) is produced by the inverse of the mechanism responsible for the fundamental absorption edge. The extrinsic part refers to the emissions related to the presence of impurities. CL emission bands in these cases are "activated" by impurity atoms or other defects and the emission features are "characteristic" of the particular activator. Such radiations can be made much more intense than intrinsic CL at ambient temperatures. The analysis of such emissions is of great importance for semiconductors and in semiconductors such as doped diamond the P or B dopants can be studied.

The first luminescence studies regarding diamond made use of X-rays or ultraviolet radiation to excite the luminescence (Matthews 1958; Dean and Male 1964). The pioneering work in diamond luminescence was developed at King's College London in the late '50 and a modified Siemens electron microscope was used for the investigations (Ralph 1960). Due to its advantages, this technique is widely used today and reviews of its applications are available (Yacobi and Holt 1986). In this thesis the CL was used to investigate the incorporation of phosphorous in diamond layers and due to the progress reported in this direction nowadays it is easier to identify the defect structure from CL analysis (Sternschulte, Horseling et al. 1996; Tanabe, Nakazawa et al. 2001; Sauer 2003). A recent study investigates the optical properties of phosphorous-doped diamond with the final purpose of quantifying the P concentration (Barjon, Desfonds et al. 2007), pointing out the capability of development regarding the CL technique, a development which was desirable for many years. Details about the experimental set-ups used to acquire CL spectra of phosphorous-doped diamonds are presented in the following sub-section.

#### *2.4.1.2 Experimental set-up*

The essential requirements of CL detection system designs are a high efficiency of light transmission and detection. For this study several CL systems were used depending if the incorporation of P was studied or a quantification mode of working for the CL set-up was needed. All cathodoluminescence spectra were acquired by the courtesy of our collaborators.

Cathodoluminescence mapping and spectra of n-type diamond thin films were performed at Groupe d'Etude de la Matière Condensée (GEMaC), University

Versailles St. Quentin – CNRS, Meudon, France. Cathodoluminescence spectroscopy and mapping at 102K made use of a Horiba Jobin Yvon SA system installed on a JEOL840 SEM. The P-doped diamond films were excited with a 20keV focussed electron beam (corresponding to a penetration depth of ~ 2.8µm).In GEMaC, the single CL spectra were typically measured with a ~10nA electron beam current whereas it was increased to ~100-200nA to provide CL spectral mappings in a reasonable acquisition time. The layers were coated with a semi-transparent gold layer (~ 5nm) in order to evacuate electric charges. The CL emission was collected by a parabolic mirror and injected with metal optics into a monocromator equipped with UV enhanced-silicon CCD camera and a 600 grooves/mm diffraction grating. The CL maps were obtained by acquiring the CL spectra of 32x32 or 64x64 points inside a 380x380µm$^2$ window or a 60x45µm$^2$ window, respectively.

A first confirmation of P incorporation in the diamond layers was done by near-band edge CL spectroscopy performed at the Friedrich-Alexander University, Erlangen-Nurnberg, Germany or at the Optical Sensor Group, Sensor Materials Centre, National Institute for Materials Science, Tsukuba, Japan. In both cases similar SEM apparatuses as the one described above were used. Their specific details will be given when the results are presented.

### 2.4.2 Secondary Ion Mass Spectrometry (SIMS)

The technique of Secondary Ion Mass Spectroscopy (SIMS) is the most sensitive of all commonly-employed surface or bulk analytical techniques. This is because of the inherent sensitivity associated with mass spectrometric-based techniques. There are a number of different variants of the technique:

- Static SIMS – used for sub-monolayer elemental analysis;
- Dynamic SIMS – used for obtaining compositional information as a function of depth below the surface;
- Imaging SIMS – used for spatially-resolved elemental analysis.

All of these variations on the technique are based on the same basic physical process. In SIMS the sample surface is subjected to bombardment by a highly energetic ion beam which leads to the ejection (or *sputtering*) of both neutral and charged (+/-) species from the surface, as shown in figure 2.16. The ejected species may be monoatomic or polyatomic and can include atoms, clusters of atoms and molecular fragments. The secondary ions in the sputtered flux are accelerated into a mass spectrometer and collected by an electron multiplier, Faraday cup or chaneltron. The mass separation makes it possible to extract compositional information of the irradiated sample. In traditional SIMS it is only the positive ions that are mass analyzed. This is primarily for practical ease but it does lead to problems with quantifying the compositional data since the positive ions are but a small, non-representative fraction of the total sputtered species. It should be further noted that the displaced ions have to be energy filtered before they are mass analyzed (i.e. only ions with kinetic energies within a limited range are mass analysed).

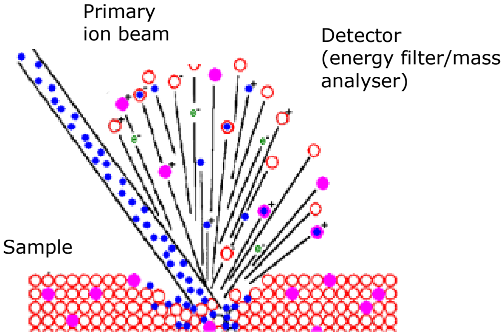

*Figure 2.16: Schematic presentation of a SIMS sputter experiment (SIMS 2008). A specimen is bombarded by a primary ion beam and ejection of atoms or clusters is possible.*

Today, SIMS is widely used for analysis of trace elements in solid materials, especially semiconductors and thin films. The SIMS ion source is one of few to produce ions from solid samples without prior vaporization. The diameter of primary ion beam can be focused less than 1µm in diameter and thus the control where the beam strikes the surface provides microanalysis, i.e. the measurement of the lateral distribution of elements on a microscopic scale.

The continuous analysis while the sample surface is slowly sputtered away produces information as a function of depth, called depth profile. When the sputtering rate is extremely slow the operating mode is called static SIMS, in contrast with dynamic SIMS used for depth profiles. For the shallow sputtering regime the damage is minimal (the escape depth of secondary ions is limited to the first atomic layer) and the ion fragmentation patterns contain information useful for identifying molecular species, while dynamic SIMS yields quantitative information. The following explanations refer only to the dynamic SIMS because this was the technique used to quantify the phosphorous in our CVD diamond layers.

Primary beam species useful for SIMS include $Cs^+$, $O^{2+}$, O, $Ar^+$ and $Ga^+$ at energies between 1 and 30keV. Primary ions are implanted and mix with sample atoms to depths of 1 to 10nm. Sputter rates in typical SIMS vary between 0.5 and 5nm/s and depend on the intensity of the ions, sample material and crystal orientation. The sputter yield is the ratio of number of atoms sputtered to the number of impinging primary ions and fall in the range from 5 up to 15.

Quantitative analysis by SIMS uses relative sensitivity factors defined according to the following equation (SIMS 2008):

$$I_R/C_R = RSF_E \times I_E/C_E \qquad (2.7)$$

where $RSF_E$ is the relative sensitivity factor for element E, $I_E$ = secondary ion intensity for element E, $I_R$ = secondary ion intensity for reference element R, $C_E$ and $C_R$ are the concentrations for E and R, respectively. The RFS is a function of the element of interest and the sample matrix.

The SIMS detection limits for most trace elements are between $1x10^{12}$ and $\sim 1x10^{18}$ atoms/$cm^3$. This limitation comes from factors such as ionization efficiency (known as ion yield and defining the fraction of sputtered atoms that become ionizied), dark current or presence of atoms found in the systems (either sputtered from mass spectrometer parts back onto the sample, either oxygen atoms present as residual gas in vacuum systems).

SIMS was discovered in 1910 by British physicist J. J. Thomson. He observed a release of positive ions and neutral atoms from a solid surface induced by ion bombardment. Improved vacuum pump technology in the 1940s enabled the first prototype experiments on SIMS by Herzog and Viehböck in 1949, at the University of Vienna, Austria. Then in the early 1960s two SIMS instruments were developed independently, one of them constructed under a NASA contract, and the other in a project initiated at University of the Orsay, France. Since then, the use of SIMS for materials characterization has grown steadily and the largest "costumers" come from the electronic materials industry (semiconductors, optoelectronic devices, etc).

SIMS has shown its applicability in a lot of different research fields: geology, biology, surface science, chemistry, physics and so on. Its good sensitivity, high dynamic range, good depth resolution as well as the fact that opposite to other depth profiling techniques (Rutherford Backscatter Spectroscopy, Medium Energy Ion Scattering, Auger Electron Spectroscopy) SIMS can detect all elements, made SIMS popular. This technique is used especially in microelectronics for investigating the distribution of dopants and contaminants in semiconductor devices. In this study SIMS is used to quantify the P in the diamond layers and evaluate the incorporation process.

Typical SIMS instruments use either a duoplasmatron or a surface ionization primary ion source (or both). The SIMS apparatus used for P quantification is located at Groupe d'Etude de la Matière Condensée (GEMaC), University Versailles St. Quentin – CNRS, Meudon, France. Secondary Ion Mass Spectrometry (SIMS) using a Cameca IMS 4f equipment was used to measure the depth distribution of phosphorus, boron, nitrogen and hydrogen atoms into the diamond films with Cs+ primary ions accelerated at 10keV. The concentration of phosphorus was quantified using implanted standards, with an accuracy estimated at ±10% under optimum conditions.

## 2.5 Electrical properties of n-type diamond: Hall measurements

Resistivity, dielectric constant or carrier mobility are a few parameters that characterize the electrical and semiconductor properties of diamond. The Hall effect measurement is the most convincing method to perform investigations of the aforementioned properties of diamond and therefore this section starts with a general presentation of the theory behind this technique. The set-up used to perform Hall measurements for all our P-doped diamond thin films is presented in the last part of the section.

### *2.5.1 Theory - van der Pauw method*

In order to determine both the mobility $\mu$ and the sheet density of the charged carriers $n_s$, a combination of a resistivity measurement and a Hall measurement is needed. The van der Pauw technique is widely used in the semiconductor industry to determine the resistivity of uniform samples and generally this method is based on the procedure developed at the National Institute of Standards and Technology (NIST 2007). As originally devised by van der Pauw (van der Pauw 1958_a; van der Pauw 1958_b), for these kind of measurements an arbitrarily shaped thin-plate sample containing four very small ohmic contacts placed on the periphery (preferably in the corners) of the plate is used. The sample should be simply connected, i.e. no holes or nonconducting islands or inclusions. A schematic of a rectangular van der Pauw configuration is shown in figure 2.17.

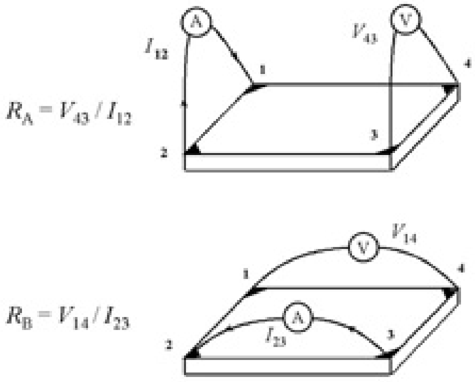

*Figure 2.17: Schematic representation of resistance measurement using the van der Pauw configuration (NIST 2007).*

Van der Pauw demonstrated that there are actually two characteristic resistances $R_A$ and $R_B$ associated with the corresponding terminals shown in figure 2.17. $R_A$ and $R_B$ are related to the sheet resistance $R_S$ through the van der Pauw equation:

$$\exp(-\pi R_A/R_S) + \exp(-\pi R_B/R_S) = 1 \qquad (2.8)$$

which can be solved numerically for $R_S$.
The bulk electrical resistivity $\rho$ can be calculated using the following mathematical relation:

$$\rho = R_S d \qquad (2.9)$$

where d is the thickness of the investigated sample.
To obtain the two characteristic resistances, a dc current $I$ injected in contact 1 and extracted out of contact 2. The voltage $V_{43}$ from contact 4 to contact 3 is measured as shown in figure 2.18. Next, the current $I$ into contact 2 and out of contact 3 is applied while measuring the voltage $V_{14}$ from contact 1 to contact 4. $R_A$ and $R_B$ are calculated by means of the following expressions:

$$R_A = V_{43}/I_{12} \text{ and } R_B = V_{14}/I_{23} \qquad (2.10)$$

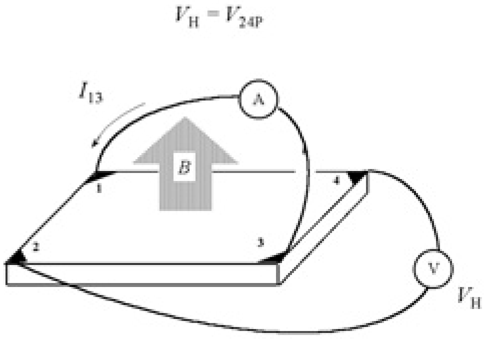

*Figure 2.18: Schematic representation of a Hall measurement using the van der Pauw configuration (NIST 2007).*

The objective of the Hall measurement in the van der Pauw technique is to determine the sheet carrier density $n_s$ by measuring the Hall voltage $V_H$. The Hall voltage measurement consists of a series of voltage measurements with a constant current $I$ and a constant magnetic field $B$ applied perpendicular to the plane of the sample. Conveniently, the same sample shown in figure 2.18, can also be used for the Hall measurement. To measure the Hall voltage $V_H$, a current $I$ is forced through the opposing pair of contacts 1 and 3 and the Hall voltage $V_H$ (= $V_{24}$) is measured across the remaining pair of contacts 2 and 4. Once the Hall voltage $V_H$ is acquired, the sheet carrier density $n_s$ can be calculated via:

$$n_s = IB/q|V_H| \tag{2.11}$$

from the known values of $I$, $B$, and $q$ (where $I$ is the current, $B$ the magnetic field, and $q$ ($1.602 \times 10^{-19}$ C) the elementary charge).
Once the sheet carrier density $n_s$ is determined, the carrier density $n$ and then the mobility $\mu$ can be calculated:

$$n = n_S/d \tag{2.12}$$

$$\mu = 1/qn_SR_S \tag{2.13}$$

There are practical aspects which must be considered when carrying out Hall and resistivity measurements. Primary concerns are (1) ohmic contact quality and size, (2) sample uniformity and accurate thickness determination, (3) thermomagnetic effects due to nonuniform temperature, and (4) photoconductive and photovoltaic effects which can be minimized by measuring in a dark environment. Also, the lateral sample dimensions must be large compared to the size of the contacts and the sample thickness. Finally, one must accurately measure the sample temperature, magnetic field intensity, electrical current, and voltage. All the above conditions are fulfilled for our measurements.

### *2.5.2 Experimental set-up*

The van der Pauw method is often used to measure the Hall effect, which can be successfully measured with a current source, voltmeter, and a magnet. Experimental set-ups that perform automatically measurements on a wide range of temperatures are nowadays available. These systems need accurate cooling and heating systems, and thus are expensive.
The Hall set-up at IMO was used to measure part of the P-doped diamond layers presented here. The experimental set-up is equipped with a 2 Tesla magnet for generating the B-field. During the measurements the samples were placed in a

home-made cryostat/oven and mounted on a custom built sample holder made for fast sample switching and easy wire bonding. The cryostat/oven is pumped down to vacuum pressures ($10^{-6}$ – $10^{-7}$ mbar) by a small turbo pump during the heating and cooling of the sample, in order to avoid oxidation and water condensation at the sample surface. The specimen temperature can vary on a wide range, reaching a maximum value of 1000K. A Keithley 6221 AC and DC current source is used. The results are collected via a computer through custom written LabVIEW software.

The Hall measurements carried out by our collaborators at the Walter Schottky Institute, TU-Munchen, Germany or at the National Institute for Materials Science, Tsukuba, Japan made use of similar configurations. Specific details will be given when the results are presented.

## 2.6 Necessary procedures for pn-junction fabrication

The performance of microelectronic devices has been improved tremendously since the first integrated circuit was introduced. Lithography processes account for 30-35% of the costs of manufacturing integrated circuits (Ho, Tay et al. 2005). This procedure is the key enabler and bottleneck controlling the device scaling, circuit performance and magnitude of integration for semiconductors. This integration drives the size, weight, cost, reliability and capability of electronic systems. Therefore the last section of the present chapter is dedicated entirely to the description of the lithography procedure used for diamond pn-junction fabrication.

### *2.6.1 Lithography*

The patterning of geometries is an essential process step in the fabrication of devices for microelectronics. The process of transferring a geometrical pattern from a mask to a radiation-sensitive resist is called *lithography* (Varadan, Vinoy et al. 2006). The procedure was discovered in 1796 by Aloys Senefelder and the word itself comes from the Greek language, literally meaning "writing on stone". The word is used today in a much broader sense and the procedure is widely spread in domains like biotechnology, fabrication of micro and nano-systems, opto-electronics, nanoelectronics, or anything else that is connected with micro and nanotechnology.

There are different types of lithography, depending on the "down-scalling" achieved after the procedure due to the use of light or other types of radiation for the transfer of patterns. The following description focuses on optical lithography since this was the technique used for our pn-junction preparation.

Figure 2.19 depicts the typical lithographic steps of this procedure.

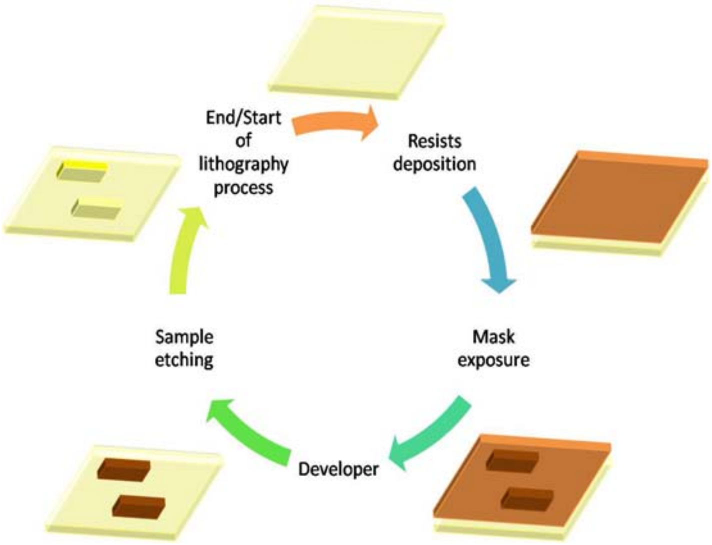

*Figure 2.19: Lithography process cycle containing the main steps for the subtractive procedure.*

Both additive and subtractive processes are employed to define features after transferring the pattern. In both cases, a first lithographic step is: suitable resists are spin-coated onto the sample surface. The sample will then be irradiated with the mask placed on top of the specimen surface. Depending on the choice of the resist material and mask, part of the resist gets cured, thereby affecting its solubility (Varadan, Vinoy et al. 2006). Thus the resist may be used either to protect areas that do not need to be etched (subtractive) or to protect areas that should not be deposited on (additive). After etching or depositing, the resist itself is removed by dissolving it in suitable chemicals.

#### 2.6.1.1 Types of radiation and exposure tools

The mission of lithography is to print a certain pattern onto a sample in a smaller and more precise way. The success in the lithographic mission depends on the lithographic exposure tool and on the way chosen to transfer the pattern. There can be electromagnetic (UV or X-rays) or particle (electrons or ions) radiation involved in the transfer process. Optical lithography is the most commercial form of lithography and several new techniques are emerging for better resolution, with a potential for mass production, especially for nanotechnology. X-ray lithography, lithography with interference or UV lithography are just a few examples of process used nowadays. Embossing lithography, also known as nanoimprinting lithography, uses a mold made by electron beam lithography to imprint the pattern onto a substrate coated with a resist. This technique is commercially important due to the nm resolution and is used for mask fabrication. Scanning probe lithography is another high-resolution method in which electrostatic discharge from the probe tip is used as the stimulant to modify (e.g. by oxidizing) the sample surface, thereby creating a pattern (Varadan, Vinoy et al. 2006; Toma, Volodin et al. 2007; Volodin, Toma et al. 2007).

The optical lithography has been developed towards smaller wavelengths, decreasing from the standard 365nm to 248nm to 193nm and is currently migrating to extreme ultraviolet lithography (13.5nm). The trend is found in the "roadmap" for semiconductors, in which the expectations of the lithographic processes are addressed and indicate that shorter wavelengths are required in the near future (Reports 2007).

Several types of lithographic tools are in use in industry. The mask aligner is an example that is used to interlock the mask and the sample before the latter is exposed. Resolution in the order of 0.5μm can be obtained with this tool. The radiation scheme employed depends on the desired resolution; electromagnetic (UV or X-rays) or particle (electrons or ions) beams may be used for the irradiation.

For the mask aligners used in optical lithography with UV radiation the feature size is the same as that one on the mask. The mask will cover the entire sample surface and one time irradiation is enough for the pattern transfer. An alternative approach uses stepper technology to improve the resolution (~0.25μm) of features (Varadan, Vinoy et al. 2006). To achieve this, the radiation is passed through a focusing lens arrangement, after it encounters the mask.

A drawback of optical lithography is the limitation in resolution of the features obtained. Significant reduction in minimum feature size is possible using electron beam lithography, which doesn't use a mask for the pattern transfer and relies on a "direct-write" technology by steering and switching of the beam in a computer controlled way. However, the writing process is time consuming and the equipment is far more expensive than optical lithography. The processing of diamond-based pn-junctions at IMO was done using a Karl Suss mask aligner (MA55) equipped with a mercury lamp (365nm).

#### *2.6.1.2 Masks*

The mask is often made on glass or quartz with a pattern on areas where we intend the radiation to be blocked from reaching the resist. As mentioned earlier, the mask itself can be made by (higher-precision) lithography. An optical blocking material, such as chromium (our case) or iron, is used to define the mask features (which are in the range of hundredths of nm).

UV light (e.g. from a high-pressure mercury lamp) is the common source of radiation that is used for mask exposure when optical lithography is used.

#### *2.6.1.3 Resists: positive vs. negative*

The mask and the selection of the proper *resist* material are crucial in the success of lithography. Geometrical patterns are transferred to resists prior to deposition or etching of films. Since optical radiation is used more often the resists are generally referred as photoresists. There are two types of resists: positive or negative, depending on the way they respond to the radiation. In figure 2.20 the process of developing positive and negative resists are compared. The positive resists become soluble in a developer after being exposed to radiation, leaving patterns on the substrate the same as that on the mask (Varadan, Vinoy et al. 2006). In contrast, when a negative resist is exposed to radiation, it becomes less soluble to the developer, thus leaving a pattern the reverse of that on the mask.

The resist is put on top of the substrate by spin-coating. By this process a uniform thin layer is deposited. The spinner motor is operated at a specific speed for good-quality films and is adapted to the type of the resist. The baking step is required to strengthen the adhesion of the resist to the sample before further processing.

A technique that uses resists to define a structural geometry on a substrate is called lift-off technique. The process steps involved in this are schematically presented in figure 2.21. The resist is spin-coated and then exposed to the radiation through a mask. A film of the desired material (e.g. a metal) is then deposited on the top of this structure. The resist will be dissolved in a specific chemical solution and will detach the film on top of the resist as well. The primary criterion for this lift-off procedure to be effective is that the thickness of the deposited thin film should be less than that of the resist. In this way some high-resolution geometry can be produced and discrete devices can be patterned.

The resists involved in the contact preparation of the diamond the pn-junctions presented in this thesis were:

- Positive resist – code S1818$^{TM}$G2 manufactured by Electronic Materials
- Negative resist – code NR7 – 300P manufactured by Futurex INC

The uniform resist layer was obtained by a spin-coating apparatus (model WS-400B-6NPP/LITE) using about 1cm$^3$ of liquid resist, which was applied in the centre of the diamond sample. Acceleration of about 3000rpm for 30s (positive resist) or 1000rpm for 40s (negative resist) were used in order to obtain a µm thick film onto the sample. The positive resist requires a pre-exposure bake at

115°C for 1 minute, while 150°C for 1 minute is necessary for the negative resist.

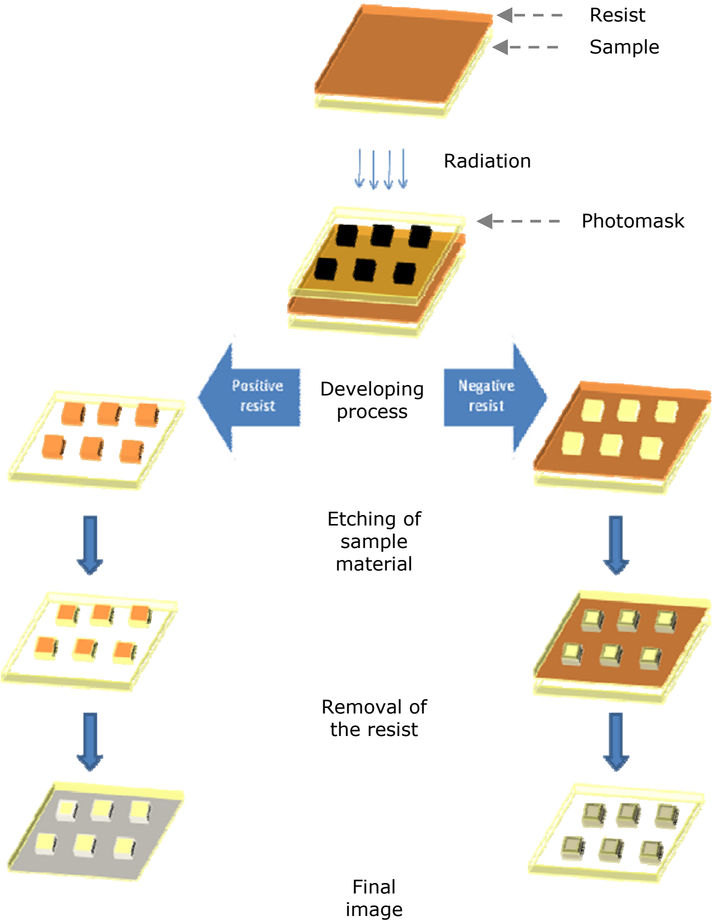

*Figure 2.20: Images formed using positive and negative resists.*

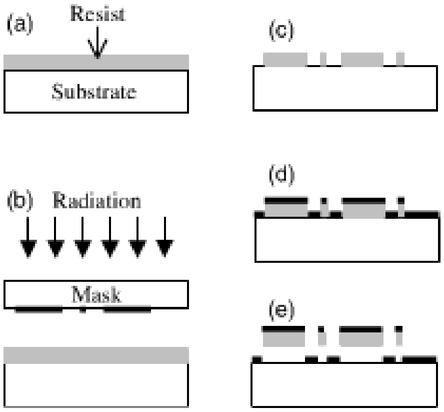

*Figure 2.21: Steps involved in the lift-off process of patterning (Varadan, Vinoy et al. 2006): a) resist deposition onto the substrate, b) transfer of the pattern by using a photomask, c) developing step, d) film deposition (metallic film) and e) dissolving of the resist and removing part of the film together with removal of the resist.*

This procedure will remove the solvent from the photoresist and improve the adhesion with the substrate. After the radiation exposure, a post-exposure bake step is necessary only for negative resist (110°C for 1 minute). Finally, the resist will be stripped away from the diamond surface using a developing solvent: RD6 developer for negative photoresist or Microposit 351 developer for positive resist.

The lift-off technique is using only the positive resist and its goal was to mark the n-type CVD diamond layers for the etching procedure. The same photoresist, as the one described for the contact preparation (see further explinations), is employed here.

### 2.6.2 Plasma etching

The etching technique is a key step for bulk processing of the devices. It can employ one or several of the following techniques:

- Wet etching – isotropic/anisotropic
- Dry etching – plasma/reactive ion

There are some process parameters: etch rate, etch selectivity and etch uniformity, characteristic for every etching technique. Wet etching is done by dipping the substrate into an etchant bath or spraying it with etchant. Dry etching is done by chemical or physical interactions between the ions in the gas and the atoms of the substrate. Wet etching is in many cases done from the back side of the sample, while plasma etching preferres the front side.

The etching process has different etch rates depending on the crystal orientation. Also, the selectivity of the process is influenced by the dopants (heavily doped regions etch slowly), or may even be altered electrochemically (e.g. etching stops upon encountering a region of different polarity in a biased p-n junction).

Non-plasma, isotropic dry etching is possible by using xenon difluorite or a mixture of interhalogen gases and provides very high selectivity for aluminium, silicon dioxide, silicon nitride, photoresists, etc.

Common methods for dry etching are plasma etching and reactive ion etching, where the external energy drives chemical reactions in low-pressure reaction chambers. As reactive gases a variety of chlorofluorocarbon gases, sulphur hexafluoride, bromide compounds or oxygen are generally used (Varadan, Vinoy et al. 2006). An advantage of the dry etching is that it provides the geometrically flexibility of patterns and sometimes less chemical contamination than the wet etching. Corrosion, reproducibility, sidewall profile and loss of critical dimensions should be taken into account when one tries to use this etching method for device fabrication.

The etching procedure for pn-junction fabrication makes use of a plasma system, thus a dry etching process. The plasma apparatus is presented in figure 2.22. During the etching procedure, oxygen gas (up to a partial pressure of $10^{-3}$ torr) was forming the discharge plasma. A power of 300W was used and, for this particular chamber design, an etching rate of ~ 75nm/min was observed in case of diamond layers.

### 2.6.3 Contact preparation

In order to investigate electronic devices metallic contacts are required. The necessary metal contacts used in this study are ohmic and are aluminium thin layers (for n-type films) or Ti/Al (for the p-type). By using the optical lithography process micrometer size contacts are patterned on top of the sample. A homemade sputtering machine was used for the deposition of thin films of very good quality, presented in figure 2.22. The base pressure of the system is around $10^{-8}$ torr, while during deposition (when the chamber is filled with Ar gas) a pressure of $10^{-3}$ torr is used. Depending on the target material and the sputtering conditions a specific thickness of the metallic layers can be obtained. For our pn-junctions generally Al layers of 50-100nm and Ti layers of about 100nm were fabricated.

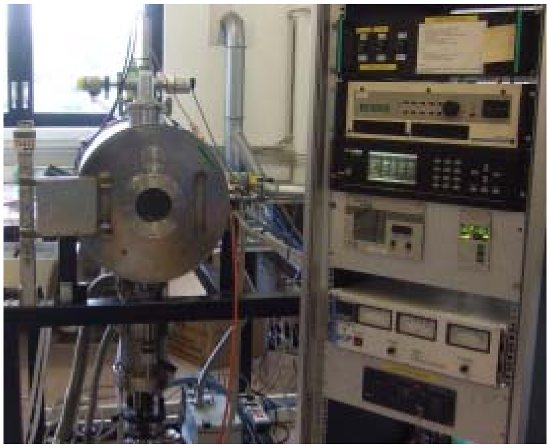

*Figure 2.22: Image of the sputtering system at IMO used for diamond pn-junction preparation.*

## 2.7 References

Axiovert Operating manual for Axiovert 40 MAT Microscope, Zeiss.

Bachmann, P. K., H. J. Hagemann, et al. (1995). "Thermal-Properties of C/H-Grown, C/H/O-Grown, C/H/N-Grown and C/H/X-Grown Polycrystalline Cvd Diamond." Diamond and Related Materials **4**(5-6): 820-826.

Barjon, J., P. Desfonds, et al. (2007). "Determination of the phosphorus content in diamond using cathodoluminescence spectroscopy." Journal of Applied Physics **101**(11): 113701_1-113701_3.

Boer, K. W. (1990). Survey of semiconductor physics - Electrons and other particles in bulk semiconductors, Van Nostrand Reinhold, ISBN 0-442-23793-6.

Bogdan, G. (2007). Growth and properties of nearly atomically-flat single crystal diamond prepared by plasma-enhanced chemical vapour deposition and its surface interactions, Hasselt University. **PhD**.

Bube, R. H. (1992). Photoelectronic properties of semiconductors, Cambridge University Press, ISBN 0-521-40491-6.

Dean, P. J. and J. C. Male (1964). "Some Properties of Visible Luminescence Excited in Diamond by Irradiation in Fundamental Absorption Edge." Journal of Physics and Chemistry of Solids **25**(12): 1369-1382.

Demirel, M. C., B. S. El-Dasher, et al. (2000). Chapter 6 - Studies on the accuracy of Electron Backscatter Diffraction measuremnts. Electron Backscatter Diffraction in Materials Science, Kluwer Academic/Plenum Publishers, ISBN 0-306-46487-X.

Haenen, K. (2002). Opto-electronic study of phosphorous-doped n-type and hydrogen-doped p-type CVD diamond films. Diepenbeek, Limburgs Universitair Centrum. **PhD**.

Ho, W. K., A. Tay, et al. (2005). "Integrated metrology and processes for semiconductor manufacturing." from http://www.scribd.com/doc/7225557/Integrated-Metrology-and-Processes-for-Semiconductor-Manufacturing.

Jongbloets, H. W. H. M. (1979). "Temperature dependence of the photothermal conductivity of high-purity germanium containing very low concentrations of Al, B and P." Physical Review B **20**(8): 3328 - 3332.

Kobashi, K. (2005). Diamond films - Chemical Vapour Deposition for Oriented and Heteroepitaxial growth, Elsevier Ltd., ISBN 0-08-044723-6.

Kravets, R., V. Ogorodniks, et al. (2002). "Fourier-transform photocurrent spectroscopy of defects in CVD diamond layers." Physica Status Solidi a-Applied Research **193**(3): 502-507.

Kravets, R., M. Vanecek, et al. (2004). "A quantitative study of the boron acceptor in diamond by Fourier-transform photocurrent spectroscopy." Diamond and Related Materials **13**(10): 1785-1790.

Liu, H. and D. S. Dandy (1995). Diamond chemical vapour deposition - Nucleation and early growth stages, Noyes Publications, ISBN 0-8155-1380-1.

Matthews, I. G. (1958). "The fluorescence of diamonds excited by X-rays." Proceedings of the Physical Society of London **72**(468): 1074-1080.

May, P. W., M. N. R. Ashfold, et al. (2007). "Microcrystalline, nanocrystalline, and ultrananocrystalline diamond chemical vapor deposition: Experiment and modeling of the factors controlling growth rate, nucleation, and crystal size." Journal of Applied Physics **101**(5): 053115_1-053115_9.

NIST. (2007, 8/14/2007). "Hall Effect Measurements." from http://www.eeel.nist.gov/812/hall.html.

Prior, D. J., A. P. Boyle, et al. (1999). "The application of electron backscatter diffraction and orientation contrast imaging in the SEM to textural problems in rocks." American Mineralogist **84**: 1741-1759.

Ralph, J. E. (1960). "Radiation Induced Changes in the Cathodoluminescence Spectra of Natural Diamonds." Proceedings of the Physical Society of London **76**(491): 688-696.

Randle, V. (1992). Microtexture determination and its applications, The Institute of Materials, London, ISBN 0-901716 35 9.

Remes, Z., M. Nesladek, et al. (2007). "Amplitude modulated step scan Fourier transform photocurrent spectroscopy of partly compensated B-doped CVD diamond thin films." Physica Status Solidi a-Applications and Materials Science **204**(9): 2950-2956.

Reports, I. (2007). "International technology roadmap for semiconductors." 2007 Edition - Lithography, from http://www.itrs.net/Links/2007ITRS/2007_Chapters/2007_Lithography.pdf.

Rose, A. (1963). Concepts in photoconductivity and allied problems. London, Interscience publishers - a division of John Wiley & Sons, New York.

Sauer, R. (2003). Luminescence from optical defects and impurities in CVD diamond. Thin-film diamond I - Semiconductors and semimetals. C. Nebel and J. Ristein, ISBN 0-12-752185-2, Elsevier **76**.

SIMS. (2008). "Introduction to Secondary Ion Mass Spectroscopy (SIMS) - Lecture Notes for MECH 343." from http://www.me.ust.hk/~mejswu/MECH343/SIMS-notes.pdf.

Sternschulte, H., J. Horseling, et al. (1996). "Characterization of doped and undoped CVD-diamond films by cathodoluminescence." Diamond and Related Materials **5**(6-8): 585-588.

Tanabe, K., K. Nakazawa, et al. (2001). "Cathodoluminescence of phosphorus doped (111) homoepitaxial diamond thin films." Diamond and Related Materials **10**(9-10): 1652-1654.

Toma, C., A. Volodin, et al. (2007). "Tip voltage controlled local modification of hydrogenated diamond surface with an atomic force microscope." Physica Status Solidi **204**(9): 2920-2924.

Tomm, J. W., A. Jaeger, et al. (1997). "Aging properties of high power laser diode arrays analyzed by Fourier-transform photocurrent measurements." Applied Physics Letters **71**(16): 2233-2235.

van der Pauw, L. J. (1958_a). "A method of measuring specific resistivity and Hall effect of discs of arbitrary shape." Philips Research Reports **13**: 1-9.

van der Pauw, L. J. (1958_b). "A method of measuring the resistivity and Hall coefficient on lamellae of arbitrary shape." Philips Technical Review **20**: 220-224.

Vanecek, M., R. Kravets, et al. (2003). "Fourier transform photocurrent spectroscopy of dopants and defects in CVD diamond." Diamond and Related Materials **12**(3-7): 521-525.

Vanecek, M. and A. Poruba (2002). "Fourier-transform photocurrent spectroscopy of microcrystalline silicon for solar cells." Applied Physics Letters **80**(5): 719-721.

Vanstreels, K. (2007). Increasing the mean grain size in copper films and features, Hasselt University **PhD**.

Varadan, V. K., K. J. Vinoy, et al. (2006). Smart material systems and MEMS: design and development methodologies, John Wiley & Sons, Ltd, ISBN 978-0-470-09361-0 (HB).

Volodin, A., C. Toma, et al. (2007). "Electrostatic force microscopy study of electrical conductivity of hydrogen-terminated CVD diamond films." Physica Status Solidi **204**(9): 2915-2919.

Yacobi, B. G. and D. B. Holt (1986). "Cathodoluminescence scanning electron-microscopy of semiconductors." Journal of Applied Physics **59**(4): R1-R24.

# 3 Growth of phosphorous-doped layers on {111} and {100}-oriented diamond substrates

With this chapter the experimental part of the present study begins. The results regarding phosphorous incorporation in the {111} and {100}-oriented diamond specimens are discussed. The P doping of single crystalline {111}-oriented diamond substrates is covered in section 3.1, while section 3.2 deals with doping of single crystalline {100}-oriented diamonds. For each case, after a short description of the synthetic HPHT substrates chosen as substrates and their preparation procedure prior growth experiments, a description of the plasma parameters is made. The obtained layers were investigated with various experimental techniques. At the end of this chapter comparisons between the results obtained on two different types of samples (in terms of crystalline orientation) were used for the doping procedure are made.

## 3.1 P-doping process using {111}-oriented single crystalline substrates

### *3.1.1 Experimental details: samples, growth and pretreatment parameters*

The choice of a good substrate is crucial for the final quality and properties of the obtained diamond film. The first successful experiments in phosphorous-doping of epitaxial diamond films were using mechanically polished {111} surfaces of type Ib synthetic diamonds (Koizumi, Kamo et al. 1997), but also bulky diamond substrates with hexagonal shaped {111} polished surfaces were used later on (Koizumi 1999). The progress in phosphorous incorporation into the monocrystalline diamond indicates that HPHT square-shaped synthetic diamond single crystals are generally preferred (Koizumi, Suzuki et al. 2008).

The substrates used in the present study include commercially available mirror-polished Sumitomo HPHT Ib {111}-oriented diamond substrates. Their dimensions are 2.5x2.5x0.5mm$^3$ and figure 3.1 shows optical images of the substrates together with AFM investigations, from which an estimation of the roughness of the sample surface is made. From these images one can evaluate the surface quality of the specimens.

Prior growing the P-doped layers by the MW PE CVD process, all substrates were chemically oxidized using an acid solution of $H_2SO_4$ and $KNO_3$ (at ~300°C on a hot plate for 30min) to remove surface contaminants, followed by rinsing in distilled water in an ultrasonic bath. For the drying procedure a flow of nitrogen gas is used. The cleaning step enables the elimination of the impurities present at the sample surface such as metallic or dust particles, which could contaminate or affect the quality of the obtained layer.

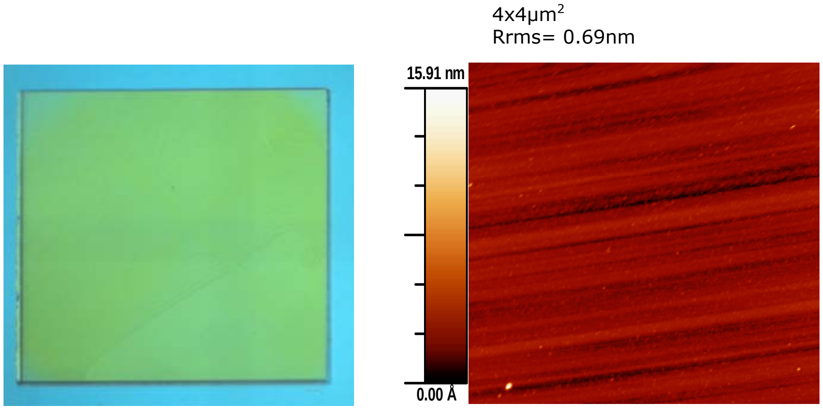

a) b)

*Figure 3.1: a) DICM image of the HPHT Ib {111}-oriented diamond substrates. The sample dimensions are 2.5x2.5mm$^2$, b) AFM image of the same diamond substrate presenting the polishing lines at the specimen surface.*

Once cleaned the diamond substrates are installed on the molybdenum substrate holder, one sample a time. After which they are introduced in the reactor chamber. Table 3.1 describes the depositions conditions necessary for lightly P-doped diamond films (Koizumi, Teraji et al. 2000; Katagiri, Isoya et al. 2004; Koizumi, Suzuki et al. 2008). The layers are grown epitaxially on synthetic HPHT type Ib {111} substrates. The source gas was 0.05% $CH_4$ (4N: purity 99.99%) diluted with $H_2$ (9N). Phosphine gas $PH_3$ (6N) was the source of phosphorous. The $[PH_3]/[CH_4]$ ratio in the source gas was varied from 100 up to 5000ppm. The gas pressure, the $H_2$ gas flow rate, the substrate temperature and the growth duration were 100torr, 500sccm, 900°C and 2 hours, respectively. The temperature of the substrate is monitored through a lateral window of the deposition chamber by an optical pyrometer. The resultant growth rate of these P-doped diamond films is estimated around 2μm/h. The different phosphine concentrations in the gas phase do not visibly influence the growth rate, however a difference is noticed when P-doped films are compared with undoped diamond layers.

*Table 3.1: Growth conditions of the P-doped CVD diamonds.*

| **Sample code** | **$PH_3/CH_4$ (ppm)** | **Pressure (torr)** | **MW power (W)** | **Temp. (°C)** | **Observations** |
|---|---|---|---|---|---|
| 60317EP | 1000 | 100 | 625 | 894 | - |
| 60510EP | 1000 | 100 | 705 | 892 | - |
| 60511EP | 500 | 100 | 690 | 896 | - |
| 60512EP | 500 | 100 | 720 | 893 | - |
| 60522EP | 500 | 100 | 665 | 897 | Pretreatment in $H_2$ plasma (for ½h) |
| 60523EP | 500 | 100 | 690 | 892 | Pretreatment in $H_2$ plasma (for ½h) |
| 60630EP | 1000 | 100 | 745 | 891 | Pretreatment in $H_2$ plasma (for ½h) |
| 60420EP | 500 | 100 | 640 | 892 | - |
| 61208EP | 100 | 100 | 693 | 891 | - |
| 70122EP | 5000 | 100 | 722 | 895 | - |
| 70201EP | 500 | 100 | 692 | 893 | Pretreatment in $O_2$+$H_2$ plasma (for 1h) |
| 70202EP | 500 | 100 | 683 | 894 | Pretreatment in $O_2$+$H_2$ plasma (for ½h) |
| 70319EP | 500 | 100 | 613 | 892 | Pretreatment in $O_2$+$H_2$ plasma (for 5 min) |
| 70330EP | 5000 | 100 | 631 | 893 | - |
| 70605EP_A | 500 | 100 | 633 | 892 | Pretreatment in $O_2$+$H_2$ plasma (for 5 min) |

| | | | | | |
|---|---|---|---|---|---|
| 70605EP_B | 500 | 100 | 625 | 891 | Pretreatment in $O_2+H_2$ plasma (for 2 min) |
| 70606EP | 2000 | 100 | 645 | 892 | - |
| 70716EP | 500 | 100 | 650 | 895 | - |
| 71115EP | 2000/<br>1000/<br>500/100 | 100 | 670 | 896 | Doping levels sequentially changed during growth |

Crystalline defects in the surface region of the substrate have unfavourable effect on the quality of the homoepitaxial diamond films. The polishing marks that are typically observed at the surface of our substrate surfaces (figure 3.1 b)) can propagate to the surface of the grown diamond films, thus the optoelectrical properties of P-doped diamond films may be altered. These marks are large (about 200nm) or small (about 20nm) periodic patterns, their height is a few nm and the patterns typically run parallel to one direction for all the substrates of as-received good quality HPHT diamond substrates. To remove the polishing-induced defects and to improve the crystalline perfection of the synthesized diamond films, some pretreatment procedures are foreseen for the homoepitaxial diamond layers (Teraji 2006). Oxygen and hydrogen plasmas are preferred as etching methods, but diamond can be etched also by gases such as nitrogen, halogens or other inert gases. Typically oxygen and hydrogen etching procedures are followed directly by synthesis and the carbon source gas is introduced in the deposition chamber. Microwave plasma, quasi-ECR microwave plasma and RF plasma are utilized for this purpose. The etching rate is typically 1μm/h under optimized etching conditions (the etched depth of diamond is ~1μm in most cases (Yamamoto, Teraji et al. 2005)). A process of surface etching in oxygen plasma or hydrogen has already been performed for P-doped films grown on top of {111} diamond substrates (Tavares, Koizumi et al. 2005). These results suggested that the quality of the overgrown CVD n-type diamond layers is improved after the RIE (reactive ion etching) pretreatments, meaning that a macroscopic flat surface can be formed after RIE RF plasma etching pretreatments.

For this study, some of the grown P-doped samples were pretreated using a microwave plasma in the same reactor used for growth of the diamond layers. In table 3.2 a comparison between the $H_2$ or $O_2/H_2$ pretreatment parameters is made. The two different gases tested for removing the damaged layer were: pure $H_2$ and a mixture of $O_2/H_2$. The pretreatment was done at 800°C in both cases. The pressure was changed depending on the process gasses: 100torr for

$H_2$ and 70torr for $O_2/H_2$. The etching time was varied in order to obtain different etching depths. The etching rates were different depending on the pretreatment type, thus a diamond etching rate of ~1µm/h for $H_2$ and ~2µm/h for $O_2/H_2$ was calculated from the weight differences before and after the plasma exposure.

*Table 3.2: Table with plasma pretreatment conditions.*

| | **$H_2$ plasma pretreatment** | **$O_2/H_2$ plasma pretreatment** |
|---|---|---|
| Temperature (°C) | 800 | |
| Pressure (torr) | 100 | 70 |
| MW power (W) | 650 | 620-740 |
| Ø (sccm) | 500 $H_2$ | 480 $H_2$<br>20 $O_2$ |
| Time (min) | 30 | 2 - 60 |
| Etching rate (µm/h) | 1 | ~2 |

### *3.1.2 Surface topography, morphology and the influence of the pretreatments*

The study regarding surface topography and morphology of P-doped diamond layers is split into two parts. The effect of the phosphine concentration is presented first, while the second part of the sub-section describes the effect of the pretreatments prior to the growth procedure.

**The effect of the doping concentration**

The surface morphology and topography of HPHT diamond specimens and the CVD diamond films, deposited with different phosphine concentration during the growth, are shown in figure 3.2. The figure is representing images for P-doped layers with phosphine concentration ($PH_3/CH_4$) of 500ppm and 5000ppm, respectively. The film thickness for both samples is ~5µm. In the low magnification DICM images (figure 3.2 – a, d and g), it is clearly observed that the polishing lines present at the substrate site are still observed after the growth process, independent from the phosphine concentration. The magnified SEM images, figure 3.2 – e and h, show that CVD films are mostly flat with few typical features observed for P-doped {111}-oriented diamond surfaces are seen, for both P doping concentrations.

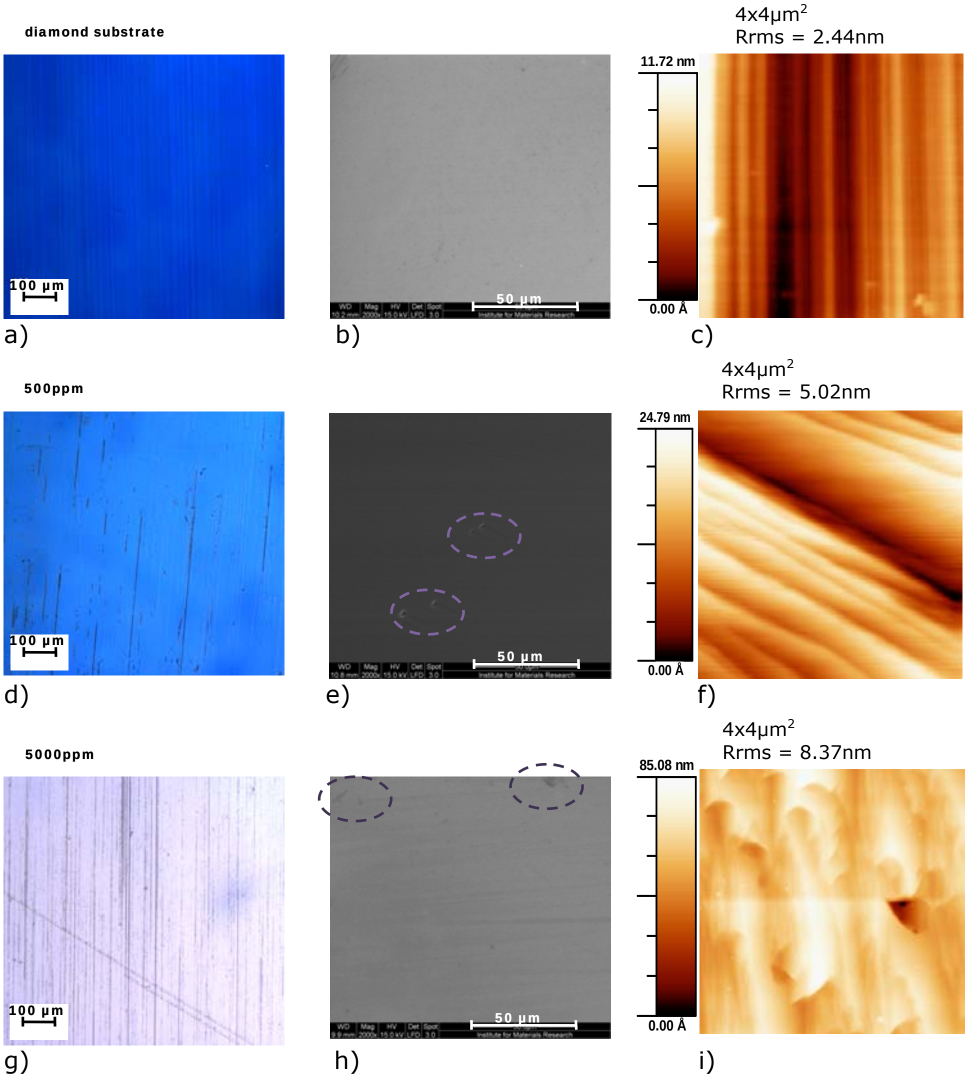

*Figure 3.2: Surface morphology and topography for a HPHT {111}-oriented diamond substrate (a) DICM, b) SEM and c) AFM images) and {111} P-doped CVD layers with 500ppm PH$_3$/CH$_4$ (d) DICM, e) SEM and f) AFM images) and 5000ppm (g) DICM, h) SEM and i) AFM images), respectively. The circles are marking the presence of "comet-like" features.*

The appearance of such “comet-like” features (Koizumi 2003) is caused by local disordering like structural defects or accidental contaminants of the sample surface. Their appearance indicates high quality thin film growth. The fact that non-epitaxial imperfections, such as unepitaxial crystallites or pyramidal hillocks, are not observed after the growth is also supporting the high quality growth process. The AFM results, figure 3.2 – c, f and i, point out that the root mean square surface roughness ($R_{RMS}$) of the P-doped diamond films remains in same range as the substrate (nm range), and only a small increase of the $R_{RMS}$ is seen. Thus, we can conclude that the addition of phosphine into the growth mixture gas doesn’t drastically change the sample surface. Moreover, increasing the phosphine concentration (up to a maximum of 5000ppm) will not lead to the appearance of special features nor to a modification of the film quality.

### The effect of the plasma pretreatments

Figure 3.3 shows surface investigations of the HPHT {111}-oriented diamond substrates etched in an $O_2/H_2$ plasma between 5 and 60min. The surface morphology changes with increasing the etching time and, as observed from the DICM micrographs (a, d and g images), a nonuniform etching of the surface occurs. The different regions present at the sample surface are probably induced by a slight substrate misorientation. The most obvious delimitation between different areas is seen for the sample etched for 60 min. Moreover, the DICM image (figure 3.3 – d) shows that triangular shaped etch pits are developed on the surface area where the etching was more obvious. The SEM images (figure 3.3 – b, e and h) indicate that for 5min etching time the polishing lines are not visible anymore and small size triangular etch pits are covering the sample surface. Increasing the exposure time will increase the feature size, as seen in the SEM image for the 30min etch. For 60min $O_2/H_2$ plasma the topography of the specimen is completely changed and step-like features are developed. The root mean square surface roughnes ($R_{RMS}$) of the investigated samples, as measured by the AFM (figure 3.3 – c, f and i), increases with increasing the exposure time but remains in the nm range.

The etching effect as previously described for $O_2/H_2$ pretreatment has not been observed in the case of $H_2$ plasma. The $H_2$ pretreatment was done at the same temperature, see table 3.2. Figure 3.4 (a – c) shows DICM, SEM and AFM images of a substrate surface pretreated for 30min in a $H_2$ plasma. The polishing lines are still visible at the substrate surface and no etching pits are observed, as in the case for a 30min $O_2/H_2$ pretreatment plasma (figure 3.3 d-f).

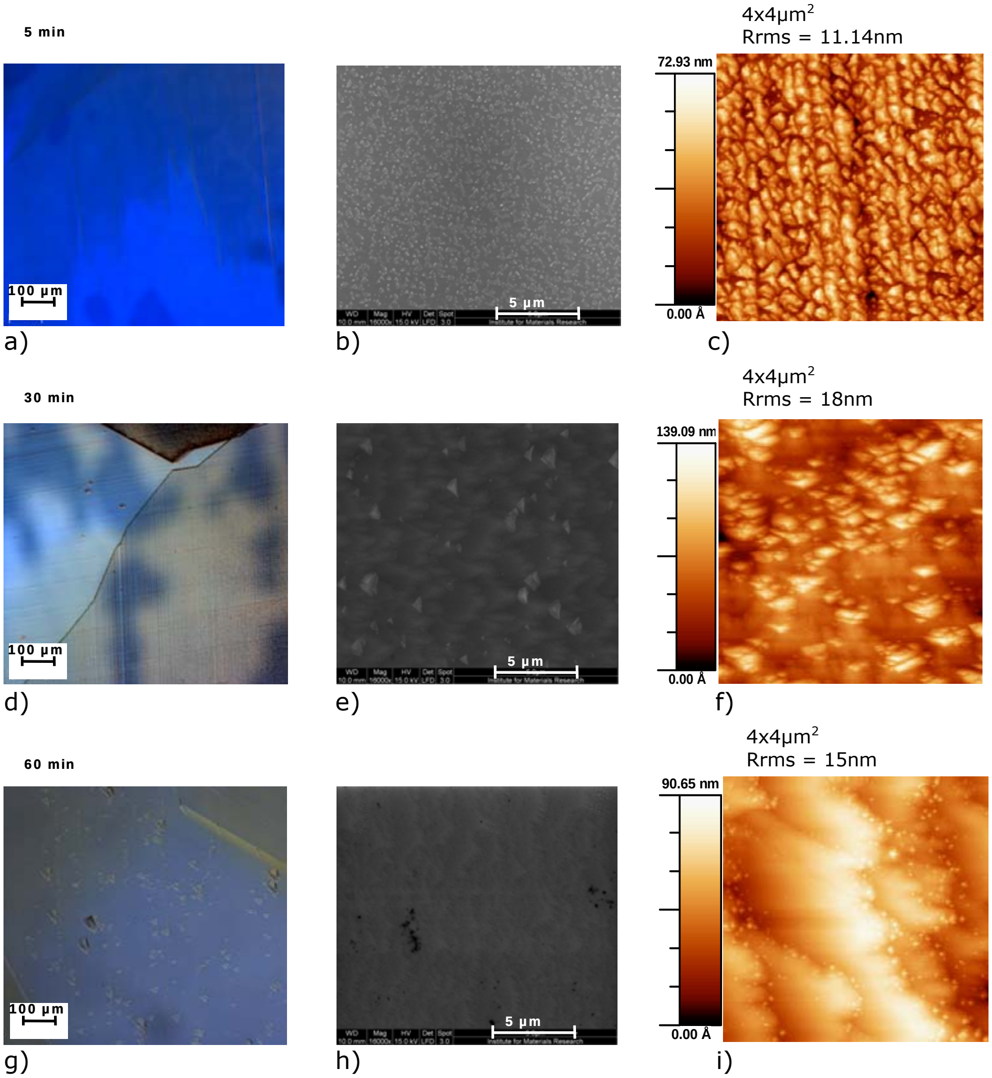

*Figure 3.3: Comparison of the surface morphology and topography for three diamond substrates pretreated in an $O_2/H_2$ plasma for: 5min (a) DICM, b) SEM and c) AFM images), 30min (d) DICM, e) SEM and f) AFM images) and 60min (g) DICM, h) SEM and i) AFM images), respectively.*

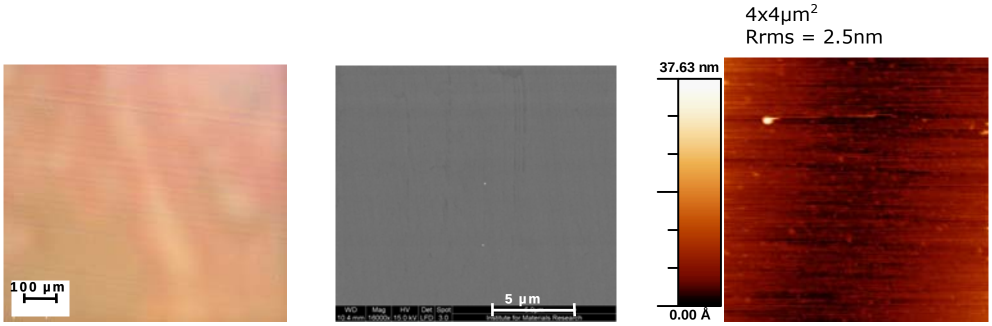

a) b) c)

*Figure 3.4: DICM (a), SEM (b) and AFM (c) images for a diamond substrate etched in a $H_2$ plasma for 30min at approximately 800°C.*

The $R_{RMS}$ of the sample, as measured by AFM in figure 3.4 – c), is almost similar to the value measured for the diamond substrates (figure 3.2 – c). Therefore the surface investigations presented indicate that this particular $H_2$ pretreatment doesn't enable any noticeable surface modification, leading to growth of diamond films which inherit the substrate polishing faults.

After the plasma pretreatment step of the substrates, P-doped homoepitaxial diamond growth was performed, using growth conditions presented in table 3.1. The following surface investigations will refer only to the results after $O_2/H_2$ pretreatment as the $H_2$ pretreatment wasn't efficient in removing substrate surface polishing lines. Figure 3.5 shows the images for the corresponding P-doped layers grown on the pretreated samples previously presented in figure 3.3. As can be observed from the optical images (figure 3.5 – a, d and g) the polishing lines are flattened and a uniform surface is only observed for the n-type film surface growth on top of a sample pretreated for 5min. For layers grown on top of substrates exposed to 30min or 60min pretreatment plasma the surface is not uniform. The film surface inherits the substrate defects after the etching step, figure 3.3 – d and g, thus a corresponding image of those defects (such as etching pits) can be seen at the layer surface.

The SEM investigation presented in figure 3.5 – b shows a flat layer surface growth after 5min pretreatment. The small etching pits, seen in figure 3.3 – b at the sample surface, are not present after the growth of P-doped layer. Thus a smooth film can be grown after such pretreatment and the layer will not inherit the surface pattern or the polishing lines.

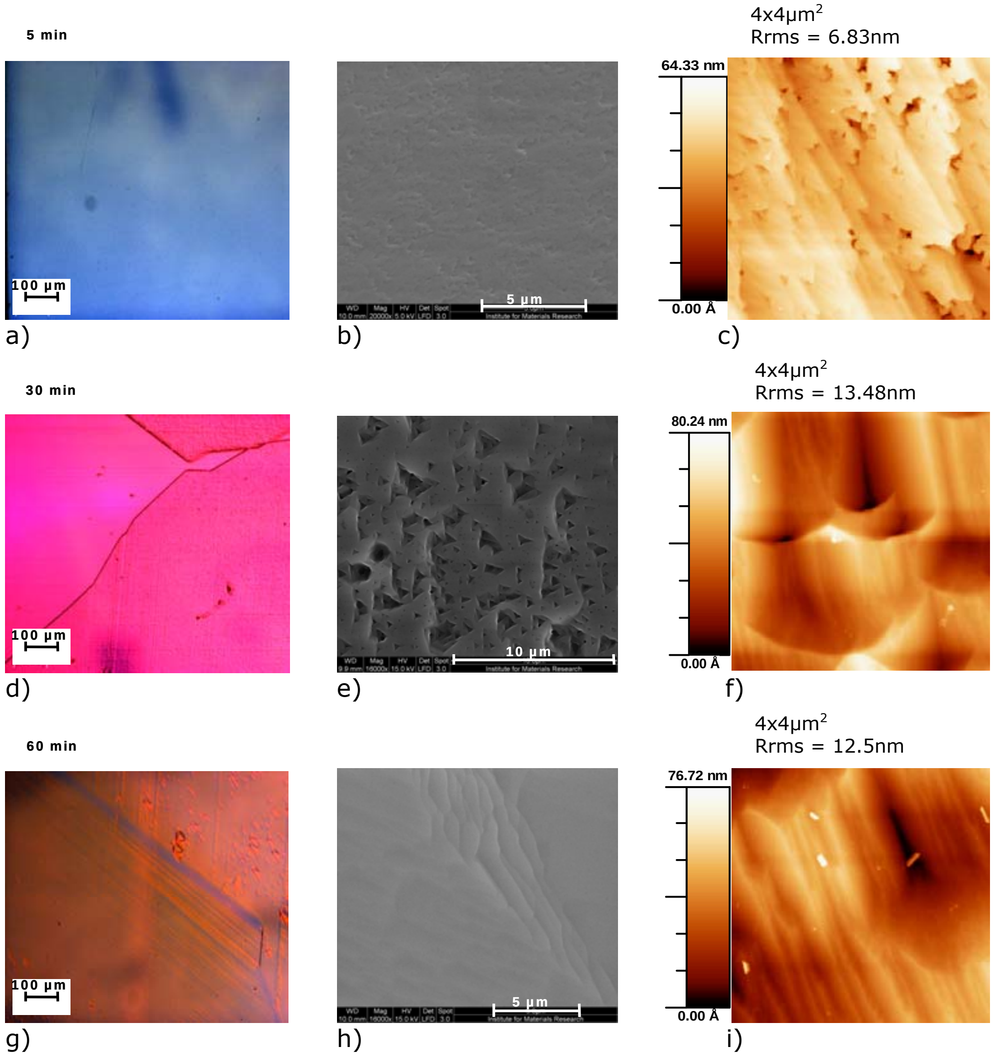

*Figure 3.5: Comparison of the surface morphology and topography of the diamond film surface, previously presented, in figure 3.3, after growth of 500ppm P-doped CVD diamond layers for 2h. The corresponding films were grown on the substrates after $O_2/H_2$ pretreatments for: 5min (a) DICM, b) SEM and c) AFM images), 30min (d) DICM, e) SEM and f) AFM images) and 60min (g) DICM, h) SEM and i) AFM images), respectively.*

For the P-doped layers grown on samples with increased pretreatment time, figures 3.5 –e and h, the film surface is not defect free and triangular features or step-like patterns are shown. The SEM micrographs indicate that these samples are macroscopically rough. The triangular marks, seen in figure 3.5 – e, are reported to be related to depressions in the surface or less diamond growth, indicating that a substantial amount of defects are created on the P-doped {111} diamond (Wada, Teraji et al. 2005). According to AFM observations, figure 3.5 – c, f and i, the flattest surface is obtained for the layer with a 5 min pretreatment step. The root mean square surface roughnes ($R_{RMS}$) on average is 6.83nm for a 4x4$\mu m^2$ scanned area, while for longer exposure time it is more than double.

These surface investigations point to the following conclusion: a 5min pretreatment step, in an $O_2/H_2$ gas mixture, prior to growth of P-doped CVD layers is necessary to diminish the polishing-related defects at the layer surface.

### *3.1.3 PC investigations*

Defect spectroscopy is a powerful tool to study impurities in semiconductors at very low concentrations and in this study it was used to identify P-related states. The first confirmation of active incorporation of P in CVD diamond and measurement of its photoionization cross-section by photocurrent measurements, PTIS and oscillatory photoconductivity, was presented in 1997 (Nesladek, Meykens et al. 1999; Nesladek, Haenen et al. 2003). Later on, the defects in CVD diamonds were also studied by the constant photocurrent method (Nesladek, Meykens et al. 1999; Nesladek, Meykens et al. 1999_a). A photoionization onset at about 0.6eV is attributed to the P impurity and this value is in good agreement with the activation energy of P level determined from Hall measurements (Nesladek, Haenen et al. 2003). This defect level was called $X_{P1}$ at that time. Since then it was generally observed in all P-doped CVD diamonds and it was attributed without doubt to substitutional phosphorus acting as an electrically active donor atom. The second defect level denoted $X_{P2}$, positioned at 0.8eV, is found in highly resistive samples and its exact origin is not known yet (Haenen 2002).

Figure 3.6 – a) shows a typical PC spectra, found in the literature, taken for a diamond sample doped with 1000ppm $[PH_3]/[CH_4]$ (Haenen 2002). The P-related donor peak is seen at 0.56eV and is marked accordingly in the figure. Further examination of the spectrum reveals the so-called oscillatory photoconductivity. The signal modulation allows the determination of the electronic structure of the P atom in the CVD diamond films. The appearance of the phenomenon is explained by the disappearance from the conduction band of a substantial part of the excited electrons by rapid thermalisation. Thus, the decrease of the photocurrent signal is seen. In the figure the N-related peak is also plotted (see the peak at 2eV).

Figure 3.6 – b) presents the liquid nitrogen temperature (LNT) photocurrent (PC) spectra of our P-doped CVD diamond thin films doped with 1000 and 500ppm [$PH_3$]/[$CH_4$], respectively. The spectra are recorded for a voltage of 100V and for Al contacts in coplanar geometry. Both samples present the P-related $X_{P1}$ peak, thus we can draw a first conclusion that the incorporation process of P in our layers is successful.

A closer examination of the spectra, for both samples, shows a gentle modulation of the photocurrent signal (marked in the spectra with blue arrows), the so called phonon-assisted oscillatory photoconductivity. By using oscillatory conductivity and PTIS it was possible to study the electronic structure of P in CVD thin films and to attribute the energies for P level excited states (Haenen, Meykens et al. 1999; Haenen, Meykens et al. 1999_a; Haenen, Meykens et al. 2000; Haenen, Meykens et al. 2000_a; Haenen, Meykens et al. 2001; Haenen, Nesladek et al. 2004).

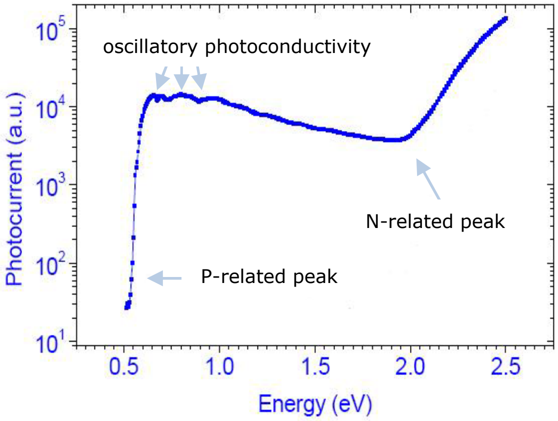

a)

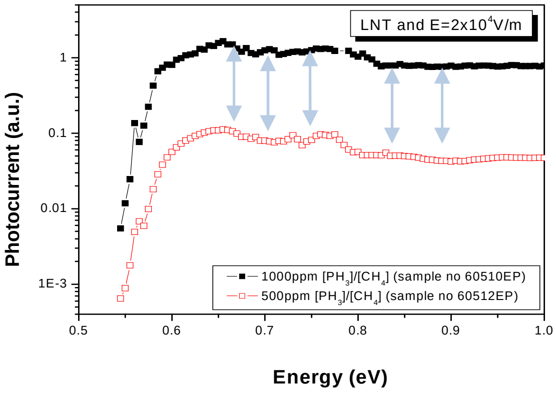

b)

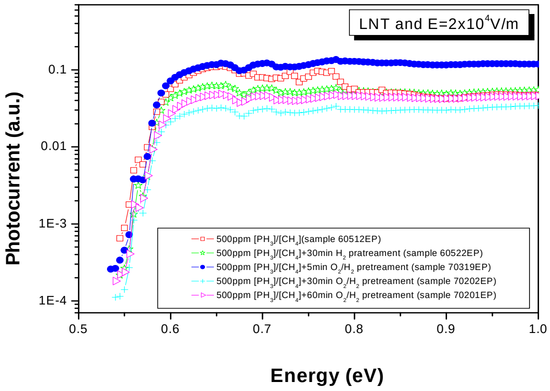

c)

*Figure 3.6: a) Typical PC spectra for P-doped CVD {111}-oriented diamond film doped with 1000ppm [PH$_3$]/[CH$_4$]* (Haenen 2002), b) *Comparison between LNT PC spectra of 1000 and 500ppm [PH$_3$]/[CH$_4$] doped films, showing the presence of substitutional P and the oscillatory photoconductivity, c) Comparison between LNT PC spectra for samples with 500ppm [PH$_3$]/[CH$_4$] doped samples, with different pretreatment time or type, showing as well the signature for substitutional P and oscillatory photoconductivity.*

In our case the 500ppm sample is showing the most well-defined minima. The enhanced quality of the spectra for the lower doped films can de due to a better film quality with less stress, resulting in less broadening of the defect levels in the band gap, which is in good agreement with the literature (Haenen, Meykens et al. 2001; Haenen 2002).The oscillatory conductivity is displayed at energies at which an emission of LO phonons leads to a fast recombination of the photo-generated free carrier on one of the excited states of phosphorus. From the oscillatory conductivity minima it is possible to determine the energy of the phosphorus excited states, calculated by subtracting the LO phonon energy from the lowest observed minimum of the cascade set, for details see (Haenen, Meykens et al. 1999; Haenen, Meykens et al. 2000; Haenen, Nesladek et al. 2004; Nesladek 2005). The energy of LO phonons (155meV) is also valid for our samples, thus it becomes apparent that P-related level present in our homoepitaxial layers are similar to the P-related states found in literature. The pretreatment step performed before the growth of our P-doped layers is not inducing noticeable changes in the PC spectra, figure 3.6 – b). All the 500ppm P-doped diamond samples are presenting similar P-related features, regardless of the pretreatment time or type.

All the PC spectra presented in figure 3.6 show a distinct sharp maximum around 0.56eV (± 0.05meV). This peak is attributed to the ground level of P which is less deep into the band gap than the 0.6eV under the CB (Haenen 2002).

The second P-related defect observed by PC measurements, called $X_{P2}$, is found for one of our samples (figure 3.7). The appearance of this particular defect is rarely seen in P-doped layers and, as it was mentioned before, it was previously only seen in attributed to resistive layers. A solution to overcome the problems regarding a sample’s high resistivity and low photoconductivity was proposed by Kravets in 2005 (Kravets 2005). The measurements described there were making use of hydrogen-terminated diamond surfaces prior FTPS investigations. On a hydrogen-terminated diamond surface, surface states pin the Fermi level close to the valence band, changing the electrical properties of the investigated material. By controlling the surface conductivity and photoconductivity of the hydrogen-terminated diamond surface it was possible to control the photosensitivity of the samples. During the hydrogenation procedure for our P-doped diamond sample the gas pressure, the $H_2$ gas flow rate, the substrate temperature were 100torr, 500sccm and 800°C, respectively. The duration of the procedure was fixed to 10min to minimise deterioration of the surface.

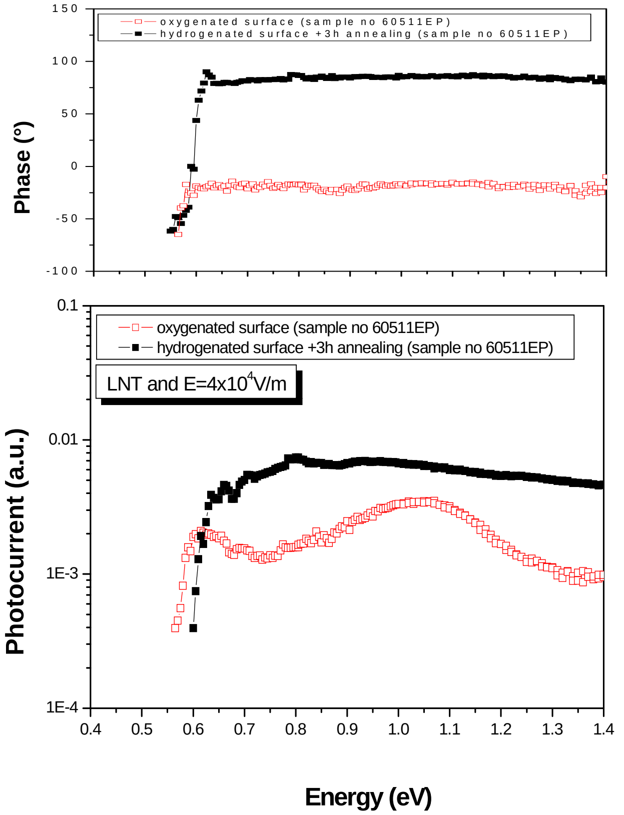

*Figure 3.7: Comparison between two LNT PC spectra of the same 500ppm [$PH_3$]/[$CH_4$] doped sample, when its surface was: oxygenated (chemically oxidized) or hydrogenated and annealed for 3h. At the top the phase of the photocurrent is given.*

The results regarding the annealing study of the hydrogenated P-doped diamond sample is presented in figure 3.7. It is well established by now that at temperatures around 200°C, in air, hydrogen leaves the surface and the surface starts to oxidize (Kravets 2005). The annealing procedure is done at 200°C in air and the duration is varied between 1 and 3 hours. After cooling down the sample typical PC coplanar contacts are deposited at the sample surface. In figure 3.7 the PC spectra of the oxidized surface is compared with the PC data of the hydrogenated surface (and annealed for 3h). An important finding of these spectra is that the photoconductivity is noticeable changed after the hydrogenation and annealing step. The $X_{P2}$ defect is no longer observed. This effect is visible only for a 3h annealing procedure. The effect can be explained by the shifting of the electron quasi-Fermi level. This modification will increase the occupation of $X_{P1}$ compared with $X_{P2}$, and thus the $X_{P1}$ level will dominate the spectrum. Also, a shifting of the threshold energy towards higher energy values is visible for the spectra with 3h annealing procedure. However, further investigations are necessary to elucidate this shifting mechanism and to detect the exact origin of this defect.

### *3.1.4 Electrical properties*

The Hall effect measurement is the most used method to characterize the electrical properties of semiconductors. Thus, in this sub-section the results obtained on for the P-doped diamond thin films grown on {111}-oriented samples are presented. Before Hall measurements, the samples were oxidized as explained earlier in section 3.1.1. This cleaning procedure is important to remove possible electrical conductivity due to the hydrogen-terminated surface. Ohmic electrodes composed of Ti capped with Au were formed on top of the P-doped diamond layers. Hall-effect measurements using the van der Pauw method were performed at the Walter Schottky Institute in Munich, Germany within the frame of the European Research Training Network collaboration (DRIVE). The measurements were carried out in an AC magnetic field of 1.8T using an Oxford Instruments cryostat (LHe up to 1000K). The measuring system consists of a Keithley 236 Source Measurement Unit and Keithley 2000 Multimeter and a Keithley 7001 Switch System with Keithley 7065 Hall Effect card for measuring the conductivity and Hall effect. An ITC502 temperature controller was used for temperature dependence experiments.

All the P-doped films show negative Hall coefficients in the temperature range from 295 to 800K, which indicates n-type conduction of the films. In figure 3.8, the results of two P-doped samples, 500 and 5000ppm, are displayed. Two conduction regimes are observed. Thermally activated conduction process by electrons in the conduction band is firstly observed. From the high-temperature region (higher than 600K) the activation energy of phosphorous in substitutional site for both samples was determined. At low temperatures (lower than 600K), the decreasing behaviour of conductivity is attributed to hopping conduction on the phosphorous band (Koizumi 2003). The hopping conduction is more pronounced when the doping level increase. This behaviour may be due to a poorer quality of the film, which induces a decrease in mobility or/and carrier concentration (figure 3.9). The poorer quality of the results can also be explained by the defective film topography, previously presented in figure 3.2. For this sample, a mobility equal to $2cm^2/Vs$ was obtained at room temperature.

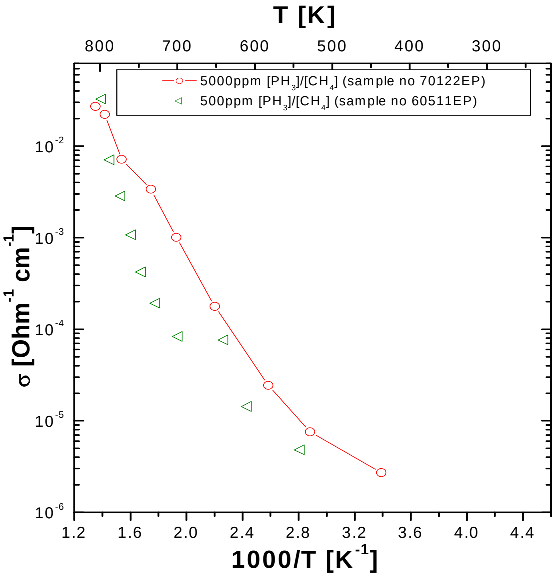

*Figure 3.8: Conductivity versus temperature for two P-doped layers (see text for details). The activation energy value in the high temperature range was ~0.5eV, for both cases. Hopping conductivity is more pronounced for higher* $[PH_3]/[CH_4]$ *concentrations.*

The present results indicate that less-defective films can be obtained when lower $[PH_3]/[CH_4]$ are used. Therefore, the P doping level of the n-type layers used for device fabrication will be less than 5000ppm $[PH_3]/[CH_4]$.

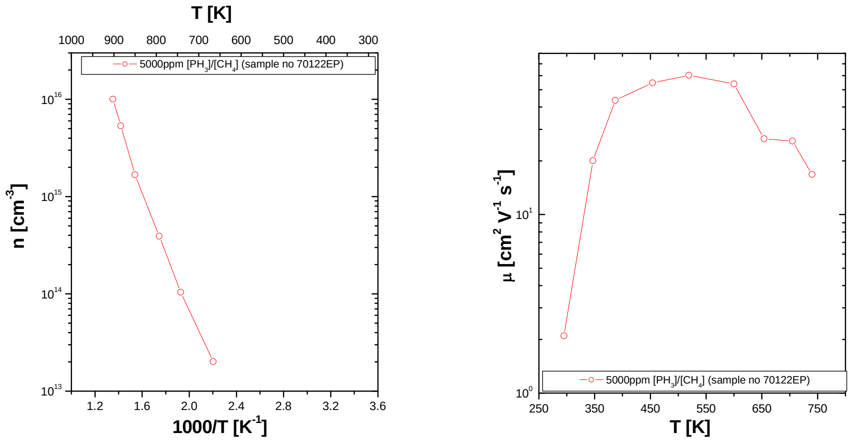

a) b)

*Figure 3.9: Hall effect measurements: carrier concentration versus temperature (a) and mobility versus temperature (b) for the sample doped with 5000ppm* $[PH_3]/[CH_4]$.

### 3.1.5 The influence of precursor concentration on P incorporation: SIMS profile

Impurity analysis is necessary to clarify the impurity concentration and distribution, therefore P-doped diamond thin films were characterized by secondary ion mass spectroscopy (SIMS). The measurements were performed at the Groupe d'Etude de la Matière Condensé (GEMaC), Versailles University St. Quentin - CNRS, Meudon, France and the experimental set-up was previously described (see chapter 2, section 2.4.2). Figure 3.10 shows the SIMS depth profiles of one sample. This sample has been formed with four different P-concentrations to check the controllability of the doping process. The P concentration has been changed sequentially during diamond growth with $[PH_3]/[CH_4]$: 2000, 1000, 500 and 100ppm every 30min. The P concentrations were estimated to be approximately $1\times10^{18}$, $9\times10^{17}$, $7\times10^{17}$ and $3\times10^{17}$ for 2000, 1000, 500 and 100ppm layers, respectively. The doping efficiency was about 3%. These results confirm the fact that our doping level is almost at the same level as the ones reported in the literature ($10^{17}$-$10^{18}$cm$^{-3}$) (Koizumi 2003; Koizumi, Suzuki et al. 2008).

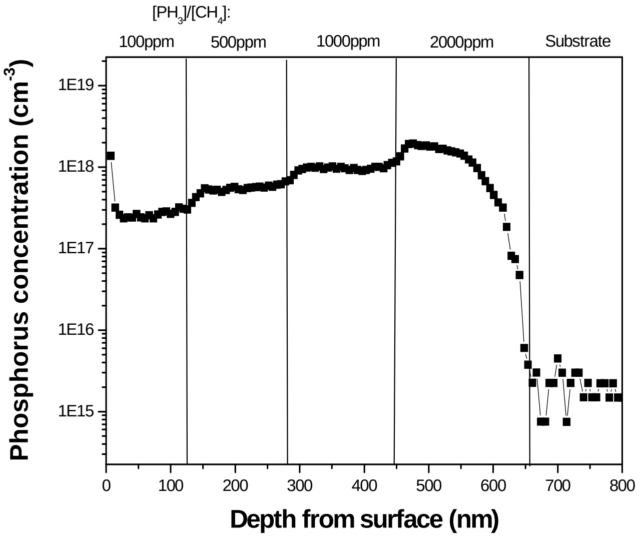

*Figure 3.10: SIMS depth profile of P atoms in a diamond film grown at ~900°C with four different $PH_3$ concentrations in the gas phase: 2000, 1000, 500 and 100ppm.*

## 3.2 P-doping process using {100}-oriented single crystalline substrates

The discovery of phosphorus doping was strictly limited to {111}-oriented surfaces for a long period of time. As explained in section 1.1.2, where a review of n-type doping in diamond was done, the development of n-type doping on {100}-oriented diamond was achieved 5 years ago (Kato, Yamasaki et al. 2005). The growth parameters were optimized and differ significantly in used $PH_3$ concentrations compared with those for {111} substrates (Kato, Futako et al. 2005; Kato, Yamasaki et al. 2005; Kato, Yamasaki et al. 2005_a; Kato, Watanabe et al. 2006; Kato, Makino et al. 2007; Kato, Makino et al. 2008; Kato, Takeuchi et al. 2008). Even though the electron mobility (at RT) is comparable or even higher to the {111} n-type doping, the layers are quite resistive (Kato, Takeuchi et al. 2008). Motivated by obtaining higher quality doped diamond films, the present study proposes doping of P on {100}-oriented diamond using atypical growth conditions. The present section investigates the P incorporation using a high temperature growth process, as inspired by the work of Teraji et al.

who used them for B-doped {100} diamond specimens (Teraji, Wada et al. 2006).

### 3.2.1 Experimental details: samples and growth parameters

Substrates were commercially available HPHT type Ib {100} single crystalline diamond substrates with a mirror-polished surface. Most of the samples size was 2x2x0.5mm$^3$, except for sample no 61121EP and 70119EP which were 3x3x1mm$^3$. The growth conditions are shown in table 3.3.

*Table 3.3: Growth conditions of {100} P-doped CVD diamonds films, grown at IMO.*

| **Sample code** | **$PH_3/CH_4$ (ppm)** | **Pressure (torr)** | **MW power (W)** | **Temp. (°C)** | **T (h)** |
|---|---|---|---|---|---|
| 60913EP | 100 | 180 | 850 | 1133 | 2 |
| 60920EP | 50 | 180 | 850 | 1131 | 2 |
| 60926EP | 500 | 180 | 955 | 1133 | 2 |
| 61107EP_A | 800 | 180 | 905 | 1132 | 2 |
| 61107EP_B | 100/800 | 180 | 972 | 1132 | 2 ½ |
| 61121EP | 800 | 180 | 766 | 1133 | 8 |
| 70119EP | 1600 | 180 | 692 | 1130 | 2 |
| 70123EP | 800 | 180 | 895 | 1132 | 8 |
| 70404EP | 5000 | 180 | 948 | 1131 | 2 |
| 70416EP | 5000 | 180 | 600 | 852 | 2 |
| 70418EP | 5000 | 180 | 680 | 954 | 2 |

The cleaning procedure is similar as the one described for {111} n-type layers, see section 3.1.1. Also the experimental system used for growing the {100}-oriented doped diamond layers was the same as the one used previously, thus the same gaseous precursors were used. The [$PH_3$]/[$CH_3$] ratio in the source gas was varied from 50 up to 5000ppm and the gas source was 1% $CH_4$. The gas pressure, the $H_2$ gas flow rate and the substrate temperature were 180torr, 495sccm, and ~1130°C, respectively.

### 3.2.2 Surface topography and morphology

The surface topography and morphology of the different phosphine concentration or growth time series of {100} homoepitaxial diamond films are shown in figure 3.11. It is found that the polishing lines seen at the substrate surface are inherited by the P-doped layer (figure 3.11 – c, f, i and l). A closer look at the SEM images (x2000) as depicted in figure 3.11 (e and h) reveals that some specific features appear at the layer surface. From the DICM images figure 3.11 (f, i and l) it is clear that the features appear independent of the $PH_3$ concentration or the growth time. Most probably these defects are caused by the polishing defects present at the substrate surface. The investigations so far show that the periodic structure seen for P-doped layers on {100}-oriented diamond is not present. The so called "step bunching" growth (Kato, Makino et al. 2007) is not observed for our samples.

From the top-view SEM images in figure 3.11 (a, d, g and j) it is clear that the growth process at the edges of the samples is different from the growth seen in the centre (see the arrows in the images). A more evident edge is present when the $PH_3$ concentration or growth time is increased. The SEM image figure 3.11 – k shows an edge detail and a number of non-epitaxial crystallites are identified as the dominant defect structures. It is believed that the formation of non-epitaxial crystallites is attributed to secondary nucleation on the surface in the initial stage of the crystal growth and that non-epitaxial crystallites and pyramidal hillocks are often seen when one tries to grow diamond on {100} homoepitaxial diamond (Kato, Makino et al. 2007).

An important parameter for diamond deposition, except the methane concentration, is the substrate temperature. By modifying this parameter it is possible to control the growth rate and crystalline quality of the layers. For P-doping on {111} and {100}-oriented diamond samples literature usually mentions about 900°C. In order to improve the surface morphology observed when the aforementioned plasma conditions are used to grow P-doped diamond films the effect of temperature was investigated. Figure 3.12 shows the morphology of three P-doped homoepitaxial films grown at temperatures of 1130°C, 954°C and 852°C, respectively.

**diamond substrate**

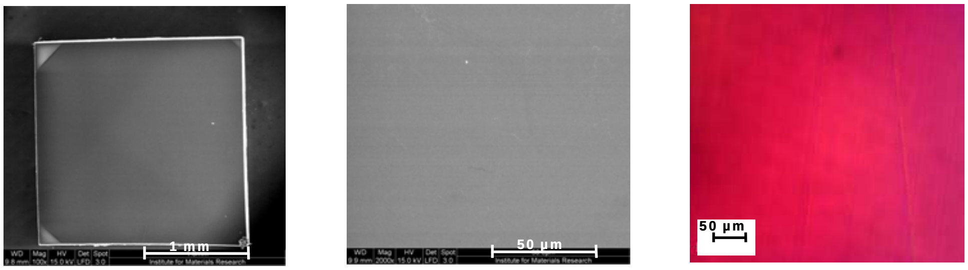

a) b) c)

**500 ppm for 2h**

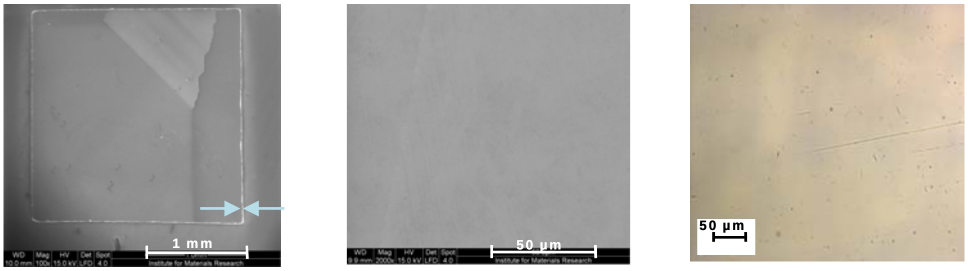

d) e) f)

**800 ppm for 2h**

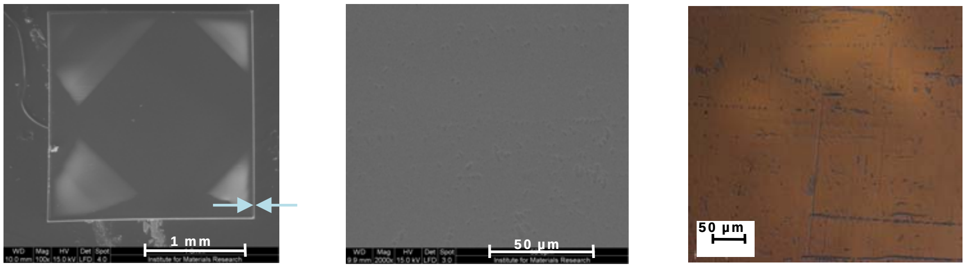

g) h) i)

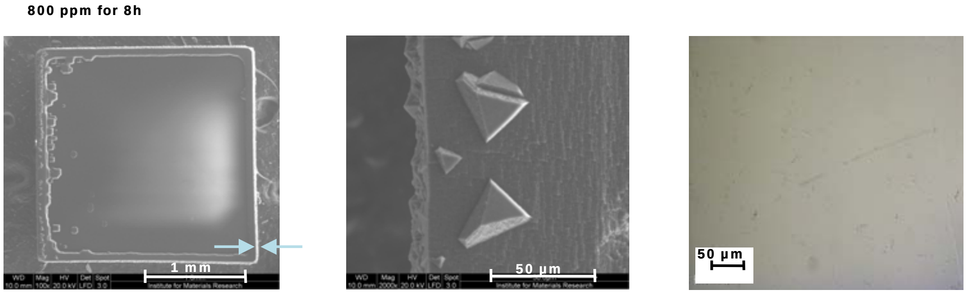

j) k) l)

*Figure 3.11: Comparison of the surface morphology and topography of the diamond substrate (a-c), the sample grown for 2h with 500ppm* $[PH_3]/[CH_4]$*(d-f), the sample grown for 2h with 800ppm* $[PH_3]/[CH_4]$*(g-i) and the sample grown for 8h with 800ppm* $[PH_3]/[CH_4]$*(j-l), respectively. SEM images of the samples are presented in the left hand side and centre positions, while DICM images are positioned in the right hand.*

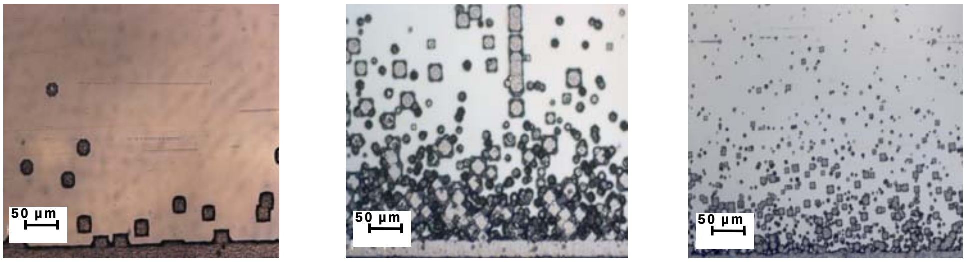

a) b) c)

*Figure 3.12: DICM images of the surface morphology of the samples grown for 2h with 5000ppm* $[PH_3]/[CH_4]$ *with a temperature of 1130°C (a), 954°C (b) and 852°C (c), respectively.*

The morphology at different substrate temperatures ($T_s$), as seen in figure 3.12, is altered. Based on these DICM images one can see a change of the surface morphology with increase of $T_s$. At higher deposition temperatures the non-epitaxial crystallites are mostly restricted at the edge of the specimen and a macroscopically smooth surface towards the centre of the layer is observed. With decreasing $T_s$ the non-epitaxial crystallites are also seen in the central part of the sample. The image of the sample grown at the lowest $T_s$ reveals a decrease in size of the defects and an increase in their density. The abovementioned results lead to the conclusion that in the given plasma parameters the best surface morphology has been obtained at a $T_s$ of ~1130°C.

### *3.2.3 PC investigations*

First PC data regarding a P-doped diamond film deposited homoepitaxially on a {100}-oriented diamond film was presented in 2001 (Haenen, Meykens et al. 2001). For the investigated layer a photoionization onset of 0.85eV was measured. The results suggested that the P atom wasn't incorporated in the substitutional position. The confirmation of the fact that P is incorporated in substitutional sites of the diamond lattice, as a donor, came in 2006 when improved growth conditions were used (Kato, Watanabe et al. 2006).

In this subsection PC data of P-doped {100}-oriented diamond layers grown in high $T_s$ conditions are presented. In figure 3.13 the rising edge of the photoconductivity spectrum is plotted for various $PH_3$ concentrations: 50, 100, 500 and 800ppm. The measurements were obtained by means of coplanar Al contacts. The recording temperature and the electric field were liquid nitrogen temperature (LNT) and $8x10^4$V/m, respectively. For all the investigated samples we can see a dominant photoionization onset around 0.55eV, which is identified as the $X_{P1}$ level (see section 3.1.3). The presence of this level in the spectra indicates that the P incorporation in the investigated diamond layers is done in susbtitutional lattice sites. A further examination of the PC spectra shows the appearance of a new defect level around 1.5eV. The intensity of this defect is more visible for samples with low $PH_3$ concentrations. This defect was noticed before in doped diamonds and multiple assumptions about its origin were made, making a P-related complex unlikely (Haenen 2002; Haenen, Lazea et al. 2007). Nonetheless its origin is unclear up till now and the fact that its appearance is randomly seen makes it difficult to characterize. However, as a similar level is seen in Li-doped, S-doped diamonds probably this is not P-related level.

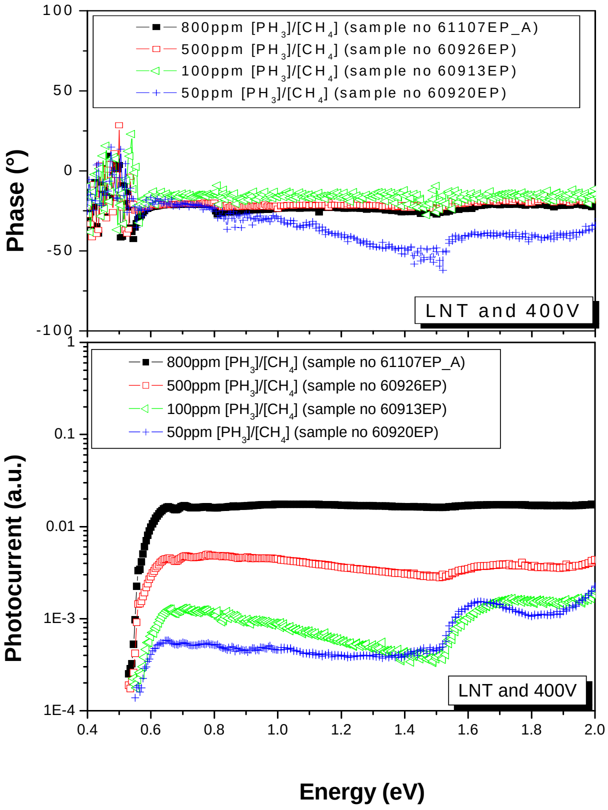

*Figure 3.13: Comparison of the photocurrent spectra for {100}-oriented samples with different PH$_3$ concentrations. The top graph shows the respective phases of the photocurrent signal.*

### *3.2.4 Electrical properties*

The Hall effect measurements for P-doped {100} homoepitaxial diamond layers were performed at the National Institute for Materials Science, Tsukuba, Japan with the courtesy of Dr. T. Teraji. The Hall set-up (ResiTest type 8300, Toyo Corp.) is equipped with a 0.53Tesla magnet for generating the AC-mode B-field. The samples were placed during the experiments in helium ambient. Two different sample holders were used to cover wide temperature range.

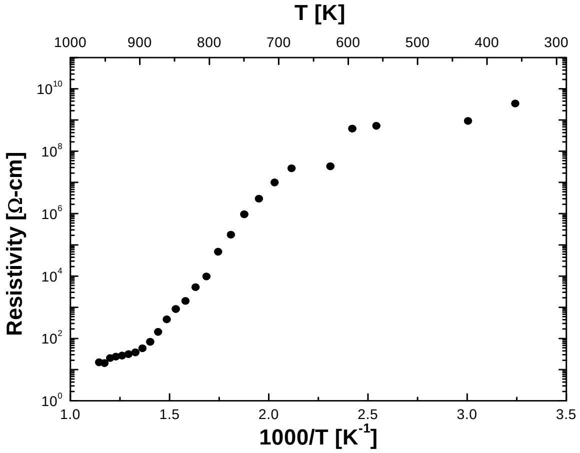

a)

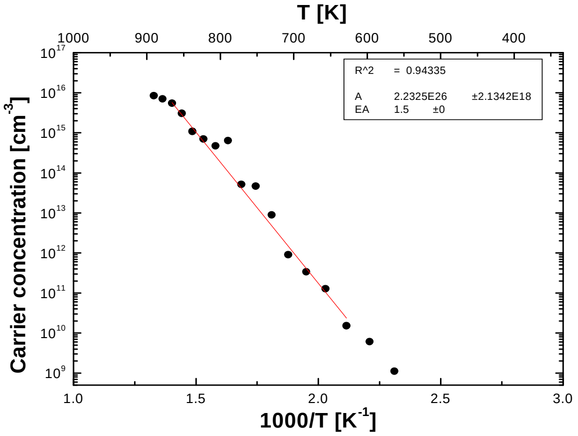

b)

*Figure 3.14: Hall effect measurements: resistance (a) and carrier concentration (b) versus temperature for a sample doped with 800ppm [$PH_3$]/[$CH_4$].*

First one is in the lower temperature range of 77K up to 473K, being controlled with a heater in a LN cryostat. Second one covers the higher range from room temperature to 800°C.The measurement data are collected to computer via GPIB connections through custom written software. In figure 3.14, the results of the electrical measurements for the sample doped with 800ppm [$PH_3$]/[$CH_4$] are displayed.

In the resistance dependence two regimes are observed. At high temperature (T>450K) the exponential behaviour indicates a thermally activated conduction process. The low temperature region is attributed to the hopping conduction (for a more precise definition of this process see section 3.1.4). These observations are consistent with the carrier concentration dependence, where we can observe the same two regimes. The activation energy value deduced at high temperature is 1.5eV. Unfortunately this value is not indicating a P-related complex (Haenen 2002; Haenen, Lazea et al. 2007) (see previous section). Also, due to the high resistivity of the sample neither n-type nor p-type conductivity was confirmed.

The electrical measurements are not confirming the PC results (from which P incorporation into substitutional sites was observed), therefore further investigations are necessary.

### *3.2.5 CL measurements*

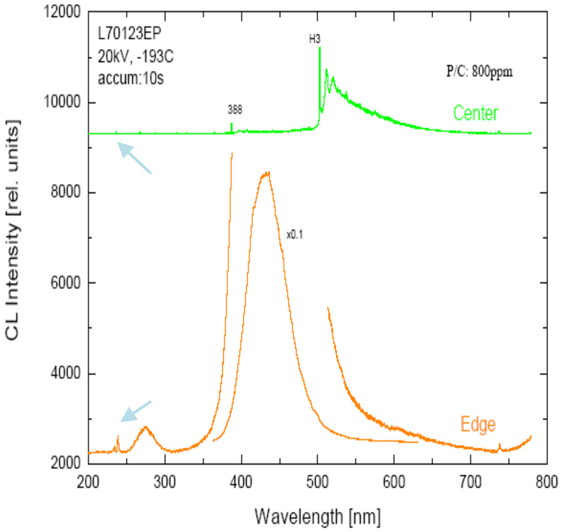

*Figure 3.15: Low temperature (~80K) near-band edge cathodoluminescence (accelerating voltage equal to 20kV). Two spectra were recorded: in the centre (upper spectra) and at the edge (lower spectra) of the sample.*

Confirmation of P incorporation into diamond films comes from three kinds of experiments: photocurrent spectroscopy, infrared spectroscopy and luminescence experiments. The results regarding P doping of {100}-oriented substrates obtained by using the third investigation method are presented in this sub-section. The near-band edge cathodoluminescence (CL) spectroscopy was performed at the National Institute for Materials Science, Tsukuba, Japan, with the courtesy of Dr. T. Teraji. The samples were examined using a SX-40A Scanning Electron Microscope (SEM) (Topcon Ltd.) fitted with a spectrometer and a CCD at 80K with an acceleration voltage of 20kV. The electron beam current was 100nA.

The behaviour, presented in figure 3.15, of the two spectra obtained when the electron beam spot was directed towards different points for the same sample is not identical. The spectrum collected in the sample's centre is similar as the one seen typically for Ib diamond substrates. The zero-phonon line at 503.4nm (2.463eV), often referred as H3 centre, is clearly observed here. This centre is the most common naturally occurring optical feature of nitrogen-containing diamond (Sauer 2003) and it is the dominant peak of this spectrum. The 388nm (3.18eV) peak is reported to be related to defects which are often formed by ion irradiation. A P-related bound exciton peak around 240nm (5.16eV) is not seen (notice the arrow in the figure 3.15).

The spectrum collected at the sample edge is presenting a strong broad signal with a maximum at 430.5nm (2.88eV). It is the band A, the most commonly observed CL emission peak of epitaxial CVD diamond grown films. It is generally attributed to extended defects such as dislocations (Sauer 2003). In addition to this peak, a P-related bound exciton peak was observed here (notice the arrow in the figure 3.15). Its position is centred around 240nm (5.16eV) and is attributed to TO-phonon assisted recombination from a phosphorous impurity. This spectrum indicates successful incorporation of phosphorus in the investigated region.

The results of CL investigations indicate that P incorporation takes place only at the edge of the sample. When correlation between the CL spectra and the microscopy observations is made (see figure 3.11 – j, k and l) one can speculate that the P incorporation is possible due to the presence of non-epitaxial crystallites which present micro facets of different orientations.

To summarize, from the CL results it is clear that P incorporation in {100}-oriented diamond samples is not homogeneous and is restricted to the edges of the samples. Therefore we can categorize it as unsuccessful, contrary to the PC results presented in sections section 3.2.3.

The aforementioned conclusions lead to the repetition of PC measurements. Figure 3.16 presents two PC spectra taken on a sample with 5000ppm $[PH_3]/[CH_4]$. The only difference between the spectra is the contact configuration: coplanar geometry or interdigital configuration (for details see section 2.2.1.3). When using coplanar Al contacts (which cover most of the samples surface, including the edge region) the presence of the P-related level is detected. Unfortunately, when using the other contacts configuration, with interdigital geometry (these contacts are located in the centre of the sample) the P-related peak is no longer present. Thus, the conclusion of the PC investigations is supporting the observations from the CL measurements. And therefore the P-incorporation in {100}-oriented diamond samples, using the growth conditions presented in section 3.2.1, was not successful.

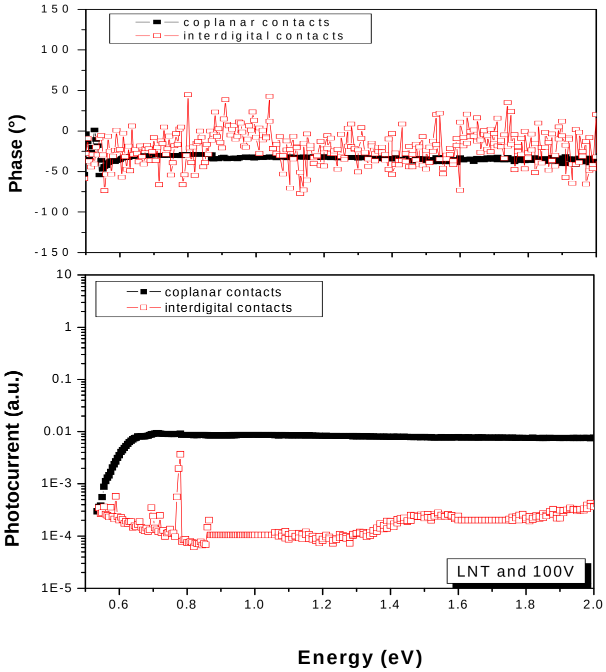

*Figure 3.16: The influence of contact geometry when recording PC spectra for a sample doped with 5000ppm [PH$_3$]/[CH$_4$]. The top graph reveals the respective phases of the photocurrent signal.*

## 3.3 Conclusions

In this chapter, experimental results obtained by different characterization techniques are presented. The phosphorus incorporation in the single crystalline diamond samples, oriented along {111} and {100} crystallographic directions, was investigated.

The quality of P-doped {111}-oriented diamond layers was investigated first by surface imaging techniques, and some pre-treatment procedures, prior to the growth step, were presented. The most effective pre-treatment for improving the layers surface morphology proved to be an oxygen containing plasma. The photocurrent measurements provided information about the P incorporation into the neutral substitutional site.

Surprisingly, a second P-related defect was observed for our samples ($X_{P2}$) and an investigation of its character was tried. The presence of P-related features in the PC spectra indicates a successful incorporation of P into {111}-oriented samples, results confirmed also by Hall measurements. The quality of our layers, as seen from SIMS spectra, was proven to be in good agreement with the experimental results obtained by other groups. Thus, it is concluded that qualitative P-doped {111}-oriented diamonds (with a mobility of $2cm^2V^{-1}s^{-1}$ at RT) can be obtained at IMO.

The results regarding P-doped {100}-oriented diamond layers are presented in the second part of the chapter. The particularity of these growth conditions was mainly the high $T_s$. As it was done for {111}-oriented sample, the surface morphology was studied by multiple surface imaging techniques. The investigations reveal surprisingly defect free morphologies. Confirmation of P incorporation into the layers was done, as previously seen, by defect spectroscopy technique (PC experiments). The presence of the substitutional P-level in the low-temperature PC spectra was presented and thus a first conclusion was drawn: successful P incorporation into {100}-oriented diamond layers was achieved. Further investigations of the PC spectra reveal, aside from the P-related peak, a new peak. This defect, situated around 1.5eV, is more pronounced when the $PH_3$ concentration is decreased. Unfortunately, the P incorporation into the investigated specimens wasn't supported by electrical measurements or by CL investigations. The observations indicate that P incorporation was observed only at the edges of the samples, where non-epitaxial crystallites were present. A confirmation of this theory was done when PC spectra were measured using different electrode configuration.

In conclusion, the results presented in this chapter indicate that high quality phosphorus-doped diamond layers can be reproducible produced in our laboratory when {111}-oriented samples are used. Unfortunately, the doping procedure failed when {100}-oriented samples were used.

## 3.4 References

Haenen, K. (2002). Opto-electronic study of phosphorous-doped n-type and hydrogen-doped p-type CVD diamond films. Diepenbeek, Limburgs Universitair Centrum. **PhD**.

Haenen, K., A. Lazea, et al. (2007). "Phosphorus doping of microcrystalline CVD diamond using modified conditions." Materials Research Society Symposium Proceedings **1093**: 1093-P17-01.

Haenen, K., K. Meykens, et al. (1999). "Low temperature photoconductivity detection of phosphorus in diamond." Physica Status Solidi a-Applied Research **174**(1): 53-58.

Haenen, K., K. Meykens, et al. (2000). "The electronic structure of phosphorus in n-type CVD diamond films: Revised." Physica Status Solidi a-Applied Research **181**(1): 11-16.

Haenen, K., K. Meykens, et al. (2000_a). "Temperature dependent spectroscopic study of the electronic structure of phosphorus in n-type CVD diamond films." Diamond and Related Materials **9**(3-6): 952-955.

Haenen, K., K. Meykens, et al. (2001). "Phonon-assisted electronic transitions in phosphorus-doped n-type chemical vapor deposition diamond films." Diamond and Related Materials **10**(3-7): 439-443.

Haenen, K., K. Meykens, et al. (1999_a). "Study of the electronic structure of the phosphorus level in n-type CVD diamond." Physica Status Solidi a-Applied Research **174**(1): R1-R2.

Haenen, K., M. Nesladek, et al. (2004). "The phosphorus level fine structure in homoepitaxial and polycrystalline n-type CVD diamond." Diamond and Related Materials **13**: 2041-2045.

Kato, H., W. Futako, et al. (2005). "Growth of phosphorus-doped diamond using tertiarybutylphosphine and trimethylphosphine." Diamond and Related Materials **14**: 340-343.

Kato, H., T. Makino, et al. (2007). "N-type diamond growth by phosphorus doping on (001)-oriented surface." Journal of Physics D-Applied Physics **40**(20): 6189-6200.

Kato, H., T. Makino, et al. (2008). "N-type diamond growth by phosphorus doping." Diamond Electronics - Fundamentals to Applications II **1039**: 39-48.

Kato, H., D. Takeuchi, et al. (2008). "Electrical activity of doped phosphorus atoms in (001) n-type diamond." Physica Status Solidi a-Applications and Materials Science **205**(9): 2195-2199.

Kato, H., H. Watanabe, et al. (2006). "N-type doping on (001)-oriented diamond." Diamond and Related Materials **15**(4-8): 548-553.

Kato, H., S. Yamasaki, et al. (2005). "Growth and characterization of phosphorus-doped diamond using organophosphorus gases." Physica Status Solidi a-Applications and Materials Science **202**(11): 2122-2128.

Kato, H., S. Yamasaki, et al. (2005). "n-type doping of (001)-oriented single-crystalline diamond by phosphorus." Applied Physics Letters **86**(22): 222111_1-222111_3.

Kato, H., S. Yamasaki, et al. (2005_a). "n-type conductivity of phosphorus-doped homoepitaxial single crystal diamond on (001) substrate." Diamond and Related Materials **14**(11-12): 2007-2010.

Koizumi, S. (1999). "Growth and characterization of phosphorus doped n-type diamond thin films." Physica Status Solidi a-Applied Research **172**(1): 71-78.

Koizumi, S. (2003). n-Type diamond growth Thin-film diamond I. C. Nebel and J. Ristein, Elsevier, ISBN 0-12-752185-2, Semiconductors and Semimetals. **76:** 239-260.

Koizumi, S., M. Kamo, et al. (1997). "Growth and characterization of phosphorous doped {111} homoepitaxial diamond thin films." Applied Physics Letters **71**(8): 1065-1067.

Koizumi, S., M. Suzuki, et al. (2008). n-Type doping of diamond. Physics and applications of CVD diamond. S. Koizumi, C. Nebel and M. Nesladek, Wiley-VCH Verlag GmbH & Co. KGaA, ISBN 978-3-527-40801-6**:** 237-256.

Kravets, R. (2005). Fourier transform phocurrent spectroscopy of CVD diamond. Prague, Czech Technical University of Prague & Institute of Physics Academy of Science of the Czech Republic. **PhD**.

Nesladek, M. (2005). "Conventional n-type doping in diamond: state of the art and recent progress." Semiconductor Science and Technology **20**(2): R19-R27.

Nesladek, M., K. Haenen, et al. (2003). Optical properties of CVD diamond. Thin film diamond I. C. Nebel and J. Ristein, Semiconductors and Semimetals, Elsevier, ISBN 0-12-752185-2. **76:** 325-378.

Nesladek, M., K. Meykens, et al. (1999). "Photocurrent and optical absorption spectroscopic study of n-type phosphorus-doped CVD diamond." Diamond and Related Materials **8**(2-5): 882-885.

Nesladek, M., K. Meykens, et al. (1999_a). "Low-temperature spectroscopic study of n-type diamond." Physical Review B **59**(23): 14852-14855.

Sauer, R. (2003). Luminescence from optical defects and impurities in CVD diamond. Thin-film diamond I - Semiconductors and semimetals. C. Nebel and J. Ristein, ISBN 0-12-752185-2, Elsevier **76:** 239-452.

Tavares, C., S. Koizumi, et al. (2005). "Effects of RIE treatments for {111} diamond substrates on the growth of P-doped diamond thin films." Physica Status Solidi a-Applications and Materials Science **202**(11): 2129-2133.

Teraji, T. (2006). "Chemical vapor deposition of homoepitaxial diamond films." Physica Status Solidi a-Applications and Materials Science **203**(13): 3324-3357.

Teraji, T., H. Wada, et al. (2006). "Highly efficient doping of boron into high-quality homoepitaxial diamond films." Diamond and Related Materials **15**(4-8): 602-606.

Wada, H., T. Teraji, et al. (2005). "Growth and characterization of P-doped CVD diamond (111) thin films homoepitaxially grown using trimethylphosphine." Applied Surface Science **244**: 305-309.

Yamamoto, M., T. Teraji, et al. (2005). "Improvement in the crystalline quality of homoepitaxial diamond films by oxygen plasma etching of mirror-polished diamond substrates." Journal of Crystal Growth **285**(1-2): 130-136.

# 4 Growth of phosphorous-doped layers on {110}-oriented diamond substrates

The reproducible and efficient n-type doping of phosphorus of {111} and {100}-homoepitaxial diamond has been successfully achieved since 1997 (Koizumi, Kamo et al. 1997; Koizumi 2003) and 2005 (Kato, Yamasaki et al. 2005), respectively. In contrast, only a few attempts reported doping of P into {110}-oriented films (Nesladek, Haenen et al. 2003). In this chapter only the results regarding phosphorus incorporation into {110}-oriented diamond films are presented, either in polycrystalline or single crystalline specimens. The doping results of the growth process on polycrystalline substrates using similar conditions as for {111} homoepitaxial growth are presented in sub-section 4.1.1, while the results concerning doping of P into polycrystalline substrates using modified plasma parameters are discussed in sub-section 4.1.2. In the second half of this chapter the first results regarding P incorporation on single crystalline {110}-oriented diamonds are presented. The chapter finishes presenting conclusions on doping on {110}-oriented diamond substrates.

## 4.1 P-doping on polycrystalline substrates

For a long time the preparation of P-doped diamond layers was limited to single crystalline diamonds. These substrates are still small, typically 3x3mm$^2$, thus making it difficult to process and manipulate the samples for diamond-based applications. The aforementioned restriction is imposing severe limitations from industrial point of view and in an attempt to overcome this impediment, growth of polycrystalline P-doped n-type diamond layers was proposed (Nesladek, Haenen et al. 2003). The first results were obtained using a growth strategy based on the fact that the addition of $PH_3$ into the gas phase strongly prefers {111}-oriented growth. The layers grown using this logic presented evidence of P incorporation and fabrication of bipolar devices was possible (Nesladek, Haenen et al. 2003; Nesladek 2005). In this section research is focused on using the same logic for P doping of polycrystalline {110}-oriented diamond layers and a complete set of experimental techniques is used to investigate the thin P doped diamond films. A specific set of new plasma growth conditions is also proposed and a comparison is made between the results obtained when using the two different doping procedures.

### *4.1.1 Experimental details and results for layers grown using conventional plasma parameters*

#### *4.1.1.1 Growth conditions*

To study P incorporation into polycrystalline diamonds, round shape polished {110}-textured CVD diamond plates of about 3mm diameter are used as substrates (Nesladek, Haenen et al. 2003) (see figure 4.1). The substrates were grown on top of 2 inch diameter Si wafer by the MW PE CVD process in an ASTeX AX6500 machine using 3% $CH_4$ in $H_2$ (figure 4.1 a). The microwave power and pressure were 6000W and 110torr, respectively. The substrate temperature during substrate growth was measured by an optical pyrometer and varied between 850 and 900°C during the total process. Total duration of the growth was 550h resulting in a 1.2mm thick polycrystalline diamond layer. Hence a growth rate of ~2.2μm/h could be established.

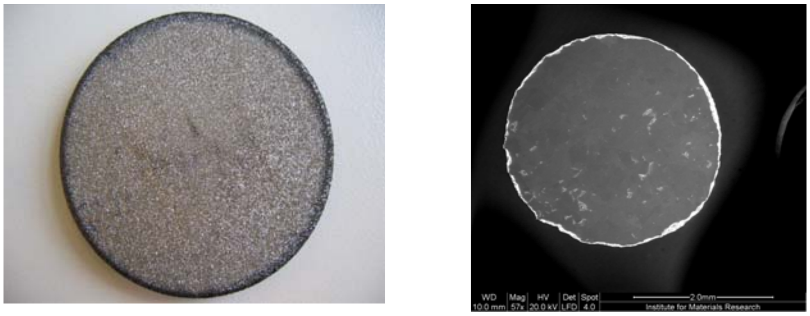

a) b)

*Figure 4.1: a) OM image of a 2inch {110}-oriented CVD polycrystalline diamond plate, b) Scanning Electron Microscopy picture of a {110}-oriented CVD polycrystalline substrate with a diameter of 3mm, cut out from the 2inch free standing CVD diamond plate and mechanically polished.*

P-doping experiments were performed in the same commercial available ASTeX system used for the growth described in the previous chapter. The source gases used were 0.05% methane (99.99% - 4N purity) and $PH_3$ (99.9999% - 6N purity), diluted in $H_2$ (99.9999999% - 9N purity). The $H_2$ flow was 500sccm and the rest of the growth conditions are shown in table 4.1. These parameters are typically used to obtain lightly P-doped epitaxial films on {111} substrates (Katagiri, Isoya et al. 2004). After 2h deposition time a ~2μm thick film was obtained.

Prior to any growth process or investigation procedure, the polycrystalline diamond specimens were chemically cleaned, as described for the single crystalline samples in section 3.1.1.

*Table 4.1: Growth conditions of the P-doped polycrystalline {110} CVD diamonds grown at IMO.*

| **Sample code** | **$PH_3/CH_4$ (ppm)** | **Pressure (torr)** | **MW power (W)** | **Temp. (°C)** |
|---|---|---|---|---|
| 60627PP | 500 | 100 | 668 | 887 |
| 60705PP | 1000 | 100 | 643 | 875 |
| 60706PP | 1000 | 100 | 600 | 861 |
| 60707PP | 1000 | 100 | 625 | 893 |
| 60714PP | 1000 | 100 | 755 | 890 |
| 60724PP | 1000 | 100 | 800 | 855 |
| 60728PP | 1000 | 100 | 725 | 807 |
| 60731PP | 1000 | 100 | 666 | 893 |

#### *4.1.1.2 Surface topography, morphology and microstructural analysis before and after growth*

To study the surface topography and morphology of P-doped diamond layers DICM and AFM investigations were performed. Figure 4.2 is showing the surface images before and after the growth of the P-doped layer, doped with 1000ppm $PH_3$. The polycrystalline substrate surfaces are macroscopically flat and microscopic defects due to the polishing procedure can be observed in the AFM image (figure 4.2 a, b). After the growth of the P-doped layer (figure 4.2 c, d and e) the surface investigations lead to the conclusion that preferential growth takes place. It is obvious that the plasma exposure affects the neighbouring grains differently. The AFM images show that neighbouring grains present different morphology and the values of the root mean square surface roughness ($R_{rms}$) for a 5x5μm$^2$ scanned area is not identical. Some of the {110} grains seem to be composed of macroscopic highly oriented {111} terraces, declined from the perfect {110} orientation. This behaviour is seen in figure 4.2 e.

The orientation of the grains of the doped polycrystalline diamond with respect to the substrate grains is investigated by electron backscatter diffraction (EBSD). Figure 4.3 shows the grain texture with respect to the film normal direction (IPF // Z), {110} texture component distribution (in plane) and pole figures for a polycrystalline diamond substrate.

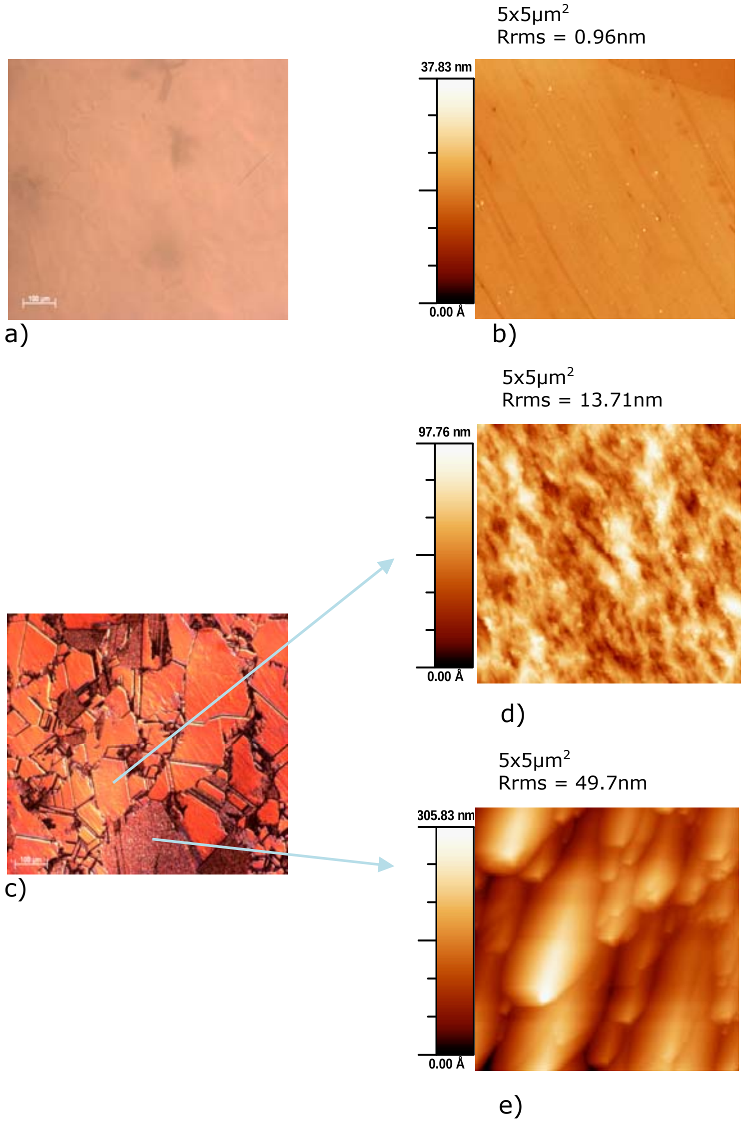

*Figure 4.2: Surface topography and morphology for a polycrystalline diamond specimen before (a – DICM image, b – AFM picture) and after growth of a 1000ppm P-doped layer (c – DICM image, d and e – AFM pictures).*

The step size (i.e. distance between two measured data points) used in these mappings was 20nm. As can be seen from the map presented in figure 4.3 - a, most of the grains have the {110} plane more or less parallel to the film surface (i.e. the green coloured grains for the IPF // Z map), but have different misorientation angles from the perfect {110} orientation. This is represented in the texture component map, figure 4.3 b.

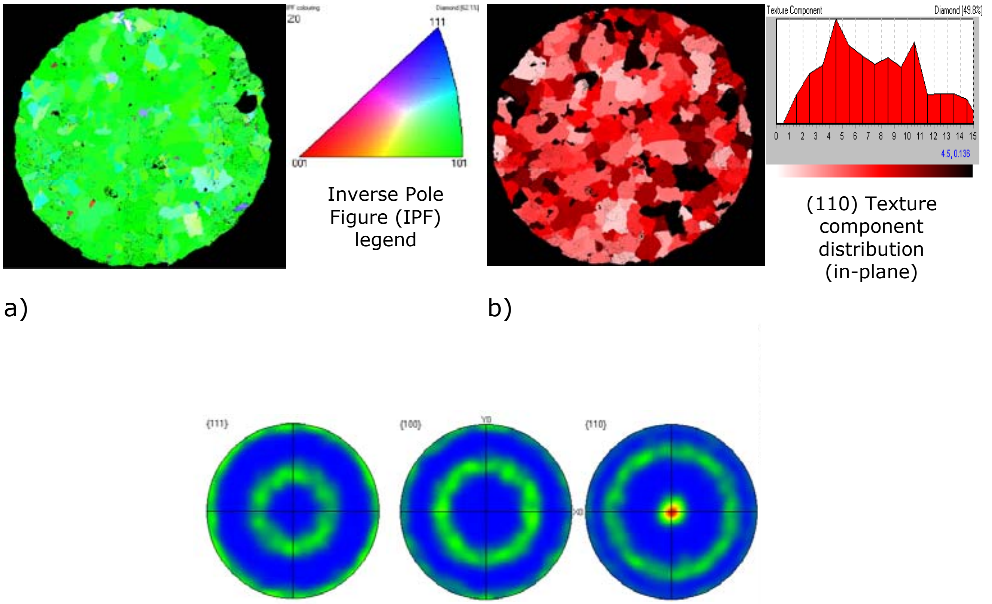

a)

b)

c)

*Figure 4.3: Top view EBSD mappings of the polycrystalline diamond substrate with 3mm diameter. The confirmation of the {110} orientation of the grains is seen in the Inverse Pole Figure mapping (a), which shows the crystallographic orientation of the surface for the individual crystallites. A unit triangle colouring scheme is presented as legend. A texture component {110} image (b) reveals the misorientation angles form the perfect {110} orientation for every grain. The preferential orientation of the data points, presented in the pole figure (c), is given related to the main crystal orientations: {100}, {111} and {110}, respectively.*

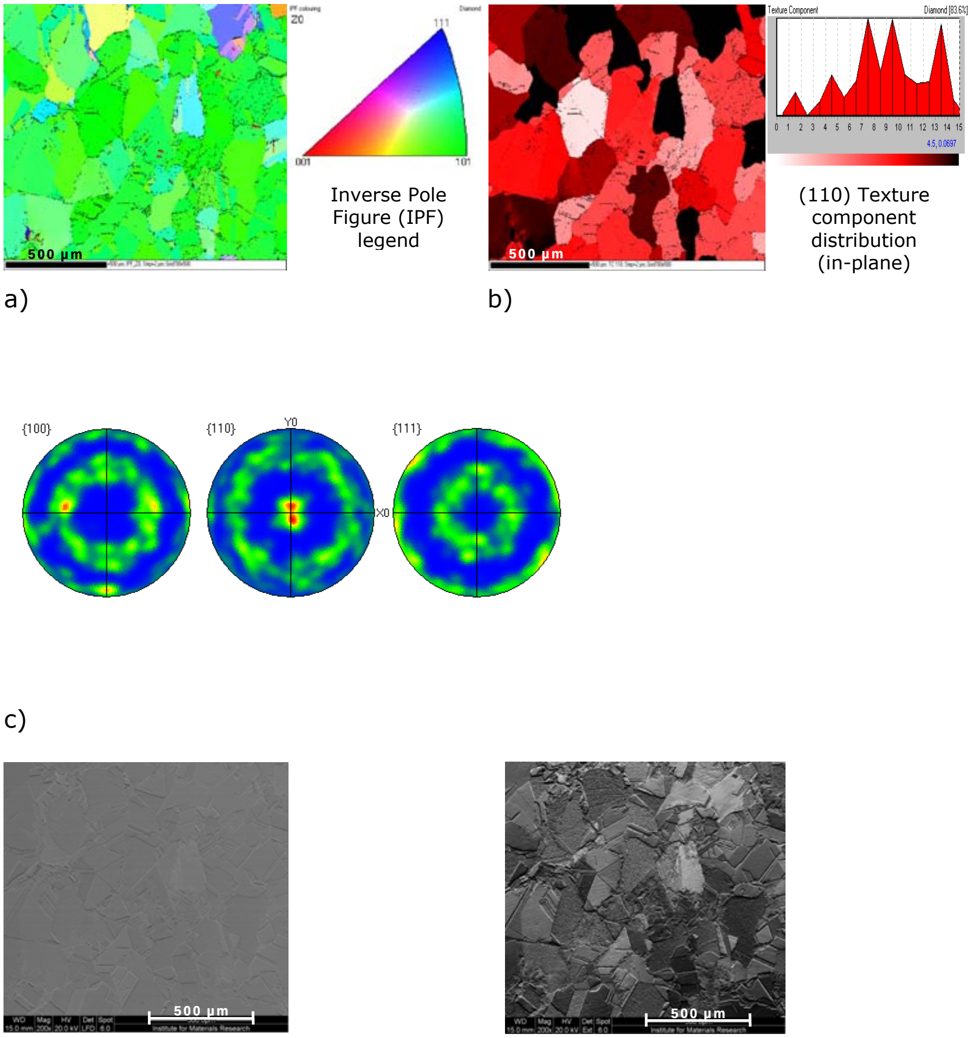

*Figure 4.4: Top view EBSD mappings and SEM images in the centre of the P-doped polycrystalline diamond specimen, doped with 1000ppm $PH_3$. a) IPF image, b) {110} texture component map, c) illustration of pole figure, d) SEM topography image (forward BSE image) and e) SEM orientation contrast and topography image.*

The scale graph of the misorientation angle is ranging from 0° to 15°. Depending on the specific orientation of each data point, a colour was attributed and thus brighter colours correspond to grains whose orientation is closer to the perfect {110} orientation, while darker grains have a larger off-angle.

As can be seen from figure 4.3 b most of the grains present a misorientation angle of less than 12°. An alternative way to present the texture of the grains for a polycrystalline diamond film is on pole figure contour plots, as shown on figure 4.3 c. The pole figures are shown for the main crystallographic planes: {100}, {111} and {110}. From the pole figures a strong {110} texture is suggested.

The influence of the growth procedure upon the grains of the polycrystalline diamond is illustrated in figure 4.4. Careful examination of the IPF mapping shows that grains with other colours than the green colouration, previously seen in the case of the polycrystalline substrate, now appear. From the representation of {110} texture components (figure 4.4 – b) it can be determined that after the growth of the P-doped layer the misorientation angle of the majority of the grains now reach a maximum of 15°. Thus, the {110} texture shown in the pole figure for the grown layer is now not that well defined, figure 4.4 – c. By looking at the grains topography shown in the SEM pictures (figure 4.4 d and e) the same conclusion can be drawn, as it was presented earlier in the DICM and AFM images, thus the neighbouring grains are affected differently by the plasma exposure.

#### *4.1.1.3 PC investigations*

The P-incorporation was investigated by photocurrent measurements. The detection of optically active P in the polycrystalline films grown at IMO is presented in figure 4.5.

The figure compares a PC spectrum of a {110}-oriented polycrystalline film with one taken on a {111}-oriented single crystalline layer deposited on a synthetic type Ib HPHT crystal (Sumitomo Electric Ltd.). Both were grown with the same plasma parameters used to lightly dope P into CVD diamond (see section 4.1.1.1). The same amount of $PH_3$ concentration was used in the gas mixture: 1000ppm. Both spectra clearly show the photoionisation related to substitutional phosphorus situated around 0.56eV (Nesladek, Meykens et al. 1999_a). This indicates successful incorporation of the phosphorus donor. However, for the polycrystalline sample the oscillatory conductivity is obviously less pronounced, while photothermal ionisation peaks cannot be seen on the rising edge of the photocurrent (Haenen, Nesladek et al. 2004).

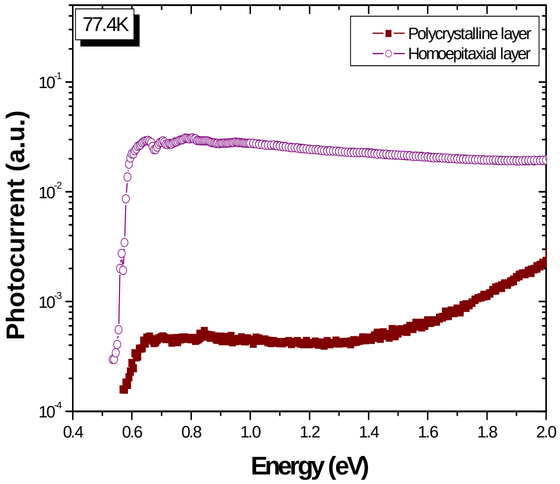

*Figure 4.5: Comparison between PC spectra taken at liquid nitrogen temperature between a {111}-oriented single crystalline and a mainly {110}-oriented polycrystalline diamond layer grown using the same conditions as the single crystalline specimen. Both are doped with 1000ppm* $[PH_3]/[CH_4]$.

In addition, these conditions lead to the presence of an extra absorption edge around 1.5eV for the polycrystalline sample. A similar level with an activation energy ~1.5eV has been seen in several CVD diamond films from different origin (Nesladek, Meykens et al. 1996; Zeisel, Nebel et al. 2000; Garrido, Nebel et al. 2002; Sternschulte, Schreck et al. 2003; Hoffman, Andrienko et al. 2005), making a P-related complex unlikely (see chapter 3). Even so, the nature of this defect remains unknown. These differences between the investigated samples clearly indicate that the layer grown on top of the single crystalline specimen has a much stronger photosensitivity and thus we can conclude that the homoepitaxial layer has a higher P-incorporation or a higher $\mu\tau$ product, where $\mu$ is the carrier mobility and $\tau$ the carrier lifetime.

Based on the above measurements we can conclude that polycrystalline CVD diamond films with active P-incorporation can be prepared when lightly P-doped plasma parameters are used. Unfortunately their quality is rather low when compared with single crystalline doped samples. One way to improve the layer quality is to grow polycrystalline films using modified growth parameters, which will be explained in the next section.

### 4.1.2 Experimental details and results for layers grown using modified plasma parameters

#### 4.1.2.1 Growth conditions

The set of growth conditions used for P-doping experiments, revealed in this subsection, represents the innovative part of the thesis. There are significant differences between this set of doping parameters and the set previously presented (see subsection 4.1.1.1), substrate temperature and $[CH_4]/[H_2]$ being the main ones (Lazea, Mortet et al. 2008). The complete sets of parameters are shown in table 4.2. The deposition time was fixed to 2h, leading to layer thicknesses of approximately 20µm. The gas pressure, the $H_2$ gas flow rate, the substrate temperature and the methane concentration were 180torr, 495sccm, ~1130°C and 1% $[CH_4]/[H_2]$, respectively. The choice for these particular conditions, presented as being atypical for P doping, was inspired by the work of Teraji et al. who also used higher than conventional methane concentrations and growth temperatures for the growth of high quality boron-doped homoepitaxial diamond (Teraji, Arima et al. 2004).

*Table 4.2: Novel growth conditions used for P doping of polycrystalline {110} CVD diamonds grown at IMO.*

| **Sample code** | **$PH_3/CH_4$ (ppm)** | **$CH_4/H_2$ (%)** | **Pressure (torr)** | **MW power (W)** | **Temp. (°C)** |
|---|---|---|---|---|---|
| 61110PP | 800 | 1 | 180 | 700 | 1133 |
| 61122PP | 500 | 1 | 180 | 665 | 1131 |
| 61128PP | 50 | 1 | 180 | 685 | 1132 |
| 61208PP | 100 | 1 | 180 | 694 | 1130 |
| 70329PP | 5000 | 1 | 180 | 668 | 1131 |
| 70405PP | 10000 | 1 | 180 | 642 | 1133 |
| 70420PP | 2000 | 1 | 180 | 635 | 1133 |
| 70503PP | 2000 | 1 | 180 | 820 | 1132 |
| 70608PP | 800 | 1 | 180 | 820 | 1134 |
| 80306PP | 200 | 1 | 180 | 775 | 1136 |
| 80307PP | 2000 | 1 | 180 | 745 | 1137 |
| 80506PP | 500 | 1 | 180 | 725 | 1138 |

#### 4.1.2.2 Surface topography, morphology and microstructural analysis before and after the growth

Figure 4.6 presents DICM and AFM pictures of a phosphorus doped layer grown using the new set of conditions. The grain boundaries are clearly seen in figure

4.6 - a and no preferential growth is present (Nesladek, Haenen et al. 2003). The AFM investigations (figure 4.6 b) reveal a microscopically rough surface and the root mean square surface roughness ($R_{rms}$) on average is ~ 90nm for a 5x5µm$^2$ scanned area. Compared with figure 4.2 d and e, where the polycrystalline sample grown using typical doping conditions is presented, the $R_{rms}$ is drastically increased and the morphology of the grains is completely changed.

From figure 4.7, which shows electron back-scattered diffraction (EBSD) images of a polycrystalline diamond sample before and after P doping, one can obtain crystallographic information when the growth is done using the nonconvetional set of plasma parameters. Depending on the specific orientation of each data point, a colour was attributed, as seen in the colour legend next to the images, giving information on the evolution of grains after the growth. As can be seen from the images the grain orientation is not modified after the growth and this proves that this particular set of plasma conditions does not influence the growth of the {110}-oriented surfaces in a similar way as in section 4.1.1.2.

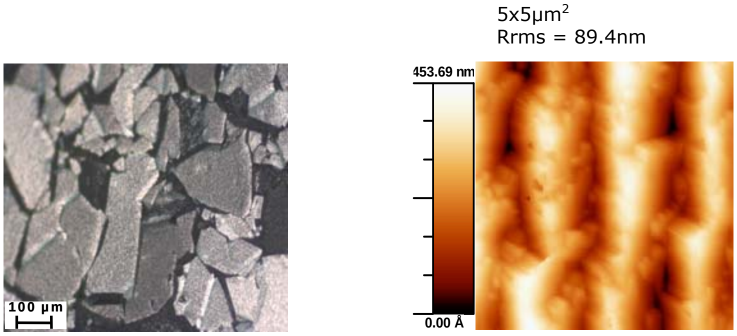

a) b)

*Figure 4.6: Surface morphology of the polycrystalline sample grown using the novel plasma parameters and doped with 500ppm [$PH_3$]/[$CH_4$] where: a) DICM image in the centre of the sample and b) AFM image of the grain surface.*

Figure 4.8 shows a SEM topography image, an EBSD texture component map and pole figures of the same polycrystalline sample as presented before. The SEM image presented in figure 4.8 confirms the non-preferential growth of the grains seen with DICM (figure 4.6 a). The degree of tilt from the ideal {110} orientation is shown in the EBSD texture component map (figure 4.8 b). Bright colours correspond to grains whose orientation is closer to the perfect {110} orientation, while darker grains have a larger off-angle. Nevertheless, the majority of grains have a tilt of less than 12° from the above mentioned orientation.

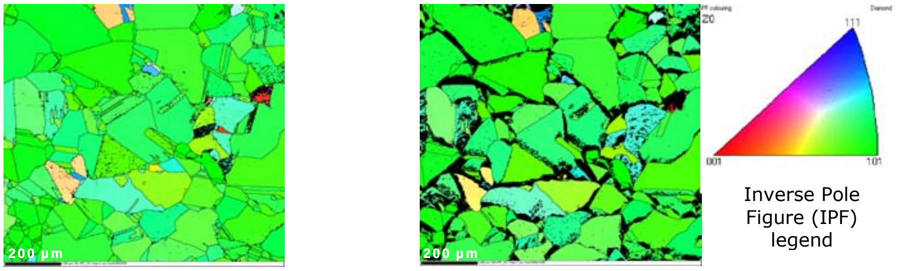

Inverse Pole Figure (IPF) legend

a) b)

*Figure 4.7: Comparison of EBSD mappings of the same polycrystalline diamond substrate: (a) before and (b) after the growth of a P-doped layer with 800ppm [$PH_3$]/[$CH_4$].*

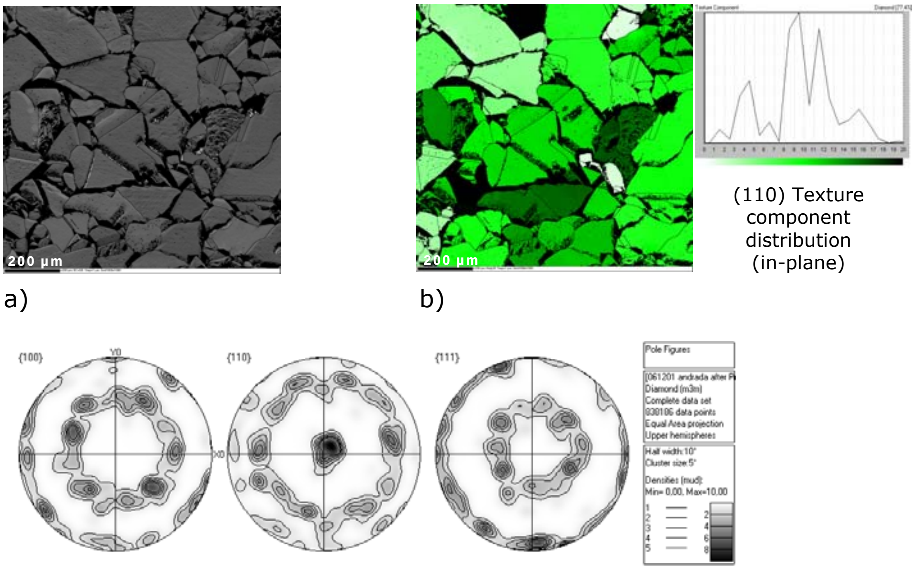

(110) Texture component distribution (in-plane)

a) b)

c)

*Figure 4.8: a) SEM topography image of a polycrystalline diamond film grown for 800ppm [$PH_3$]/[$CH_4$], b) EBSD texture component map (1x1mm$^2$) of the same sample illustrating the degree of tilt from the perfect (110) direction for each diamond grain on a). The scale bar ranging from 0° to 20° indicates that the majority of grains have a tilt of less than 12° compared with the perfect {110} orientation. c) {100}, {111} and {110} pole figure contour plots of the same sample as in images a) and b).*

According to this analysis the grain orientation after growth remains unmistakably {110}, with all grains showing continued growth when compared with the substrate. The pole figure presented in figure 4.8 c is showing a strong {110} texture, which is in agreement with the observation seen for the polycrystalline substrate (see figure 4.3). These results point to a first indication that the employed conditions in combination with a phosphine containing gas mixture does not prohibit growth of {110}-oriented surfaces (Lazea, Mortet et al. 2008).

#### *4.1.2.3 PC and FTPS investigations*

To study the incorporation of phosphorus and possible unwanted defects, quasi-steady-state photocurrent measurements (PC) and Fourier-Transform Photocurrent Spectroscopy (FTPS) were performed. The details of the techniques were described previously in section 2.2, chapter 2. Figure 4.9 presents the subsequent photocurrent signals of four P-doped polycrystalline layers, doped with 50ppm, 100ppm, 500ppm and 800ppm, respectively. Remarkably, the signal becomes much stronger and richer in details for all the investigated samples when compared with the PC spectra taken for the polycrystalline sample grown with conventional plasma parameters, see figure 4.5. Now all the samples present the so-called oscillatory photoconductivity.

The first order minimum is the most pronounced one and it becomes broadened as the phosphine concentration increases. All this can be considered a direct proof that the novel set of doping conditions presented in this chapter lead to an incorporation of substitutional phosphorus on {110}-orientated substrates. Moreover, the defect level at higher energy has disappeared. It is speculated that this is due to the higher substrate temperature during deposition, removing the defect.

Comparing the photoresponse obtained at identical electric fields ($2x10^4$V/m) for different doping levels also reveals that an increase of the dopant concentration in the gas phase leads to a shift of the photocurrent onset towards lower energy values. For the 800ppm doped sample, photocurrent can be detected as low as 485meV, more than 100meV below the ionisation energy of the phosphorous donor (which is ~560meV) (Nesladek, Meykens et al. 1999_a). This result can be explained by impurity-assisted electron tunnelling, i.e. in samples with a higher incorporation of phosphorus, the donor atoms are closer to each other faciliting tunnelling of the electrons. A similar shift induced by using higher electrical fields has already been reported for {111} single crystalline layers doped with P (Knuyt, Haenen et al. 2006). In addition, the signal intensity also increased with the dopant concentration sustaining the statement that more P can be found in these layers.

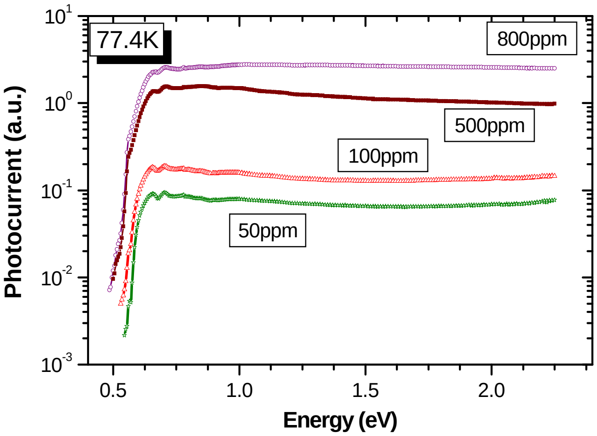

*Figure 4.9: Comparison of PC spectra taken at liquid nitrogen temperature for {110}-oriented polycrystalline layers grown using the novel set of plasma parameters with different [$PH_3$]/[$CH_4$] ratios.*

In order to obtain details of the electronic structure regarding the incorporated phosphorus an even more sensitive technique, such as FTPS, can be used. Figure 4.10 shows a comparison between the PC and FTPS spectra obtained for a sample doped with 800ppm. The FTPS spectra didn't reveal new electronic levels in the P energy level structure due to phosphorus excited states (Haenen, Nesladek et al. 2004). All the peaks were previously seen in the PC spectra. The only difference is a slight improvement regarding the sharpness of the peaks. Nevertheless, it has to be noted that FTPS is a technique that is faster than conventional PC (Vanecek and Poruba 2002).

Thus, it can be concluded that a first confirmation of the P incorporation into the polycrystalline {110} diamond samples grown with novel plasma parameters has been given by defect spectroscopy techniques.

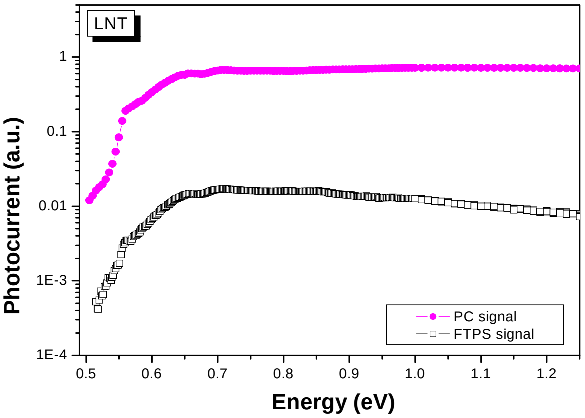

*Figure 4.10: PC and FTPS spectra taken at liquid nitrogen temperature on a 800ppm [$PH_3$]/[$CH_4$] doped polycrystalline layer grown using the novel set of plasma parameters.*

#### *4.1.2.4 CL results and the correlation between grain orientation and P incorporation*

To confirm the obtained PC results, the samples have been investigated by cathodoluminescence spectroscopy (CL). The CL spectra presented in figure 4.11 were performed at the Friedrich-Alexander University Erlangen-Nurnberg, Erlangen, Germany, within the framework of the European Research Training Network DRIVE and by the courtesy of Prof. Dr. J. Ristein and P. Geithner. The polycrystalline doped diamond samples were excited with a 200µm wide 8kV electron beam using 500nA beam current, leading to a resolution of about 8meV in the spectral range involved. Figure 4.11 displays two CL spectra taken on two P-doped polycrystalline samples with different doping concentration. The spectra clearly show two important peaks in the excitonic region: the free exciton ($FE^{TO}$) peak at 5.27eV and the P-bound exciton ($BE^{TO}$) peak at 5.18eV, both for the case of recombinations assisted with the emission of transverse optical phonons and their replicas (Sauer, Teofilov et al. 2004). In figure 4.11 a, besides the above mentioned peaks, also the peak labelled $BE_P^{NP}$ is observed. This peak can actually be induced by the sum of free exciton recombination assisted by transverse acoustic phonons ($FE^{TA}$) and P-bound exciton assisted by no-phonon ($BE_P^{NP}$) transitions. However, usually the intensity of the $FE^{TA}$ peak is a couple of times smaller then the intensity of $FE^{TO}$ excitation, behaviour also seen here. As expected, the incorporation of P as confirmed by the amplitude of the P-bound exciton signal is higher in the layer grown with 500ppm (figure 4.11 b). On single crystalline diamond one can quantify the substitutional phosphorus concentration found in the diamond layer from the ratio between the BE and FE luminescence intensities (Barjon, Desfonds et al. 2007). Thus, it is safe to conclude that the intensity of the CL BE-peak confirms the behaviour seen in PC spectra, which showed that a higher $PH_3$ concentration in the gas phase leads to higher active P-incorporation in the obtained diamond layer (Lazea, Mortet et al. 2008). This is corroborated as well by significant broadening of the spectral features in figure 4.11 b compared to figure 4.11 a.

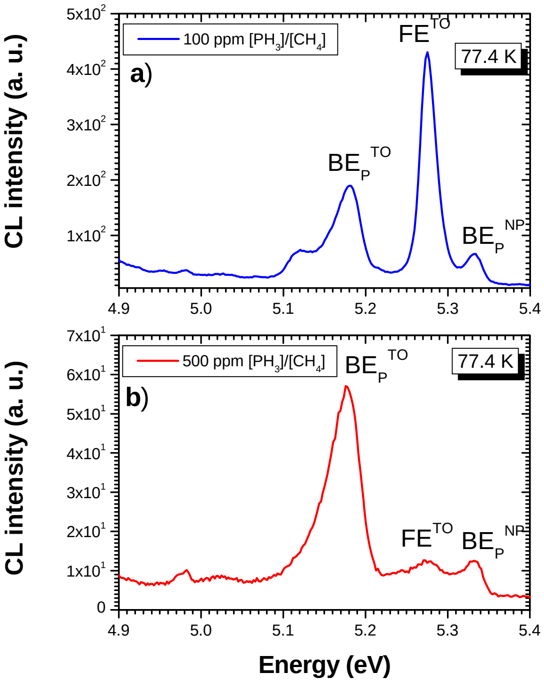

*Figure 4.11: Cathodoluminescence spectra taken at liquid nitrogen temperature for two polycrystalline samples grown with set II of plasma conditions. (a) 100ppm $[PH_3]/[CH_4]$. (b) 500ppm $[PH_3]/[CH_4]$. The peak attributed to the $BE_P^{NP}$ likely contains a contribution of the $FE^{TA}$ exciton.*

A different set of CL measurements on the same polycrystalline P-doped diamonds were kindly provided by Dr. T Teraji from the National Institute for Materials Science, Tsukuba, Japan. The CL spectra shown in figure 4.12 were carried out in a SX-40A scanning electron microscope (Topcon Ltd.) fitted with a spectrometer and at 80K, with an acceleration voltage of 20kV and an electron beam current of 90nA. In this case the beam was focused on different grains with different orientations at the sample surface, see figure 4.12. A comparison of CL measurements taken on 100ppm $[PH_3]/[CH_4]$ and 500ppm $[PH_3]/[CH_4]$ doped samples can be made. The identification of the grain orientation is made from the EBSD images. These mappings are located in the centre of the figure 4.12.

From figure 4.12 a) one can observe two CL spectra for the polycrystalline sample doped with 100ppm $[PH_3]/[CH_4]$. The spectra presented in the left and right sides of the figure are taken when the electron beam was focused on different grains of different orientation, which are marked correspondingly. The P-bound exciton peak ($BE^{TO}$), located at 5.18eV (239nm), is present for both grains. Its intensity and broadening is almost identical, indicating that the P incorporation is almost similar for the investigated grains, regardless of their orientation. Figure 4.12 b) shows similar investigations for a sample doped with 500ppm $[PH_3]/[CH_4]$. In this case a more noticeable difference is seen between the CL spectra recorded for the two grains. Here it is more evident that the intensity of the P-bound exciton ($BE^{TO}$) is increased when the grain doesn’t present a perfect {110}-orientation (see the left hand side CL spectra from figure 4.12 b). This result suggests that the incorporation efficiency of P might depend on the grain misorientation angle from the perfect [110], but complementary analyses are necessary to confirm this theory.

To further elucidate the role of the substrate orientation on the P-incorporation efficiency in separate grains, electron back-scattered diffraction (EBSD) and cathodoluminescence (CL) mapping were compared, yielding spatial information on the phosphorus concentration [P] according to the grain orientation (Lazea, Barjon et al. 2009). Cathodoluminescence (CL) spectroscopy and mapping were performed at Groupe d’Etude de la Matière Condensée (GEMaC), University Versailles St. Quentin – CNRS, Meudon, France by the courtesy of Dr. J. Barjon. The experimental details are enclosed in chapter 2, see section 2.4.1.2. In figure 4.13 the CL results for a 500ppm $[PH_3]/[CH_4]$ sample obtained at 102K are displayed. As discussed by Barjon et al. (Barjon, Desfonds et al. 2007; Barjon, Pinault et al. 2007), it is possible to determine the active P-concentration in CVD diamond by making use of the ratio of the free and P-bound exciton luminescence intensities. Hence, it is necessary that both types of exciton luminescence are detectable in the CL spectra to make a successful estimation.

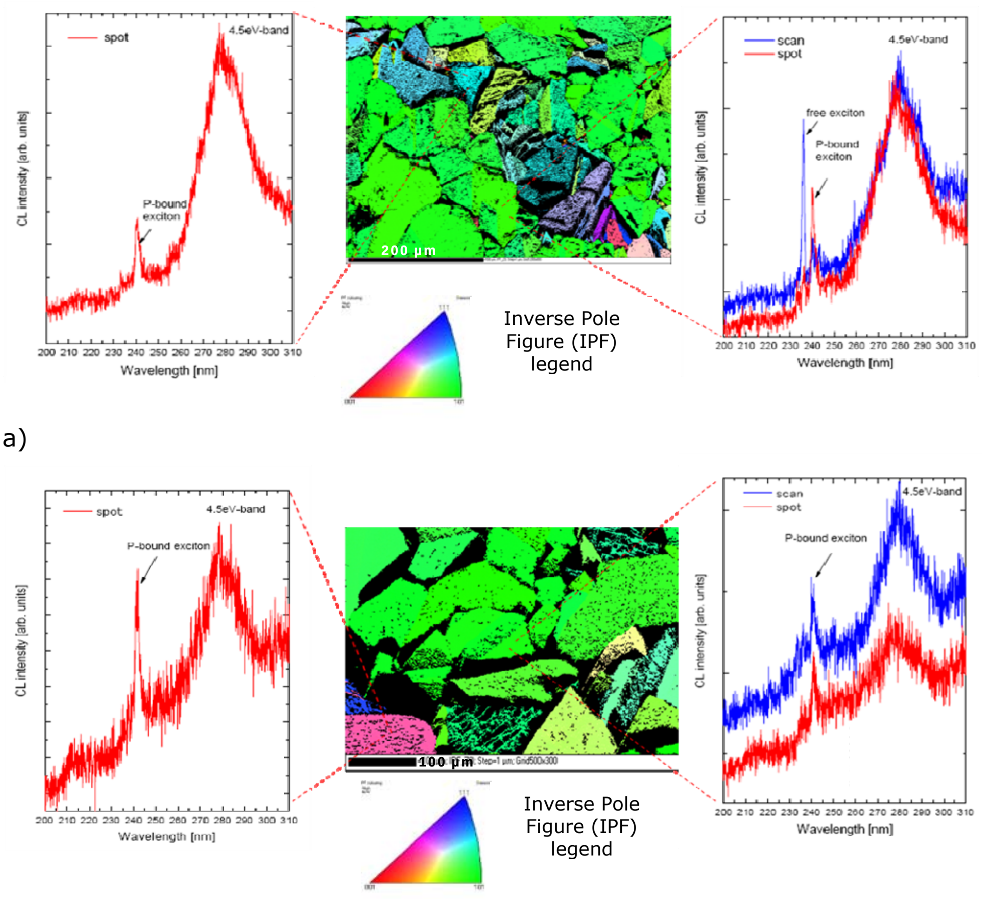

a)

b)

*Figure 4.12: Comparison of cathodoluminescence spectra taken at liquid nitrogen temperature when the electron beam was focused on two different grains of the polycrystalline samples doped with: a) 100ppm [$PH_3$]/[$CH_4$] and b) 500ppm [$PH_3$]/[$CH_4$]. The centre images represent the EBSD mappings of the samples, from which an identification of the grain orientation is possible.*

However, when investigating films grown with 500ppm [$PH_3$]/[$CH_4$] in the gas phase, as presented in figure 4.13, nearly all the exciton-related emission is attributed to the P-bound exciton, and this for different spots on the film, i.e. different oriented grains marked accordingly.

The absence of the free exciton emission points to an overall [P] that is higher than $10^{18}$cm$^{-3}$, i.e. the phosphorus donor is efficiently incorporated using the applied growth conditions.

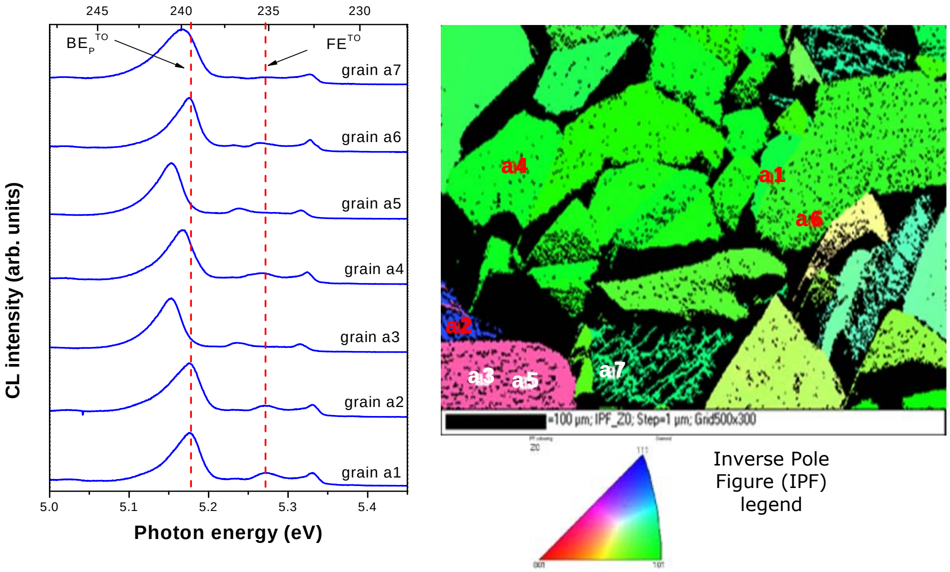

a) b)

*Figure 4.13: a) CL spectra taken at ~100K on seven different oriented grains of a {110}-textured 500ppm [PH$_3$]/[CH$_4$] doped film (see figure 4.11-b). All grains shows almost no free exciton emission and a very pronounced P-bound exciton emission, pointing to an overall P incorporation higher than $10^{18}$cm$^{-3}$ for different spots on the film. b) The EBSD map presenting the orientation of the grains of the investigated sample. The grains are marked accordingly to the CL spectra.*

Figure 4.14 shows CL spectra taken on 2 different grains from a film grown using less phosphorus in the gas phase, i.e. with 100ppm [PH$_3$]/[CH$_4$]. The two grains, which are in close proximity, and are marked accordingly in figure 4.15 a, fulfil both the conditions enabling the quantification of the P-concentration by CL. The spectra shows distinguishable peaks which can be attributed to free (FE) and P-bound (BE$_P$) excitons, labelled TO or TA when assisted with a transverse optical or acoustic phonon respectively and NP in the case of a no phonon transition (Araujo, Tajani et al. 2004; Sauer, Teofilov et al. 2004; Barjon, Desfonds et al. 2007; Barjon, Pinault et al. 2007). $O^{\Gamma}$ is the phonon involved in the optical replica. Although both grains show several types of exciton emission, including $FE^{TO}$ and $BE_P^{TO}$ signals used for [P] quantification, it is clear that there is a large difference in their intensity and position. In grain 1 the spectrum is dominated by free exciton recombination. In contrast, the situation for grain 2 is clearly different. The bound exciton related emission is much larger than the signal related to free excitons, indicating a larger incorporation of substitutional phosphorus in grain 2. In addition, the energetic positions of all exciton recombinations are shifted towards lower energies in grain 2. Such a lowering in energy has already been reported in the case of polycrystalline P-doped films deposited directly on silicon, pointing to a large position dependent tensile stress, and, as a result, a local band gap reduction (Ghodbane, Omnés et al. 2008). The presence of strain inside grains is also coherent with the large $BE_P^{TO}$ linewidths (43meV) observed here. Such linewidths are well above those obtained for homoepitaxial layers (23meV) (Barjon, Desfonds et al. 2007; Barjon, Pinault et al. 2007).

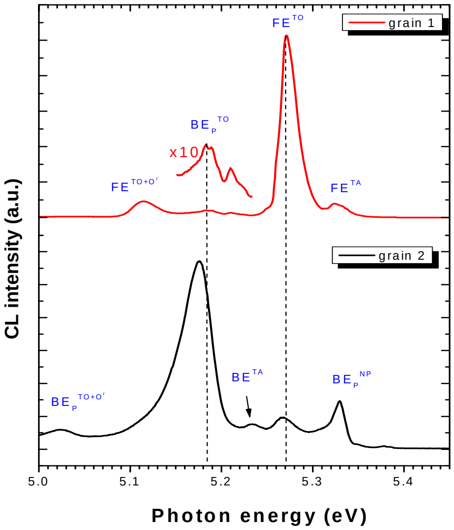

*Figure 4.14: CL spectra taken at ~100K on two different oriented grains of a {110}-textured 100ppm $[PH_3]/[CH_4]$doped film (see figure 4.15). Grain 2 shows more P-bound exciton emission than grain 1, pointing to a higher incorporation of the substitutional P donor (Lazea, Barjon et al. 2009).*

The key point of immediate interest is the difference in the ratio of $FE^{TO}$ and $BE_P^{TO}$ emission for grain 1 and 2 indicating that the amount of incorporated P is clearly different for both grains, with a clear enhanced incorporation of P in grain 2 where [P] > $10^{17}$cm$^{-3}$. To study the incorporation in the film, the whole surface was mapped by CL and [P] was determined. Figure 4.15 a) shows a typical result of a 380x300µm$^2$ area. The CL mapping confirms that there is a large variation of the phosphorus concentration from one grain to another, with values ranging between $10^{15}$ and $10^{18}$ cm$^{-3}$.

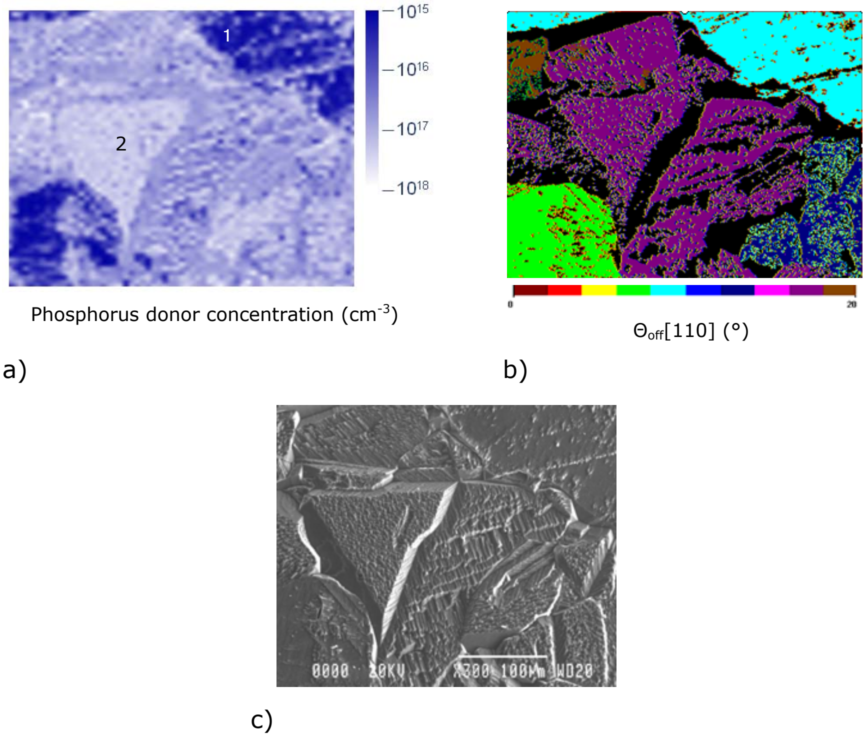

a) b)

c)

*Figure 4.15: a) P-concentration map based on the ratio of intensities of neutral phosphorus-bound exciton and free exciton emission as determined with CL mapping. "1" and "2" mark the two spots where the CL spectra featured in figure 4.14 were taken. b) Corresponding EBSD map showing the miscut angle of the substrate grains with respect to the exact [110] direction. The colour legend corresponds to off-angles between 0° and 20°, with a resolution of 2°. c) SEM picture of the region featured in a) and b) (Lazea, Barjon et al. 2009).*

To correlate these results with the grain orientation, a corresponding EBSD map was made showing the misorientation angle $\Theta_{\mathrm{off}\,[110]}$ of the grains with respect to the perfect [110] direction. All grains fall within the 4° to 20° interval. Comparing both figures, it is remarkable that the P-incorporation efficiency is smaller for grains oriented closer to [110] direction, while there is systematically a large amount of phosphorus donor atoms incorporated when these angles are higher than 12°.

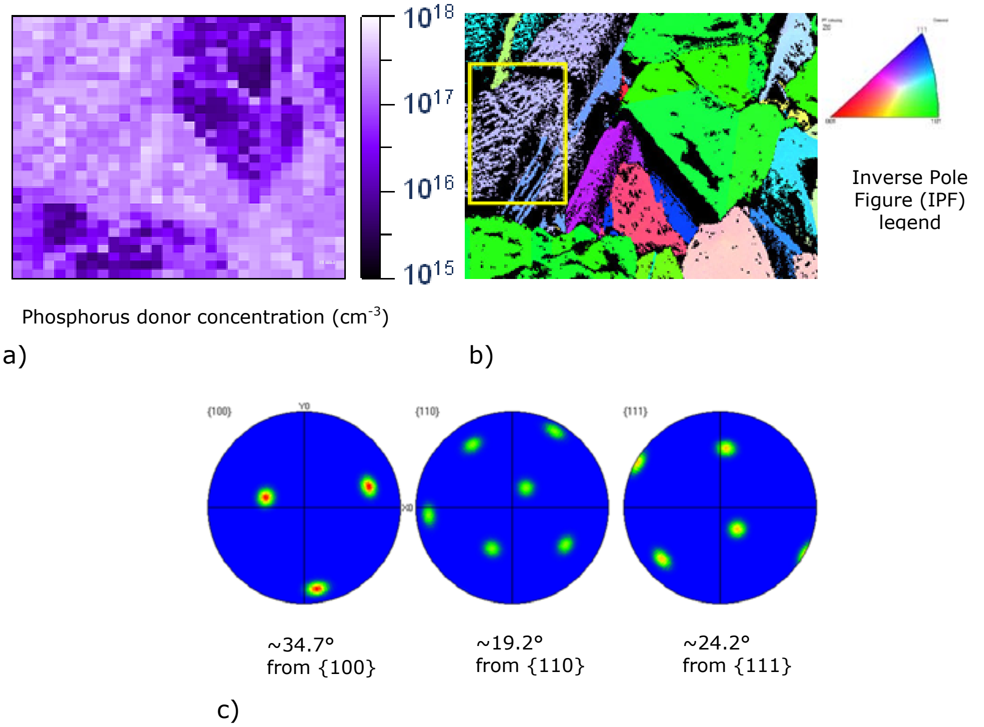

*Figure 4.16: a) P-concentration map based on CL mapping, b) EBSD mapping showing the inverse pole figure plot. The boxed section shows a grain that is not perfectly {110}-oriented as indicated by the purple coloration and c) the pole figures show with more accuracy the misorientation angles, with respect to the main crystallographic orientations, of the grain boxed in figure b): 35°, 19° and 24°.*

EBSD also provides the possibility to determine the off-angle with respect to the other major crystallographic orientations, i.e. {100} and {111}. This is useful when certain grains have an intermediate orientation with respect to the main crystallographic orientations. An example is given in the boxed part of figure 4.16 b). A correlation between the orientation for the grain and the P concentration indicated in the CL mapping, presented in figures 4.16 a) and b), suggests that grains with a certain off-angle from the ideal [110] direction will incorporate a higher P concentration of ~$10^{18}$ $cm^{-3}$. The exact misorientation angle from the perfect {110}-orientation, corresponding to this part of the film, is shown by the pole figures depicted in figure 4.16 c).

Based on the aforementioned results a relation between the orientation of the grains and the donor concentration is plotted in figure 4.17.

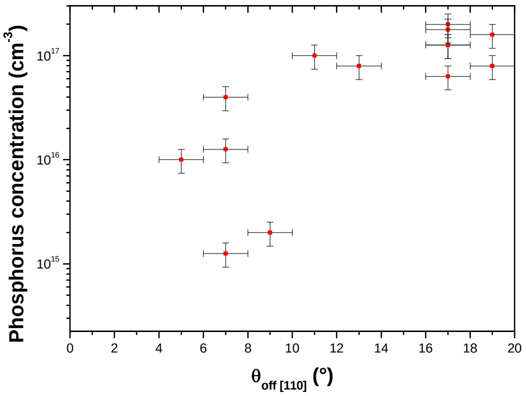

*Figure 4.17: Phosphorus concentration in function of the off-angle of the grain surface orientation with respect to the perfect [110] axis (Lazea, Barjon et al. 2009).*

While the influence of the misorientation is obvious, the lack of a clear one-to-one relation between the two quantities [P] and $\Theta_{off\ [110]}$, leads to the assumption that there is at least a second element that plays a key role. The influence of the substrate misorientation angle was studied before for single crystalline n-type {100}-orientated diamond layers, where it was found that small angles of 2° or 3° were useful in enhancing step flow growth and the phosphorus incorporation (Kato, Makino et al. 2007). The beneficial influence was explained by the need to control the step growth and thus to reduce the presence of the non-epitaxial crystallites and pyramidal hillocks. Nevertheless, the amount of phosphine gas needed to obtain similar [P] as presented here was two orders of magnitude higher. When looking in detail to the surface of the grain 2 (figure 4.15 (c)), it becomes obvious that a certain roughness is present (see figure 4.6 (b)), which is also evident in the granular-like parts of figure 4.13 b). It is proposed that the surface features consist out of {111}-oriented microfacets that facilitate the incorporation of P. Studies on single crystal diamond growth have already pointed out that the incorporation efficiency of {111}-oriented layers is several orders of magnitude higher than for {100}-oriented films (Kato, Makino et al. 2007). Moreover, van Enckevort and co-workers have shown that growth on top of {110} facets is stabilized through the formation of microfactes, leading to the rough appearance as seen in figure 4.15 (c) (van Enckevort, Janssen et al. 1993). According to Nishitani-Gamo et al. these microfacets develop predominantly in {111} facets (Nishitani-Gamo, Loh et al. 1999). In addition, the calculations of Battaile et al. lead to believe that a certain misorientation with respect to the exact [110] axis can have an advantageous effect on the growth rate, enhancing locally the growth and subsequently the phosphorus incorporation of suitable orientated grains (Battaile, Srolovitz et al. 1998). Contrary to this, grains with a misorientation angle lower than 10° show much less to no microfacets at all, maintaining their {110} orientation. As a result, these regions generally have an [P] below $10^{16}$cm$^{-3}$. Examples can be seen in the bottom left and top right corners of figure 4.15 a).

To summarize, in this section a detailed investigation of the P-doping of {110}-oriented microcrystalline diamond was achieved by CL and EBSD mapping. The combination of these two techniques is a powerful tool in the local determination of dopant incorporation as a function of the substrate orientation. Such data can yield information on the incorporation of P as function of the substrate miscut orientation and they may be transposed to the case of homoepitaxial growth of P-doping on single and polycrystalline CVD diamond layers. In particular, it was shown that the phosphorus concentration in one film can vary over three orders of magnitude, although a misorientation angle of more than 10° with respect to the perfect [110] axis is needed to incorporate more than $10^{17}$ cm$^{-3}$. In addition, it was proposed that the different surface morphology facilitate the local incorporation of P via the formation of {111}-oriented microfacets on most of the grains.

#### *4.1.2.5 Electrical properties*

The P-doped layers grown on polycrystalline {110}-oriented CVD diamond samples were investigated with Hall measurements. The Hall effect measurements were performed at the National Institute for Materials Science, Tsukuba, Japan by courtesy of Dr. S. Koizumi. The set-up is equipped with a 0.7Tesla magnet for generating the AC magnetic field (0.52Trms) with frequencies ranging from 10mHz~200mHz. During the measurements the samples were placed in a high temperature cryostat/oven operated in He ambient at a pressure of 1Pa evacuated by a turbo molecular pump. The specimen temperature can vary on a wide range, reaching a maximum value of

1073K. A Keithley 6517A DC current source is used. The results are collected via a computer through custom written Toyo Resitest 8310 software.

In figure 4.18, the results of the electrical measurements are displayed for a 500ppm polycrystalline P-doped sample (sample no 61122PP).

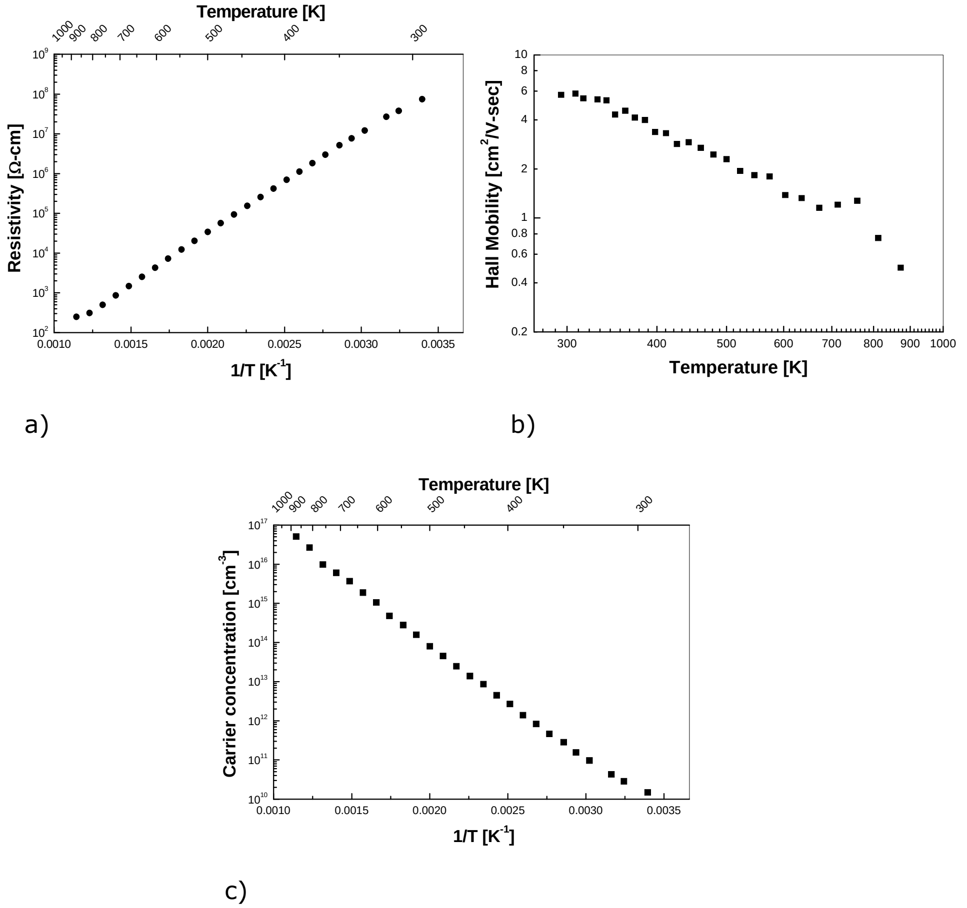

a) b)

c)

*Figure 4.18: Hall effect measurements: resistance, mobility and carrier concentration versus temperature (or reciprocal temperature scale) for sample grown with a phosphorus concentration $[PH_3]/[CH_4]$ = 500ppm (active donor concentration in the layer equal to $1.8\times10^{17}$cm$^{-3}$).*

Hall effect measurements confirmed that the investigated sample is effectively n-type doped and a mobility equal to 6cm$^2$/Vs was obtained at 300K (room temperature).

The mobility of such n-type polycrystalline diamond layers is lower than the ones presented, for instance, for undoped single crystalline CVD diamond films (see table 1.3 from chapter I). Keeping in mind that this value is measured for polycrystalline diamond layers, thus a large number of compensating defects may be present, this is a reasonable value. Comparable mobility values are seen in the previous works dealing with phosphorus incorporation in polycrystalline diamond layers (Nesladek, Haenen et al. 2003).

The resistance behaviour, figure 4.18 a, indicates an exponential behaviour that points to a thermally activated process by electrons in the conduction band. This behaviour is seen for the entire temperature range on which the sample was investigated. From the temperature dependence of the carrier concentration, figure 4.18 c, we see that the carrier concentration is proportional to the P concentration into the layer, as estimated by CL mapping in figure 4.15. By fitting the carrier concentration profile of figure 4.18 c the activation energy was estimated at 0.55eV. This value is almost similar to the photoionization value found by PC investigation, which is attributed to P substitutional incorporation.

These results confirm that n-type diamond layers containing phosphorus atoms can be obtained when one prepares the samples using the novel set of plasma parameters proposed in this chapter.

### ***4.1.2.6 Micro-Raman Spectroscopy investigation***

#### *4.1.2.6.1 Theory and experimental set-up*

A useful method in material identification is laser Raman spectroscopy. This technique is a straightforward, non-destructive method requiring no large sample preparation and consists in illuminating the specimen with monochromatic light and examining the scattered light by using a spectrometer. When the electromagnetic radiation is scattered by a molecule or by a crystal, one photon of the incident radiation is annihilated and, at the same time, one photon of the scattered radiation is created. The scattering mechanism can be classified on the basis of the difference between the energies of the incident and scattered photons. If the energy of the incident photon is equal to that of the scattered one, we speak of *Rayleigh scattering*. If the energy differs than the process is inelastic and it is called *Raman scattering*. When the light is scattered to a lower energy the lines are called Stokes lines. The others, having higher energy are called anti-Stokes. Most of the time only one of the processes, Stokes or anti-Stokes scattering, is considered. A Raman spectrum is plotted as the intensity versus the difference in wavenumber between the incident radiation and the scattered light. From the Raman spectra one can obtain information on the vibrational, rotational and low-frequency modes in a system with bonds that can cause these modes. Different materials have different vibrational modes, therefore characteristic Raman spectra.

Crystals, as is the case of diamond, do not behave as if composed of molecules with specific vibrational energy levels; instead, the crystal lattice undergoes vibration. These macroscopic vibrational modes are called phonons. Natural diamond exhibits a sharp first-order peak (triply degenerate) in the Raman spectrum at ~1332.44cm$^{-1}$ and a weak second-order feature centred at ~2750cm$^{-1}$ (Solin and Ramdas 1970). In principle the first order peak should have a Lorentzian line shape with full-width at half maximum (FWHM) typically ≤2 cm$^{-1}$. In diamond films grown by HPHT or CVD techniques, various growth sectors can contain different concentrations of defects and carbon can be incorporated into the films in non diamond forms such as graphitic or amorphous carbon regions. By using Raman and photoluminescence spectroscopy these impurities and structural imperfections can be investigated. Recently the Raman technique was improved and nowadays Raman spectroscopic imaging is frequently used.

In this subsection the Raman technique was used to study the structural perfection of the diamond crystal when P-doped layers were grown on top of the {110}-oriented polycrystalline specimens. The experiments were performed at Groupe d'Etude de la Matière Condensée (GEMaC), University Versailles St Quentin – CNRS, Meudon, France by the courtesy of Dr. J. Barjon and Dr. Nada Habka. Confocal and micro-Raman (µRaman) spectroscopy and mapping of the 1332cm$^{-1}$ diamond line were performed using a Horiba Jobin-Yvon confocal micro-Raman HR800. The µRaman emission was recorded in the backscattered geometry. Excitation was performed with the 632.81nm line of a He-Ne laser. The laser beam was focused at the surface of the sample with a x100 objective (spot size <1µm and power ~10mW). By using a 1800st/mm grating and a confocal hole of 50µm, the spectral resolution was 0.5cm$^{-1}$ in the range of the diamond peak.

When Raman mapping was performed, full spectra were recorded for each point and then stored in an "image file". Therefore, data contained the complete information locally resolved within the studied spectral window and sample area. The width of the spectral window depends on the excitation wavelength and especially on the acquisition mode of the spectrometer.

#### *4.1.2.6.2 Strain effect in diamond grains after the P doping of polycrystalline substrates*

The aim of the Raman spectroscopy investigations is to obtain preliminary information about the crystal quality of the polycrystalline diamond samples. Also, the presence and influence of the impurities, such as P, present in the doped specimens can be studied. To this purpose a 500ppm [$PH_3$]/[$CH_4$] polycrystalline sample was analyzed by Raman spectroscopy (see figure 4.19). In this subsection Raman spectra and 2D spectral images are discussed. Figure 4.19 shows two Raman spectra recorded for two different grains of the 500ppm [$PH_3$]/[$CH_4$] diamond layer. The analyzed grains were previously investigated by CL measurements and are marked accordingly (see figure 4.13). In both spectra 2 Raman peaks are observed: the diamond Raman first order peak, usually situated at 1332cm$^{-1}$ in natural diamond crystals (Palnichenko, Jonas et al. 1999) as well as in homoepitaxial (Linares and Doering 1999) and polycrystalline CVD diamond (Ferrari and Robertson 2001), is present. A second peak is a down shifted peak (up to 6cm$^{-1}$) with respect to the expected diamond line. This shift indicates that the layer is under strong tensile stress at the surface (Yanchuck, Valakh et al. 2004).

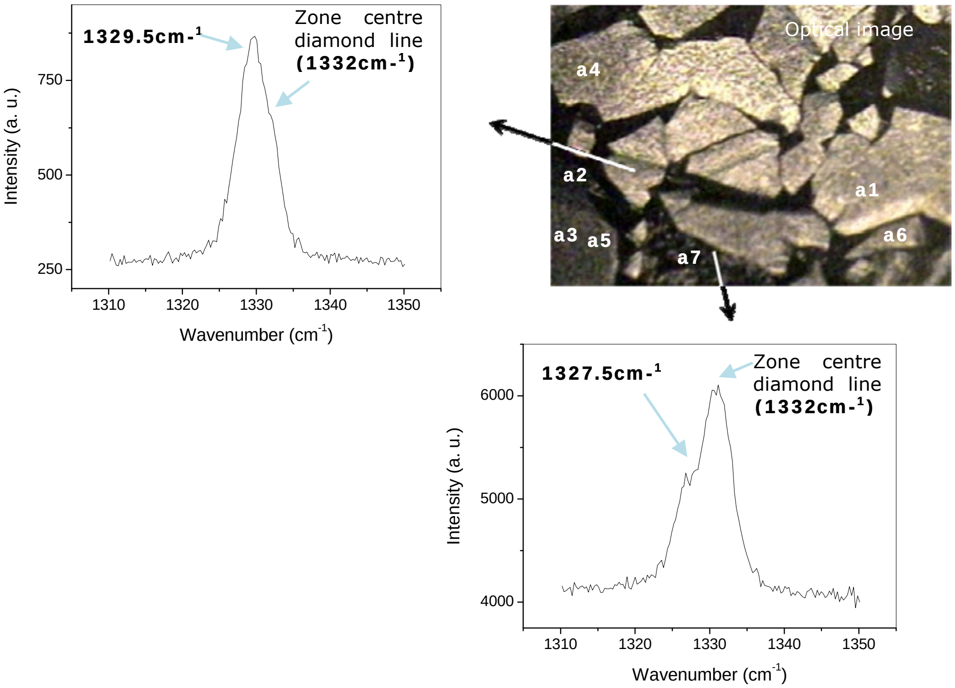

*Figure 4.19: Raman spectra of two grains of the sample doped with 500ppm [$PH_3$]/[$CH_4$]. The grains are marked accordingly in the optical microscope image.*

Nevertheless, from the Raman spectra it is confirmed that the crystalline perfection of the P-doped films, when novel doping conditions are applied, is close to the quality of the polycrystalline diamond.

In order to study the local variation of the Raman-line parameters, high resolution (1µm$^2$ step) 2D mapping of one grain was performed (see figure 4.20). The Raman mapping shows the stress evaluation by monitoring the changes in the diamond peak position. The 1326cm$^{-1}$ peak position mapping (figure 4.20 b) exhibits areas with different colouration which point to a noticeable difference in the layers strain (according to the legend posted next to the Raman map). Thus it is possible to observe regions with a higher or a lower strain. This result proofs that the strain observed at the investigated grain surface is not homogenous.

From the aforementioned Raman results the presence of the diamond peak position for the {110}-oriented polycrystalline diamond layers was revealed. A preliminary stress evaluation map was presented, indicating a non-uniform stress at the layer surface. Further investigations are necessary for an exact identification of the stress origin, work which is currently in progress.

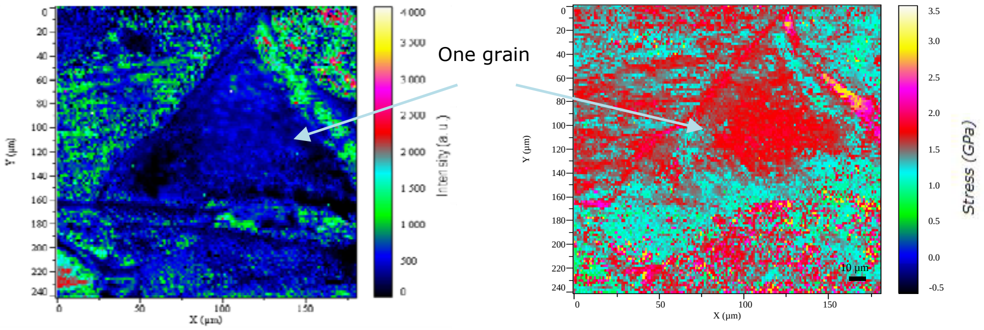

Total intensity

Stress in the layer

a)

b)

*Figure 4.20: µRaman 2D images of the same grain of the sample doped with 500ppm [PH$_3$]/[CH$_4$], evaluating the stress into the diamond sample (left) and into the doped diamond layer (right), by mapping the 1326cm$^{-1}$ peak position.*

## 4.2 P-doping process using {110}-oriented single crystalline substrates

### 4.2.1 Experimental details and results for layers grown using novel plasma parameters

The successful results regarding P doping of {110}-oriented polycrystalline diamonds, when the novel set of plasma conditions was used, represents the motivation for the experiments presented in this sub-section. This study presents the first investigations of phosphorus-doped single crystalline diamond films deposited on {110}-oriented substrates. The presence of P into the layers is confirmed by means of defect spectroscopy techniques. The n-type character of the layer, carrier concentration and mobility were investigated by Hall measurements.

#### 4.2.1.1 Growth conditions

The CVD diamond layers were grown in similar growth conditions as the ones previously described in this chapter (see sub-section 4.1.2). Thus, a higher methane concentration (1%) and a higher temperature (~1135°C), than usually employed for P-doping, are the distinct signature of the growth described here. The only difference between the polycrystalline and single crystalline growth conditions is the deposition time. For the single crystalline layers the time is changed from a maximum of 2h down to a minimum of 30min, as can be seen from the table 4.3.

*Table 4.3: Growth conditions used for P doping of single crystalline {110} CVD diamonds grown at IMO.*

| **Sample code** | **$PH_3/CH_4$ (ppm)** | **$CH_4/H_2$ (%)** | **Time (min)** | **Pressure (torr)** | **MW power (W)** | **Temp (°C)** |
|---|---|---|---|---|---|---|
| 80415EP | 500 | 1 | 120 | 180 | 776 | 1135 |
| 80418EP | 1000 | 1 | 120 | 180 | 885 | 1135 |
| 80522EP | 500 | 1 | 120 | 180 | 965 | 1133 |
| 80717EP | 500 | 1 | 30 | 180 | 820 | 1131 |
| 80723EP | 1000 | 1 | 30 | 180 | 860 | 1134 |
| 80731EP | 500 | 1 | 60 | 180 | 833 | 1135 |
| 80812EP | 250 | 1 | 60 | 180 | 855 | 1132 |
| 80818EP | 100 | 1 | 60 | 180 | 810 | 1135 |

For these experiments HPHT synthetic {110}-oriented single crystalline diamonds were chosen, on which homoepitaxial (doped) layers were deposited.

The substrates used in this work belong to the same Ib HPHT {100}-oriented sample which was polished into 2x2x0.5cm$^3$ samples, with the main surface orientated along the [110] crystallographic axis.

#### *4.2.1.2 Surface topography, morphology and microstructural analysis before and after the growth*

The surface morphology of different phosphine concentration series of {110} homoepitaxial diamond films are shown in figure 4.21. It was found that the doped diamond layers do not inherit the polishing lines seen at the substrate surface and when the phosphine concentration is increased the surface morphology is changed as a consequence (figure 4.21 a, c and e). As can be seen from figure 4.21 b, d and f, representing a closer examination of the samples surface by AFM, the typical root mean square surface roughness ($R_{rms}$) for a 5x5µm$^2$ scanned area is drastically increased when higher phosphine concentrations are added to the gas mixture. This observation clearly proves that in this case the phosphine addition directly influences the growth process, and possibly the deposition rate. An estimation of the growth rate is made in figure 4.22, where a SEM image is presenting a lateral view of the sample grown with 500ppm [$PH_3$]/[$CH_4$]. The growth rate (~50µm/h) is higher than the growth rate seen for the polycrystalline layers grown using identical conditions. Further investigations are necessary to explain this phenomenon.

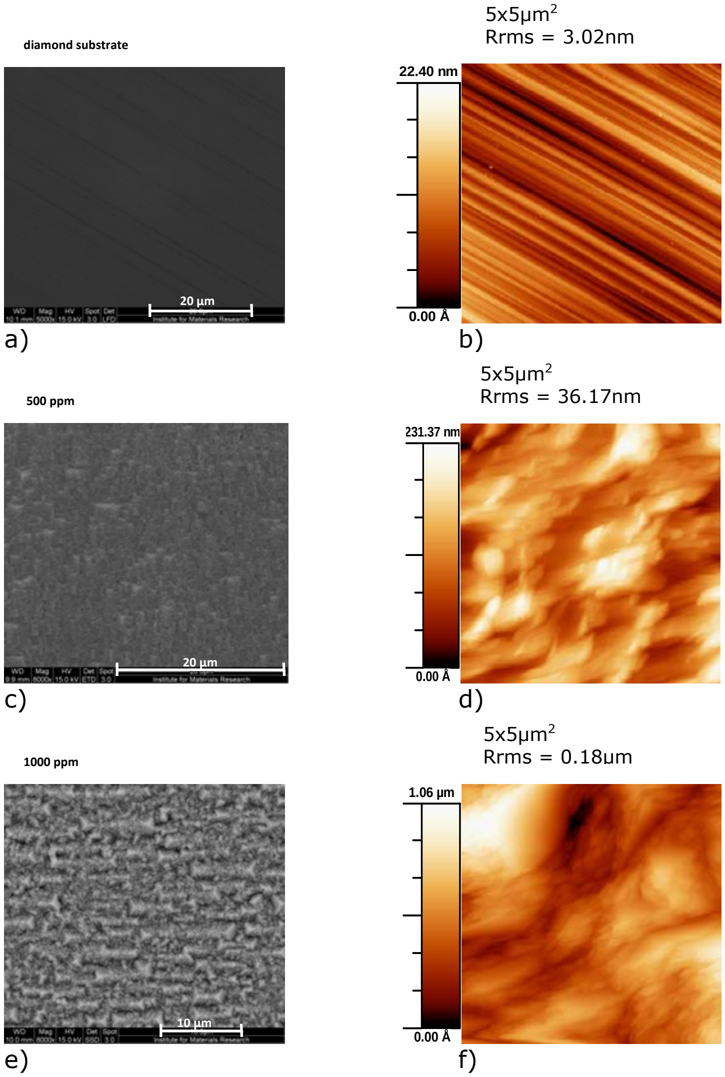

*Figure 4.21: Comparison of the surface morphology of a single crystalline homoepitaxial {110}-oriented diamond substrate (a, b), a homoepitaxial layer grown with 500ppm [$PH_3$]/[$CH_4$] (c, d) and homoepitaxial layer grown with 1000ppm [$PH_3$]/[$CH_4$] (d, e). Where SEM images are a, c and e; AFM images of the samples are: b, d and f.*

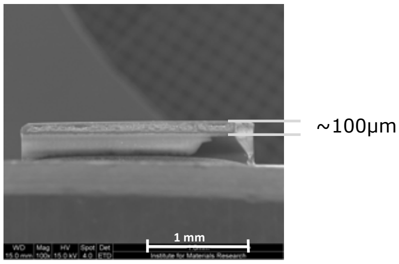

*Figure 4.22: SEM image of the homoepitaxial layer grown with 500ppm [$PH_3$]/[$CH_4$]. The lateral view which reveals the thickness of the layer after 2h growth, corresponding with a growth rate of ~50µm/h.*

The microstructural and textural development of the P-doped diamond layer after doping with 500ppm [$PH_3$]/[$CH_4$] is presented in figure 4.23. Figure 4.23 a) and b) shows the single crystalline diamond sample texture with respect to the film normal direction (IPF // Z) and the pole figure contour plots. As can be seen from the triangle colouring scheme, the diamond sample is mainly {110}-orientated, having a green colouration. The behaviour is confirmed by the pole figures. After the growth of the P-doped layer, EBSD investigations are presented in figure 4.23 c) and d). According to the EBSD map (figure 4.23 c) the layer orientation after growth remains unmistakably {110}, showing continued growth when compared with the substrate. The defect seen in the centre down part of the layer is due to the cleaning procedure, rather than the growth process. The pole figure presented in figure 4.23 d) is showing a strong {110} texture, which is in agreement with the observation seen for the polycrystalline substrate (see figure 4.3).

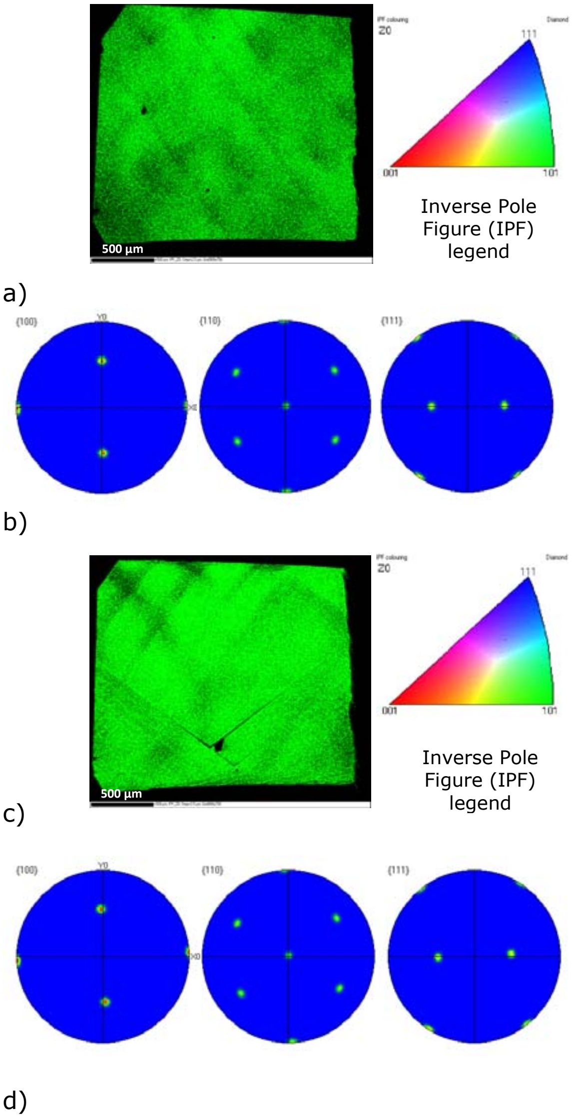

*Figure 4.23: Top view EBSD maps of a single crystalline {110}-oriented substrate (a) and of a 500ppm $[PH_3]/[CH_4]$ homoepitaxial layer (c). {100}, {110} and {111} pole figures of the substrate and the P-doped layer are presented in images (b) and (d), respectively.*

#### 4.2.1.3 PC and FTPS investigations

In this sub-section P-doped {110}-oriented single crystalline diamond thin films were investigated by defect spectroscopy techniques. A first set of PC measurements are presented in figure 4.24. The measurements were done using interdigital electrode configuration, thus the possible edge-located defects influences are excluded. Note that there are several differences between the investigated samples. Figure 4.24 a) compares the incorporation of phosphorus into 1000ppm $[PH_3]/[CH_4]$ samples grown for 120 min and 30 min, respectively. Both spectra clearly show the photoionization onset related to substitutional phosphorus situated around 0.56eV (Nesladek, Meykens et al. 1999_a) and the oscillatory conductivity, indicating the successful incorporation of the phosphorus donor. However, the sample grown for less time presents a small intensity of the photocurrent and a less obvious oscillatory photoconductivity. This observations lead to the conclusions that less P is incorporated for the sample grown for 30min plasma exposure. Even so, the PC spectra reveal the successful incorporation of P into single crystalline {110}-oriented diamonds using these atypical growth parameters.

In order to optimize the P incorporation into the layers, samples were grown for 60min plasma exposure. Figure 4.24 b) presents the PC spectra taken at liquid nitrogen temperature for two samples doped with 500ppm $[PH_3]/[CH_4]$ and 250ppm $[PH_3]/[CH_4]$, respectively. The spectra reveal photocurrent signals much richer in detail and both spectra present oscillatory photoconductivity. As it was previously observed for the polycrystalline samples grown in similar plasma condition (see figure 4.9), the first order minima seen for single crystalline samples becomes more broadened as the phosphine concentration is increased. From all the aforementioned results it can be concluded that doping using this set of plasma parameters is leading to incorporation of substitutional phosphorus also on single crystalline {110}-oriented substrates.

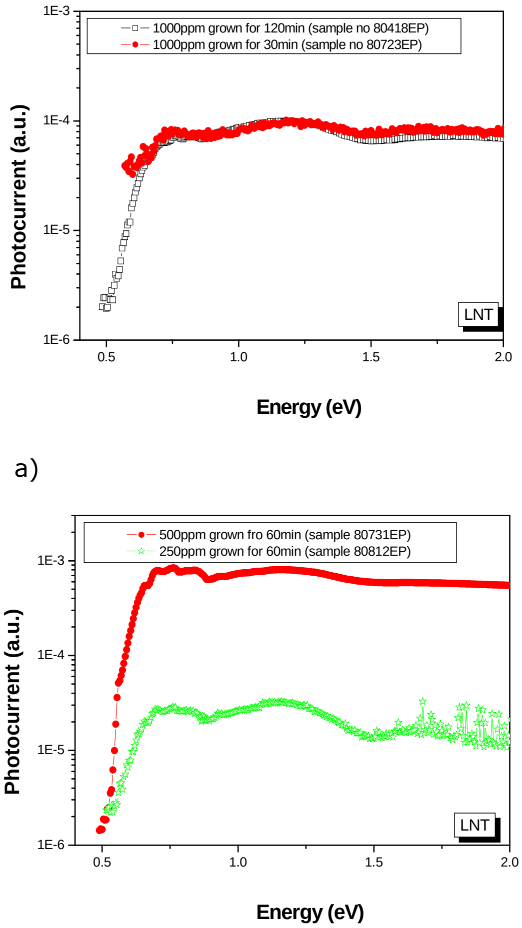

a)

b)

*Figure 4.24: PC spectra taken at liquid nitrogen temperature of P-doped {110}-oriented single crystalline diamond layers: a) doped with 1000ppm [$PH_3$]/[$CH_4$] grown for different time, b) doped with 500ppm [$PH_3$]/[$CH_4$] and 250ppm [$PH_3$]/[$CH_4$], respectively, grown for 60min.*

FTPS measurements of homoepitaxial P-doped {110}-oriented diamond layers were performed at the Institute of Physics, Department Optical Crystals, Academy of Sciences of the Czech Republic, courtesy of Dr. Zdeněk Remeš, within the frame of the European Research Training Network (DRIVE). Figure 4.25 shows a FTPS spectrum obtained for a sample doped with 500ppm $[PH_3]/[CH_4]$. The FTPS spectrum presents the same P-related peak as seen with the PC technique. However, the FTPS spectrum presents a sharper rising edge of the peak and a activation energy closer to the 0.56eV value of the excited states of P. This is due to the 3 operating advantages of the technique, such as: short acquisition time, high resolution and high light throughput giving good signal to noise ratio.
Thus, it can be concluded that a first confirmation of the P incorporation into the single crystalline {110} diamond samples, grown in novel plasma parameters, have been given by PC measurements as well as FTPS analyses.

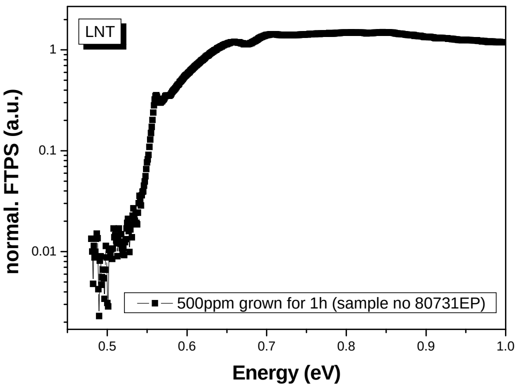

*Figure 4.25: FTPS spectra taken at liquid nitrogen temperature of P-doped {110}-oriented single crystalline diamond layer doped with 500ppm $[PH_3]/[CH_4]$ and grown for 60min in atypical plasma conditions.*

#### *4.2.1.4 Electrical properties*

Hall effect measurements were performed at IMO. The experimental details were presented in chapter 2, sub-section 2.5.2. From the experiments the n-type character of the layer was confirmed and figure 4.26 displays the results for carrier concentration, resistance and mobility versus temperature. The behaviour seen in the resistance graph is typically observed for P-doped diamond layers. The exponential decrease of the resistance towards higher temperatures indicates a thermally activated conduction process by electrons in the conduction band (see figure 4.26 a). From the carrier concentration dependence the activation energy is provided, figure 4.26 b). The value is in accordance with the optical ionisation energy of ~0.56eV of phosphorus established in the previous subsection and activation energy values obtained on {111} and {100}-oriented P-doped diamonds .

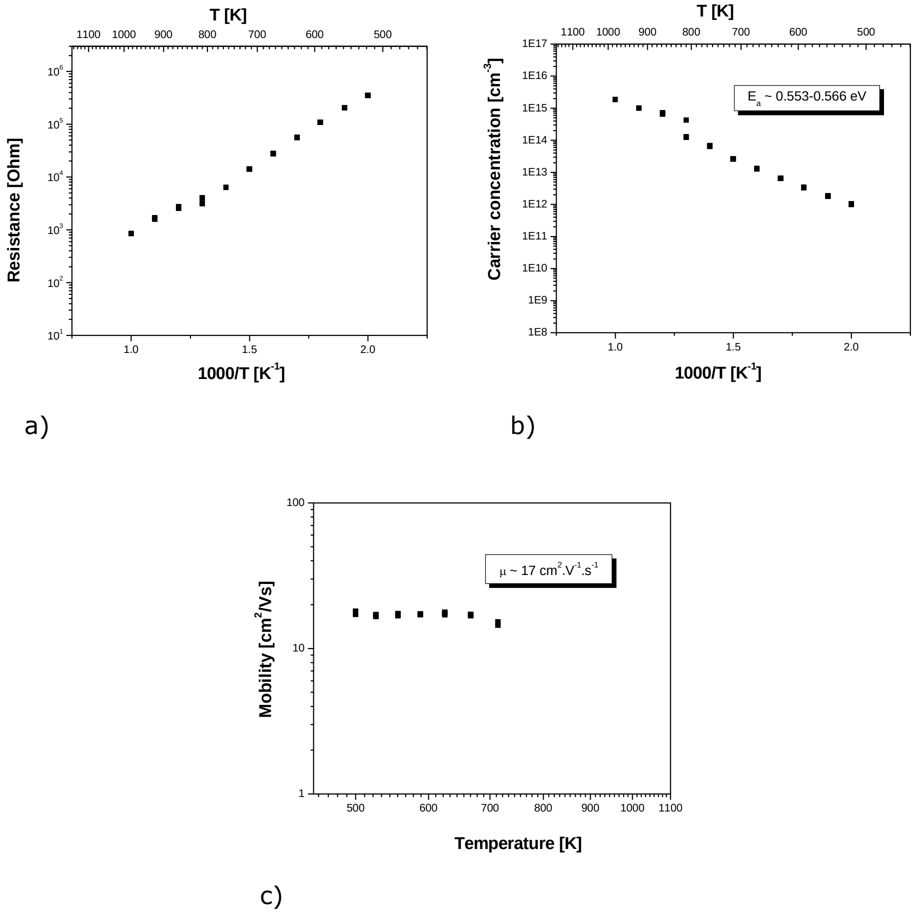

*Figure 4.26: Hall effect measurements taken for a P-doped {110}-oriented single crystalline diamond layer doped with 500ppm [$PH_3$]/[$CH_4$] and grown for 60min: resistance (a) carrier concentration (b), and mobility (c) versus temperature.*

This value is a further confirmation of the incorporation of phosphorus in the homoepitaxial diamond layer. The temperature dependence of the mobility, presented in figure 4.23 c), indicates a value of $17 cm^2V^{-1}s^{-1}$ in the range of high temperatures (~500K). Even at higher temperatures (~700K) the mobility seems to be limited. The origin of this behaviour is not yet determined and further investigations are necessary in order to establish its cause.

#### *4.2.1.5 Impurity analysis: SIMS profile*

To check the impurity concentration and the profile in the grown P-doped diamond layers, SIMS measurements were performed. The measurements were carried out at the Groupe d’Etude de la Matière Condensé (GEMaC), Versailles University St. Quentin - CNRS, Meudon, France and the experimental set-up was previously described (see chapter 2, section 2.4.2).

Figure 4.27 compares the SIMS depth profiles of impurities in two P-doped films grown with 500ppm and 1000ppm, respectively, of $PH_3$ in $CH_4$. The P concentration in the 500ppm sample was estimated to be around $10^{18}cm^{-3}$, while boron signal is close to the detection limit (figure 4.27 a)). The SIMS depth profile of 1000pm P-doped sample, see figure 4.27 b, presents a P concentration of $\sim 3x10^{19}cm^{-3}$ . The boron signal for this sample is observed rather strongly if we simply compare its intensity to the one observed for the 500ppm P-doped sample. The cause of this contamination is unclear for the moment. However, one can speculate that boron presence is related to its presence in the diamond substrate, since it was only observed for this layer. Nevertheless, further investigations are required in order to elucidate the contamination source.

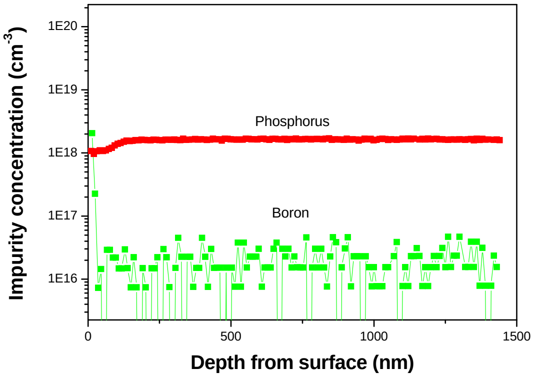

a)

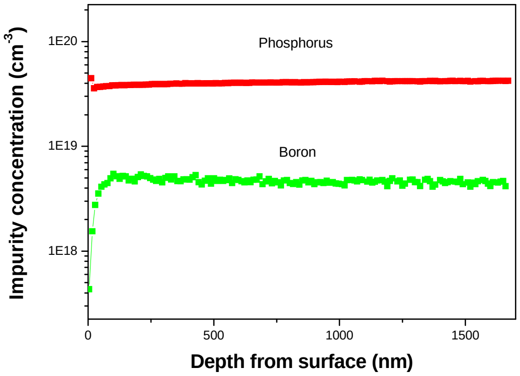

b)

*Figure 4.27: SIMS depth profile of P and B atoms in diamond films doped with $PH_3$ concentrations in the gas phase of 500ppm (a) and 1000ppm (b).*

## 4.3 Conclusions

The main aim of chapter 4 was to present the growth and characterization of phorphorus doped CVD diamond films on {110} oriented substrates.

First, the growth and doping results when polycrystalline {110}-oriented diamond substrates were used was presented. The first doping process followed a growth strategy based on the plasma parameters used for the P diamond doping of {111}-oriented single crystalline samples. The quality of P-doped {110}-oriented diamond layers was established from defect spectroscopy measurements and surface imaging results. A confirmation of the P incorporation was done, but a preferential growth process of the grains was observed. Overall, the doping process had a lower quality, when one compares it with the single crystalline doping process. Therefore, a novel set of plasma parameters was proposed.

The new set of doping conditions is atypical for the P incorporation process, mainly due to the higher substrate temperature and methane concentration. To study the P incorporation and possible unwanted defects, the doped CVD polycrystalline diamond layers were firstly investigated by defect spectroscopy techniques. The results indicate a successful P incorporation and a higher quality of the polycrystalline diamond layers when compared with the single crystalline P-doped diamond layers. The surface imaging and microsturctural investigations point out that the growth mechanism does not have a preferential behaviour. The grains of the polycrystalline {110}-oriented diamond substrate clearly grow after exposure to the plasma while the surface of the grains keep the same orientation of the substrate, i.e. {110} orientated. From corroboration of the microstructural information with the CL measurements, a first conclusion can be drawn: the novel set of plasma conditions is suitable for P incorporation in {110}-oriented diamond grains. Surprisingly, the combination of these two techniques proofs to be a powerful tool in the local determination of the dopant incorporation as a function of the substrate orientation. In particular, it was shown that the phosphorus concentration in one film may vary over three orders of magnitude, although a certain missorientation angle with respect to the perfect [110] axis is needed to incorporate more than $10^{17}$cm$^{-3}$ P atoms. In addition to this new information, it was proposed that the morphology of the grains facilitates the local incorporation of P via formation of {111}-oriented microfacets when a certain off-angle is present.

The successful P doping of polycrystalline layers when using optimized plasma conditions inspired the doping of single crystalline {110}-oriented diamond substrates. The presence of P-related features in the PC spectra indicates a successful incorporation of P into {110}-oriented samples when the novel set of plasma parameters is used. The preliminary surface imaging results reveals that the phosphine addition directly influences the growth process, and possibly the deposition rate. For this growth and doping process high growth rates are observed. Confirmation of P incorporation into the layers, as observed by PC method, is done by FTPS experiments. The presence of substitutional P defect in the low-temperature FTPS spectra was presented and thus the successful P incorporation into {110}-oriented single crystalline diamond layers was achieved. This is the first time, that P incorporation is successful into {110}-oriented single crystalline diamond layers. However, the question remains if the microfacets present at the sample surface play a role in P incorporation or not. Up till now the scientific literature focused exclusively on doping into {111} and {100}-oriented diamond layers, therefore n-type character was studied for these types of layers. In this chapter, preliminary electrical investigations of the {110}-oriented single crystalline layers indicate the n-type character of the obtained diamond thin films, proving that the novel set of plasma parameters is suitable for donor doping of the {110}-oriented single crystalline diamond layers.

In conclusion, the results presented in this chapter indicate that phosphorus-doped diamond layers can be reproducibly produced in our laboratory when {110}-oriented samples are used. The doping procedure can be achieved when one uses either polycrystalline or single crystalline diamond layers. The atypical set of doping parameters, proposed in this chapter, proved to be suitable for successful P incorporation.

## 4.4 References

Araujo, D., A. Tajani, et al. (2004). "Study of the phosphorus incorporation in n-doped diamond films by cathodoluminescence." Journal of Physics-Condensed Matter **16**(2): S287-S292.

Barjon, J., P. Desfonds, et al. (2007). "Determination of the phosphorus content in diamond using cathodoluminescence spectroscopy." Journal of Applied Physics **101**(11): 113701_1-113701_3.

Barjon, J., M. A. Pinault, et al. (2007). "Cathodoluminescence as a tool to determine the phosphorus concentration in diamond." Physica Status Solidi a-Applications and Materials Science **204**(9): 2965-2970.

Battaile, C. C., D. J. Srolovitz, et al. (1998). "Atomic-scale simulations of chemical vapor deposition on flat and vicinal diamond substrates." Journal of Crystal Growth **194**(3-4): 353-368.

Ferrari, A. C. and J. Robertson (2001). "Resonant Raman spectroscopy of disordered, amorphous, and diamondlike carbon." Physical Review B **64**(7): 075414.

Garrido, J. A., C. E. Nebel, et al. (2002). "Electrical and optical measurements of CVD diamond doped with sulfur." Physical Review B **65**(16): 165409_1-165409_6.

Ghodbane, S., F. Omnés, et al. (2008). "n-type phosphorus-doped polycrystalline diamond on silicon substrates." Diamond and Related Materials **17**(7-10): 1324-1329.

Haenen, K., M. Nesladek, et al. (2004). "The phosphorus level fine structure in homoepitaxial and polycrystalline n-type CVD diamond." Diamond and Related Materials **13**: 2041-2045.

Hoffman, A., I. Andrienko, et al. (2005). "Electron trapping and detrapping in ion-beam-damaged diamond surfaces." Applied Physics Letters **86**(4): 044103_1-044103_3.

Katagiri, M., J. Isoya, et al. (2004). "Lightly phosphorus-doped homoepitaxial diamond films grown by chemical vapor deposition." Applied Physics Letters **85**(26): 6365-6367.

Kato, H., T. Makino, et al. (2007). "N-type diamond growth by phosphorus doping on (001)-oriented surface." Journal of Physics D-Applied Physics **40**(20): 6189-6200.

Kato, H., S. Yamasaki, et al. (2005). "Growth and characterization of phosphorus-doped diamond using organophosphorus gases." Physica Status Solidi a-Applications and Materials Science **202**(11): 2122-2128.

Knuyt, G., K. Haenen, et al. (2006). "Photoconductivity observations on phosphorous-doped n-type CVD diamond at low temperature and varying electric field." Diamond and Related Materials **15**(1): 29-33.

Koizumi, S. (2003). n-Type diamond growth Thin-film diamond I. C. Nebel and J. Ristein, Elsevier, ISBN 0-12-752185-2, Semiconductors and Semimetals. **76:** 239-260.

Koizumi, S., M. Kamo, et al. (1997). "Growth and characterization of phosphorous doped {111} homoepitaxial diamond thin films." Applied Physics Letters **71**(8): 1065-1067.

Lazea, A., J. Barjon, et al. (2009). "Incorporation of phosphorus donors in (110)-textured polycrystalline diamond." Journal of Applied Physics - in press.

Lazea, A., V. Mortet, et al. (2008). "Growth of polycrystalline phosphorous-doped CVD diamond layers." Chemical Physics Letters **454**(4-6): 310-313.

Linares, R. and P. Doering (1999). "Properties of large single crystal diamond." Diamond and Related Materials **8**(2-5): 909-915.

Nesladek, M. (2005). "Conventional n-type doping in diamond: state of the art and recent progress." Semiconductor Science and Technology **20**(2): R19-R27.

Nesladek, M., K. Haenen, et al. (2003). "N-type P-doped polycrystalline diamond." Physica Status Solidi a-Applied Research **199**(1): 77-81.

Nesladek, M., K. Haenen, et al. (2003). Optical properties of CVD diamond. Thin film diamond I. C. Nebel and J. Ristein, Semiconductors and Semimetals, Elsevier, ISBN 0-12-752185-2. **76:** 325-378.

Nesladek, M., K. Meykens, et al. (1999_a). "Low-temperature spectroscopic study of n-type diamond." Physical Review B **59**(23): 14852-14855.

Nesladek, M., K. Meykens, et al. (1996). "Investigation of n-doping in CVD diamond using gap states spectroscopy." Diamond and Related Materials **5**(9): 1006-1011.

Nishitani-Gamo, M., K. P. Loh, et al. (1999). "Surface morphology of homoepitaxially grown (111), (001), and (110) diamond studied by low energy electron diffraction and reflection high-energy electron diffraction." Journal of Vacuum Science & Technology a-Vacuum Surfaces and Films **17**(5): 2991-3002.

Palnichenko, A. V., A. M. Jonas, et al. (1999). "Diamond formation by thermal activation of graphite." Nature **402**(6758): 162-165.

Sauer, R., N. Teofilov, et al. (2004). "Radiative recombination in phosphorus-doped CVD diamond." Physica Status Solidi a-Applied Research **201**(11): 2405-2413.

Solin, S. A. and A. K. Ramdas (1970). "Raman Spectrum of Diamond." Physical Review B **1**(4): 1687-1698.

Sternschulte, H., M. Schreck, et al. (2003). "Growth and properties of CVD diamond films grown under H2S addition." Diamond and Related Materials **12**(3-7): 318-323.

Teraji, T., K. Arima, et al. (2004). "High-quality boron-doped homoepitaxial diamond grown by high-power microwave-plasma chemical-vapor deposition." Journal of Applied Physics **96**(10): 5906-5908.

van Enckevort, W. J. P., G. Janssen, et al. (1993). "CVD Diamond Growth Mechanisms as Identified by Surface-Topography." Diamond and Related Materials **2**(5-7): 997-1003.

Vanecek, M. and A. Poruba (2002). "Fourier-transform photocurrent spectroscopy of microcrystalline silicon for solar cells." Applied Physics Letters **80**(5): 719-721.

Yanchuck, I. B., M. Y. Valakh, et al. (2004). "Raman scattering, AFM and nanoindentation characterisation of diamond films obtained by hot filamnet CVD." Diamond and Related Materials **13**: 266-269.

Zeisel, R., C. E. Nebel, et al. (2000). "Photoconductivity study of Li doped homoepitaxially grown CVD diamond." Physica Status Solidi a-Applied Research **181**(1): 45-50.

# 5 Devices and applications of P-doped diamond layers

In the present chapter the fabrication of diamond-based devices is explored. The devices which make used of either homoepitaxial diamond layers or diamond layers grown on non-diamond substrates are presented in separate subsections. In subsection 5.1.1 the results regarding pn-junction fabrication and characterization of single crystalline {111}-oriented diamond layers are shown. The following sub-section, 5.1.2, presents the results obtained when pn-junctions are fabricated using polycrystalline {110}-oriented diamond films. These results show the successful fabrication of devices when nonconventional P-doping conditions of polycrystalline diamond thin films are used. The performed investigations show that the polycrystalline diamond pn-junctions can be a good alternative to single crystalline devices.

The last part of the chapter is dedicated to devices which made use of P-doped diamond layers grown on non-diamond substrates. More precisely, for these applications the polycrystalline doped diamond thin films were grown on top of metallic substrates, appropriate for thermionic electron sources.

## 5.1 Fabrication and characterization of homoepitaxial diamond based devices

For application of diamond to electrical devices it is very important to control the impurity conductivity and to form pn and pin-junctions. Diamond pn and pin-junctions have numerous applications. For example, such devices are used as UV and particle detectors (Nesladek 2005). Also, diamond pin-junctions can be a good alternative to photoresistors because the photoresponse is temperature insensitive and additionally the detectors can operate in photovoltaic mode. The progress made in this direction was recently demonstrated by the diamond VUV photodetectors with high sensitivity that were chosen to be launched onboard satellite PROBA-2 (PRoject for ON-Board Autonomy) for solar UV radiation analysis (BenMoussa, Schuhle et al. 2006; BenMoussa, Soltani et al. 2008).

A first diamond pn-junction device was constructed in 2001 and was considered as the real breakthrough in the CVD diamond electronic device area (Koizumi, Watanabe et al. 2001). For its fabrication single crystalline {111}-oriented diamond layers were used. However, {111}-oriented diamond pn-junctions have limitations due to mechanical polishing, film quality etc. The development and optimisation of P-doped (Kato, Makino et al. 2008) and B-doped layers (Teraji 2008) brought the possibility to construct such devices on {100}-oriented diamond layers (Makino, Kato et al. 2005; Makino, Tokuda et al. 2006). Based on these successes, also polycrystalline diamond pn-junctions were prepared in 2005 (Nesladek 2005). In line with this research trend, numerous groups all over the world contribute to the improvement of diamond devices and a variety of pn or pin-junctions were fabricated (Koizumi, Watanabe et al. 2002; Suzuki, Yoshida et al. 2004; Tajani, Tavares et al. 2004; Makino, Kato et al. 2005; Tavares, Tajani et al. 2005; Makino, Kato et al. 2006; Makino, Tokuda et al. 2007; Tavares, Muret et al. 2007; Makino, Kato et al. 2008; Makino, Sung-Gi et al. 2009). The differences between these devices pertain to (except from the substrate orientation such as {111} or {100}-oriented single crystalline diamond substrates) the presence of heavily B or P-doped layers as well as growth of intrinsic thin diamond layers. Depending on the particular specifications of the devices, maximum rectification ratios of $10^6$ at ±15V (at RT) (Makino, Sung-Gi et al. 2009) and $10^{10}$ at ±25V (at RT) (Makino, Tokuda et al. 2006) were observed for diamond-based pn-junctions fabricated from {111} and {100}-oriented diamonds, respectively .

In this subsection, we shall focus on the characterization of the devices fabricated at IMO, which make use of single crystalline {111}-oriented thin films as well as polycrystalline {110}-oriented diamond layers.

### 5.1.1 pn-Junctions of single crystalline {111}-oriented diamond layers

#### 5.1.1.1 Introduction and experimental details

As described in chapter 1, see sub-section 1.2.3, obtaining a diamond-based *pn-junction* requires the fabrication of p and n type semiconducting material by doping diamond with acceptor and donor impurities. B-doped and P-doped diamond layers were independently grown using two separate MW PE CVD systems and the corresponding plasma parameters of each layer are presented in table 5.1. The reason behind growing first the B-doped layer and then the P-doped layer is due to the fact that B-doped thin films have less defective surfaces when compared with P-doped layers. For preparation of the doped layers a mixture of $CH_4$ and $H_2$ gas was used and HPHT synthetic Ib {111}-oriented single crystalline diamonds were used as substrates. The substrate size was $2.5x2.5x0.5mm^3$. The growth conditions for the P-doped layers are similar to that one given in chapter 3, with a typical ratio of $[CH_4]/[H_2]$ of 0.05%.

After the growth, square shaped mesa structures of $250μm^2$ were fabricated by conventional photo-lithography and plasma etching processes (see chapter 1). Finally, electrodes were formed on the n-type layer and at the p-type diamond film. For the n-type layer, Al (100nm) square shaped electrodes were deposited, while for the p-type layer, L-shape Ti (100nm)/Al(100nm) metallic contacts were fabricated. The samples were annealed in vacuum (~$10^{-6}$torr) at 450°C for 45min to ensure the formation of ohmic contacts on p-type layers. The diode structures are presented in figure 5.1, where a top view and a sketched of the cross-section are shown.

*Table 5.1: Experimental conditions for boron- and phosphorus-doped diamond growth.*

| | **B-doped diamond** | **P-doped diamond** |
|---|---|---|
| Source gases | TMB, $CH_4$, $H_2$ | $PH_3$, $CH_4$, $H_2$ |
| $CH_4/H_2$ | 0.126% | 0.05% |
| TMB,$PH_3/H_2$ | 635ppm | 2000-5000ppm |
| Total gas pressure | 82.5torr | 100torr |
| Total gas flow | 500sccm | 500sccm |
| Substrate temperature | ~1000°C | ~900°C |
| Growth duration | 2h | 2h |

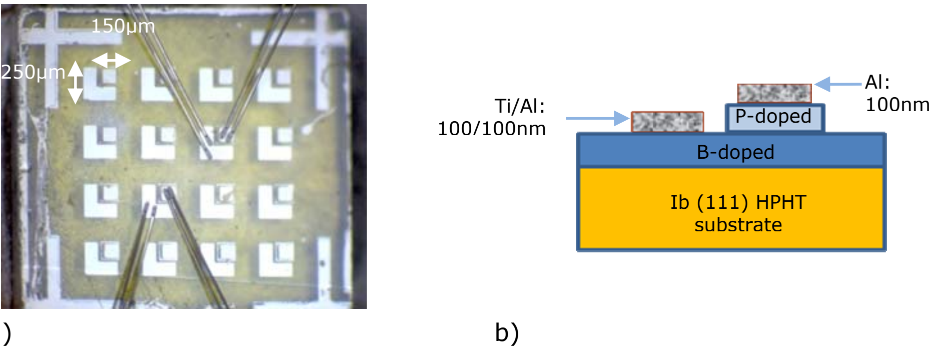

a) b)

*Figure 5.1: CVD diamond pn-junction device fabricated on Ib {111}-oriented HPHT diamond substrate: a) top view OM image and b) schematics of the diode.*

### *5.1.1.2 Experiments: IV characteristics*

This sub-section presents the current-voltage (I-V) characteristics measured for the diamond-based pn-junctions. These measurements were carried out using a 2400 Keithley Source Meter Unit. All the electrical properties were measured at room temperature and in air. Aluminium wires were used to connect the ohmic metallic contacts of the pn-junctions with the sample holder. The I-V data have been automatically recorded through a custom made LabVIEW program.

Under RT conditions, a d.c. bias (±40V) could be applied to this structures and the resulting I(V) characteristics, shown in figure 5.2, are clearly rectifying. In figure 5.2 the two distinct curves represent two different pn-junctions, on the same substrate. A slight difference is seen between the two curves. However, in both cases the data are typically show a diode character. The pn-junction that presents a "better" response shows a rectification ratio at +/- 40V of four orders of magnitude and is identified as the 2nd diode curve in figure 5.2. The high values of current at reverse bias current can be due to some local imperfections of the pn-junction surface which may cause some current leakages, affecting the reverse current. Nevertheless, these preliminary results point out the successful fabrication of diamond-based pn-devices at IMO using photo-lithography processes.

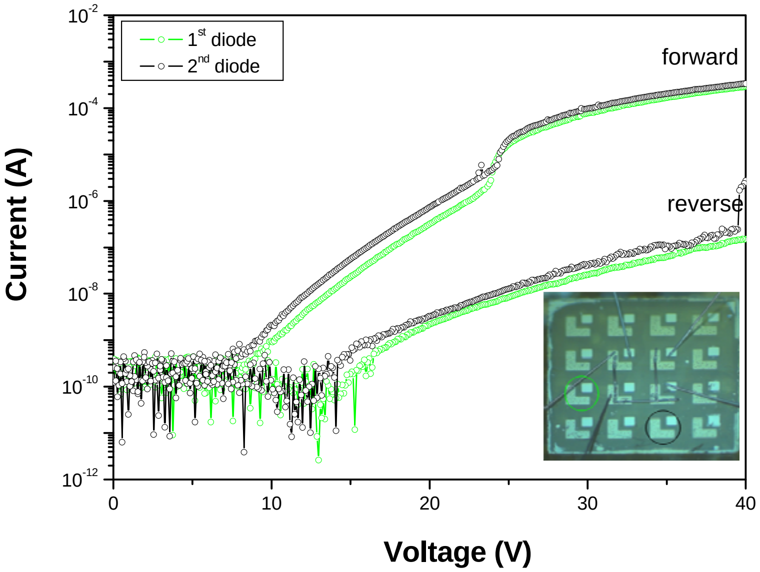

*Figure 5.2: I(V) characteristics of two pn-junctions formed on the sample doped with 635ppm B and 2000ppm P. The measurements were obtained at room temperature. The "forward" direction corresponds to the case when the positive voltage was applied to the p-type diamond.*

### 5.1.2 pn-Junctions of polycrystalline {110}-oriented diamond layers

#### 5.1.2.1 Introduction and experimental details

The fabrication of pn-junctions using polycrystalline diamond substrates finds its motivation in the fact that the polycrystalline diamond layers are interesting due to the possibility of deposition over large areas. Thus, the difficulty to manipulate and process small (typically 3x3mm$^2$) single crystalline diamond samples can be diminished. The first result regarding the successful fabrication of pn-junction using polycrystalline diamond layers was reported in 2005 (Nesladek 2005). The growth of these P-doped layers was obtained using the single crystalline doping strategy, i.e. conditions for doping of {111}-oriented single crystalline diamonds were used. In this subsection we shall focus exclusively on the pn-junction characterization when P-doped polycrystalline layers were grown in a non-conventional set of plasma growth conditions (see chapter 4).

The growth of P-doped thin films, necessary for pn-junction fabrication, has been done on top of B-doped polycrystalline {110}-oriented diamond substrates. The p-type layers were grown on top of a 2 inch Si wafer by MW PE CVD in an ASTeX AX6500 machine using 3% $CH_4$ in $H_2$. The microwave power, pressure and substrate temperature were 6000W, 100torr and 850-900°C, respectively. The [TMB]/[$CH_4$] ratio was 100ppm. Total duration of growth was 300h resulting in a 0.4mm thick B-doped polycrystalline diamond layer, hence the deposition rate was 1.3µm/h. The orientation of the grains, according to the EBSD measurements, was mainly {110} as will be shown later on. After the growth, the B-doped layer was detached from the Si substrate and round shape samples (3mm diameter) were laser cut and polished. The P-doping plasma conditions are similar to the ones presented in chapter 4 and are called *novel n-type growth parameters*. Table 5.2 presents the growth conditions used for the polycrystalline pn-junctions, i.e. the B-doped substrate as well as the P-doped diamond layers.

*Table 5.2: Experimental conditions for boron- and phosphorus-doped diamond growth.*

| | **B-doped diamond substrates** | **P-doped diamond layers** |
|---|---|---|
| Source gases | TMB, $CH_4$, $H_2$ | $PH_3$, $CH_4$, $H_2$ |
| $CH_4/H_2$ | 3% | 1% |
| TMB,$PH_3/H_2$ | 100ppm | 100-800ppm |
| Total gas pressure | 100torr | 180torr |
| Total gas flow | ~500sccm | ~500sccm |
| Substrate temperature | 850-900°C | ~1130°C |
| Growth duration | 300h | 2h |
| Layer thickness | ~0.4mm | ~20-30µm |

#### *5.1.2.2 Surface topography and microstructural analysis of the pn-junction*

The surface topography and microstructural analyses of the polycrystalline {110}-oriented diamond samples, before and after the growth of P-doped layers, were studied in chapter 4 (see sub-section 4.1.1.2). In this section the doping process takes place on top of B-doped polycrystalline diamonds. The aim of this study is to observe if there are any influences of the B-doped substrate upon the growth of the n-type layers and if the behaviour already observed in chapter 4 (see sub-section 4.1.1.2.) is somehow altered.

Figures 5.3, 5.4 and 5.5 display the EBSD images for a polycrystalline diamond sample before and after P doping. One can obtain information regarding the crystallographic orientation of the B-doped substrate (figure 5.3) and of the layers grown with 100ppm [$PH_3$]/[$CH_4$] (figure 5.4) and 500ppm [$PH_3$]/[$CH_4$] (figure 5.5), respectively. Figure 5.3 represents the EBSD investigations of the B-doped diamond substrate and the investigations sustain the {110} texture of the grains, see the IPF and the pole figures. From the EBSD texture component investigation it is observed that most of the grains have a misorientation angle of less than 15° from the perfect {110} orientation. For the P doped layers, the EBSD investigations show that the grain orientation is similar to the substrate, see IPF images (figure 5.4 a) and 5.5 a)). The pole figures sustain this observation (figures 5.4 c and 5.5 c)), where a strong {110} texture is seen for the case of P doped layers. According to the EBSD texture component maps, the degree of tilt from the ideal {110} orientation is identical as the one presented for the substrate, most of the grains present a misorientation angle of less than 15° from the perfect {110} orientation (see figures 5.4 b and 5.5 b)). This behaviour is in accordance with the conclusions drawn in chapter 4, sub-section 4.1.1.2.

To study the surface topography of the P-doped diamond layers SEM images were performed. Figure 5.6 is showing the surface images for the same P-doped layers as previously investigated by EBSD. The samples surfaces present a uniform growth of the grains, regardless of the doping concentration. This observation is in accordance with the behaviour seen for the P-doped layers grown on top of the undoped polycrystalline diamond substrates, see chapter 4, section 4.1.1.2.

Thus, we can conclude that the doping process has not been influenced by the fact that the polycrystalline diamond substrates were B-doped.

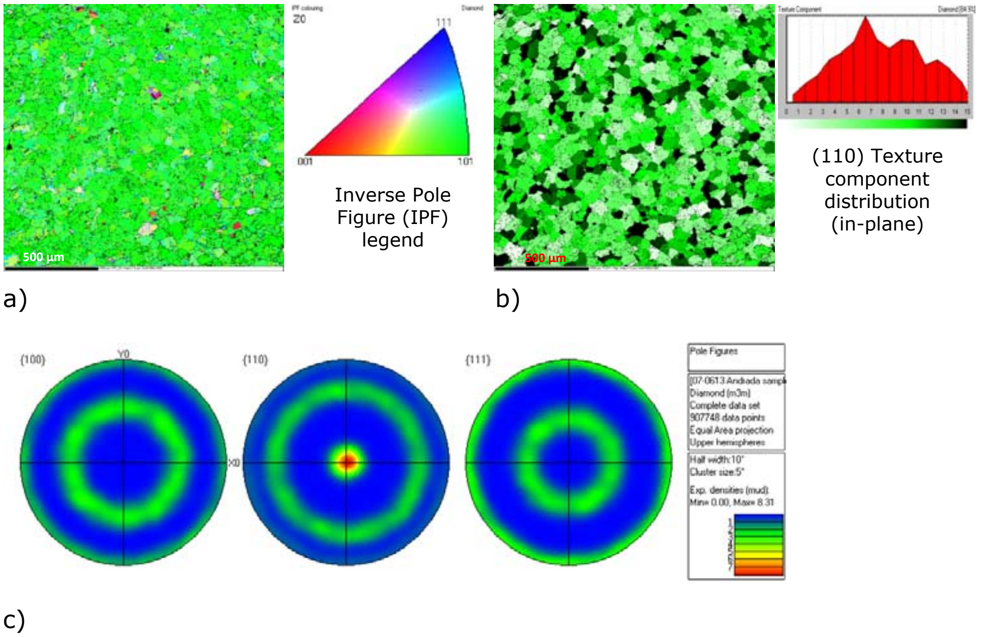

*Figure 5.3: EBSD mappings of the polycrystalline B-doped diamond substrate: (a) IPF map; (b) texture component map (1x1mm$^2$) of the same sample, illustrating the degree of tilt from the perfect {110} direction for each diamond grain on a. The scale bar ranging from 0° to 15° indicates that the majority of grains have a tilt of less than 12°; (c) {100}, {111} and {110} pole figure contour plots of the same sample as in images a) and b).*

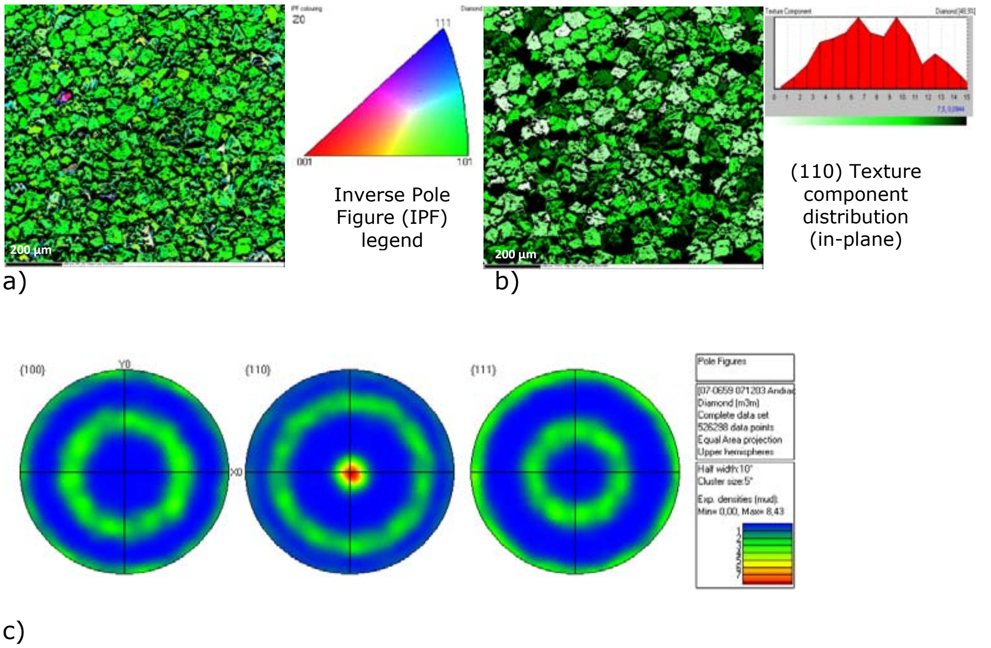

*Figure 5.4: EBSD mappings of the polycrystalline P-doped layer with 100ppm [$PH_3$]/[$CH_4$]: (a) IPF map; (b) texture component map (1x1mm$^2$) of the same sample, illustrating the degree of tilt from the perfect {110} direction for each diamond grain on a. The scale bar ranging from 0° to 15° indicates that the majority of grains have a tilt of less than 12°; (c) {100}, {111} and {110} pole figure contour plots of the same sample as in images a) and b).*

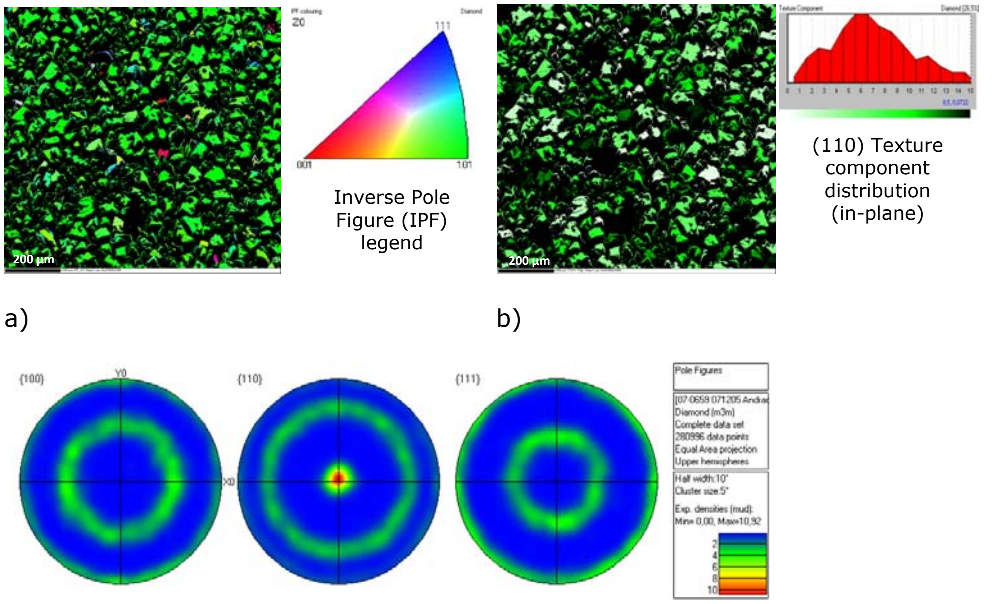

a)

b)

c)

*Figure 5.5: EBSD mappings of the polycrystalline P-doped layer with 500ppm [$PH_3$]/[$CH_4$]: (a) IPF map; (b) texture component map (1x1mm$^2$) of the same sample, illustrating the degree of tilt from the perfect {110} direction for each diamond grain on a. The scale bar ranging from 0° to 15° indicates that the majority of grains have a tilt of less than 12°; (c) {100}, {111} and {110} pole figure contour plots of the same sample as in images a) and b).*

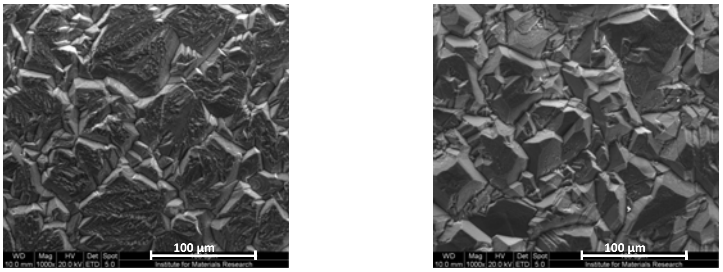

a) b)

*Figure 5.6: Comparison of the SEM images of two polycrystalline P-doped diamond layers, doped with 100ppm [$PH_3$]/[$CH_4$] (a) and 500ppm [$PH_3$]/[$CH_4$] (b), respectively.*

### 5.1.2.3 Experiments: IV characteristics and photoresponse

Current-voltage (I-V) characteristics of the polycrystalline diamond pn-junctions were measured using the experimental set-up previously described in sub-section 5.1.1.2. The fabricated polycrystalline diamond-based structures are presented in the figure 5.7. It must be mentioned that the metallic electrodes of the pn-junctions are also similar to the ones used for investigating the single crystalline pn-junctions: circular Al contacts for n-type layer (Ø=~100µm) and circular Ti/Al for p-type layer (Ø=~3mm).

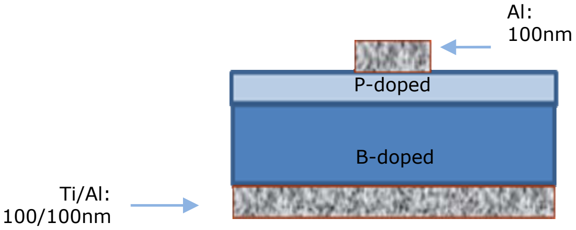

*Figure 5.7: Schematic of the freestanding CVD polycrystalline diamond pn-junction device fabricated at IMO.*

Figure 5.8 presents the rectification ratio for three freestanding polycrystalline pn-junctions, the only differences between the devices is the $PH_3$ concentration used during growth. All the pn-junctions present rectifying properties, the highest rectification ratio was over five orders of magnitude when a forward (n-type negative) and reverse (n-type positive) voltage of ±15V was applied to the pn-junction with 100ppm [$PH_3$]/[$CH_4$]. The other two pn-junctions, with 500ppm and 800ppm [$PH_3$]/[$CH_4$] respectively, presented a rather high reverse current. This behaviour may be caused by different factors. One can speculate it is due to the probable leakage of current caused by the polycrystalline nature of the sample or due to the surface imperfections caused by the surface roughness, which in turn can affect the adhesion of the contacts. One solution to overcome the surface imperfections may be the decrease in exposure time, thus growing thinner layers.

Nevertheless, the results presented here indicate that the quality of the polycrystalline pn-junctions, which were obtained by doping P in nonconventional plasma conditions, are practically comparable to the results found in the literature regarding polycrystalline diamond-based pn-junctions (Nesladek 2005).

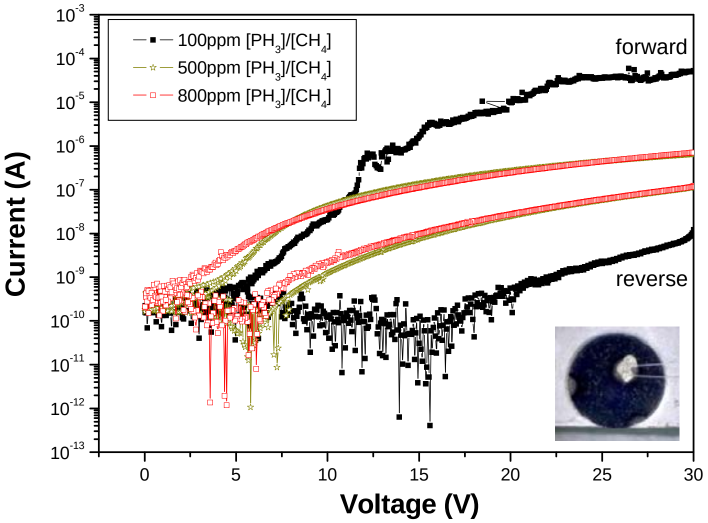

*Figure 5.8: I(V) characteristics of three pn-junctions, formed when the n-type layer was doped with 100ppm, 500ppm and 800ppm, respectively. The measurements were obtained at room temperature. The "forward" direction corresponds to the case when the positive voltage was applied to the p-type diamond.*

Figure 5.9 shows the photoresponse at room temperature for the same pn-junctions as previously characterized by IV curves (see figure 5.8). The spectra are measured from IR to UV, showing a maximum responsivity at about 210nm (5.9eV) and a strong rejection towards the visible part of the spectrum. This strong rejection of low energies predestines these detectors for solar blind detection of UV and XUV radiation. Such detectors are suitable for space applications and were recently tested (BenMoussa, Schuhle et al. 2006; BenMoussa, Soltani et al. 2008). The rejection factor between the responsivity maximum at 210nm (5.9eV) and the photocurrent at 500nm (2.48eV) is over three orders of magnitude in the case of the device doped with 100ppm [$PH_3$]/[$CH_4$]. To our knowledge this is comparable with similar measurements of polycrystalline CVD diamond pn junctions found in literature (Nesladek 2005).

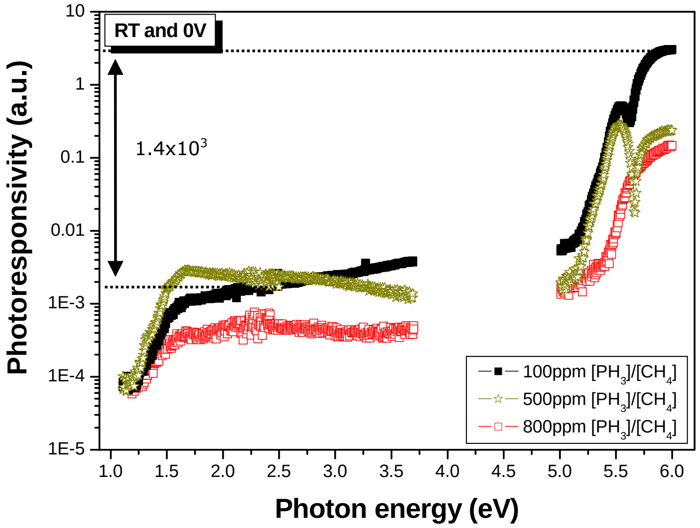

*Figure 5.9: Polycrystalline CVD diamond pn junction photodetector devices. The detector's photoresponsivity in the UV and visible part of the solar spectrum is shown. Circular Al (Ø=~100µm) for n-type layers and circular Al/Ti contacts (Ø=~3mm) p-type layers were used for.*

An attentive look at the photoresponsivity spectra points out that the signal presents a fluctuation around 220nm (5.6eV). The signal fluctuation tends to be more pronounced when the P concentration in the n-type layer of the device reaches 500ppm [$PH_3$]/[$CH_4$]. However, this signal fluctuation is not seen for the highest P concentration, namely 800ppm $[PH_3]/[CH_4]$. The nature of this signal fluctuation is not well understood and is currently under investigation.

In an attempt to improve the characteristics of the polycrystalline diamond pn-junctions, previously presented in figure 5.8, the IV measurements were re-measured. One of the investigated devices had a selectively grown P-doped layer on half of its surface (by simply covering a part of its surface with a Molybdenum metallic plate). The metallic contacts were fabricated by means of photolithography, identical to the case of pn-junctions previously presented in this subsection. The layers of the two different pn-junctions were grown in similar plasma conditions and for both samples the n-type layer was doped with 100ppm $[PH_3]/[CH_4]$. A schematic cross-section of the pn structure with a preferential growth of the n-type diamond layer and a top-view image sample are shown in figure 5.10.

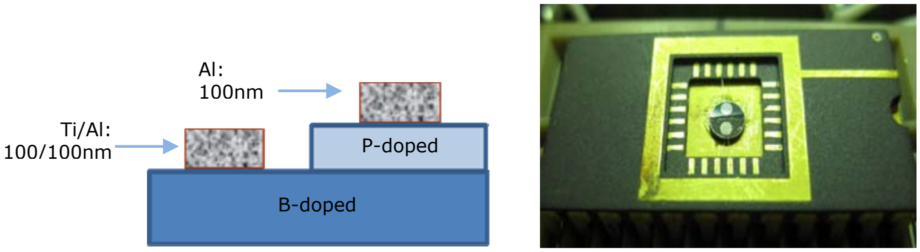

a) b)

*Figure 5.10: a) Schematics of the freestanding CVD polycrystalline diamond pn-junction device fabricated at IMO by means of preferential growth and photolithography, b) OM top-view image of a 3mm diameter pn-junction placed on a substrate holder for IV measurements.*

Figure 5.11 shows the I-V characteristics of the pn-junctions, with and without preferential growth of the P-doped layer. It is easily noticed that the signal of the device with preferential growth structure is less noisy. This could be explained by the fact that the current has a shorter trajectory through the sample and thus current leakage is less probable. Another positive observation is regarding the turn-on voltage. A turn on voltage of 2-3V is observed, compared with 4-5V for the device without preferential growth structures. This value is closer to the values found in literature for the devices which are based on single or polycrystalline diamond samples (Koizumi, Watanabe et al. 2002; Nesladek 2005) and proofs the high quality of our devices based on polycrystalline diamond specimens.

To summarize, in this sub-section the successful fabrication of diamond-based devices was presented. It was proven that the polycrystalline P-doped layers grown in atypical growth conditions generate n-type layers which may be used to produce pn-junctions. The characterization of such devices point out that the growth of P-doped polycrystalline layers, using nonconventional plasma conditions, may be used for diamond-based devices. An improvement of the results was done by selectively growing the P-doped layer at the surface of the polycrystalline sample. These devices are interesting due to the possibility of deposition on larger areas or to the more accessible price of the polycrystalline diamond substrates when compared with single crystalline diamond samples.

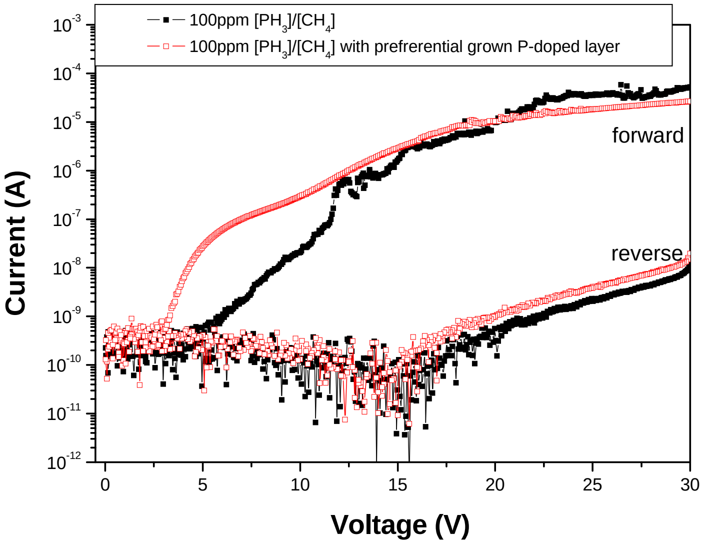

*Figure 5.11: I(V) characteristics of two polycrystalline diamond pn-junctions, formed with n-type layers grown using atypical plasma parameters and doped with 100ppm [$PH_3$]/[$CH_4$]. The measurements were obtained at room temperature. The only difference between the pn-junctions was that for one of them the P-doped layer was preferentially grown on half of the sample.*

## 5.2 Fabrication and characterization of diamond based devices grown on non-diamond material

Realization of diamond-based devices with expected properties is not an easy task and the development of such devices requires high quality diamond substrates or films of large size. One solution to overcome these limitations is the use of polycrystalline diamond films and the successful device fabrication based on this type of films was presented in the previous section of the chapter. The films presented earlier were homoepitaxial grown diamonds. In this subsection we shall focus on the merits of growth on non-diamond substrates and the possibility to fabricate devices based on these diamond films.

### *5.2.1 Phosphorus doped polycrystalline diamond films for thermionic electron emission*

#### *5.2.1.1 Introduction and experimental details*

Electron emission from carbon based materials has long been under investigation due to prospects of providing efficient electron sources. These emitters, diamond, nanocrystalline and carbon nanotube films, were mainly characterized with respect to electron field emission at room temperature (Koeck, Nemanich et al. 2009). The emission mechanism for nanostructured materials was based on field enhancement and penetration effects. Diamond thin films with small rms roughness exhibit negligible field enhancement effects and emission originated from states due to dopants as well as negative electron affinity (NEA) effects.

A thermionic electron source is based on the phenomenon of thermionic electron emission where electrons gain sufficient kinetic energy to escape the surface and thus are released in vacuum (Koeck, Nemanich et al. 2009). Thermionic electron emitters are a key component in applications ranging from travelling wave tubes for communications, space propulsion and direct energy conversion. As the conventional approach based on metallic emitters requires high operating temperatures the negative electron affinity (NEA) characteristics of diamond surfaces in conjunction with suitable donors would allow an electronic structure corresponding to a low effective work function. For this purpose we have prepared phosphorus-doped polycrystalline diamond films on metallic substrates by plasma assisted CVD where the NEA surface characteristics was induced by exposure of the film surface to a hydrogen plasma.

The substrates were 25mm in diameter and 1mm thick metallic molybdenum substrates, and were provided to us by courtesy of Dr. F. Koeck and Prof. Dr. R. Nemanich from the Department of Physics, Arizona State University, Tempe, USA. The substrate preparation includes ultrasonic abrasion in a nanodiamond-dimethil sulfoxide (DMSO) suspension for 60min (Koeck, Nemanich et al. 2009).

This was followed by a rinse in methanol and drying with nitrogen gas. Growth of the emitter structure was performed by plasma assisted chemical vapour deposition utilizing $PH_3$ as a phosphorus source and a set of unconventional plasma parameters, as given in the table 5.3.

*Table 5.3: Experimental conditions for phosphorus-doped polycrystalline diamond growth.*

| | **P-doped diamond** |
|---|---|
| Source gases | $PH_3$, $CH_4$, $H_2$ |
| $CH_4/H_2$ | 1% |
| TMB,$PH_3/H_2$ | 800ppm |
| Total gas pressure | 50torr |
| Total gas flow | ~500sccm |
| Substrate temperature | 1130-1200°C |
| Growth duration | 120min |

Examples of the morphology of the obtained P-doped polycrystalline diamond films grown on metallic substrates are presented in figure 5.12. From the SEM images it can be seen that the exposure to the plasma it generates a uniform polycrystalline layer only for the growth at higher temperatures. A lower substrate temperature promotes layers with visible macroscopic pin holes and line defects (see figure 5.12 a) and b)). The grain size is also temperature dependent, thus grains with a well-defined structure are observed for samples grown at 1200°C (see figure 5.12 c) and d)).

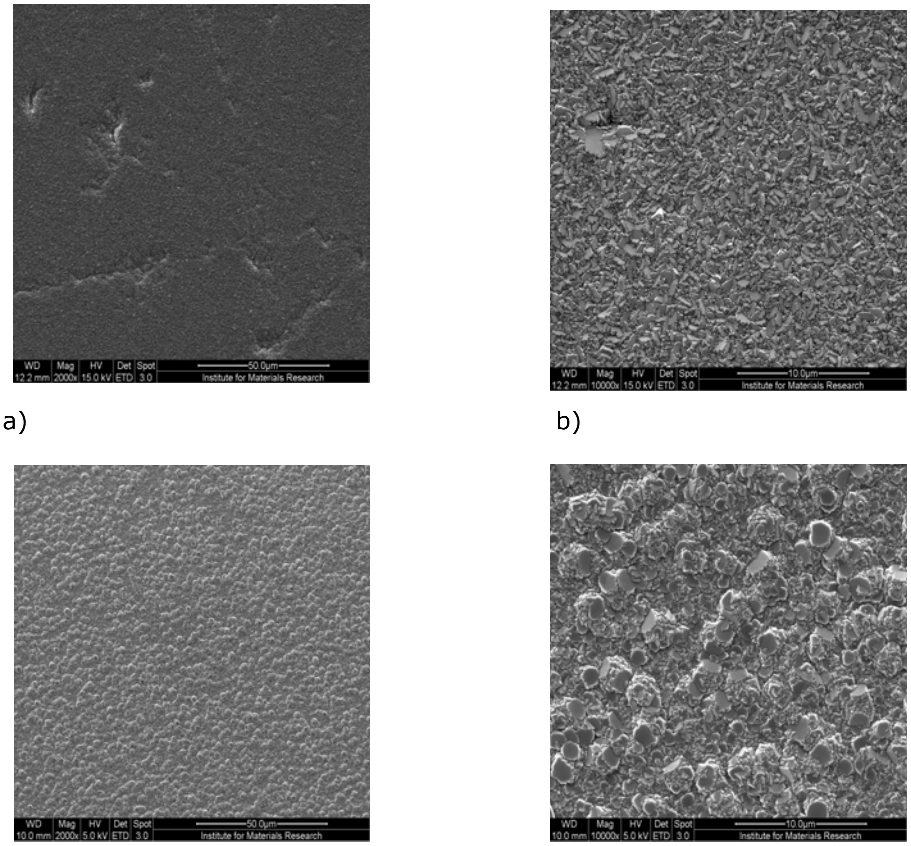

a) b)

c) d)

*Figure 5.12: Top-view SEM images of the two polycrystalline P-doped diamond layers, doped with 800ppm [$PH_3$]/[$CH_4$] and grown at 1130°C (a) and b)) or ~1200°C (c) and d)), respectively.*

### *5.2.1.2 Results: thermionic emission characterization*

Prior to emission measurements the samples were exposed to a hydrogen plasma with microwave power at 600W, sample temperature <600°C and chamber pressure at 20torr (Koeck, Nemanich et al. 2009). This results in NEA of the diamond surface.

Thermionic emission measurements were provided to us by courtesy of Dr. F. Koeck and Prof. Dr. R. Nemanich from the Department of Physics, Arizona State

University, Tempe, USA. The P-doped polycrystalline diamond layers grown on metallic substrates were characterized with respect to the Richardson – Dushman relation (5.1). Establishing an emission current from a metallic solid is dependent on the materials parameters, the work function $\varphi$ and an emission parameter $A_R$. Richardson and Dushman, in a theoretical approach, formulated a relationship between the emission current J(T) and material parameters in their corresponding law expressed by:

$$J(T)=A_R\,T^2 \exp(-\varphi/k_BT), \tag{5.1}$$

where $\varphi$ is the material work function and $A_R$ the Richardson's constant, with the emitter at temperature T, and $k_B$ Boltzmann's constant (Koeck, Nemanich et al. 2009).

The emission current for our samples was recorded as a function of emitter and the data – set fit to the theoretical equation is shown in figure 5.13 (Koeck, Nemanich et al. 2009). Electron emission from this structure commences at temperature <375°C and increases following the law of Richardson – Dushman. Evaluation of the data – fit presents an effective work function of 0.9eV, significant lower than the results from previously reported nitrogen-doped diamond emitters (Koeck, Nemanich et al. 2009; Koeck and Nemanich 2009_a). At elevated temperatures of 765°C the emission current was observed to exhibit stability within the measurement intervals of ~1h indicating stability of the NEA surface.

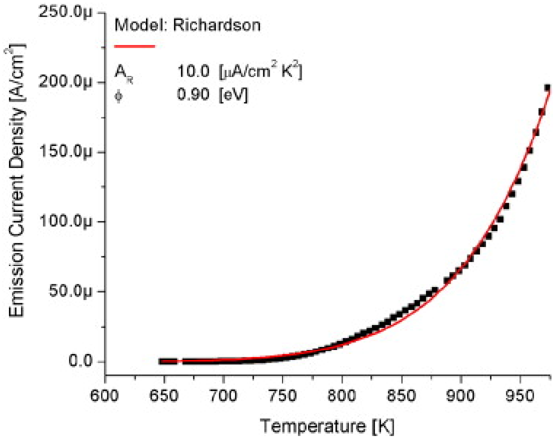

*Figure 5.13: Thermionic electron emission data (squares) and fit to the Richardson relation (line) from P-doped polycrystalline diamond (Koeck, Nemanich et al. 2009).*

In conclusion, the prepared P-doped polycrystalline diamond films on metallic substrates were characterized by thermionic electron emission measurements. The investigation compared with the Richardson – Dushman relation presented an effective work function of 0.9eV and the thermionic emission sustained a stable current up to 765°C.

## 5.3 Conclusions

In this chapter the capability of fabrication of diamond based devices at IMO was demonstrated. The phosphorus doped diamond layers were used to obtain two distinct types of applications. The first part of the present chapter was dedicated to the fabrication of pn-junctions. The devices were obtained by means of the photolithography technique and single as well as polycrystalline P-doped diamond samples, grown homoepitaxially, were obtained.

The electrical characterization of the single crystalline pn-junctions demonstrated that promising rectification ratios could be obtained. However, their performances could still be improved if we want to reach a superior quality of our devices similar to the ones reported in the literature by the leader in this field.

For the devices based on polycrystalline diamond layers it was shown that n-type phospshorus layers deposited in unconventional plasma parameters can be used to form pn-junctions. Electrical measurements of our devices have demonstrated that promising rectification ratios around $10^5$ could be obtained at room temperature. These values were obtained even without mesa-etching and this points to the high quality of the freestanding diamond-based pn-junctions. Their performances were slightly improved when preferential growth of P-doped layers was obtained and their characterisation ends the section dedicated to pn-junction devices.

Since the success in exploiting diamond based applications starting from homoepitaxial growth was shown, the second part of the chapter focused on the growth of P-doped diamond layers using non-diamond substrates. For this purpose the production of n-type diamond thin films on metallic substrates was investigated. The growth conditions used here were similar to the atypical set of plasma parameters used for production of n-type polycrystalline CVD diamond films. The thermionic electron emission measurements were successful and have indicated that the polycrystalline P-doped layers grown on top of molybdenum substrates present the lowest measured work function of any known material.

As a general conclusion, it was demonstrated that the atypical growth set of plasma parameters are appropriate conditions to generate P-doped diamond layers which can be successfully used in device fabrication.

## 5.4 References

BenMoussa, A., U. Schuhle, et al. (2006). "Radiometric characteristics of new diamond PIN photodiodes." Measurement Science & Technology **17**(4): 913-917.

BenMoussa, A., A. Soltani, et al. (2008). "New developments on diamond photodetector for VUV solar observations." Semiconductor Science and Technology **23**(3): 1-7.

Kato, H., T. Makino, et al. (2008). "N-type diamond growth by phosphorus doping." Diamond Electronics - Fundamentals to Applications II **1039**: 39-48.

Koeck, F. A. M. and R. J. Nemanich (2009_a). "Low temperatue onset for thermionic emitters based on nitrogen incorporated UNCD films." Diamond and Related Materials **18**(2-3): 232-234, doi: 10.1016/j.diamond.2008.11.023.

Koeck, F. A. M., R. J. Nemanich, et al. (2009). "Thermionic electron emission from low work-function phosphorus doped diamond films." Diamond and Related Materials: in press, doi:10.1016/j.diamond.2009.01.024.

Koizumi, S., K. Watanabe, et al. (2001). "Ultraviolet emission from a diamond pn junction." Science **292**(5523): 1899-1901.

Koizumi, S., K. Watanabe, et al. (2002). "Formation of diamond p-n junction and its optical emission characteristics." Diamond and Related Materials **11**(3-6): 307-311.

Makino, T., H. Kato, et al. (2006). "Electrical and optical characterizations of (001)-oriented homoepitaxial diamond p-n junction." Diamond and Related Materials **15**(4-8): 513-516.

Makino, T., H. Kato, et al. (2005). "Strong excitonic emission from (001)-oriented diamond P-N junction." Japanese Journal of Applied Physics Part 2-Letters & Express Letters **44**(37-41): L1190-L1192.

Makino, T., H. Kato, et al. (2008). "Homoepitaxial diamond p-n(+) junction with low specific on-resistance and ideal built-in potential." Diamond and Related Materials **17**(4-5): 782-785.

Makino, T., H. Kato, et al. (2005). "Electrical characterization of homoepitaxial diamond p-n+ junctions." Diamond and Related Materials **14**: 1995-1998.

Makino, T., R. Sung-Gi, et al. (2009). "Electrical and light-emitting properties from {111}-oriented homoepitaxial diamond p-i-n junctions." Diamond and Related Materials: - in press, doi:10.1016/j.diamond.2009.01.016.

Makino, T., N. Tokuda, et al. (2007). "Electrical and light-emitting properties of (001)-oriented homoepitaxial diamond p-i-n junction." Diamond and Related Materials **16**: 1025-1028.

Makino, T., N. Tokuda, et al. (2006). "High-efficiency excitonic emission with deep-ultraviolet light from (001)-oriented diamond p-i-n junction." Japanese Journal of Applied Physics Part 2-Letters & Express Letters **45**(37-41): L1042-L1044.

Nesladek, M. (2005). "Conventional n-type doping in diamond: state of the art and recent progress." Semiconductor Science and Technology **20**(2): R19-R27.

Suzuki, M., H. Yoshida, et al. (2004). "Electrical characterization of phosphorus-doped n-type homoepitaxial diamond layers by Schottky barrier diodes." Applied Physics Letters **84**(13): 2349-2351.

Tajani, A., C. Tavares, et al. (2004). "Homoepitaxial {111}-oriented diamond pn junctions grown on B-doped Ib synthetic diamond." Physica Status Solidi a-Applied Research **201**(11): 2462-2466.

Tavares, C., P. Muret, et al. (2007). "Static and transient electrical properties of (111) diamond p-n diodes." Physica Status Solidi a-Applications and Materials Science **204**(9): 2985-2990.

Tavares, C., A. Tajani, et al. (2005). "{111}-oriented diamond films and p/n junctions grown on B-doped type Ib substrates." Diamond and Related Materials **14**(3-7): 522-525.

Teraji, T. (2008). Chemical vapour deposition of homoepitaxial diamond films. Physics and applications of CVD diamond. S. Koizumi, C. Nebel and M. Nesladek, Wiley-VCH Verlag GmbH & Co. KGaA, ISBN 978-3-527-40801-6**:** 29-76.

# 6 General conclusions and outlook

Diamond is a fabulous gemstone and in the last decades it has received a lot of attention for its large range of exceptional and extreme properties. The present study focuses on diamond's semiconducting properties which have promoted this material as an appropriate candidate for optoelectronic devices and applications. Due to the continuous research efforts in doping of diamond, particularly in n-type doping, good quality n and p-doped diamond thin films were obtained, and since 2001 the bottleneck, represented by the fabrication of bipolar diamond-based devices, was solved (Koizumi, Watanabe et al. 2001). However, the need to improve the quality of the doped diamond layers led to an increasing interest in this research topic and thus, due to the fashionable nature of the subject, in 2006 the present study began.

The first steps of my work were directed towards the necessity to improve the reproducibility and efficiency of n-type doping of {111} and {100} homoepitaxial diamond growth. For this reason, the {111}-oriented diamond samples were firstly addressed. It was possible to obtain at IMO n-type layers of a comparative quality with the ones reported by other research groups worldwide. In order to obtain a high crystalline quality of the n-type diamond epilayers at IMO a specific surface $O_2/H_2$ plasma pre-treatment procedure was developed to reduce crystallographic defects during growth that originate from the substrate. Using the optimized growth conditions, together with the substrate pretreatment, the preparation of n-type {111}-oriented diamond layers is reproducibly obtained.

Regarding the doping of diamond layers grown on {100}-oriented substrates, in 2005 Kato et al. demonstrated that P-doped homoepitaxial layers with n-type conductivity can be obtained (Kato, Yamasaki et al. 2005). However, when the present study started, the quality of the P-doped layers on {100}-oriented substrates was inferior to the P-doped {111}-oriented diamond thin films and this triggered the interest in the topic. In this study, I have tried a different approach than the general tendency for P-doping, thus a range of new doping conditions was investigated. The plasma parameters explored in this case are different from usual P doping conditions: higher substrate temperature and higher methane concentration during growth. Several measurement techniques, such as photocurrent and cathodoluminescence, were involved to characterize the P-doped homoepitaxial {100}-oriented diamonds. After careful investigation, it was concluded that P-doping was unsuccessful for the {100}-oriented diamond substrates grown using the newly introduced plasma parameters.

Whereas the efficient n-type doping of phosphorus of {111} and {100}-oriented diamond layers has been successfully achieved since 1997 (Koizumi, Kamo et al.

1997) and 2005 (Kato, Yamasaki et al. 2005), respectively, the research of doping of {110}-oriented diamond thin films was restricted. The first results regarding P-doping on samples presenting this orientation were achieved using polycrystalline {110} diamond substrates (Nesladek, Haenen et al. 2003). However, the literature indicates that further improvements are necessary to reach the efficiency level observed for the doped {111} and {100}-oriented, and, thus I have started investigating the {110}-oriented diamonds. Initial findings in this direction presented the growth and doping results when polycrystalline diamond substrates were obtained using a doping strategy employed for growth of homoepitaxial {111}-oriented layers. The quality of the P-doped layers was established from defect spectroscopy measurements and surface imaging results. A confirmation of the P incorporation was done. Nevertheless, a preferential growth process of the grains was observed. Overall, the aforementioned doping process had a lower quality when compared to the single crystalline doping process. Therefore, a new approach was tried by P doping in an atypical set of plasma parameters. This unconventional set of growth conditions, previously used unsuccessfully for the doping of {100}-oriented diamond samples, was now tested on polycrystalline {110}-oriented diamond substrates.

Due to its particularities, mainly the higher substrate temperature and methane concentration, these plasma parameters generate uniform growth of the diamond substrate. The P incorporation into the {110}-oriented polycrystalline diamond samples and the possible incorporation of unwanted defects were originally investigated by defect spectroscopy techniques. The results indicate a successful P incorporation and a comparative quality of the layers with the single crystalline P-doped diamond layers. The surface imaging and microsturctural investigations point out that the growth mechanism does not have a preferential behaviour. The grains of the polycrystalline {110}-oriented diamond substrate clearly grow after exposure to the plasma while the surface of the grains keeps the same orientation of the substrate, i.e. {110}-oriented. From corroborating the microstructural information with the CL measurements, a first conclusion can be drawn: the novel set of plasma conditions is suitable for P incorporation in {110}-oriented diamond grains. Surprisingly, the combination of these two techniques proves to be a powerful tool in the local determination of the dopant incorporation as a function of the substrate orientation. In particular, it was shown that the phosphorus incorporation efficiency is smaller for grains closer to the perfect [110] direction, while there is systematically a large amount of P donor atoms incorporated when these angles are higher than 12°. In addition to this new information, it was observed into detail the surface morphology of the grains and it was seen that the surface presents a certain roughness. It is proposed that the surface features consists out of {111}-oriented microfacets that facilitates the local incorporation of P.

The successful P doping of polycrystalline layers, when using optimized plasma conditions, inspired the doping of single crystalline {110}-oriented diamond substrates. Higher growth rates were observed for the grown layers and ~100µm thick diamond thin films were achieved within 2 hours deposition. The presence of P-related features in the PC spectra indicates a successful incorporation of P into these layers. The preliminary surface imaging results reveal a surprising morphology which presents microfacets at the sample surface. Their exact orientation needs further investigations. A confirmation of P incorporation into the layers, as seen with PC, was done by FTPS experiments. The incorporation of phosphorus donor was further studied with several techniques. From SIMS data and Hall measurements it was revealed that high P concentrations can be incorporated (as high as $\sim 10^{19}$cm$^{-3}$) and a confirmation of the n-type behaviour of the deposited layers was done. These results point to the following conclusion: successful P incorporation into {110}-oriented single crystalline diamonds was observed. However, further analyses are necessary to establish the importance of the microfacets in the P localization at the sample surface. Preliminary electrical investigations of the obtained layers indicate the n-type character of the achieved diamond thin films, proving that the novel set of plasma parameters is suitable for donor doping of the {110}-oriented single crystalline diamond layers.

The closing part of the study presents the applications and device fabrication based on the P-doped layers obtained at IMO. First, several pn-junctions were made using phosphorus and boron-doped CVD diamond layers. The bipolar devices based on single crystalline {111}-oriented substrates showed good rectification ratio, however the focus of the applications was on the {110} polycrystalline-based devices. Successfully freestanding pn-junctions were obtained when P-doped layers were grown using the our novel plasma parameters introduced in chapter 4. A good rectification ratio up to $\sim 10^5$ at ±15V was obtained. Moreover, these measurements could be slightly improved when preferential growth of P-doped layer was obtained at the sample surface. Finally, the second type of applications refers to thermionic electron emission from low work-function P-doped polycrystalline diamond films. These results prove that our novel plasma parameters produce P-doped diamond layers of sufficient quality for device fabrication.

This work is meant to be a contribution to the development of semiconducting diamonds. It introduced a new set of CVD diamond P-doping conditions. The quality of the n-type {110}-oriented diamond layers and their bipolar devices fabricated at IMO demonstrate the effective applicability of these new plasma conditions. Even if the progress is significant, the possibility to explore the doping of the {110}-orientated diamonds still remains and further work in this direction may address the stabilization of {110} facets during the growth, and thus, to increase the crystalline quality of diamond thin films.

## 6.1 References

Kato, H., S. Yamasaki, et al. (2005). "n-type doping of (001)-oriented single-crystalline diamond by phosphorus." Applied Physics Letters **86**(22): 222111_1-222111_3.

Koizumi, S., M. Kamo, et al. (1997). "Growth and characterization of phosphorous doped {111} homoepitaxial diamond thin films." Applied Physics Letters **71**(8): 1065-1067.

Koizumi, S., K. Watanabe, et al. (2001). "Ultraviolet emission from a diamond pn junction." Science **292**(5523): 1899-1901.

Nesladek, M., K. Haenen, et al. (2003). "N-type P-doped polycrystalline diamond." Physica Status Solidi a-Applied Research **199**(1): 77-81.

# List of symbols and abbreviations

$\alpha$ – absorption coefficient
Å – Angstrom
a-C – amorphous carbon
Al – aluminum
AFM – atomic force microscopy
A – Ampere
AC – alternative current
Ar – argon
AM – amplitude modulation
ASTeX – Applied Science and Technology (now Seki Technotron Inc.)
Au – gold
B – boron
**B** – magnetic field
BE – bound exciton
BSE – back scattered electrons
$B_2CH_6$ – diborane
$(B(CH_3)_3$ – trimethylboron
C – Carbon
$CH_4$ – methane
$CH_3$ – methyl
cm – centimeter
°C – Celsius
CL – cathodoluminescence
Cs – cesium
CCD – charged-coupled device
$CaF_2$ – calcium fluoride
CB – conduction band
CVD – chemical vapor deposition
DC – direct current
DLC – diamond like carbon
D – Deuterium
d – thickness
DICM – differential interference contrast microscopy
3D – tridimensional
2D – two-dimensional
$e$ – electron charge
E – electrical field
$E_a$ – activation energy (eV)
e-C – evaporated amorphous carbon

eV – electron volt (unit of energy)
EBSD – electron backscatter diffraction
EBSP – electron backscatter pattern
EIU – electronic interface unit
EL – electroluminescence
$F$ – electric field
fcc – face-centered cubic
FE – free exciton
FTIR – Fourier-transform infrared spectroscopy
FTPS – Fourier-transform photocurrent spectroscopy
FWHM – full width at half maximum
FEG – field emission gun
$\Phi$ – gas flow (sccm)
GaAs – gallium arsenide
$H_2$ – hydrogen gas
HeNe – helium-neon laser
HF – hot filament
hkl – Miller indices
HPHT – high pressure high temperature
Hz – hertz (measure of frequency)
$H_2SO_4$ – sulfuric acid
IMO – Instituut voor Materiaalonderzoek, Diepenbeek, Belgium (Institute for Materials Research, Diepenbeek, Belgium)
IR – infrared
I – current
IPF – inverse pole figure
$KNO_3$ – potassium nitrate
k – Boltzman constant ($1.380650(24)x10^{-23}J/K$)
k – Kelvin
kg - kilograme
LNT – liquid nitrogen temperature (77K)
LHe – helium liquid temperature (4.22K)
Li – lithium
$\mu$ - mobility ($cm_2/V$)
μm – micrometer
Mo – molybdenum
MW – microwave
MW PE – microwave plasma enhanced
min – minute
mm - milimetre
N – nitrogen
Ni – nichel

Na – sodium
nm – nanometre
NIRIM – National Institute for Research in Inorganic Materials, Tsukuba, Japan
$N_{ph}$ – number of photons
NIST – National Institute of Standards and Technology, U.S.
n – carrier density ($m^{-3}$)
$O_2$ – oxygen gas
OC – orientation contrast
OM – optical microscopy
Ω – Ohm (the unit, in direct current, of electrical resistance)
p – pressure (torr)
*P* – power (W)
P – phosphorus
Pa – Pascal (the unit of pressure, stress, Young’s modulus and tensile stress)
ppm – part per million
ppb – part per billion
PC – photocurrent
$PH_3$ – phosphine
PL – photoluminescence
RF – radio frequency (Hz)
$R_{rms}$ – root mean square surface roughness
R – resistance (Ω)
RIE – reactive ion etching
RT – room temperature
ρ – electrical resitivity (Ohm $m^{-1}$)
SE – secondary electrons
SEM – scanning electron microscopy
sccm – cubic centimeter per minute at standard temperature and pressure
Si – silicon
STM – scanning tunneling microscopy
s – second
SIMS – Secondary Ion Mass Spectroscopy
σ – Conductivity ($Ohm^{-1}cm^{-1}$)
TA – transverse acoustic
TO – transverse optical
TEM – transmission electron microscopy
Ti – titanium
$T_s$ – substrate temperature
T – temperature
TBP – tertiarybutylphosphine
V – volt (unit of voltage)
Θ – misorientation angle

UNCD – ultrananocrystalline diamond
UV – ultraviolet
XRD – X-ray diffraction

# List of publications for the present study

1. V. Mortet, O. Elmazria, W. Deferme, M. Daenen, J. D'Haen, **A. Lazea**, A. Morel, K. Haenen, M. D'Olieslaeger
*Titanium nitride grown by sputtering for contacts on boron-doped diamond*
Plasma Processes and Polymers, 2007, 4/S1, S139 – S143.

2. K. Haenen, **A. Lazea**, V. Mortet, J. D'Haen, P. Geithner, J. Ristein
*Phosphorous doping of microcrystalline CVD diamond using modified conditions*
Materials Research Society Symposium Proceedings, 1039, 1093-P17-01, 49-55. In "Diamond Electronics – Fundamentals to Applications II", Eds. C. E. Nebel, R. B. Jackman, R. J. Nemanich, M. Nesládek, ISBN 978-1-55899-986-2.

3. **A. Lazea**, V. Mortet, J. D'Haen, P. Geithner, J. Ristein, M. D'Olieslaeger, K. Haenen
*Growth of polycrystalline phosphorous-doped CVD diamond layers using novel doping conditions*
Chemical Physics Letters, 2008, 454/4-6, 310-314.

4. V. Mortet, M. Daenen, T. Teraji, **A. Lazea**, V. Vorlicek, J. D'Haen, K. Haenen, M. D'Olieslaeger
*Characterization of boron doped diamond epilayers grown in a NIRIM type reactor*
Diamond and Related Materials, 17/7-10, 2008, 1330-1334.

5. F. A. M. Koeck, R. J. Nemanich, **A. Lazea**, K. Haenen
*Thermionic electron emission from low work-function phosphorus doped diamond films*
Diamond and Related Materials, in press, 2009, doi: 10.1016/j.diamond.2009.01.024.

6. **A. Lazea**, J. Barjon, J. D'Haen, V. Mortet, M. D'Olieslaeger, K. Haenen
*Incorporation of phosphorus donors in (110)-textured polycrystalline diamond*
Journal of Applied Physics, 105/8, 2009, 083545.

7. K. Haenen, **A. Lazea**, J. Barjon, J. D'Haen, N. Habka, T. Teraji, S. Koizumi, V. Mortet
*(110)-Textured P-doped microcrystalline diamond: growth, characterization and devices*

Journal of Physics: Condensed Matter, accepted for publication, 2009. Invited article.

8. N. Habka, J. Barjon, **A. Lazea**, K. Haenen
*Raman mapping of strain in phosphorus doped polycrystalline CVD diamond layers*
To be submitted, 2009.

9. K. Haenen, **A. Lazea**, S. Koizumi
*UV-response of diamond p(i)n-junctions*
To be submitted, 2009. Invited article.

10. **A. Lazea**, V. Mortet, J. Barjon, N. Habka, F. Jomard, Z. Remes, K. Haenen
*Growth and characterization of phosphorous-doped {110}-oriented single crystalline diamond films*
To be submitted, 2009.

# Curriculum Vitae

| | |
|---|---|
| **NAME** | **LAZEA Ileana-Andrada** |
| **DATE OF BIRTH** | 01 September 1979 |
| **NATIONALITY** | Romanian |

## EDUCATION

| | |
|---|---|
| BSc (1998-2002) | University of Bucharest, Bucharest, ROMANIA<br>Faculty of Physics, Degree in Medical Physics<br>Thesis: *"Laser Cavitation"* |
| MSc (2002-2004) | University of Bucharest, Bucharest, ROMANIA<br>Faculty of Physics, Medical physics and Biophysics<br>Thesis: *"Modification of Polymeric Membranes Induced By Plasma Treatments"* |
| PhD (2006–2009) | IMEC wzv, Division IMOMEC, Wetenschapspark, No. 1, 3590 Diepenbeek, Limburg, BELGIUM<br>and<br>University of Hasselt, 3590 Diepenbeek, Limburg, BELGIUM<br>Thesis: *"Growth and characterization of phosphorus n-type Chemical Vapour Deposition (CVD) diamond films of various orientations and devices/applications based on these layers"* |